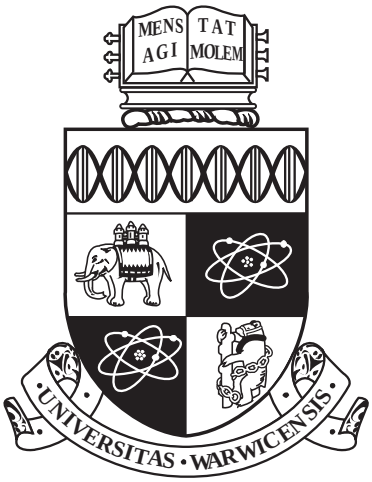

Performance Analysis for Cooperative Wireless Communications

by

Kezhi Wang

Thesis

Submitted to University of Warwick in partial

fulfilment of the requirements for the degree of

Doctor of Philosophy

School of Engineering

October 2014

THE UNIVERSITY OF
WARWICK

Contents

Acknowledgments

First and foremost, I would like to express my greatest gratitude to my supervisor, Dr. Yunfei Chen from the School of Engineering at University of Warwick for his careful supervision, constructive suggestions and valuable time. It would simply not have been possible to produce this work without his patient guidance, inspiration, encouragement and warm support. It is my very great privilege to have been his student. Also, I would like to thank him for supporting me to attend the international conference in Canada.

My special thanks also goes to Warwick Graduate School for awarding me Chancellor's International Scholarship, which has been making my study in U.K. come true. Without this scholarship, I would not have come and been studying here and achieved this point.

I also would like to take this opportunity to express my appreciations to Climate-KIC and European Institute of Innovation and Technology (EIT) for supporting me to attend summer school in Netherlands and Germany and then supporting me to attend conferences in Poland and Hungary. I have learned a lot from these training courses.

More importantly, I would like to thank my beloved parents for their unconditional sacrifices, constant encouragement, continuous support and endless love. They always have faith in me and are proud of me. I would like to dedicate this thesis to them.

It is my fortune to meet my girl friend during my Ph.D. study in War-

wick. I would like to thank her for the companionship during the happy and hard time.

Last but not the least, I was very lucky to have met so many good friends in U.K., especially the members from Communications Systems Laboratory (ComSysLab) in University of Warwick. I would like to thank them all.

Declarations

This thesis is submitted in partial fulfillment for the degree of Doctor of Philosophy under the regulations set out by the Graduate School at the University of Warwick. This thesis is solely composed of research completed by Kezhi Wang, except where stated, under the supervision of Dr. Yunfei Chen between the dates of October 2011 and October 2014. This thesis has not previously been presented in identical or similar form to any other examination board.

Kezhi Wang

October, 2014

Abstract

Cooperative relaying has been proposed as a promising solution to mitigate and combat the deleterious effects of fading by sending and receiving independent copies of the same signal at different nodes. It has attracted huge attention from both industry and academia. The purpose of this thesis is to provide an analytical performance evaluation of the cooperative wireless systems while taking some realistic conditions into consideration.

To achieve this, first, performance analysis of amplify-and-forward (AF) relaying using pilot-aided maximum likelihood estimation is studied in this thesis. Both disintegrated channel estimation (DCE) and cascaded channel estimation (CCE) are considered. Based on this analysis, optimal energy allocation is proposed.

Then, performance analysis for AF relaying corrupted by interferers are investigated. Both randomly distributed and fixed interferers are considered. For random interferers, both the number and the locations of the interferers are random while for fixed interferers, both the number and the locations are fixed.

Next, multihop relaying and multiple scattering channels over α - μ fading are analyzed. Channels with interferences and without interferences are considered. Exact results in the form of one-dimensional integral are derived. Also, approximate results with simplified structure and closed-form expressions are provided.

Finally, a new hard decision fusion rule that combines arbitrary numbers of bits for different samples taken at different nodes is proposed. The best thresholds for the fusion rules using 2 bits, 3 bits and 4 bits are obtained through simulation. The bit error rate (BER) for hard fusion rule with 1 bit is provided.

Numerical results are presented to show the accuracy of our analysis and provide insights. First, they show that our optimal energy allocation methods outperform the conventional system without optimal energy allocation, which could be as large as several dB's in some cases. Second, with the increase of signal-to-interference-plus-noise ratio (SINR) for AF relaying with interference, the outage probability decreases accordingly for both random and fixed interferers. However, with the change of interference-to-noise ratio (INR) but with the SINR fixed, the outage probability for random interferers change correspondingly while the outage probability for fixed interferers remains almost the same. Third, our newly derived approximate expressions are shown to have acceptable performances in approximating outage probability in wireless multihop relaying system and multiple scattering channel considering interferences and without interferences. Last, our new hard decision fusion rule is shown to achieve better performance with higher energy efficiency. Also they show that there is a tradeoff between performance and energy penalty in the hard decision fusion rule.

List of Publications

Journal Papers

- **Kezhi Wang**, Yunfei Chen, Mohamed-Slim Alouini, Xu Feng, "BER and Optimal Power Allocation for Amplify-and-Forward Relaying Using Pilot-Aided Maximum Likelihood Estimation", *IEEE Transactions on Communications*, (DOI: 10.1109/TCOMM.2014.2358219).

- **Kezhi Wang**, Yunfei Chen, Marco Di Renzo, "Outage Probability of Dual-Hop Selective AF With Randomly Distributed and Fixed Interferers", *IEEE Transactions on Vehicular Technology*, (DOI: 10.1109/TVT.2014.2366727).

- **Kezhi Wang**, Tian Wang, Yunfei Chen, Mohamed-Slim Alouini, "Statistics of α - μ Random Variables and Their Applications in Wireless Multihop Relaying and Multiple Scattering Channels", *IEEE Transactions on Vehicular Technology*, (DOI: 10.1109/TVT.2014.2345258).

- Yunfei Chen, **Kezhi Wang**, Jiming Chen, "Hard-Decision Fusion With Arbitrary Numbers of Bits for Different Samples", *IEEE Transactions on Vehicular Technology*, vol.62, no.2, pp. 879 - 884, Feb. 2013.

- **Kezhi Wang**, Yunfei Chen, Jiming Chen, "ALRT-Based Energy Detection Using Uniform Noise Distribution", *Wireless Communications and Mobile Computing*, (second round of reviewing).

Conference Papers

- **Kezhi Wang**, Tian Wang, Yunfei Chen, Mohamed-Slim Alouini, "Sum of Ratios of Products for α - μ Random Variables in Wireless Multihop Relaying and Multiple Scattering", in *IEEE 80th Vehicular Technology Conference (VTC2014-Fall)*, Vancouver, Canada, Sep. 2014.

- **Kezhi Wang**, Yunfei Chen, Mohamed-Slim Alouini, Feng Xu, "Pilot Power Optimization for AF Relaying Using Maximum Likelihood Channel Estimation", in *IEEE 80th Vehicular Technology Conference (VTC2014-Fall)*, Vancouver, Canada, Sep. 2014.

List of Figures

List of Tables

Abbreviations

AF Amplify-and-forward

ASK Amplitude-shift keying

AWGN Additive white Gaussian noise

BER Bit error rate

BPSK Binary phase-shift keying

BFSK Binary frequency-shift keying

CCE Cascaded channel estimation

CDF Cumulative distribution function

CDMA Code division multiple access

CSI Channel state information

DF Decode-and-forward

DCE Disintegrated channel estimation

EGC Equal gain combining

EHF Extremely high frequency

FDMA Frequency division multiple access

FSK Frequency-shift keying

GA Gamma approximation

GG Generalized Gamma

GGA Generalized Gamma approximation

GGRA Generalized Gamma ratio approximation

GRA Gamma ratio approximation

i.i.d. Independent and identically distributed

INR Interference-to-noise ratio

ISI Inter-symbol interference

LOS Line-of-sight

LMMSE Linear minimum mean squared error

LTE Long term evolution

MGF Moment generating function

MISO Multiple-input-single-output

MIMO Multiple-input-multiple-output

ML Maximal likelihood

M-PAM M-ary pulse amplitude modulation

MRC Maximal ratio combining

NCFSK Noncoherent frequency-shift-keying

PDF Probability density function

PPP Poisson point process

PSK Phase-shift keying

QPSK Quadrature phase-shift keying

QoS Quality of service

RSP Ratio of sums of products

RV Random variable

SNR Signal-to-noise ratio

SRP Sum of ratios of products

SP Sum of products

SIR Signal-to-interference ratio

SIMO Single-input-multiple-output

SINR Signal-to-noise-plus-interference ratio

TDMA Time division multiple access

UHF Ultra high frequency

UWB Ultra-wideband

WLAN Wireless local area networks

WSNs Wireless sensor networks

4-PAM 4-pulse amplitude modulation

Important Symbols

$B(\cdot,\cdot)$ Beta function

$E(\cdot)$ Expectation operator

$G_{a,b}^{c,d}(\cdot)$ Meijer's G-function

$K_v(\cdot)$ vth order modified Bessel function of the second kind

$L^{-1}(\cdot)$ Inverse transformation operator

$N(\cdot,\cdot)$ Normal distribution

$V(\cdot)$ Variance operator

$\Gamma(\cdot)$ Gamma function

$\Gamma(\cdot,\cdot)$ Upper incomplete Gamma function

$\kappa_\nu(\cdot)$ Complete elliptic integral of the νth kind

${}_2F_1(\cdot,\cdot;\cdot;\cdot)$ Hypergeometric function.

$\Re(\cdot)$ Real part

$\Im(\cdot)$ Imaginary part

$Q(\cdot)$ Gaussian Q-function

$\lceil\cdot\rceil$ Ceiling function

$sign(\cdot)$ Signum function

$\gamma(\cdot, \cdot)$ Lower incomplete Gamma function

Chapter 1

Introduction

1.1 Wireless Communications

With the extensive development of wireless technologies over the past four decades, wireless communications have now become an indispensable part of people's daily lives and various industries. The attractive advantage of wireless communication systems is that the mobile devices are free to take, move, install and relocate with little additional cost of setting and rewiring. Also, it is very convenient to add other wireless devices or remove some from the existing systems without causing serious problems to the rest of systems, with proper hardware and software configurations.

The information produced in a wireless source could be either a digital signal, such as the signal in digital electronics, the output of a computer, or an analogue signal, such as a temperature, light, sound or video signal. In digital wireless communication systems, the information at source will be transformed into a sequence of binary digits for transmission [1]. Compared with analog communications, which were used a long time ago, digital communications

have the advantage of high efficiency, flexibility, compatibility and reliability [1]. Also, digital signals are more tolerant to noise and easy to store. The most commonly used media of wireless communications can be radio waves but can also be other electromagnetic technologies, such as infrared [2]. Radio waves have the longest wavelength in the electromagnetic spectrum. The frequencies of radio waves are between 3 Hz to 300 GHz. Microwaves can be considered as a sub-class of the radio waves that start from UHF (ultra high frequency) to EHF (extremely high frequency) which cover the frequencies between 300 MHz to 300 GHz. The higher frequencies of microwaves are called millimeter waves which may be applied in future 5G cellular communications to tackle the bandwidth shortage problems [3, 4].

Over the past several years, many types of wireless communication systems have been proposed, such as wireless personal area networks (WPAN), wireless local area networks (WLAN), wireless metropolitan area networks (WMAN) and wireless wide area networks (WWAN). The wireless technologies have also been developed rapidly, including bluetooth, ad hoc networks, ZigBee, Ultra-wideband (UWB), wireless fidelity (Wi-Fi), worldwide interoperability for microwave access (WiMax), etc.

1.2 Evolution of Mobile Communication Systems

The last four decades have seen unprecedented growth in mobile communication systems. The evolution and features of wireless mobile communication systems are summarized as follows.

In the early 1980s, the first-generation or 1G network was launched based on frequency division multiple access (FDMA), which can only provide the basic mobile speech service using the analogue cellular technologies.

Around the late 1980s, second-generation or 2G network was introduced, based on code division multiple access (CDMA) or time division multiple access (TDMA) technologies, which provided better coverage and spectrum efficiency than 1G. In 1991, Global System for Mobile Communications (GSM) was launched, which can allow people to use picture messages (MMS), text messages (SMS), emails and Internet services (WAP). Then, the General Packet Radio Service (GPRS) was introduced (or referred as 2.5G), which added packet switched capability to existing 2G networks, improving services such as e-mail and Internet access. Later in 2003, enhanced data rates for GSM evolution (EDGE) was developed (referred as 2.75G or enhanced GPRS), which is considered as a pre-3G communication technology. It can provide typical bit rates of up to 400 kbit/s and peak bit rates of up to 1 Mbit/s.

Third-generation or 3G network was introduced in late 2002, which brought us faster Internet services and video calling. In 3G network, some universal global standards were designed and defined by International Telecommunication Union (ITU) and its partners such as the 3rd Generation Partnership Project (3GPP). Universal Mobile Telecommunications System (UMTS) was used in Europe and it selected wideband code division multiple access (W-CDMA) as an air interface. Time division synchronous code division multiple access (TD-SCDMA) was proposed in China, and code division multiple access 2000 (CDMA2000) EV-DO was used in the United States. Shortly after 3G, high speed packet access (HSPA) protocols (or referred to as 3.5G) were released, which can provide the peak data rates of up to 5.76 Mbit/s in the

uplink and 14 Mbit/s in the downlink. Later in 2008, a further improved standard, HSPA+ (or referred to as Evolved HSPA), was released, which brought the data rates of the uplink and downlink to around 22 Mbit/s and 168 Mbit/s, respectively.

Two fourth-generation or 4G standard candidates: worldwide interoperability for microwave access (WiMAX) and long term evolution (LTE) were first commercially deployed at around 2007 and 2009, respectively. WiMAX was introduced by WiMAX Forum, which was described as "a standards-based technology enabling the delivery of last mile wireless broadband access as an alternative to cable and DSL" [5]. LTE was developed by 3GPP, which is a natural upgrade path for UMTS, HSPA and EDGE networks. Their purposes were both for high speed data transmission and high capacity of mobile phones and data terminals. The above two wireless technologies cannot be called as true 4G as they did not meet the technical requirements set by ITU.

In 2010, WirelessMAN-Advanced (known as IEEE 802.16m or Mobile WiMAX) standardized by IEEE and LTE-Advanced standardized by 3GPP reached the ITU requirements and became the true 4G standard. Several core techniques have been investigated and adopted in LTE-Advanced, such as multiple-input-multiple-output (MIMO), orthogonal frequency-division multiple access (OFDMA), cooperative wireless communications, heterogeneous deployment networks, self-organizing operation [6]. In particular, relaying via cooperative wireless communications has been considered as one of the key technologies in the future generation commercial wireless communication systems [7].

1.3 Cooperative Wireless Communications

Recently, the demands for lower bit error rate (BER), larger system capacity, better quality of service (QoS) and wider coverage area have been increasing rapidly. However, the performance of wireless communication systems is always influenced by path loss, interference from other users, fading in wireless channels, etc. In high density mobile environments, such as in big cities, the mobile terminals are often subject to multi-path deep fading. To reduce the degradation of signal integrity, diversity is important in receiving the correct information. The core idea of diversity is that different antennas can receive different copies of the the signal. The chances of all these versions being in a deep fade is much smaller than one signal being in a deep fade, if they are independent. A simple two-branch transmit diversity technique for wireless communications was proposed in [8].

Traditional space diversity systems using multiple antenna arrays deployed at the transmitter and/or the receiver are proposed to address these challenges. Based on the number of antennas, they can be mainly categorised as single-input-multiple-output (SIMO), multiple-input-single-output (MISO) and MIMO. Multiple antenna arrays can potentially and theoretically combat multipath fading propagation effects and increase the channel capacity by sending and receiving multiple copies. However, they may be physically complex, large-size and not cost-efficient. Therefore, in mobile communication systems, it is more practical to install multiple antennas in the base station than in the mobile node as the node is always complexity-limited and power-limited.

Therefore, cooperative/collaborative wireless communication systems,

which are composed of multiple mobile nodes, have come into being [9, 10]. They enable single-antenna mobiles to have part of the advantages of the MIMO systems. In this case, multiple users / sensors / nodes can cooperate with each other and share their antennas as relays. In this sense, they can create a virtual MIMO system, thereby generating virtual multiple antenna arrays and improving the performance of their own and the whole networks. These nodes not only have their own information to send, but also can act as relays to help other mobile nodes to transmit. Thus, they can combat and mitigate the deleterious effects of fading by sending and receiving multiple independent copies of the same signal, and they can effectively improve the QoS and enhance the transmission robustness of the networks.

Also, cooperative wireless systems can extend the network coverage by using idle nodes as relays or multihops in the network [11]. Since the power consumed by sending the signal through direct link by a signal antenna can be very high if the transmission distance is long, it is not acceptable by some mobile node which is power-limited or battery-driven. Cooperative relaying can overcome the problem of the insufficient power in transmitting the signal in long distance, as it can shorten the transmission distance between each mobile node by using relays or multihops. The joint routing, scheduling and power control problem for multi-hop wireless networks were studied in [12].

Another advantage of cooperative wireless systems is by using intermediate relay nodes, the systems can deal with the path loss concerns to some extent. Because the whole transmission distance between the source and destination can be divided into at least two parts by the intermediate relay nodes. It is shown in [13] that the sum of path loss of each part is less than the path loss of the entire direct path. This advantage can be found in as path loss

gain [13].

Several aspects of the design and optimization of conventional coded multiple-antenna transmission diversity methods are explored in [14]. Compared with traditional space diversity systems [14], cooperative wireless communication systems can achieve the same diversity gain as the traditional space diversity system without the installation of multiple antennas at the source or at the destination. It was also reported in [10] that less power is required in cooperative wireless systems than the conventional methods to achieve the same level of performance.

Distributed space-time coded cooperative diversity protocols for combating multipath fading in wireless networks were proposed in [15]. Several practical implications, signal schemes, and requirements on system design for cooperative communication systems were discussed in [7]. They provide an effective way for multiple wireless nodes to cooperate with each other, thereby exploiting spatial diversity in the network. Also, the low-complexity cooperative diversity protocols are developed and analyzed in [10]. They considered certain implementation constraints in the cooperating networks, such as half-duplex transmission, nonergodic and delay-constrained scenarios.

The new cooperative transmission protocols for delay-limited coherent fading channels composed of half-duplex nodes were proposed in [16]. Single, multiple relay selection and their achievable diversity orders were studied in [17]. Relay selection by allowing more than one relay to cooperate was generalized and several SNR-suboptimal multiple relay selection schemes were proposed in [17]. The power allocation problem in the transmit diversity wireless systems in Rayleigh fading with mean channel gain information was studied in [18]. The power allocation that minimizes the outage probability under

the total power constraint was considered in [18]. The optimal joint relay selection and power allocation scheme for two-way relay networks were proposed in [19]. The scheme in [19] was based on the maximization of the smaller of the received SNRs of the two transceivers subject to the total transmit power constraint. Apart from power allocation, [20] has proposed to design cooperative communication protocols by considering time domain as well. Then, [20] has shown that one should allocate more time and energy to the source than the relay.

In [21], the relay-based multi-user cooperative communication systems for the 4G uplink have been proposed. In the system, the multiple users' data streams are coded at the relay and then being forwarded to the base station. Also, the low-complexity coded modulation schemes in 4G wireless systems for distributed relaying have been studied in [22]. The block-based selective orthogonal frequency division multiplexing decode-and-forward relaying schemes for 4G systems have been proposed in [23], while the relay based cellular broadband networks of low complexity and low cost for suburban environment have been studied in [24]. In [25], relay nodes with the interference consisting of two single antenna transmitters and receivers have been studied. The relay systems have also been studied for the 5G systems [26]. In [26], two-way wireless relaying with multiple antennas using decode and forward protocol for 5G systems have been presented.

To sum up, cooperative wireless communications are expected to provide significant improvement in terms of system capacity, network coverage, reception reliability, energy efficiency, device size, cost and hardware implementation [10]. Because of these advantages, cooperative wireless relaying has attracted extensive attention from not only academia, but also industry.

They have recently been adopted by several new wireless standards, such as Mobile Multihop Relay (MMR, IEEE 802.16j), WiMAX (IEEE 802.16m) [27] and LTE-Advanced standard (3GPP) [28].

1.4 Thesis Outline

1.4.1 Research Motivation

Although cooperative wireless relaying communication systems has been extensively researched and applied as an effective way to mitigate the detrimental effects of wireless channels, there are still a lot of problems which need to be considered thoroughly.

First of all, for early research in cooperative relaying networks, perfect channel state information (CSI) is assumed to be available at some or all the network nodes. However, in reality, the training process is always necessary for a node to obtain an estimate of the exact CSI. Such estimation is always imperfect owing to the existence of fading or noise. Thus, the channel estimation process is important in wireless relay communications [29]. Recently, two channel estimation methods, i.e. disintegrated channel estimation (DCE) and cascaded channel estimation (CCE) are used in most wireless relaying systems [30]. However, DCE and CCE considering performance, power efficiency and complexity are still not available and are urgently needed. Also, in practice, the total power assigned to each node or to the whole networks are often limited such that an optimal power allocation method between the pilots (use for channel estimation in the training process) and the data (use for information transmission) is required. For some other applications, the optimal

power allocation method between the source node, relay and destination node is also required.

Secondly, in cooperative wireless system, existing work has mainly focused on the ideal situation with no interference during the relaying transmission process. Although this assumption can simplify theoretical analysis and present useful insights, it cannot be applied in practical scenarios, such as in simultaneous multi-user transmissions [31]. In reality, the nodes usually suffer from interference and the interference always causes the degradation of the performance of the system, which can not be ignored in the practical system analysis and design. For the applications in multiple-access systems with mobile nodes, the number and the locations of the interferers can be random while for the applications in fixed-access wireless systems with fixed nodes, the number and the locations of the interferers can be fixed. Therefore, the performance analysis for cooperative wireless systems with either random or fixed interferers is needed, as they can provide a number of useful insights and suggestions to the design of practical cooperative systems.

Then, for multihop relaying and multiple scattering channels, the system structure is more complex than the dual-hop wireless channels. Therefore, the exact results in terms of BER and outage probability are very complicated to obtain and not convenient to use, most of which have no closed-form expressions or are in terms of complicated special functions. If considering interference in those systems, their structure becomes even more complex than the systems without considering interference. Therefore, proper approximation methods with simplified form for those systems are highly required.

Last, but not least, decision making is essential in wireless communications, such as cooperative relaying systems, wireless sensor networks (WSNs)

and cognitive radio [32]. Since there are a variety of impairments such as noise, attenuation, fading, interference and distortion contributing to errors in the wireless channels, which will affect the signal transmission, it is important to understand how to receive the information transmitted by the source to the maximum possible extent. Therefore, the best fusion rule is highly needed in wireless communication systems.

1.4.2 Chapter Outlines

Motivated by the above observations, the performance of the cooperative wireless communications is analytically evaluated in this thesis, while taking several realistic conditions into account. Approximate methods with simplified form and the best fusion rule are provided for specific applications. An introduction and conclusion are given in most chapters to provide the readers with overviews and summaries of these chapters. Mathematical derivations and expressions are provided and several practical scenarios of cooperative wireless systems are examined and discussed. Numerical results are also given to verify those derivations and insights are presented as well. The structure of this thesis is organized as follows.

In Chapter 2, several fading channels used in this thesis are introduced while a review of modulation schemes including higher order modulations is given. Then, a comprehensive overview of the cooperative wireless relaying is presented. The details of the two main decision methods, i.e. soft-decision and hard-decision, are also discussed in this chapter. Finally, widely used performance measures for evaluating the system and related research methods applied in this thesis are introduced.

In Chapter 3, BER and outage probability expressions for amplify-and-forward (AF) relaying systems with two different channel estimation methods, DCE and CCE, using a pilot-aided maximum likelihood method in slowly fading Rayleigh channels, are derived. Based on the BERs, the optimal values of pilot energy under the total transmitting energy constraints at the source and the optimal values of pilot energy under the total transmitting energy constraints at the relay are obtained, separately. Moreover, the optimal energy allocation between the pilot energy at the source, the pilot energy at the relay, the data energy at the source and the data energy at the relay are obtained when their total transmitting energy is fixed.

In Chapter 4, the outage probability performance of a dual-hop AF selective relaying system with global relay selection is analyzed for Nakagami-m fading channels in the presence of multiple interferers at both the relays and the destination. Two different cases are considered in this chapter. In the first case, the number of interferers is assumed to be random, as are their locations. Outage probability using the generalized Gamma approximation (GGA) in the form of a one-dimensional integral is derived. In the second case, the number and locations of the interferers are assumed to be fixed. Exact outage probability in the form of a one-dimensional integral is derived. For both cases, closed-form expressions of lower bounds and asymptotic expressions for high signal-to-interference-plus-noise ratio (SINR) are also provided. Simplified closed-form expressions of outage probability for special cases (e.g., dominant interferences, independent and identically distributed interferers, Rayleigh distributed signals) are studied.

In Chapter 5, exact results for the probability density function (PDF) and cumulative distribution function (CDF) of the sum of ratios of products

(SRP) and the sum of products (SP) of independent α - μ random variables (RVs) are derived. They are in the form of a one-dimensional integral based on the existing works on the products and ratios of α - μ RVs. To simplify the exact results, approximate expressions in closed-form are also provided as follows: generalized Gamma ratio approximation (GGRA) is proposed to approximate SRP; Gamma ratio approximation (GRA) is proposed to approximate SRP and the ratio of sums of products (RSP); GGA and Gamma approximation (GA) are used to approximate SP. The proposed results of the SRP can be used to calculate the outage probability for wireless multihop relaying systems or multiple scattering channels with interferences. The proposed results of the SP can be used to calculate the outage probability for these systems without interferences. Also, the proposed approximate result of the RSP can be used to calculate the outage probability of the signal-to-interference ratio (SIR) in a multiple scattering system with interference.

In Chapter 6, a new hard decision fusion rule that combines arbitrary numbers of bits for different samples taken at different nodes is proposed. The best thresholds for the fusion rules using 2 bits, 3 bits and 4 bits are obtained through simulation. The BER for the hard fusion rule with 1 bit is also derived using characteristic function. The new scheme shows that there is a tradeoff between performance and energy penalty in the decision fusion rule in wireless communication systems.

Finally in Chapter 7, the research results and findings are summarized and discussed. Also, the possible future work directions and suggestions are given.

Chapter 2

Background

2.1 Channel Models

Mathematical models are usually applied in wireless communication systems to characterize the physical channels and to clearly and conveniently reflect the important characteristics of the transmission medium. In the following, a brief introduction of the mathematical models that are used in this thesis is provided.

2.1.1 AWGN

The simplest model to describe the practical communication model is the additive noise channel. In this case, the transmitted signal $s(t)$ is influenced by an additive random noise, which may be caused by amplifiers or interference. If this noise is generated mainly by amplifiers at the receiver or electronic components, it can be named as thermal noise. This sort of noise can be generalized statistically to a Gaussian noise process [1]. Therefore the model for these channels is usually called additive white Gaussian noise (AWGN).

Due to its mathematical tractability and application to a large class of physical channels, it has been applied to many system analyses and research [1]. The mathematical model of AWGN is

$$u(t) = s(t) + n(t) \tag{2.1}$$

where $u(t)$ is the received signal in the communication system, $n(t)$ is the additive white Gaussian noise in the channel and t is the discrete time symbol. The PDF of a Gaussian RV X is described in terms of the mean μ and variance σ^2 as

$$f_X(x) = \frac{1}{\sqrt{2\pi\sigma^2}} e^{-\frac{(x-\mu)^2}{2\sigma^2}}. \tag{2.2}$$

Denote that X follows the Gaussian distribution (or Normal distribution) as $X \sim N(\mu, \sigma^2)$. The CDF of a Gaussian RV is defined as

$$F_X(x) = 1 - Q(\frac{x-\mu}{\sigma}) \tag{2.3}$$

where $Q(\cdot)$ is the Q function defined as [1]

$$Q(x) = \frac{1}{\sqrt{2\pi}} \int_x^\infty e^{-\frac{t^2}{2}} dt. \tag{2.4}$$

Also, Q function can be approximated as [1]

$$Q(x) \approx \frac{1}{2} e^{-\frac{x^2}{2}}, \quad x > 0. \tag{2.5}$$

Note that (2.5) is a very good approximation for Gaussian Q-function normally when $x \gg 3$, which has been used in some literature, such as [33].

2.1.2 Rayleigh Fading Channels

Apart from being influenced by the thermal noise, the transmitting signal usually undergoes fading through wireless channels as well. When a signal experiences fading during transmission, both its phase and envelope fluctuate over time.

Depending on the nature of the radio propagation, there are different models describing the statistical behaviour of the fading channel. The basic one of them is Rayleigh fading channel [34], which can be applied to describe the multipath fading with no direct line-of-sight (LOS) path. Rayleigh fading can be used in tropospheric and ionospheric signal propagation as well as heavily built-up urban environment [1]. Rayleigh fading is a reasonable model for the environment where there are many objects scatter the radio signal before it reaches the destination. Following the central limit theorem, if there is sufficiently scatter and no direct LOS path, then the channel impulse response will be well-modelled as a Gaussian process and have zero mean and phase evenly distributed between 0 and 2 π radians [35]. If X_1, X_2 are assumed to be two independent and identically distributed (i.i.d.) Gaussian RVs such that $X_1,\ X_2 \sim N(0, \sigma^2)$, then

$$X = \sqrt{X_1^2 + X_2^2} \tag{2.6}$$

is a Rayleigh RV. Thus, the PDF of a Rayleigh RV is given by

$$f_X(x) = \frac{x}{\sigma^2} e^{-\frac{x^2}{2\sigma^2}}, \quad x \geq 0. \tag{2.7}$$

In this case, X can be seen as the channel fading amplitude. The CDF of a

Rayleigh RV is given by

$$F_X(x) = 1 - e^{-\frac{x^2}{2\sigma^2}}, \quad x \geq 0. \tag{2.8}$$

If the instantaneous SNR per symbol is defined as $\gamma = X^2 E_s/N_0$ and the average SNR per symbol as $\bar{\gamma} = \Omega E_s/N_0$, where E_s is the energy per symbol, $\Omega = E(X^2)$, $E(\cdot)$ is the expectation operator, X^2 is the received instantaneous signal power such that $E(X^2) = 2\sigma^2$ and N_0 is the power of the Gaussian noise, the instantaneous SNR follows an exponential distribution with the PDF as [34]

$$f_\gamma(\gamma) = \frac{1}{\bar{\gamma}} e^{-\frac{\gamma}{\bar{\gamma}}}, \quad \gamma > 0. \tag{2.9}$$

2.1.3 Ricean Fading Channels

If X_1 and X_2 are distributed as $X_1 \sim N(\mu_1, \sigma^2)$ and $X_2 \sim N(\mu_2, \sigma^2)$ respectively, then, $X = \sqrt{X_1^2 + X_2^2}$ can be defined as a Ricean RV which is used to describe the multipath fading when one of the paths, typically a line of sight signal, is much stronger than the others. Thus, the PDF of a Ricean RV is given by [1, pp. 50]

$$f_X(x) = \frac{x}{\sigma^2} I_0(\frac{sx}{\sigma^2}) e^{-\frac{x^2+s^2}{2\sigma^2}}, \quad x > 0 \tag{2.10}$$

where $s = \sqrt{\mu_1^2 + \mu_2^2}$ and $I_0(x)$ is written as $I_0(x) = \sum_0^\infty (\frac{x^k}{2^k k!})^2$.

2.1.4 Nakagami-m Fading Channels

The Nakagami-m distribution gives the general version of the Rayleigh distribution. It can describe a complex fading environment through a shape

parameter m. The PDF of a Nakagami-m RV X can be given by [1]

$$f_X(x) = \frac{2m^m x^{2m-1}}{\Omega^m \Gamma(m)} e^{-\frac{mx^2}{\Omega}}, \; x \geq 0 \tag{2.11}$$

where Ω is defined as $\Omega = E(X^2)$ and m is defined as the ratio of moments or the fading parameter ranging from 1/2 to ∞ as [1]

$$m = \frac{\Omega^2}{E[(X^2 - \Omega^2)^2]}. \tag{2.12}$$

In (2.12), m=1 gives the Rayleigh model and $\Gamma(\cdot)$ is the Gamma function which is defined as $\Gamma(z) = \int_0^\infty t^{z-1} e^{-t} dt$ [36].

Simulators for the Rayleigh and Nakagami fading channels were reported in [37, 38]. Then, following the definition as in (2.9), the instantaneous SNR γ of (2.11) is distributed according to a gamma distribution with the PDF given by [34]

$$f_\gamma(\gamma) = \frac{m^m \gamma^{m-1}}{\bar{\gamma}^m \Gamma(m)} e^{-\frac{m\gamma}{\bar{\gamma}}}, \; \gamma \geq 0. \tag{2.13}$$

The Nakagami-m fading channel can provide more flexible and accurate match to the experimental signal statistics than the Rayleigh fading channel. Also, Nakagami-m fading can be used to model fading channel either more or less severe than Rayleigh fading by adjusting the parameter m [1]. [39] has shown that the Nakagami-m fading can provide the best fit for the data signals received in urban radio multipath channels.

2.1.5 α - μ Fading Channels

The α - μ distribution, which is in fact a rewritten form of the generalized Gamma (GG) distribution, can be applied to model more complex multipath

fading, as it includes the distributions of Gamma, Nakagami-m, exponential, Weibull, one-sided Gaussian, central Chi-squared and Rayleigh fading [40]. The PDF of a α - μ RV X is [40]

$$f_X(x) = \frac{\alpha\mu^{\mu}}{\Gamma(\mu)\hat{\gamma}^{\alpha\mu}} x^{\alpha\mu-1} e^{-\frac{\mu x^{\alpha}}{\hat{\gamma}^{\alpha}}}, x \geq 0 \tag{2.14}$$

where $\alpha > 0$ is related to the non-linearity of the environment [41], $\hat{\gamma} = E^{1/\alpha}(X^{\alpha})$ is a α-root mean value, $\mu = \frac{E^2(X^{\alpha})}{V(X^{\alpha})}$ is the inverse of the normalized variance of X^{α}, and $V(\cdot)$ are the variance operators [40]. One can get Nakagami-m fading when setting $\alpha = 1$, Weibull fading when setting $\mu = 1$ and Rayleigh fading when setting $\alpha = \mu = 1$ in (2.14). α - μ fading can be used to explore the non-linearity of the propagation medium, as sometimes fading model like Nakagami-m fading may not result in a moderate fitting [42]. [43] has shown that α - μ distribution can describe a signal composed of clusters of multipath waves propagating in a nonhomogeneous environment.

2.1.6 Characteristics of Fading Channels

Slow and Fast Fading

If the coherence time of the channel T_c is larger than the symbol duration time T_s, the channel can be defined as the slow fading channel, while if the coherence time T_c is smaller than the symbol duration time T_s, the channel is called as the fast fading channel [34]. The coherence time T_c can be related to the channel Doppler spread f_d as

$$T_c \simeq \frac{1}{f_d}. \tag{2.15}$$

Frequency Flat and Frequency Selective Fading

If the transmitted signal bandwidth f_s is much smaller than the coherence bandwidth of the channel f_c, the channel is called as frequency flat fading, while if the signal bandwidth f_s is much larger than the coherence bandwidth of the channel f_c, the channel is called as frequency selective fading. The coherence bandwidth of the channel f_c is related to the maximum delay spread τ_{max} given by [34]

$$f_c \simeq \frac{1}{\tau_{max}}. \tag{2.16}$$

2.2 Modulation Scheme

The data which needs to be transmitted through wireless channels can be both an analog signal or a digital signal. Digital signal transmission is more popular than the analog signal transmission. For instance, digital audio broadcasting (DAB) and digital video broadcasting (DVB) systems can broadcast radio and video signals through terrestrial digital transmissions, which allow for more efficient uses of frequency spectrum and can provide better quality of the sound and picture than traditional analogue methods.

Before transmission, the transmitted signal has to be encoded using either analog or digital modulation techniques to fit the channel. There are basically three types of analog modulation schemes: frequency modulation (FM), amplitude modulation (AM) and phase modulation (PM); while there are also three major classes of digital modulation techniques: frequency-shift keying (FSK), amplitude-shift keying (ASK) and phase-shift keying (PSK) [34]. The major advantage that digital modulation has over analog is that it can achieve greater fidelity. This is because digital modulation is the combination of 0 and

1 and any noise is virtually eliminated once the receiver decides whether a 0 or a 1 was transmitted. In the following, some modulation schemes used in this thesis will be introduced.

2.2.1 Binary Phase Shift Keying

Introduction

PSK is the digital modulation scheme that can convey the transmitted data through the phase of the carrier wave by modulating the reference signal. In this case, the digital data can be represented by a finite number of distinct signals. For instance, the M signal waveforms can be represented by [1]

$$s(t) = Re\{g(t)e^{j\frac{2\pi(m-1)}{M}}e^{j2\pi f_c t}\}, \quad m = 1, 2, \cdots, M \tag{2.17}$$

where $g(t)$ is the signal pulse shape and $\frac{2\pi(m-1)}{M}, m = 1, 2, \cdots, M$ is the M possible phases of the carrier and f_c is the carrier frequency. A convenient way to represent PSK schemes is to use a constellation diagram, such as constellation diagram for binary phase shift keying (BPSK) and quadrature phase-shift keying (QPSK) as follows [1]

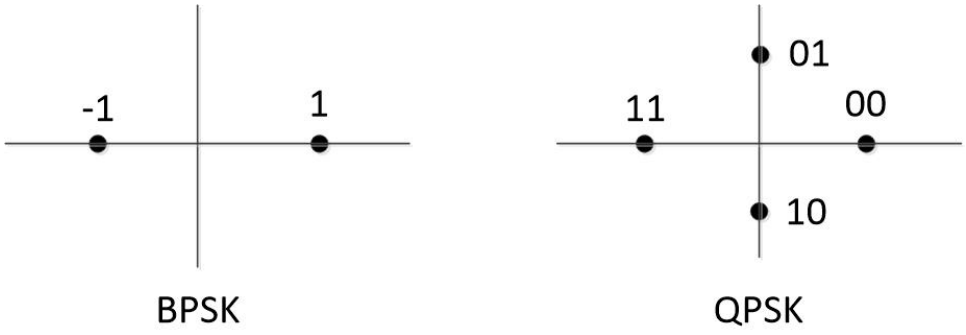

Figure 2.1: Constellation diagram for BPSK and QPSK

BPSK is the modulation with the robust and simplest implementation, which attracts great interest among the researchers and applications. It has only two phase states which are represented by the sinusoid, and two phases are different by 180 degree. During the modelling and calculation, $s(t)$ is always denoted as 1 and -1 for its two states. If one considers the signal transmitting in AWGN, the received signal $y(t)$ can be denoted as follows:

$$y(t) = \sqrt{E_d} + n(t) \tag{2.18}$$

where E_d is the transmitted signal energy per symbol when 1 is transmitted and,

$$y(t) = -\sqrt{E_d} + n(t) \tag{2.19}$$

when -1 is transmitted [1]. In the performance analysis below, the time indexes will be omitted.

Performance Analysis

In BPSK modulation, assume the probabilities of sending message 1 and -1 are p and $1-p$, respectively, and assume $s_1 = \sqrt{E_d}$ and $s_2 = -\sqrt{E_d}$. Using (2.18) and (2.19), and defining the decision threshold as r_{th}, then the decision regions can be shown as Fig. 2.2. Thus, the BER performance can be given

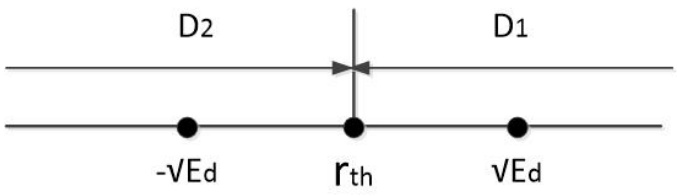

Figure 2.2: Decision regions

Table 2.1: Popular modulation schemes

Attributes	Characteristics
Carrier schemes	Frequency, phase, amplitude.
Number of bits	If the alphabet consists of $M = 2^N$ alternative symbols, each symbol represents a message of N bits.
Detection methods	Coherent, noncoherent, differentially coherent, partially coherent.

as [1]

$$\begin{aligned} P_e &= p \int_{D_2} Pr(y|s = \sqrt{E_d})dy + (1-p) \int_{D_1} Pr(y|s = -\sqrt{E_d})dy \\ &= p\, Q(\frac{\sqrt{E_d} - r_{th}}{\sqrt{\frac{N_0}{2}}}) + (1-p)\, Q(\frac{r_{th} + \sqrt{E_d}}{\sqrt{\frac{N_0}{2}}}) \end{aligned} \tag{2.20}$$

If $p = 1/2$, one can have $r_{th} = 0$, and the error probability can be simplified as

$$P_e = Q\left(\sqrt{\frac{2E_d}{N_0}}\right) \tag{2.21}$$

where $Q(\cdot)$ is the Gaussian Q-function and N_0 is the noise power. BPSK signaling can be used with rectangular pulses, which has constant envelope. However, in practice, filtered pulse shapes are more preferred and employed [1]. Also, a root-raised-cosine filter (RRC) are usually used as the transmit and receive filter in the digital communication system to perform matched filtering, which helps to minimize the inter-symbol interference (ISI).

2.2.2 Higher Order Modulations

Higher-order modulation schemes are the modulations usually with an order of four or higher such as QPSK, and 4-pulse amplitude modulation (4-PAM). Although BPSK gives the better BER performance than QPSK and 4-PAM, QPSK and 4-PAM can transmit twice the data rate in a given bandwidth compared to BPSK. Thus there is a tradeoff between reliability and data rate.

Other popular modulation schemes can be a combination of the attributes listed in Table. 2.1, which are based on (1) carrier schemes, such as the frequency, phase and amplitude; (2) the number of levels assigned to the modulated carrier schemes; (3) the detection schemes, such as coherent, partially coherent, noncoherent, differentially coherent [34]. According to the needs of specific wireless communication channels, sometimes a more sophisticated modulation scheme is required, which can be realized by modulating more than one attribute, such as modulating phase and amplitude together. This can satisfy the performance / power / bandwidth / reliability requirements of the specific system channel. Details and analysis about these modulation schemes are presented in Chapter 3 of [34].

2.3 Cooperative Wireless Relaying

Nowadays, cooperative wireless relaying has been extensively studied as an effective way to provide extra spatial diversity, combat fading, enhance the reliability and improve QoS in conventional single antenna transceiver systems [9, 44–47]. Most recently, cooperative wireless relaying has been adopted in LTE-Advanced as a key technique for future generation wireless communications [6].

A typical cooperative wireless communication system with a cooperative diversity link is shown in Fig. 2.3 [44]. In Fig. 2.3, the source terminal S

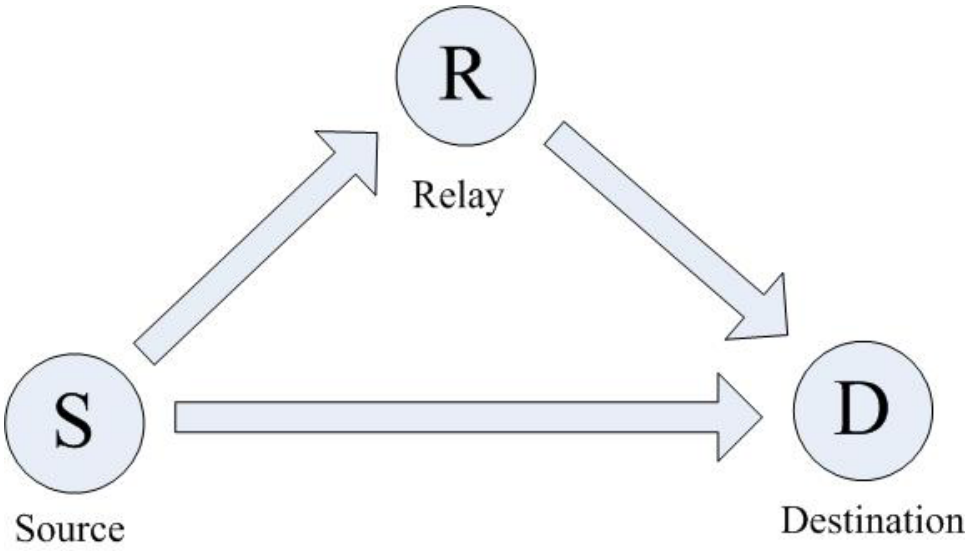

Figure 2.3: A typical cooperative wireless communication system with a cooperative diversity link.

can not only communicate with the destination terminal D directly but also can communicate through a relay R to D. In this case, the communication period can be divided into two intervals. In the first interval, S communicates with the R and D while in the second interval, only the relay R communicates with D. The destination D can combine the two received signals from those two transmission periods. In this system, one can see that if the direct link is faded deeply, then the relay link is an effective way to compensate for that, which may still achieve the acquired performance. The end-to-end performance analysis and a selection combining scheme for this system is presented in [44].

In the LTE-Advanced standard, source terminal S in Fig. 2.3 is referred to as a base station (eNodeB), destination terminal D in Fig. 2.3 is referred to

as user equipment (UE) and R in Fig. 2.3 is referred to as a relay node (RN), as in Fig. 2.4. The link between eNodeB and RN is denoted as a backhaul link or Un interface, whereas the link between RN and UE is denoted as access link or Uu interface. The eNodeB can transmit the signal at a higher power,

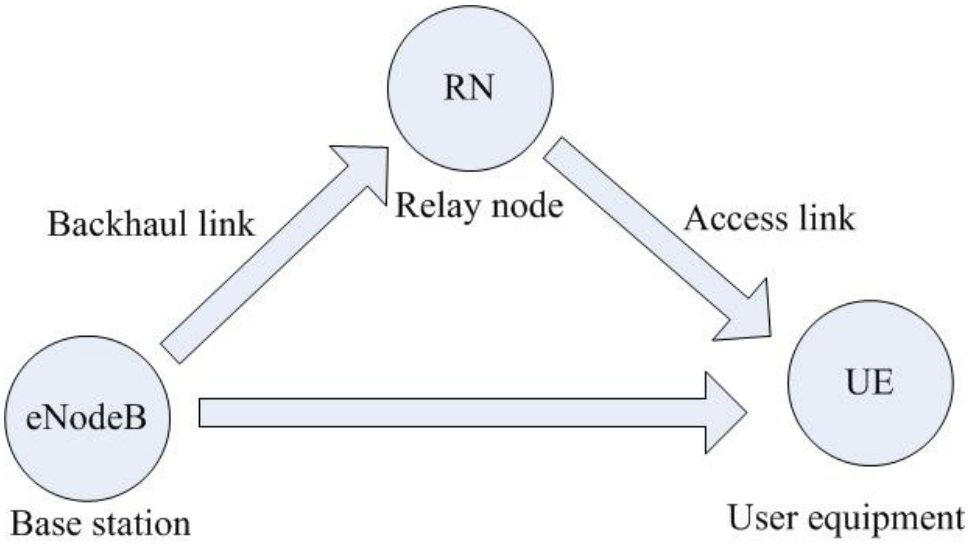

Figure 2.4: Cooperative wireless relaying in LTE-Advanced standard.

which is able to cover a larger area than the RN. Thus, each UE can either communicate with the eNodeB via the help of low-power RNs or directly with the eNodeB. In this case, the remote UEs or cell edge UEs can be well served and therefore the capacity and coverage of the network can be improved [6].

2.3.1 Cooperative Techniques and Performance Analysis

Several cooperative strategies have been proposed in the past few years, such as AF, decode-and-forward (DF) [10], compress-and-forward (CF) [48], and coded cooperation [49]. Among them, AF (non-regenerative) and DF (regenerative) relaying are perhaps the most widely used ones. In AF relaying, the source

broadcasts its information to the relays in the first phase and then the relays simply amplify the received signals from the source and forward them to the destination in the second phase, while in DF relaying, the source broadcasts its information in the first phase but the relays have to decode the received signals from the source and then re-encode the signals before forwarding them to the destination [9]. AF relaying can be seen as an analog cooperative method whereas DF relaying can be seen as a digital cooperative method. For systems with relatively bad backhaul links, AF relaying is more favourable than DF relaying [6].

For AF relaying in the LTE-Advanced standard, the relay node RN only operates as a repeater, such that the signals are simply amplified and forwarded from the eNodeB to the UE. Thus, only the radio frequency protocol layer is equipped in RN [50]. Also, the interference or the noise are amplified by the RN to the UE in this case. For DF relaying in the LTE-Advanced standard, the RN first decodes the transmitted signal from the eNodeB and then re-encodes the signal to the UE. In this case, the radio frequency layer and physical layer are both needed in RN [50]. Therefore, DF relaying has a more complex structure than AF relaying and the processing delay in DF relaying in terms of decoding and encoding can be longer than AF relaying [50]. However, DF relaying has better received SINR than AF relaying as the noise and the interference can be removed in DF relaying. Due to the lower complexity and simpler structure, AF relaying is more attractive than DF relaying for some source-limited or power-limited applications [46]. End-to-end performance of two-hop wireless communication systems with AF relaying over flat Rayleigh fading channels is analyzed in [47]. Outage probability and average BER expressions for noise limited systems are presented in [47].

AF relaying can be further categorized into relays with channel state information (CSI) and relays without CSI (blind relaying). For the former case, the relays can use instantaneous CSI of the first hop to control the amplification gain. Thus, in this case, the power of the retransmitted signal in the relay side can be fixed [46]. For the latter case, relays without CSI do not need instantaneous CSI of the first hop but use the fixed amplification gain. In this case, the power of the retransmitted signal in the relay side is variable [46]. Although the relays with CSI have better performance than the relays without CSI, an estimator is needed to obtain CSI in CSI-aided relays and therefore, the complexity of relays with CSI increases [46]. The exact outage probability of two-hop CSI-aided AF relaying over Nakagami-m fading channel is proposed in [51]. A comprehensive framework for the performance analysis of AF relaying with CSI-assisted over several fading channels is presented in [52]. In [52], a simple lower bound for outage probability is given based on the moment generating function (MGF).

In a multiple-access system or a frequency-reused cell, interference from other transmitting sources, i.e. interferers, may cause a performance degradation and therefore, cannot be ignored in the performance analysis. In [53], the outage probability and average BER of a dual-hop relaying system with fixed gain over Nakagami-m fading channel in the presence of a single interferer are investigated. It was shown in [53] that the presence of the interferer at the destination and at the relay leads to a floor point in the BER performance and outage probability. A tight lower bound for BER of dual-hop AF with CSI-aided over Nakagami-m fading channel in the presence of multiple interferers at the relay is derived in [54]. Closed-form expressions for the exact outage probability is given in [54]. Also, outage probability of two-hops AF

relaying systems with co-channel interference over Nakagami-m fading is investigated in [55]. In [55], multiple co-channel interferers at both the relay and destination are considered.

2.3.2 Cooperative Relaying

In mobile networks, in order to achieve the improvement in coverage, throughput, adaptability, connectivity, deployment and capacity and less transmit power in each individual node, packets are more likely to propagate from the source through several intermediate relaying nodes before they can reach the destination. This is known as multihop transmission, which can be applied to WLAN, cellular, ad-hoc, and hybrid networks [11].

The diagram of multihop transmission can be found in Fig. 2.5. In

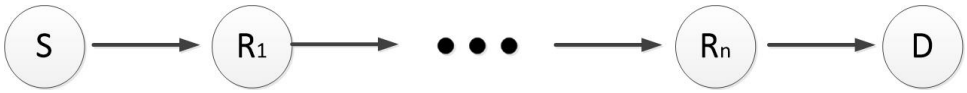

Figure 2.5: Multihop transmission.

multihop systems, the signal can be transmitted from the source S to the destination D through several intermediate relaying nodes $R_1 \cdots R_n$. Multihop systems have the benefits of broadening the network without using a large amount of transmitting power and improving connectivity in each node [11,56]. Also, they can promote higher data rates resulting in higher throughput, and they make use of wireless medium more efficient.

Reference [11] presented and characterized four channel models for multihop wireless communication systems, and introduced the concept of multihop diversity. An analytical framework for the evaluation of the end-to-end outage probability of multihop wireless relaying systems over Nakagami-m channels is

reported in [57]. Closed-form lower bounds for the performance of the multihop transmissions with nonregenerative relays over not necessarily identically distributed Nakagami-m fading channels are presented in [56]. The benefits of the multihop relaying are emphasized in [58] for broadband cellular mesh networks. Also, the design suggestion on spectrum allocation, relay deployment are given in [58]. The tight closed-form upper bound for the ergodic capacity and outage probability performance of multihop relaying with an arbitrary number of cooperative intermediate relays and no direct link between the source and destination nodes over Nakagami-m fading are investigated in [59].

2.3.3 Relay Combining

In a cooperative communication system, idle nodes acting as virtual antennas are employed to forward signals from the source to the destination to achieve cooperative space diversity. In this case, combining method is used in destination D to combine signals from the source S through relays R_1, R_2,...,R_n, as shown in Fig. 2.6.

The most frequently used relay combining schemes are maximum ratio combining (MRC) [60], equal gain combining (EGC) [60] and relay selection combining [61]. Performance analysis of EGC and MRC receivers operating on α-μ fading channels has been conducted in [60]. An exact average BER for the distributed spatial diversity wireless systems with K relays over a Rayleigh fading channel is analysed in [62]. It has been shown that the conventional MRC is the optimum detection scheme and it could achieve the full diversity order of $K+1$. [62] has also considered the direct link between the source and

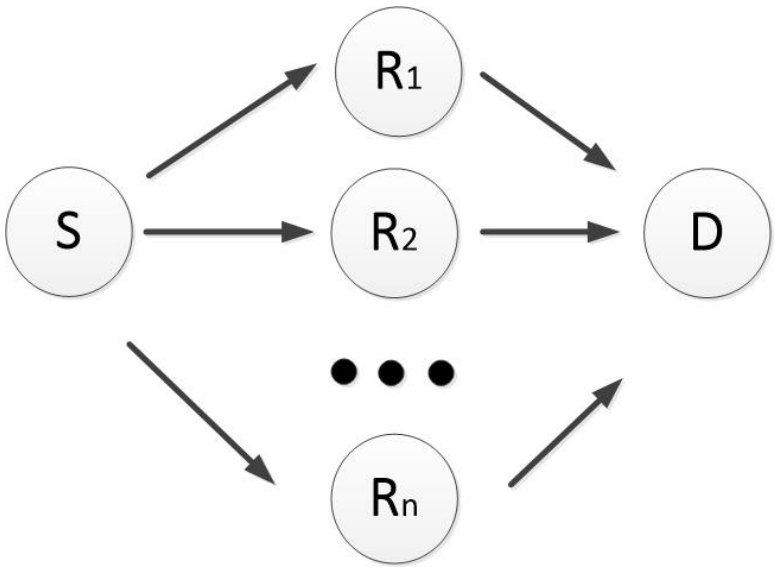

Figure 2.6: Two-hop cooperative relay combining.

destination.

Diversity order of MRC with L antennas using amplify and forward in Nakagami-m fading channels was studied in [63]. The bit error rate and outage probability for EGC over independent non-identical Nakagami-m fading using MGF were studied in [64]. Also, the error performance and diversity of multi-source multi-relay wireless networks have been analyzed in [65]. Binary Network-coded cooperative diversity protocols and MRC schemes have been used in [65].

The diversity performance of cooperative communication improves as the number of idle nodes increases [62]. However, the complexity of the network also become larger as the number of the idle nodes increases. In the applications such as WSNs, performance is less important than complexity since the main goal for WSNs is to achieve long battery life once the minimum performance requirement is met [66]. Moreover, the relays have different locations such that each transmitted signal through different paths causes different

attenuations, resulting in different performance. Therefore, relay selection is vital in reducing the network complexity in cooperative communication systems [66].

A comprehensive overview of relay selection is introduced in [61], where single-relay selection approaches and multiple-relay selection approaches are reviewed. Reference [67] proposed a novel scheme by selecting the best relay from a set of K available relays and then applies these relays for combination between the destination and the source. Reference [68] presented the optimal selection scheme for AF relaying among a set of multiple relays over Rayleigh fading channels under an aggregate power constraint. Also, reference [69] proposed the selection scheme for AF relaying by comparing the instantaneous SNR with a preset threshold from a subset of idle nodes.

Then, new partial relay selection schemes (i.e. selecting the idle user with the strongest second-hop instantaneous SNR or using the received signal amplitude for selection) for cooperative AF relaying over Nakagami-m fading channels was proposed in [70]. In [66], the partial selection schemes were compared with the optimal selection scheme. [66] has shown that the new partial selection scheme with the simpler structure has almost the same performance as the full selection scheme in some cases. Although the partial relay selection schemes cannot perform as well as the optimal selection schemes, they can reduce the complexity of hardware and software designed for the systems greatly [70].

Receiver selection diversity in the Rayleigh fading using BPSK and Alamouti transmission scheme in the presence of channel estimation error was studied in [71]. Space-time sum of squares combining selection and space-time sum of magnitudes selection were presented in [71], which has shown that these

two schemes have the simpler structures and with nearly the same performance as SNR selection. The exact end-to-end error probability using full channel state information selection combining for decode and forward system in a flat Rayleigh fading environment was studied in [72]. [72] has shown that the full channel state information selection combining can effectively utilize the instantaneous SNR of the source to relay channel at the destination. An orthogonal space-time block code with a minimum-selection generalized selection combining was presented in [73]. Dual-hop systems with multiple antennas have been studied in [74], where some realistic propagation conditions have been taken into consideration, such as keyhole channels, spatial correlation and co-channel interference. The analytical expressions of the symbol error rate and outage probability have been presented in [74]. Moreover, the performance of the optimum combining with the decode and forward relaying over Nakagami-m fading in the presence of co-channel interference at the relays and at the destination has been reported in [75].

2.4 Decision Fusion

Since there are a variety of impairments such as noise, attenuation, fading, interference and distortion contributing to errors in the wireless channel, which will affect the signal transmission, it is important to understand how to receive the information transmitted by the source to the maximum possible extent. Data fusion is a technique that can combine data from different mobile nodes, multiple sensors, secondary users and diversity branches to achieve the improved accuracies and performance [33].

The diagram of decision fusion composed of fusion centre and N nodes

is shown in Fig. 2.7. For instance, in cognitive radio, each secondary user

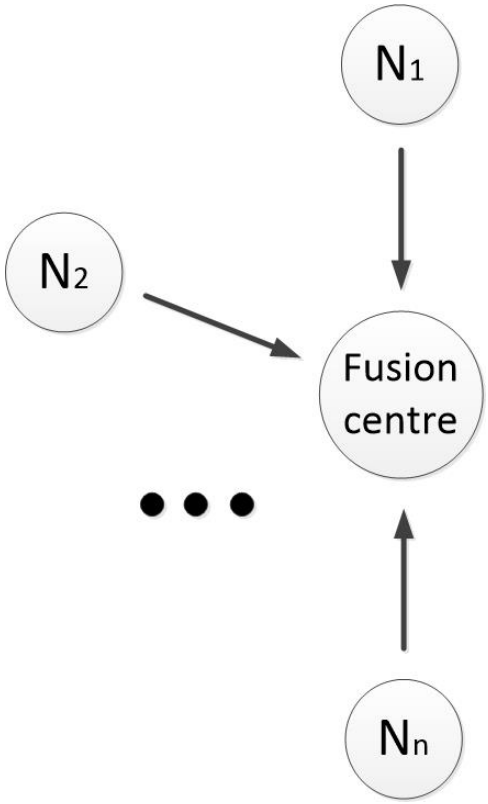

Figure 2.7: Decision fusion composed of fusion center and N nodes.

can be equipped with the detector, which can make a local sensing and then forward the information to a fusion centre to make a final decision about the existence of the primary user [76]. Also, in WSNs, considering there are a large number of tiny autonomous sensors which can detect a target or a situation at the same time. Each sensor determines a local decision according to the target and transmits the data to the fusion centre which will combine these detection results to produce the final decision [33, 77].

Hard-decision and soft-decision fusion rules are the most used decision methods [78]. In hard-decision combining strategy, each cooperative node performs a local observation and then transmits a binary number indicating

status of the situation to a fusion centre. On the other hand, in soft-decision combining strategy, each cooperative node sends its full observation of the situation to the fusion centre. Theoretically, soft-decision fusion method can achieve optimum performance at the expense of large communication bandwidth and cost [79]. It was shown in [78, 79] that the performance of hard decision fusion using multiple bits is not as good as soft decision fusion where the whole samples are sent to the fusion centre, but hard decision fusion requires less communication bandwidth with simpler structure [80]. Therefore, there is a tradeoff between complexity and performance in both hard-decision and soft-decision fusion rule.

Three algorithms for suboptimal signal detection applied to the additive mix of orthogonal sinusoidal signals have been reported in [81]. Also, the weighted partial decision detectors have been analyzed in [82] for arbitrary signal-to-noise ratios under Gaussian noise. In [83], the Neyman-Pearson optimum generalized multinomial detectors that minimize the error probability for deterministic signals were studied. In [84], diversity schemes with distributed decision combining for direct sequence CDMA have been studied in a shadowed Rician fading channel. The diversity schemes with maximal ratio, selection and distributed decisions have also been analyzed in [84].

2.5 System Performance Measures

In the digital communication system, many measurements can be used to predict or evaluate the system performance and then can provide insights and guidelines to the practical system design. The most important ones are introduced below.

2.5.1 Signal-to-Noise Ratio

SNR is a very important performance measure in the digital communication system. It serves as an effective indicator of the overall fidelity of the system and is defined as the power ratio of a signal (meaningful information) to the background noise (unwanted signal) as [34]

$$\gamma = \frac{P_s}{N_0} X^2 \tag{2.22}$$

where X is a random variable, γ denotes the instantaneous SNR, P_s is the signal power and N_0 is the noise power. The average SNR $\bar{\gamma}$ can be given as

$$\bar{\gamma} = \int_0^\infty \gamma f(\gamma) d\gamma \tag{2.23}$$

where $f(\gamma)$ is the PDF of instantaneous SNR γ. ML estimations of SNR using digitally modulated signals for sampled signal processing receivers and continuous time signal processing receivers are reported in [85].

2.5.2 Outage Probability

Outage probability is another measure that is widely used in wireless channels for the evaluation of the performance of wireless communication systems. It is defined as the probability that the instantaneous error probability exceeds a specified value or equivalently the probability that the output SNR falls below a certain threshold as [34]

$$P_{out}(\gamma_{th}) = Pr(\gamma < \gamma_{th}) = \int_0^{\gamma_{th}} p_\gamma(\gamma) d\gamma \tag{2.24}$$

where γ_{th} denotes the receiver sensitivity. Also, γ_{th} can be given as $\gamma_{th} = 2^{2R} - 1$, where R is the transmission rate. One can show that (2.24) is the CDF of SNR γ as well.

2.5.3 Bit Error Rate

The BER is defined as the error probability of a detection scheme and it is a nonlinear function of the instantaneous SNR [34]. BER is a very important measure which can be applied to examine the nature of the wireless communication system. It can be expressed for general form of coherent binary modulations as [86]

$$P_e = aQ(\sqrt{bx}) \tag{2.25}$$

where x is the instantaneous signal-to-noise ratio, $(a, b) = (1, 2)$ is for BPSK, $(a, b) = (1, 1)$ is for binary frequency-shift keying (BFSK), $(a, b) = (2\frac{M-1}{M}, \frac{6}{M^2-1})$ is for M-ary pulse amplitude modulation (M-PAM) and $Q(\cdot)$ denotes the Gaussian Q-function.

For Non-coherent modulations, the general form of BER can be represented as [86]

$$P_e = ae^{-bx} \tag{2.26}$$

where x is the instantaneous signal-to-noise ratio, $(a, b) = (0.5, 1)$ is for differential binary phase-shift keying (DBPSK), $(a, b) = (0.5, 0.5)$ is for non-coherent binary frequency-shift keying (NCBFSK). Other BER expressions are presented in [34]. To get the average BER, a further integral on the instantaneous BER expression with respect to the instantaneous SNR, with the help of the PDF expression of SNR is needed.

2.6 Related Methods

2.6.1 Moment Generating Function

The MGF of a RV X can be defined as [87]

$$M_X(s) = \int_{-\infty}^{\infty} f_X(x) e^{sx} dx \tag{2.27}$$

where $f_X(x)$ is the PDF of X. MGF provides an alternative method to analyze the performance, different from working directly with PDF or CDF of the RV. If X_1, X_2, ... X_n is a sequence of independent RVs and if

$$S_n = \sum_{i=1}^{n} a_i X_i \tag{2.28}$$

where a_i is the constant which represents the weight of X_i. One can see that the PDF of S_n is the convolution of PDF of each $a_i X_i,\ i = 1, 2...n$. With the help of MGF, one can get the PDF of S_n as

$$\begin{aligned} f_{S_n}(t) &= L^{-1}[M'_X(s)] \\ &= \frac{1}{2\pi j} \int_{\sigma - j\infty}^{\sigma + j\infty} M'_X(s) e^{-st} ds \end{aligned} \tag{2.29}$$

where σ is chosen to make the integral converge in the complex s plane. $M'_X(s) = M_{X_1}(a_1 s) M_{X_2}(a_2 s) ... M_{X_n}(a_n s)$ and $L^{-1}(\cdot)$ is the inverse transformation operator. MGF is a very convenient method and widely used in analyzing the performance of cooperative wireless systems [88]. For instance, the outage

probability can be derived using the MGF as [34]

$$P_{out}(\gamma_{th}) = \frac{1}{2\pi j}\int_{\sigma-j\infty}^{\sigma+j\infty}\frac{M_X(-s)}{s}e^{s\gamma_{th}}ds. \tag{2.30}$$

Also, the BER can be obtained using MGF as

$$P_e = \frac{1}{2\pi j}\int_{\sigma-j\infty}^{\sigma+j\infty}\frac{M_{D|\gamma}(-s)}{s}ds \tag{2.31}$$

where $M_{D|\gamma}(s)$ denotes the MGF of the decision variable $D|\gamma$, which can be found in [34, pp. 9] for different modulation schemes.

2.6.2 Characteristic Function

The characteristic function of a RV X is defined as [87]

$$\Phi_X(\omega) = \int_{-\infty}^{\infty} f_X(x)e^{jwx}dx \tag{2.32}$$

where $f_X(x)$ is the PDF of variable X. If jw is changed to s, the characteristic function becomes the moment generating function of X. In this case, the PDF is given by

$$f_X(x) = \frac{1}{2\pi}\int_{-\infty}^{\infty}\Phi_X(\omega)e^{-jwx}dw. \tag{2.33}$$

Unlike MGF, which may not exist, as the integrals may not converge absolutely in (2.27), the characteristic function always exists. Then in some cases, characteristic function is more suitable to use, such as the case in [33].

2.6.3 Moment-Matching Method

The moment-matching method is widely used to fit an analytically complicated distribution or a distribution of empirical data by using a more tractable one [60,89–93]. The most popular used approximation distributions in cooperative wireless communications are Gaussian distribution, GG distribution and Gamma distribution.

Gaussian Distribution

The PDF of a Gaussian distribution RV Y is given by

$$f_Y(y) = \frac{1}{\sqrt{2\pi\sigma^2}} e^{-\frac{(y-\mu)^2}{2\sigma^2}}. \tag{2.34}$$

One can use (2.34) to approximate another analytically complicated distribution, such as the applications in [92, 93]. One can see that there are two unknown parameters in (2.34), which can be determined by using

$$\mu = E(I) \tag{2.35}$$

and

$$\sigma^2 = E(I^2) - E^2(I) \tag{2.36}$$

where I is the RV of another complicated distribution.

Generalized Gamma Distribution

The PDF of a GG distribution RV Y is given by

$$f_Y(y) = \frac{p\, a^{-d} y^{d-1} e^{-\left(\frac{y}{a}\right)^p}}{\Gamma\left(\frac{d}{p}\right)},\ y > 0 \tag{2.37}$$

where $d > 0, p > 0$ are shape parameters and $a > 0$ is the scale parameter. GG distribution is also named as α - μ distribution [40], which can be seen as a generalization of the two parameter Gamma distribution. One can have the c-th order moment $E(Y^c)$ of (2.37) as [94]

$$E(Y^c) = \frac{a^c \Gamma\left(\frac{d+c}{p}\right)}{\Gamma\left(\frac{d}{p}\right)}. \tag{2.38}$$

By matching the first, second and third moment of GG distribution to the first, second and third moment of another analytically complicated distribution or the empirical data, three unknown parameters a, d and p in (2.37) can be determined. Thus the following equations (2.39) have to be solved numerically to obtain a, d and p.

$$\begin{cases} \frac{a\Gamma\left(\frac{d+1}{p}\right)}{\Gamma\left(\frac{d}{p}\right)} = E(I) \\ \frac{a^2\Gamma\left(\frac{d+2}{p}\right)}{\Gamma\left(\frac{d}{p}\right)} = E(I^2) \\ \frac{a^3\Gamma\left(\frac{d+3}{p}\right)}{\Gamma\left(\frac{d}{p}\right)} = E(I^3) \end{cases} \tag{2.39}$$

where I is the RV of the complicated distribution to be approximated, such as the application in [89, 95, 96].

Gamma Distribution

By setting $p = 1$ in (2.37), the PDF of a Gamma distribution RV Y can be given as

$$f_Y(y) = \frac{y^{k-1}e^{-y/\theta}}{\theta^k \Gamma(k)},\ y > 0. \tag{2.40}$$

One can see that there are two unknown parameters k and θ in (2.40), which can be determined by [60, 90, 91]

$$k = \frac{E^2(I)}{V(I)} \tag{2.41}$$

and

$$\theta = \frac{V(I)}{E(I)} \tag{2.42}$$

where I can be seen as the RV of another complicated distribution.

Chapter 3

Performance Analysis and Optimal Energy Allocation for Amplify-and-Forward Relaying Using Pilot-Aided Maximum Likelihood Estimation

3.1 Introduction

Dual-hop transmission has been commonly used in cooperative wireless communications [9, 30, 45–47, 97–100]. It can be mainly categorized into AF and DF relaying as it is introduced in the previous chapter. Depending on the nature and complexity of the AF relays, the amplification gain of the AF relay can be classified as variable gain or fixed gain [46], [47]. A variable gain AF relay requires the instantaneous CSI of the first hop while a fixed gain AF relay

does not. Although a fixed gain relay is not expected to perform as well as a variable gain relay, it has lower power consumption due to the saved power on the acquisition of the instantaneous CSI at the relay. In practice, CSI is often acquired by estimation which can be performed by using either unknown or known symbols [1]. A pilot-symbol-aided system was proposed to obtain CSI using known symbols [101]. For example, linear minimum mean squared error (LMMSE) channel estimation with pilot symbols for AF relaying was studied in [98, 102, 103]. In a variable gain AF, the instantaneous CSI can be estimated both at the relay in order to determine the variable gain and at the destination for coherent demodulation, separately. This is termed as DCE, as was studied in [30, 98]. Unlike a variable gain AF, in a fixed gain AF, since no CSI is required at the relay, only a CCE consisting of both the source-to-relay link and the relay-to-destination link can be used to estimate CSI at the destination [30, 98–100, 104].

In all these aforementioned works, the estimation accuracy or the performance of the channel estimator were considered assuming unlimited power, while in practice the total power is often limited such that an optimal power allocation for pilots may be required. The authors in [105] used outage probability as a measure to obtain the optimal power allocation and they considered the allocation between training and data symbols under the total transmitting power constraint at the source but did not consider the power allocation at the relay. However, the relay is usually complexity- and power-limited. Therefore, optimal power allocation at the relay is equally important and cannot be ignored. The authors in [106] considered the power allocation between training and data symbols both at the relay and at the source using a signal-to-noise ratio measure. However, it was reported in [107] that power allocation scheme

using BER measure often achieves considerable BER performance gain over that using SNR measure, when the relay is closer to the source than to the destination.

Moreover, [106] considered two power constraints: a total transmit power constraint between source and relay as well as individual power constraints at source and relay, respectively. The former can be applied in the case when the total power saving is more important, such as fixed nodes which can be charged, while the latter can be used in the case when the individual battery power or the individual lifetime is more important, such as moving nodes. The authors in [108] also considered similar power allocation between training and data symbols as in [106] but used an outage probability measure instead. Since a further integral on SNR is needed, derivations of BER and outage probability are often more difficult than that of SNR in most AF systems. Therefore, one can choose to obtain the optimal power allocation according to the application and the complexity of the AF system using the specific measure, such as SNR, outage probability or BER.

Furthermore, the authors in [105], [106] and [108] all considered the case when the signal experiences fast fading such that LMMSE is necessary and must be used in channel estimation. In this case, the system model is so complex such that derivations of SNR, outage probability or BER using channel estimates are very difficult, if not impossible. As a result, power allocations based on SNR, outage probability or BER often do not have closed-form in this case.

However, in many previous works [109], [110] and in high data-rate applications [111], the channel coherence time is much larger than the bit interval such that the signal only experiences slow or even block fading. In

this case, since the channel gain is not time-varying, maximum likelihood estimation with a much simplified structure is more suitable to obtain the channel estimates [85]. To the best of the authors' knowledge, none of the works in the literature have considered the optimal energy allocation for AF relaying in the slowly fading channel using ML estimation.

In this chapter, the performance for an AF relaying system in a slowly fading Rayleigh channel using pilot-symbol-aided ML channel estimation is analyzed. Also, the optimal energy allocation of these channels are derived. The contributions of this chapter can be summarized as follows:

• The pilot-symbol-aided ML estimation methods for both DCE and CCE are first introduced. For DCE, the case when the fading gain is estimated at the relay as well as the case when the fading gain is estimated at both the relay and destination are considered, separately. For CCE, the case when the fading gain is estimated at the destination is considered. Based on these, the outage probabilities of AF relaying for DCE and CCE are derived for variable and fixed gains, respectively.

• Then the general form of the BER expressions for high order modulations with DCE and CCE is derived. Two kinds of closed-form approximations for DCE with different complexity and accuracy are provided while the closed-form approximations for CCE with two kinds of amplification factors are provided.

• More importantly, using these BER expressions of both DCE and CCE, the optimal values of pilot energy under the total transmitting energy constraints at the source and at the relay are obtained, separately. This is the case when the source, relay or destination are battery-limited moving nodes. Moreover, the optimal energy allocation between the pilot energy at the source,

the pilot energy at the relay, the data energy at the source and the data energy at the relay are obtained when their total transmitting energy are fixed. This is the case when the source, relay and destination are fixed nodes that can be charged.

• Finally, numerical results are presented to illustrate and verify our theoretical analysis. They show that the derived simple closed-form expressions match well with the simulation. Also, they show that the optimal energy values of the data and pilot from our derived methods are nearly the same as what are observed from the BER simulation curves. More importantly, they show that our optimal energy allocation methods outperform the conventional system without optimal energy allocation, which could be as large as several dB's in some cases.

The remainder of this chapter is organized as follows. Section 3.2 introduces the system model while Section 3.3 shows the pilot-aided ML estimation methods for DCE and CCE. Section 3.4 derives the BER and outage probability of AF using a variable gain in DCE, whereas Section 3.5 derives the BER and outage probability of AF using a fixed gain in CCE, based on which, the approximation expressions and the optimal energy allocations are obtained. Numerical results are presented in Section 3.6, followed by concluding remarks in Section 3.7.

Meijer's G-Function

Meijer's G-function is a very general function which can be reduced to many special functions in many common cases. The Meijer G-function is defined

by [112]

$$G_{p,q}^{m,n}\left(x\middle|\begin{matrix}a_1,...,a_p\\ b_1,...,b_q\end{matrix}\right)=\frac{1}{2\pi i}\int_L \frac{\prod_{j=1}^{m}\Gamma(b_j-s)\prod_{j=1}^{n}\Gamma(1-a_j+s)}{\prod_{j=m+1}^{q}\Gamma(1-b_j+s)\prod_{j=n+1}^{p}\Gamma(a_j-s)}x^s ds \tag{3.1}$$

where $\Gamma(\cdot)$ is the gamma function. This integral may be considered as an inverse Mellin transformation and can be reduced to many special functions such as [113]

$$G_{0,1}^{1,0}\left(-x\middle|\begin{matrix}-\\ 0\end{matrix}\right)=e^x, \tag{3.2}$$

$$G_{2,2}^{1,2}\left(x\middle|\begin{matrix}1,1\\ 1,0\end{matrix}\right)=ln(1+x) \tag{3.3}$$

and etc. The Meijer's G-function will be extensively used in this thesis.

3.2 System Model

In this chapter, an AF cooperative system with one source S, one destination D and one relay R is considered. Also, assume there is no direct link between the source and the destination, as shown in Fig. 3.1. In the first time slot, the

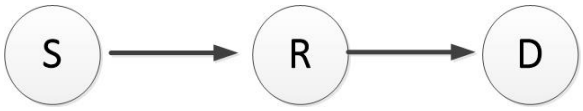

Figure 3.1: AF cooperative system with one source, one destination and one relay.

source transmits the signal to the relay such that the received signal at the

relay can be expressed as

$$u(t) = \sqrt{E_d}\, h_1\, s(t) + n_1(t) \tag{3.4}$$

where h_1 is the complex fading gain in the channel between the source and the relay, E_d is the transmitted signal power per data symbol, $s(t)$ is the transmitted data symbol with the unit power such that $E(|s(t)|^2) = 1$, and n_1 is the complex AWGN in the channel between the source and the relay with noise power N_1.

In the second time slot, the received signal at the relay is amplified and forwarded such that the received signal at the destination can be given by

$$y(t) = G\, h_2\, u(t) + n_2(t) \tag{3.5}$$

where h_2 is the complex fading gain in the channel between the relay and the destination, n_2 is the complex AWGN in the channel between the relay and the destination with noise power N_2, and G is the amplification factor in the relay side.

Assume that all the links experience Rayleigh fading with $E(|h_1|^2) = \Omega_1$ and $E(|h_2|^2) = \Omega_2$. Assume that r is the path-loss exponent and that d_1 and d_2 are the distances between the source and the relay, the relay and the destination, respectively. Therefore, one has $\Omega_1 = Ld_1^{-r}$ and $\Omega_2 = Ld_2^{-r}$, where L is a constant that takes antenna gains and other power factors into account. Also assume that all nodes have similar transmitter/receiver settings such that L is the same for all hops. Define the instantaneous SNR between the source and the relay, and between the relay and the destination as $\gamma_1 = E_d\, |h_1|^2/N_1$

and $\gamma_2 = E_s\ |h_2|^2/N_2$, respectively, and the average SNR as $\bar{\gamma}_1 = E_d\ \Omega_1/N_1$ and $\bar{\gamma}_2 = E_s\ \Omega_2/N_2$, respectively, where E_s is the transmitted power per data symbol at the relay that is included in G. Therefore, the PDFs of γ_1 and γ_2 can be given by $f(\gamma_1) = \frac{1}{\bar{\gamma}_1} e^{-\frac{\gamma_1}{\bar{\gamma}_1}}$ and $f(\gamma_2) = \frac{1}{\bar{\gamma}_2} e^{-\frac{\gamma_2}{\bar{\gamma}_2}}$, respectively [1].

Consider the case when W_1 pilot symbols each with transmitted power E_{w_1} are inserted before D data symbols at the source, giving a frame of $W_1 + D$ symbols. At the relay, in DCE, W_2 pilot symbols each with the transmitted power E_{w_2} are inserted into the frame received from the source, while in CCE, the same pilot symbols W_1 from the source are amplified and forwarded to the destination with transmitted power E_{w_2} such that no additional pilots are inserted at the relay. Note that this chapter still uses the notation W_2 to denote the number of pilot symbols at the relay for CCE but $W_2 = W_1$ in this case, as shown in Fig. 3.2.

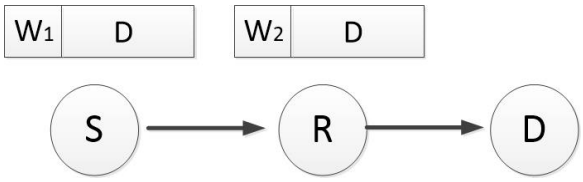

Figure 3.2: Symbol frame for CCE and DCE.

Assume that n_{w_1} and n_{w_2} are the complex AWGN in the channel between source and relay, and the channel between relay and destination with noise power N_{w_1}, N_{w_2}, during the transmission of W_1, W_2 pilot symbols, respectively. Note that N_{w_1} and N_{w_2} can be the same as N_1 and N_2, respectively, but can also be different from N_1 and N_2, if one considers the different noise that occurs in the pilot or data transmission periods separately. Also, assume block fading channels such that the fading gains remain the same during the whole frame. Let P_T, P_1, P_2, P_d, P_s, P_{w_1} and P_{w_2} be the total energy, the

total energy at the source, the total energy at the relay, the total data energy at the source, the total data energy at the relay, the total pilot energy at the source and the total pilot energy at the relay, respectively. Therefore, one has $P_T = P_1 + P_2$, $P_1 = P_d + P_{w_1}$, $P_2 = P_s + P_{w_2}$, $P_d = D\ E_d$, $P_s = D\ E_s$, $P_{w_1} = W_1\ E_{w_1}$, $P_{w_2} = W_2\ E_{w_2}$ in both DCE and CCE. Let $H_1 = D + W_1$, $H_2 = D + W_2$ and $H = H_1 + H_2$. Also, let P_1^*, P_2^*, P_d^*, P_s^*, $P_{w_1}^*$ and $P_{w_2}^*$ be the optimal total energy at the source, the optimal total energy at the relay, the optimal data energy at the source, the optimal data energy at the relay, the optimal pilot energy at the source and the optimal pilot energy at the relay, respectively.

Note that this chapter considers the optimal energy for the whole frame in terms of P_d^*, P_s^*, $P_{w_1}^*$ and $P_{w_2}^*$, instead of the optimal power for one symbol as in [108, 114]. In this case, one can adjust either the number of symbols or the power of one symbol to achieve this under the total energy constraints for specific application, which is more general and also more flexible than the optimal power for one symbol. Note also that this chapter considers the case when the signal experiences block fading channel such that the channel gain keeps the same in one frame. Therefore, pilot symbols can be either interleaved with the data symbols or inserted as a preamble before the data symbols, as they do not need to sample the fading process. In fast fading channels, since the fading process is time-varying, these two schemes may be different and the interleaving rate will depend on the fading rate. In the next section, the amplification factor in relay and ML estimation for both DCE and CCE will be introduced.

3.3 Pilot-Aided Maximum Likelihood Estimation

3.3.1 Disintegrated Channel Estimation

In DCE, the amplification factor G is defined as [9]

$$\hat{G}_{var}^2 = \frac{E_s}{E_d \left|\hat{h}_1\right|^2 + N_1}. \tag{3.6}$$

In this case, the relay and the destination estimate h_1 and h_2, separately. Let $h_1 = x_1 + iy_1$, where x_1, y_1 are independent and identically distributed RVs with zero mean and variance $\Omega_1/2$. Assume that $\hat{h}_1 = \hat{x}_1 + i\hat{y}_1$, where $\hat{h}_1$, $\hat{x}_1$ and $\hat{y}_1$ are estimates of h_1, x_1 and y_1 respectively. Using the pilot-symbol-aided ML estimation [85], one can have $\hat{x}_1 \sim N(x_1, \frac{N_{w_1}}{2\,E_{w_1}W_1})$ and $\hat{y}_1 \sim N(y_1, \frac{N_{w_1}}{2\,E_{w_1}W_1})$, where $N(x, y)$ denotes the normal distribution with mean x and variance y. Therefore, one can get the PDF of $|\hat{h}_1|$ as

$$f_{|\hat{h}_1|}(x) = \frac{2xe^{-\frac{x^2 E_{w_1} W_1}{N_{w_1} + E_{w_1}\Omega_1 W_1}} E_{w_1} W_1}{N_{w_1} + E_{w_1}\Omega_1 W_1}, \quad x \geq 0. \tag{3.7}$$

Similarly, one can get the PDF of $|\hat{h}_2|$ as

$$f_{|\hat{h}_2|}(x) = \frac{2xe^{-\frac{x^2 E_{w_2} W_2}{N_{w_2} + E_{w_2}\Omega_2 W_2}} E_{w_2} W_2}{N_{w_2} + E_{w_2}\Omega_2 W_2}, \quad x \geq 0. \tag{3.8}$$

Define the estimated instantaneous SNR in the channel between the source and the relay, and that between the relay and the destination as $\hat{\gamma}_1 = E_d\,|\hat{h}_1|^2/N_1$ and $\hat{\gamma}_2 = E_s\,|\hat{h}_2|^2/N_2$, or $\hat{\gamma}_1 = \frac{P_d}{D}\,|\hat{h}_1|^2/N_1$ and $\hat{\gamma}_2 = \frac{P_s}{D}\,|\hat{h}_2|^2/N_2$, respectively.

Therefore, one can calculate the estimated average SNR as $\bar{\hat{\gamma}}_1 = \bar{\gamma}_1 + \gamma_{\varepsilon_1}$ and $\bar{\hat{\gamma}}_2 = \bar{\gamma}_2 + \gamma_{\varepsilon_2}$, respectively, where γ_{ε_1} and γ_{ε_2} are defined as the statistics of the channel estimation errors between source and relay, and between relay and destination, respectively, with the values of $\gamma_{\varepsilon_1} = \frac{E_d N_{w_1}}{N_1 E_{w_1} W_1}$ and $\gamma_{\varepsilon_2} = \frac{E_s N_{w_2}}{N_2 E_{w_2} W_2}$. Thus, the PDF of $\hat{\gamma}_1$ and $\hat{\gamma}_2$ can be given by $f(\hat{\gamma}_1) = \frac{1}{\hat{\gamma}_1} e^{-\frac{\hat{\gamma}_1}{\hat{\gamma}_1}}$ and $f(\hat{\gamma}_2) = \frac{1}{\hat{\gamma}_2} e^{-\frac{\hat{\gamma}_2}{\hat{\gamma}_2}}$, respectively.

3.3.2 Cascaded Channel Estimation

In CCE, the amplification factor G for the data symbols at the relay can be written as [46]

$$\begin{aligned} G^2_{d_{fix_1}} &= E\left[\frac{E_s}{E_d h_1^2 + N_1}\right] \\ &= \frac{E_s e^{\frac{N_1}{E_d \Omega_1}} \Gamma\left(0, \frac{N_1}{E_d \Omega_1}\right)}{E_d \Omega_1} \end{aligned} \tag{3.9}$$

or [115]

$$\begin{aligned} G^2_{d_{fix_2}} &= \frac{E_s}{E\left[E_d h_1^2 + N_1\right]} \\ &= \frac{E_s}{E_d \Omega_1 + N_1}. \end{aligned} \tag{3.10}$$

Similarly, the amplification factor for the pilot symbols at the relay is [46]

$$\begin{aligned} G^2_{w_{fix_1}} &= E\left[\frac{E_{w_2}}{E_{w_1} h_1^2 + N_{w_1}}\right] \\ &= \frac{E_{w_2} e^{\frac{N_{w_1}}{E_{w_1} \Omega_1}} \Gamma\left(0, \frac{N_{w_1}}{E_{w_1} \Omega_1}\right)}{E_{w_1} \Omega_1} \end{aligned} \tag{3.11}$$

or [115]

$$\begin{aligned} G^2_{w_{fix_2}} &= \frac{E_{w_2}}{E\left[E_{w_1} h_1^2 + N_{w_1}\right]} \\ &= \frac{E_{w_2}}{E_{w_1} \Omega_1 + N_{w_1}}. \end{aligned} \tag{3.12}$$

Instead of estimating h_1 and h_2 separately at the relay and at the destination as in DCE, this section estimates the product of h_1 and h_2 at the destination in CCE. In this case, the relay uses a fixed gain which remains constant and no estimator is needed at the relay to simplify the structure of the relay. On the other hand, in DCE, extra power is consumed to estimate the instantaneous CSI for $\hat{G}_{var}$, although DCE has a slightly better performance than CCE in some regions [47]. Define the instantaneous equivalent channel gain between the source and the destination as H. Then the received pilot symbol at destination can be written as

$$y = \sqrt{E_{w_1}}\ H\ G_{w_{fix_1}}\ s + n_w \tag{3.13}$$

where $H = h_1\ h_2$ and $n_w = G_{w_{fix_1}}\ h_2\ n_{w_1} + n_{w_2}$. The PDF of $|H|$ is given as [116]

$$f_{|H|}(x) = \frac{4xK_0\left(2\sqrt{\frac{x^2}{\Omega_1\Omega_2}}\right)}{\Omega_1\Omega_2}, \quad x > 0. \tag{3.14}$$

Define the estimated instantaneous equivalent channel gain between the source and the destination as $\hat{H}$. Also, n_w in (3.13) is non-Gaussian but can be approximated as Gaussian [106], which helps to derive (3.15). Thus, using the pilot-symbol-aided ML estimation [85] and following the same process as in DCE in Section 3.3.1, one can get the PDF of $|\hat{H}|$ as

$$f_{|\hat{H}|}(x) = \frac{4xK_0\left(2\sqrt{\frac{x^2}{\Omega}}\right)}{\Omega}, \quad x > 0 \tag{3.15}$$

where $\Omega = \Omega_1\Omega_2 + \Omega_\varepsilon$, $\Omega_\varepsilon = \frac{N_{w_2} + G^2_{w_{fix_1}} N_{w_1}\Omega_2}{E_{w_1} G^2_{w_{fix_1}} W_1}$ can be considered as the variance of the channel estimation error. Then, the PDF of $|\hat{H}|$ using $G_{w_{fix_2}}$ can also

be obtained.

3.4 BER and Optimal Energy Allocation in Disintegrated Channel Estimation

This section first derive the outage probability and BER of AF using a variable gain in DCE and then study the optimal energy allocation under the total transmitting energy constraint. In the first subsection, the case when the relay estimates h_1 and the destination has perfect knowledge of h_2 is considered. This is the case for mobile relays with limited complexity and power but fixed destination with enough power for accurate h_2. It serves as a benchmark for the case when both are estimated. In the second subsection, the case when both the relay estimates h_1 and the destination estimates h_2 is considered, separately. From this case, one can see that with the power at the destination increasing, the estimation accuracy also improves, which will be verified in Section 3.6.

3.4.1 Estimation of CSI at the Relay

Outage Probability and BER

The received signal at the destination can be written by omitting the time indexes as

$$y = \sqrt{E_d}\, h_1\, h_2\, \hat{G}_{var}\, s + \hat{G}_{var}\, h_2\, n_1 + n_2. \tag{3.16}$$

Since $\hat{h}_1$ is the estimate of h_1 with $\hat{h}_1 = h_1 + \varepsilon_1$, where ε_1 is the channel estimation error, one has

$$y = \sqrt{E_d}\,(\hat{h}_1 - \varepsilon_1)\; h_2\; \hat{G}_{var}\; s + \hat{G}_{var}\; h_2\; n_1 + n_2. \tag{3.17}$$

After simplification, one has

$$y = \sqrt{E_d}\;\hat{h}_1\; h_2\; \hat{G}_{var}\; s - \sqrt{E_d}\;\varepsilon_1\; h_2\; \hat{G}_{var}\; s + \hat{G}_{var}\; h_2\; n_1 + n_2. \tag{3.18}$$

The end-to-end SNR can be derived from (3.18) as

$$\gamma_{end_1} = \frac{\gamma_2 \hat{\gamma}_1}{\gamma_2 + \hat{\gamma}_1 + 1 + \gamma_{\varepsilon_1}\;\gamma_2} \tag{3.19}$$

where $\gamma_{\varepsilon_1} = \frac{E_d N_{w_1}}{N_1 E_{w_1} W_1}$, $E(|\varepsilon_1|^2) = \frac{N_{w_1}}{E_{w_1} W_1}$ and $E(|s|^2) = 1$ are assumed, and other symbols are defined as before. The value of ε_1 is considered as random disturbance, similar to noise. That is why ε_1 does not appear in (3.19) and only its statistics do. It is derived in Appendix A.1 that the outage probability using the end-to-end SNR in (3.19) is

$$F_{\gamma_{end_1}}(\gamma_{th}) = 1 - \frac{2e^{-\frac{\gamma_{th}(\gamma_{\varepsilon_1}\;\bar{\gamma}_2 + \bar{\hat{\gamma}}_1 + \bar{\gamma}_2)}{\bar{\hat{\gamma}}_1 \bar{\gamma}_2}} K_1\left(\frac{2}{\sqrt{\frac{\bar{\gamma}_2 \bar{\hat{\gamma}}_1}{\gamma_{th}(\gamma_{\varepsilon_1}\;\gamma_{th} + \gamma_{th} + 1)}}}\right)}{\sqrt{\frac{\bar{\gamma}_2\;\bar{\hat{\gamma}}_1}{\gamma_{th}\left(\gamma_{\varepsilon_1}\;\gamma_{th} + \gamma_{th} + 1\right)}}}, \tag{3.20}$$

where $K_v(\cdot)$ is the vth order modified Bessel function of the second kind [36]. Using (3.20), the BER can be calculated as [86]

$$P_e = \frac{a}{2}\sqrt{\frac{b}{2\pi}} \int_0^\infty \frac{e^{-\frac{b}{2}x}}{\sqrt{x}} F_{\gamma_{end_1}}(x) dx \tag{3.21}$$

where a and b are modulation-specific constants including $(a,b) = (1,1)$ for BFSK, $(a,b) = (1,2)$ for BPSK and $(a,b) = (2\frac{M-1}{M}, \frac{6}{M^2-1})$ for M-PAM. Also, the BER expression in (3.21) is a good approximation to the BER of some higher order modulations, such as $(a,b) = (2, 2\ sin^2(\pi/M))$ for M-PSK.

The BER in (3.21) can be approximated in two ways. First, one can approximate the BER as

$$P_e \approx \frac{1}{2} a \left(1 - \frac{\sqrt{b}}{\sqrt{b + 2\beta_2}}\right) \tag{3.22}$$

where $\beta_2 = \frac{\bar{\hat{\gamma}}_1 + \bar{\gamma}_2 \gamma_{\varepsilon_1} + \bar{\gamma}_2}{\bar{\hat{\gamma}}_1 \bar{\gamma}_2}$. This approximation can be used in the case when $\bar{\hat{\gamma}}_1, \bar{\gamma}_2 \to \infty$.

Proof: See Appendix A.2.

Second, one can get the approximate BER as

$$P_e \approx \frac{1}{2} a \sqrt{b} \times \left(\frac{\sqrt{\beta_1} \left((b + 2(\beta_1 + \beta_2)) \kappa_1 \left(-\frac{b - 2\beta_1 + 2\beta_2}{4\beta_1} \right) - 2(b + 2\beta_2) \kappa_2 \left(-\frac{b - 2\beta_1 + 2\beta_2}{4\beta_1} \right) \right)}{(b - 2\beta_1 + 2\beta_2)(b + 2(\beta_1 + \beta_2))} + \frac{1}{\sqrt{b}} \right) \tag{3.23}$$

where $\beta_1 = \frac{2\sqrt{\gamma_{\varepsilon_1} + 1}}{\sqrt{\bar{\hat{\gamma}}_1 \bar{\gamma}_2}}$ and $\kappa_\nu(\cdot)$ is the complete elliptic integral of the νth kind defined in [36] with $\kappa_1(k) = \int_0^{\pi/2} \frac{dx}{\sqrt{1 - k \sin^2(x)}}$, $\kappa_2(k) = \int_0^{\pi/2} \sqrt{1 - k \sin^2(x)}\, dx$. This approximation can be used in the case when $\gamma_{\varepsilon_1}\ \gamma_{th} + \gamma_{th} \gg 1$.

Proof: See Appendix A.3.

Optimal Energy Allocation

Since this subsection considers the case when the relay estimates h_1 and the destination has perfect knowledge of h_2, it only derives the optimal energy allocation between P_d and P_{w_1} under the fixed total energy P_1 at the source.

Since (3.22) is simpler than both (3.21) and (3.23), (3.22) is used to derive the optimal allocation. One can observe that minimizing (3.22) is equivalent to minimizing β_2. Inserting $E_d = \frac{P_d}{D}$, $E_{w_1} = \frac{P_{w_1}}{W_1}$ and $P_d = P_1 - P_{w_1}$ into β_2, one can get

$$\beta_2 = \frac{DP_{w_1}N_1}{(P_1 - P_{w_1})(P_{w_1}\Omega_1 + N_{w_1})} + \frac{N_2}{E_s\Omega_2} + \frac{N_{w_1}}{P_{w_1}\Omega_1 + N_{w_1}}. \tag{3.24}$$

Differentiating (3.24) with respect to P_{w_1}, equating it to zero and solving the equation, the optimal value of P_{w_1} can be found as

$$P^*_{w_1} = \frac{\mu_1 - P_1 N_{w_1}\Omega_1}{DN_1\Omega_1 - N_{w_1}\Omega_1} \tag{3.25}$$

where $\mu_1 = (-D^2P_1N_1^2N_{w_1}\Omega_1 + DP_1^2N_1N_{w_1}\Omega_1^2 + DP_1N_1N_{w_1}^2\Omega_1)^{1/2}$. Then, by using $P^*_{w_1}$ of (3.25), the optimal value of P_d can be found as $P^*_d = P_1 - P^*_{w_1}$. With the help of MATHEMATICA software, one can see from (3.25) that the optimal pilot energy at the source increases when Ω_1 increases, or when the distance between the source and the relay decreases, as $\Omega_1 = Ld_1^{-r}$.

3.4.2 Estimation of CSI at Both the Relay and Destination

Outage Probability and BER

In this case, the received signal at destination can be written as

$$y = \sqrt{E_d}\, h_1\, h_2\, \hat{G}_{var}\, s + \hat{G}_{var}\, h_2\, n_1 + n_2. \tag{3.26}$$

Let $\hat{h}_1$, $\hat{h}_2$ be the estimates of h_1, h_2, respectively, with $\hat{h}_1 = \varepsilon_1 + h_1$ and $\hat{h}_2 = \varepsilon_2 + h_2$ where ε_1 and ε_2 are the channel estimation errors. Thus,

$$y = \sqrt{E_d}\,(\hat{h}_1 - \varepsilon_1)\,(\hat{h}_2 - \varepsilon_2)\,\hat{G}_{var}\,s + \hat{G}_{var}\,(\hat{h}_2 - \varepsilon_2)\,n_1 + n_2. \tag{3.27}$$

The end-to-end SNR in this case can be written as

$$\gamma_{end_2} = \frac{\hat{\gamma}_2\hat{\gamma}_1}{\hat{\gamma}_2\gamma_{\varepsilon_1} + \hat{\gamma}_1\gamma_{\varepsilon_2} + \gamma_{\varepsilon_1}\,\gamma_{\varepsilon_2} + \hat{\gamma}_2 + \hat{\gamma}_1 + 1 + \gamma_{\varepsilon_2}} \tag{3.28}$$

where $E(|s|^2) = 1$, $E(|\varepsilon_1|^2) = \frac{N_{w_1}}{E_{w_1}W_1}$, $E(|\varepsilon_2|^2) = \frac{N_{w_2}}{E_{w_2}W_2}$ and other symbols are defined as before. It is derived in Appendix A.4 that the outage probability of the end-to-end SNR in (3.28) is

$$F_{\gamma_{end_2}}(\gamma_{th}) = 1 - \frac{2e^{-\frac{\gamma_{th}(\gamma_{\varepsilon_1}\bar{\gamma}_2 + \gamma_{\varepsilon_2}\bar{\gamma}_1 + \bar{\gamma}_1 + \bar{\gamma}_2)}{\bar{\gamma}_1\bar{\gamma}_2}} K_1\left(\frac{2}{\sqrt{\frac{\bar{\gamma}_1\bar{\gamma}_2}{\gamma_{th}(\gamma_{\varepsilon_1}\gamma_{th} + \gamma_{th} + (\gamma_{\varepsilon_1}+1)\gamma_{\varepsilon_2}(\gamma_{th}+1)+1)}}}\right)}{\sqrt{\frac{\bar{\gamma}_1\bar{\gamma}_2}{\gamma_{th}((\gamma_{\varepsilon_1}+1)\gamma_{\varepsilon_2}(\gamma_{th}+1) + \gamma_{\varepsilon_1}\gamma_{th} + \gamma_{th} + 1)}}}. \tag{3.29}$$

The BER is given by

$$P_e = \frac{a}{2}\sqrt{\frac{b}{2\pi}}\int_0^\infty \frac{e^{-\frac{b}{2}x}}{\sqrt{x}} F_{\gamma_{end_2}}(x)dx. \tag{3.30}$$

Using the same approximations as before, the BER in (3.30) can be approximated as

$$P_e \approx \frac{1}{2}a\left(1 - \frac{\sqrt{b}}{\sqrt{b + 2\beta_4}}\right) \tag{3.31}$$

or

$$P_e \approx \frac{1}{2}a\sqrt{b}\times \left(\frac{\sqrt{\beta_3}\left((b+2(\beta_3+\beta_4))\kappa_1\left(-\frac{b-2\beta_3+2\beta_4}{4\beta_3}\right)-2(b+2\beta_4)\kappa_2\left(-\frac{b-2\beta_3+2\beta_4}{4\beta_3}\right)\right)}{(b-2\beta_3+2\beta_4)(b+2(\beta_3+\beta_4))}+\frac{1}{\sqrt{b}}\right) \tag{3.32}$$

where $\beta_3 = \frac{2\sqrt{(\gamma_{\varepsilon_1}+1)(\gamma_{\varepsilon_2}+1)}}{\sqrt{\bar{\gamma}_1\bar{\gamma}_2}}$ and $\beta_4 = \frac{\bar{\gamma}_1\gamma_{\varepsilon_2}+\bar{\gamma}_1+\bar{\gamma}_2\gamma_{\varepsilon_1}+\bar{\gamma}_2}{\bar{\gamma}_1\bar{\gamma}_2}$.

Optimal Energy Allocation

The first part of this subsection considers the optimal allocation between P_d and P_{w_1} under fixed P_1, and the optimal allocation between P_s and P_{w_2} under fixed P_2, separately. The second part considers the optimal allocation between P_d, P_s, P_{w_1}, P_{w_2} under the fixed total energy P_T. Similarly, β_4 in (3.31) is used to derive the optimal energy allocation below.

Firstly, by inserting $E_d = \frac{P_d}{D}$, $E_s = \frac{P_s}{D}$, $E_{w_1} = \frac{P_{w_1}}{W_1}$, $E_{w_2} = \frac{P_{w_2}}{W_2}$, $P_d = P_1 - P_{w_1}$ and $P_s = P_2 - P_{w_2}$ into β_4, one can get

$$\beta_4 = \frac{DP_{w_1}N_1 + N_{w_1}(P_1 - P_{w_1})}{N_{w_1}(P_1 - P_{w_1}) + P_{w_1}\Omega_1(P_1 - P_{w_1})} + \frac{DP_{w_2}N_2 + N_{w_2}(P_2 - P_{w_2})}{N_{w_2}(P_2 - P_{w_2}) + P_{w_2}\Omega_2(P_2 - P_{w_2})}. \tag{3.33}$$

Differentiating (3.33) with respect to P_{w_1}, P_{w_2} and equating to zero, the optimal values of P_{w_1} and P_{w_2} can be found as

$$P^*_{w_1} = \frac{\mu_1 - P_1 N_{w_1}\Omega_1}{DN_1\Omega_1 - N_{w_1}\Omega_1} \tag{3.34}$$

and

$$P^*_{w_2} = \frac{\mu_2 - P_2 N_{w_2}\Omega_2}{DN_2\Omega_2 - N_{w_2}\Omega_2} \tag{3.35}$$

where $\mu_2 = (-D^2P_2N_2^2N_{w_2}\Omega_2 + DP_2^2N_2N_{w_2}\Omega_2^2 + DP_2N_2N_{w_2}^2\Omega_2)^{1/2}$. Then, by using $P_{w_1}^*$ of (3.34) and $P_{w_2}^*$ of (3.35), the optimal values of P_d and P_s can be found as $P_d^* = P_1 - P_{w_1}^*$ and $P_s^* = P_2 - P_{w_2}^*$.

Secondly, inserting $P_{w_1}^*$, $P_{w_2}^*$, P_d^*, P_s^* and $P_2 = P_T - P_1$ into β_4 in (3.33), differentiating it with respect to P_1, equating to zero and solving the equation, one can get

$$\begin{aligned}&\frac{\alpha_7^2\left(2\Omega_2\alpha_6^2(DN_2\alpha_8 + N_{w_2}\alpha_5) + \alpha_9(\alpha_5(\alpha_6 - \alpha_8) + \alpha_6\alpha_8)\right)}{\alpha_5^2\alpha_6\alpha_8^2}\\ &+ \frac{\alpha_{10}^2(\alpha_3 - 2DN_1\Omega_1\alpha_4)}{\alpha_1^2\alpha_2} + \frac{\alpha_{10}^2(\alpha_4(\alpha_3 - 2N_{w_1}\Omega_1\alpha_4) - \alpha_2\alpha_3)}{\alpha_1\alpha_2^2\alpha_4} = 0\end{aligned} \tag{3.36}$$

where $\alpha_1 = \alpha_4 - DP_1N_1\Omega_1$,

$\alpha_2 = DN_1N_{w_1} - P_1N_{w_1}\Omega_1 - N_{w_1}^2 + \alpha_4$,

$\alpha_3 = DP_1N_1N_{w_1}\Omega_1^2 - DN_1N_{w_1}\Omega_1(DN_1 - P_1\Omega_1 - N_{w_1})$,

$\alpha_4 = [-DP_1N_1N_{w_1}\Omega_1(DN_1 - P_1\Omega_1 - N_{w_1})]^{1/2}$,

$\alpha_5 = \alpha_6 - DN_2\Omega_2(P_T - P_1)$,

$\alpha_6 = [-DN_2N_{w_2}\Omega_2(P_T - P_1)(DN_2 - \Omega_2(P_T - P_1) - N_{w_2})]^{1/2}$,

$\alpha_7 = N_{w_2} - DN_2$,

$\alpha_8 = DN_2N_{w_2} - N_{w_2}\Omega_2(P_T - P_1) - N_{w_2}^2 + \alpha_6$,

$\alpha_9 = DN_2N_{w_2}\Omega_2(DN_2 - \Omega_2(P_T - P_1) - N_{w_2}) - DN_2N_{w_2}\Omega_2^2(P_T - P_1)$, and

$\alpha_{10} = N_{w_1} - DN_1$. Note that (3.36) does not lead to a closed-form expression for the optimal value of P_1^* but can be calculated numerically by using mathematical software packages, such as MATLAB, MATHEMATICA and MAPLE. With the optimal value of P_1^* obtained from (3.36), one can easily calculate the optimal value of P_2^* and the following optimal values of P_d^*, P_s^*, $P_{w_1}^*$ and $P_{w_2}^*$ under the fixed total energy P_T. Note that the optimal value of P_1^* obtained from (3.36) is the exact optimal value for the total energy at the

source. In the following, a simpler approximate closed-form value for P_1^* under high SNR conditions is given. When the SNR is high ($N_{w_1} \to 0, N_{w_2} \to 0$), β_4 in (3.33) can be approximated as

$$\beta_5 \approx \frac{DP_{w_1}N_1 + N_{w_1}(P_1 - P_{w_1})}{P_{w_1}\Omega_1(P_1 - P_{w_1})} + \frac{DP_{w_2}N_2 + N_{w_2}(P_2 - P_{w_2})}{P_{w_2}\Omega_2(P_2 - P_{w_2})}. \tag{3.37}$$

Differentiating (3.37) with respect to P_{w_1}, P_{w_2} and equating them to zero, respectively, the optimal values of P_{w_1} and P_{w_2} can also be found as

$$P_{w_1}^* = \frac{P_1\mu_5}{\mu_3} \tag{3.38}$$

and

$$P_{w_2}^* = \frac{P_2\mu_6}{\mu_4} \tag{3.39}$$

respectively, where $\mu_3 = DN_1 - N_{w_1}, \mu_4 = DN_2 - P_{w_2}, \mu_5 = \sqrt{DN_1N_{w_1}} - N_{w_1}$ and $\mu_6 = \sqrt{DN_2N_{w_2}} - N_{w_2}$. By using $P_{w_1}^*$ in (3.38) and $P_{w_2}^*$ in (3.39), the optimal values of P_d and P_s can be found as $P_d^* = P_1 - P_{w_1}^*$ and $P_s^* = P_2 - P_{w_2}^*$, respectively. One can see from (3.38) and (3.39) that the optimal pilot powers at the source and at the relay increase with the increases of P_1 and P_2, respectively. Then, by inserting $P_{w_1}^*$, $P_{w_2}^*$, P_d^*, P_s^* and $P_2 = P_T - P_1$ into β_4 in (3.33) and differentiating it with respect to P_1, and equating to zero, one can get

$$\sqrt{\frac{\Omega_1\mu_3\mu_5(\mu_4 - \mu_6)(DN_1\mu_5 + N_{w_1}(\mu_3 - \mu_5))}{\Omega_2\mu_4\mu_6(\mu_3 - \mu_5)(DN_2\mu_6 + N_{w_2}(\mu_4 - \mu_6))}} = \frac{P_1\Omega_1\mu_5 + N_{w_1}\mu_3}{(P_T - P_1)\Omega_2\mu_6 + N_{w_2}\mu_4}. \tag{3.40}$$

Letting $\mu_7 = \sqrt{\frac{\Omega_1\mu_3\mu_5(\mu_4-\mu_6)(DN_1\mu_5+N_{w_1}(\mu_3-\mu_5))}{\Omega_2\mu_4\mu_6(\mu_3-\mu_5)(DN_2\mu_6+N_{w_2}(\mu_4-\mu_6))}}$, one can get

$$P_1^* = \frac{P_T\Omega_2\mu_6\mu_7 - N_{w_1}\mu_3 + N_{w_2}\mu_4\mu_7}{\Omega_1\mu_5 + \Omega_2\mu_6\mu_7}. \tag{3.41}$$

With the value of P_1^* obtained in (3.41), one can easily calculate the value of P_2^* and the following optimal values of P_d^*, P_s^*, $P_{w_1}^*$ and $P_{w_2}^*$ under the fixed total energy P_T. Note that from our simulations, it is found that the values of $P_{w_1}^*$ in (3.38) and $P_{w_2}^*$ in (3.39) are nearly the same as the values of $P_{w_1}^*$ in (3.34) and $P_{w_2}^*$ in (3.35), respectively. Thus (3.38) and (3.39) are very good approximations. Also, the optimal value of P_1^* obtained from (3.41) is nearly the same as the value obtained in equation (3.36), but (3.41) gives a closed-form expression of P_1^*, which is preferable in some applications.

3.5 BER and Optimal Energy Allocation in Cascaded Channel Estimation

This section first derives the outage probability and BER of AF using a fixed gain in CCE, and then derive the optimal energy under the total transmit energy constraints. The first subsection uses $G_{d_{fix_1}}$ and $G_{w_{fix_1}}$, while the second subsection uses $G_{d_{fix_2}}$ and $G_{w_{fix_2}}$.

3.5.1 Using $G_{d_{fix_1}}$ and $G_{w_{fix_1}}$

Outage Probability and BER

In this case, the received signal at the destination is

$$y = \sqrt{E_d}\, h_1\, h_2\, G_{d_{fix_1}}\, s + G_{d_{fix_1}}\, h_2\, n_1 + n_2. \tag{3.42}$$

Assuming $H = h_1\, h_2$ and $n = G_{d_{fix_1}}\, h_2\, n_1 + n_2$, (3.42) becomes

$$y = \sqrt{E_d}\, H\, G_{d_{fix_1}}\, s + n. \tag{3.43}$$

Let $\hat{H}$ be the estimate of H, and $\hat{H} = H + \varepsilon$, where ε denotes the channel estimation error. One has

$$y = \sqrt{E_d}\, \hat{H}\, G_{d_{fix_1}}\, s - \sqrt{E_d}\, \varepsilon\, G_{d_{fix_1}}\, s + n. \tag{3.44}$$

The end-to-end SNR can be derived from (3.44) as

$$\gamma_{fix} = \frac{E_d\, \hat{H}^2\, G_{d_{fix_1}}^2}{E_d\, \Omega_\varepsilon\, G_{d_{fix_1}}^2 + N} \tag{3.45}$$

where $N = G_{d_{fix_1}}^2 N_1 \Omega_2 + N_2$ and $E(|s|^2) = 1$. It is derived in Appendix A.5 that the outage probability of the end-to-end SNR in (3.45) can be written as

$$F_{\gamma_{fix}}(\gamma_{th}) = 1 - 2\sqrt{\frac{\gamma_{th}(E_d \Omega_\varepsilon G_{d_{fix_1}}^2 + N)}{E_d G_{d_{fix_1}}^2 \Omega}} K_1\left(2\sqrt{\frac{\gamma_{th}(E_d \Omega_\varepsilon G_{d_{fix_1}}^2 + N)}{E_d G_{d_{fix_1}}^2 \Omega}}\right). \tag{3.46}$$

Using γ_{fix} in (3.45), the BER is derived as

$$P_e = \int_0^\infty aQ\left(\sqrt{b\,\frac{E_d\,\hat{H}^2\,G_{d_{fix_1}}^2}{E_d\,\Omega_\varepsilon\,G_{d_{fix_1}}^2+N}}\right) f_{\hat{H}}(\hat{H})d\hat{H}. \tag{3.47}$$

One can use the PDF of $\hat{H}$ in (3.15) with [36, (6.62)] to solve the integral as

$$P_e = \frac{aG_{2,3}^{2,2}\left(\frac{2(E_d\Omega_\varepsilon G_{d_{fix_1}}^2+N)}{bE_dG_{d_{fix_1}}^2\Omega}\Big|\begin{matrix}\frac{1}{2},1\\1,1,0\end{matrix}\right)}{2\sqrt{\pi}} \tag{3.48}$$

where a, b are defined as in (3.21) and $G_{a,b}^{c,d}(\cdot)$ denotes the Meijer's G-function [36]. When $x \gg 1$, using the approximation $\Gamma[0,x] \approx \frac{e^{-x}}{x}$ [36] in (3.9) and (3.11), one can have $G_{d_{fix_1}}^2 \approx \frac{E_s}{N_1}$ and $G_{w_{fix_1}}^2 \approx \frac{E_{w_2}}{N_{w_1}}$. Therefore, the BER in (3.48) can be approximated as

$$P_e \approx \frac{aG_{2,3}^{2,2}\left(\frac{2(E_dE_sN_{w_1}(N_{w_2}+E_{w_2}\Omega_2)+E_{w_1}E_{w_2}N_1(N_2+E_s\Omega_2)W_1)}{bE_dE_s(N_{w_1}(N_{w_2}+E_{w_2}\Omega_2)+E_{w_1}E_{w_2}\Omega_1\Omega_2W_1)}\Big|\begin{matrix}\frac{1}{2},1\\1,1,0\end{matrix}\right)}{2\sqrt{\pi}}. \tag{3.49}$$

Optimal Energy Allocation

Denote β_6 as

$$\beta_6 = \frac{2(E_dE_sN_{w_1}(N_{w_2}+E_{w_2}\Omega_2)+E_{w_1}E_{w_2}N_1(N_2+E_s\Omega_2)W_1)}{bE_dE_s(N_{w_1}(N_{w_2}+E_{w_2}\Omega_2)+E_{w_1}E_{w_2}\Omega_1\Omega_2W_1)}. \tag{3.50}$$

From the graph depicted by Matlab software and the numerical calculation, one can observe that minimizing P_e in (3.49) is equivalent to minimizing β_6. However, β_6 in (3.50) is a complicated function that does not lead to any closed-

form expressions for the optimal energy allocation. Therefore, the equation for high SNR ($N_{w_2} \to 0, N_2 \to 0$) is simplified as

$$\beta_6 \approx \frac{2E_d N_{w_1} + 2E_{w_1} N_1 W_1}{bE_d E_{w_1} \Omega_1 W_1 + bE_d N_{w_1}}. \tag{3.51}$$

Note that the high SNR approximation is used only to derive the closed-form solutions of the energy allocation but the derived optimal values can be used for all SNRs and BERs, which will be justified in Section 3.6. By inserting $E_d = \frac{P_d}{D}$, $E_{w_1} = \frac{P_{w_1}}{W_1}$ and $P_d = P_1 - P_{w_1}$ into β_6 in (3.51) and differentiating it with respect to P_{w_1}, then equating it to zero, one can get the optimal value of P_{w_1} as

$$P^*_{w_1} = \frac{\mu_1 - P_1 N_{w_1} \Omega_1}{DN_1\Omega_1 - N_{w_1}\Omega_1}. \tag{3.52}$$

Then, the optimal value of P_d can be found as $P^*_d = P_1 - P^*_{w_1}$. One can see that (3.51) does not include E_s and E_{w_2} due to high SNR approximation. Therefore, β_6 of (3.50) is used to get the optimal values of P_s and P_{w_2}. By inserting $E_s = \frac{P_s}{D}$, $E_{w_2} = \frac{P_{w_2}}{W_2}$ and $P_s = P_2 - P_{w_2}$ into β_6 of (3.50) and differentiating it with respect to P_{w_2}, then equating it to zero, one can get the optimal value of P_{w_2} as

$$P^*_{w_2} = \frac{\mu_8 + P_2 N_{w_1} N_{w_2} \Omega_2 W_1 (DN_1 - P_d \Omega_1)}{D^2 N_1 N_2 \Omega_2 (P^*_{w_1}\Omega_1 + N_{w_1}) + N_{w_1} N_{w_2} \Omega_2 W_1 (DN_1 - P_d \Omega_1)} \tag{3.53}$$

where $\mu_8 = [D^2 P_2 N_1 N_2 N_{w_1} N_{w_2} \Omega_2 W_1 ((P^*_{w_1}\Omega_1 + N_{w_1})(-D^2 N_1 N_2 + D(-P_2) N_1 \Omega_2 + P_2 P_d \Omega_1 \Omega_2) + N_{w_1} N_{w_2} W_1 (P_d \Omega_1 - DN_1))]^{1/2}$. Then, the optimal value of P_s can be found as $P^*_s = P_2 - P^*_{w_2}$. In this case, the optimal energy allocation between P_d, P_s, P_{w_1}, P_{w_2} under the fixed total energy P_T can be obtained by first inserting $P^*_{w_1}$, $P^*_{w_2}$, P^*_d, P^*_s and $P_2 = P_T - P_1$ into β_6 in (3.50) and

differentiating it with respect to P_1, then equating it to zero. However, the results are not presented here since it is very complicated and do not provide much insight to the performance analysis, although it can be easily extracted using the well-known mathematical software packages. The next subsection will provide the optimal energy allocation between P_d, P_s, P_{w_1}, P_{w_2} under fixed P_T for the case when $G_{d_{fix_2}}$ in (3.10) and $G_{w_{fix_2}}$ in (3.12) are used.

3.5.2 Using $G_{d_{fix_2}}$ and $G_{w_{fix_2}}$

Outage Probability and BER

In this case, using $G_{d_{fix_2}}$ in (3.10) and $G_{w_{fix_2}}$ in (3.12), the outage probability can be easily obtained by replacing $G_{d_{fix_1}}$ and $G_{w_{fix_1}}$ in (3.46) with $G_{d_{fix_2}}$ and $G_{w_{fix_2}}$, respectively. Also, the BER expression P_e in (3.47) can be solved in closed-form as

$$P_e = a \frac{G_{2,3}^{2,2}\left(\frac{2E_dE_s(E_{w_1}N_{w_2}\Omega_1+N_{w_1}(N_{w_2}+E_{w_2}\Omega_2))+2E_{w_1}E_{w_2}(E_dN_2\Omega_1+N_1(N_2+E_s\Omega_2))W_1}{bE_dE_s(N_{w_1}(N_{w_2}+E_{w_2}\Omega_2)+E_{w_1}\Omega_1(N_{w_2}+E_{w_2}\Omega_2W_1))}\middle| \begin{matrix}\frac{1}{2},1\\ 1,1,0\end{matrix}\right)}{2\sqrt{\pi}} \tag{3.54}$$

where a, b are defined as in (3.21). Using the approximations of $G_{d_{fix_2}}^2 \approx \frac{E_s}{E_d\Omega_1}$ and $G_{w_{fix_2}}^2 \approx \frac{E_{w_2}}{E_{w_1}\Omega_1}$ in high SNR, the BER expression in (3.54) can be approximated as

$$P_e = \frac{aG_{2,3}^{2,2}\left(\frac{2(E_dE_s(E_{w_1}N_{w_2}\Omega_1+E_{w_2}N_{w_1}\Omega_2)+E_{w_1}E_{w_2}(E_dN_2\Omega_1+E_sN_1\Omega_2)W_1)}{bE_dE_s(E_{w_2}N_{w_1}\Omega_2+E_{w_1}\Omega_1(N_{w_2}+E_{w_2}\Omega_2W_1))}\middle| \begin{matrix}\frac{1}{2},1\\ 1,1,0\end{matrix}\right)}{2\sqrt{\pi}}. \tag{3.55}$$

Optimal Energy Allocation

Denote β_7 as

$$\beta_7 = \frac{2(E_{w_1}E_{w_2}W_1(E_dN_2\Omega_1 + E_sN_1\Omega_2) + E_dE_s(E_{w_1}N_{w_2}\Omega_1 + E_{w_2}N_{w_1}\Omega_2))}{bE_dE_s(E_{w_1}\Omega_1(E_{w_2}\Omega_2W_1 + N_{w_2}) + E_{w_2}N_{w_1}\Omega_2)}. \tag{3.56}$$

From the graph depicted by Matlab software and the numerical calculation, one can observe that minimizing P_e in (3.55) is equivalent to minimizing β_7. However, β_7 in (3.56) is a complicated function that does not lead to any closed-form expressions for optimal energy allocation. Therefore, β_7 is simplified for high SNR ($N_{w_2} \to 0$) as

$$\beta_7 \approx \frac{2E_dE_{w_1}E_{w_2}N_2\Omega_1W_1 + 2E_dE_{w_1}E_sN_{w_2}\Omega_1 + 2E_dE_{w_2}E_sN_{w_1}\Omega_2 + 2E_{w_1}E_{w_2}E_sN_1\Omega_2W_1}{bE_dE_{w_1}E_{w_2}E_s\Omega_1\Omega_2W_1 + bE_dE_{w_2}E_sN_{w_1}\Omega_2}. \tag{3.57}$$

Firstly, by inserting $E_d = \frac{P_d}{D}$, $E_s = \frac{P_s}{D}$, $E_{w_1} = \frac{P_{w_1}}{W_1}$, $E_{w_2} = \frac{P_{w_2}}{W_2}$, $P_s = P_2 - P_{w_2}$ and $P_d = P_1 - P_{w_1}$ into β_7 in (3.57) and differentiating it with respect to P_{w_1} and P_{w_2}, then equating them to zero, respectively, one can get the optimal value of P_{w_2} as

$$P^*_{w_2} = \frac{P_2\sqrt{N_2DN_{w_2}} - P_2N_{w_2}}{DN_2 - N_{w_2}} \tag{3.58}$$

and the optimal value of P_{w_1} as

$$P^*_{w_1} = \frac{\mu_9 + P_1N_{w_1}\Omega_1(DP^*_{w_2}N_2 + P_s(N_{w_2} - P^*_{w_2}\Omega_2))}{\Omega_1(DP^*_{w_2}(P_sN_1\Omega_2 + N_2N_{w_1}) + P_sN_{w_1}(N_{w_2} - P^*_{w_2}\Omega_2))} \tag{3.59}$$

where $\mu_9 = (-DP_1P^*_{w_2}P_sN_1N_{w_1}\Omega_1\Omega_2(DP^*_{w_2}(N_2(P_1\Omega_1 + N_{w_1}) + P_sN_1\Omega_2) + P_s(P_1\Omega_1 + N_{w_1})(N_{w_2} - P^*_{w_2}\Omega_2)))^{1/2}$. Then, by using $P^*_{w_1}$ in (3.59) and $P^*_{w_2}$ in (3.58), the optimal values of P_d and P_s can be found as $P^*_d = P_1 - P^*_{w_1}$ and

$P_s^* = P_2 - P_{w_2}^*$, respectively. Note that this optimal allocation method can be seen as the suboptimal method due to approximation being used. Also note that $P_{w_1}^*$ and $P_{w_1}^*$ should be greater than zero to have physical meanings.

Secondly, in order to get the optimal energy allocation between P_d, P_s, P_{w_1}, P_{w_2} under fixed P_T, $P_{w_1}^*$ in (3.59) and $P_{w_2}^*$ in (3.58) must be approximated to obtain simpler forms. Following the same process as that in Section 3.4.2, β_7 in (3.57) can be approximated as

$$\beta_8 \approx \frac{2\left(DP_{w_1}\left(\frac{N_1}{P_1 - P_{w_1}} + \frac{N_2\Omega_1}{P_2\Omega_2 - P_{w_2}\Omega_2}\right) + \frac{P_{w_1}N_{w_2}\Omega_1}{P_{w_2}\Omega_2} + N_{w_1}\right)}{b(P_{w_1}\Omega_1 + N_{w_1})}. \tag{3.60}$$

Differentiating β_8 in (3.60) with respect to P_{w_1}, P_{w_2} and equating both of them to zero, respectively, the approximate optimal values of P_{w_1} and P_{w_2} can be found as

$$P_{w_1}^* = \frac{P_1\mu_5}{\mu_3} \tag{3.61}$$

and

$$P_{w_2}^* = \frac{P_2\mu_6}{\mu_4} \tag{3.62}$$

respectively. One can see that $P_{w_1}^*$ and $P_{w_2}^*$ in (3.61) and (3.62) are the same as the optimal values obtained in Section 3.4.2 for DCE. By using $P_{w_1}^*$ in (3.61) and $P_{w_2}^*$ in (3.62), the approximate optimal values of P_d and P_s can be found as $P_d^* = P_1 - P_{w_1}^*$ and $P_s^* = P_2 - P_{w_2}^*$ respectively. Then, by inserting those approximate $P_{w_1}^*$, $P_{w_2}^*$, P_d^*, P_s^* and $P_2 = P_T - P_1$ into β_8 and differentiating it with respect to P_1, then equating it to zero, one can get

$$P_1^* = \frac{\sqrt{P_T^2\mu_{11}\mu_{12} - \mu_{10}\mu_{11} + \mu_{10}\mu_{12}} - P_T\mu_{12}}{\mu_{11} - \mu_{12}} \tag{3.63}$$

where $\mu_{10} = P_T N_{w_1} \mu_3 \mu_4 (\mu_3 - \mu_5)(DN_2\mu_6 + N_{w_2}(\mu_4 - \mu_6))$, $\mu_{11} = \Omega_1 \mu_4 \mu_5 (\mu_3 - \mu_5)(DN_2\mu_6 + N_{w_2}(\mu_4 - \mu_6))$ and $\mu_{12} = \Omega_2 \mu_3 \mu_6 (\mu_4 - \mu_6)(DN_1\mu_5 + N_{w_1}(\mu_3 - \mu_5))$. With the value of P_1^* obtained in (3.63), one can easily calculate the value of P_2^* and the following optimal values of P_d^*, P_s^*, $P_{w_1}^*$ and $P_{w_2}^*$ under the fixed total energy P_T. Similarly, these approximate optimal values are nearly the same with the exact values from our simulations, as will be shown later.

3.6 Numerical Results and Discussion

In this section, numerical results are presented to illustrate and verify our theoretical analysis. In the first subsection, the BER expressions of AF using a variable gain in DCE and using two types of fixed gain in CCE are examined. In the simulation, 10^6 Monte-Carlo simulation runs are used. Each run has a different channel realization but the same bit. There is no iteration. In the second subsection, the BER performances with optimal energy values are compared with the conventional system without optimal energy allocation. $(a, b) = (1, 2)$ is used for BPSK; $(a, b) = (1.5, 0.4)$ is used for 4-PAM and $(a, b) = (2, 1)$ is used for the approximation of QPSK. Also, $L = 1$, the path-loss exponent $r = 3$, $W_1 = 5$, $W_2 = 5$ and $D = 45$ are used in the examples below.

Note that the total pilot energy and the total data energy, not the individual symbol powers, are optimized in this chapter. As a result, one can either fix the individual symbol powers and optimize the symbol numbers, or fix the symbol numbers and optimize the individual symbol powers, or both. The examples below fix the symbol numbers and optimizes the individual symbol powers. Other values of W_1, W_2 and D or other methods of optimization

can be examined in a similar way but are omitted here. They have the same effects as it is the total energy that determines the system performance and that is optimized.

Denote the BER expressions in (3.21), (3.30), (3.48) or (3.54) as "Exact", the BER expressions in (3.22), (3.31), (3.49) or (3.55) as "Approximation-1" and BER expressions in (3.23) or (3.32) as "Approximation-2". Exact BER expressions in (3.21) and (3.30) in the form of one-dimensional integral are calculated numerically by using the "NIntegrate" method in MATHEMATICA software package while other BER expressions in closed-form are calculated directly.

3.6.1 Validation of BER Expressions

Fig. 3.3 - Fig. 3.5 show the BERs vs. $\bar{\gamma}_1$, where $d_1 = 1$, $d_2 = 1$, $N_1 = 1$, $N_2 = 1$, $N_{w_1} = 1$, $N_{w_2} = 1$, $\gamma_{\varepsilon_1} = -10$ dB and $\bar{\gamma}_1 = 2\bar{\gamma}_2$ are set. One can see from Fig. 3.3 - Fig. 3.5 that BPSK gives the best BER performance while 4-PAM gives the worst BER performance. But QPSK and 4-PAM can transmit twice the data rate in a given bandwidth compared to BPSK. Thus it is a tradeoff between reliability and rate.

Fig. 3.3 (a) compares the BERs obtained by simulation, "Exact" in (3.21), "Approximation-1" in (3.22) and "Approximation-2" in (3.23) when h_1 is estimated using pilot symbols in DCE for Rayleigh fading channels with perfect knowledge of h_2. Fig. 3.3 (b) compares the BERs obtained by simulation, "Exact" in (3.30), "Approximation-1" in (3.31) and "Approximation-2" in (3.32) when both h_1 and h_2 are estimated in DCE with $\gamma_{\varepsilon_2} = -10$ dB. One sees that the "Exact" results in (3.21) or (3.30) agree well with simulation for

BPSK and 4-PAM in Fig. 3.3 (a) and Fig. 3.3 (b). The slight mismatch in low $\bar{\gamma}_1$ is caused by the numerical evaluation of the integrals for "Exact" in (3.21) or (3.30). One also sees that "Approximation-2" in (3.23) or (3.32) are close to the simulation, especially at high $\bar{\gamma}_1$. On the other hand, "Approximation-1" in (3.22) or (3.31) have larger differences from the simulation results, but they have the simplest structures. It can be seen that the approximation error is reduced by increasing $\bar{\gamma}_1$. The mismatch between "Approximation-1", "Approximation-2" and simulation is caused by the use of different approximations to "Exact" in Appendices A.2 and A.3 with different complexities and accuracies. Generally, all the BER curves are nearly the same and they match well with simulation when $\bar{\gamma}_1$ is above 25 dB for BPSK and above 30 dB for 4-PAM. For QPSK, similar behaviour can be observed from Fig. 3.3 (a) and Fig. 3.3 (b). However, a slight mismatch still exists between "Exact", "Approximation-1", "Approximation-2" and simulation in high $\bar{\gamma}_1$, again, due to different accuracies of the approximations used in different ranges.

Fig. 3.4 compares BERs between the case when h_1 is estimated but with perfect knowledge of h_2 and the case when both h_1 and h_2 are estimated in DCE. "Exact" in (3.21) and (3.30) are used. It is obvious that BERs with perfect knowledge of h_2 give the best performance and with the increase of γ_{ε_2}, the BER performances of BPSK, QPSK and 4-PAM deteriorate, respectively. This is because with the deterioration of the relay-to-destination channel, the BER performances become worse accordingly.

Fig. 3.5 (a) compares the BERs obtained by simulation, "Exact" in (3.48) and "Approximation-1" in (3.49) when the product of h_1 and h_2 is estimated in the destination in CCE using fixed gains $G_{d_{fix_1}}$ and $G_{w_{fix_1}}$ for Rayleigh fading channels. Fig. 3.5 (b) compares the BERs obtained by sim-

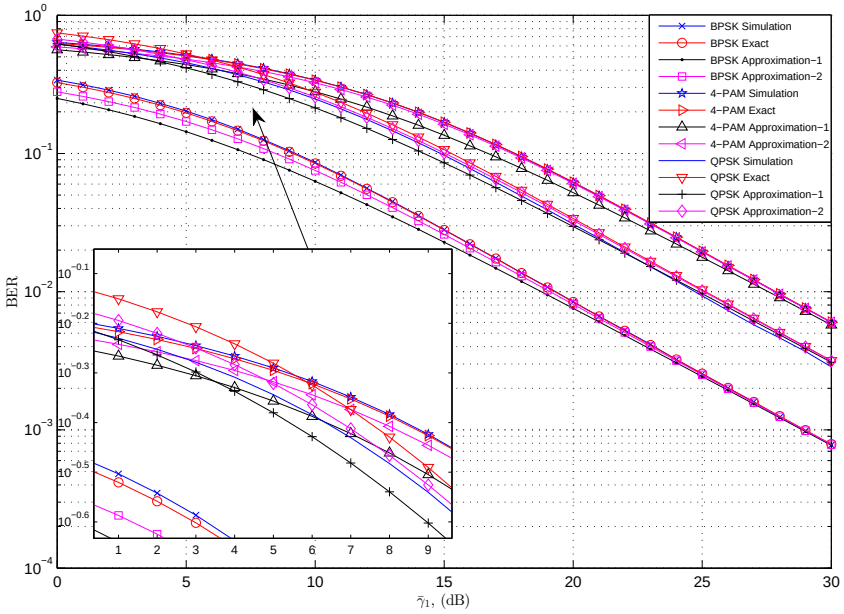

(a)

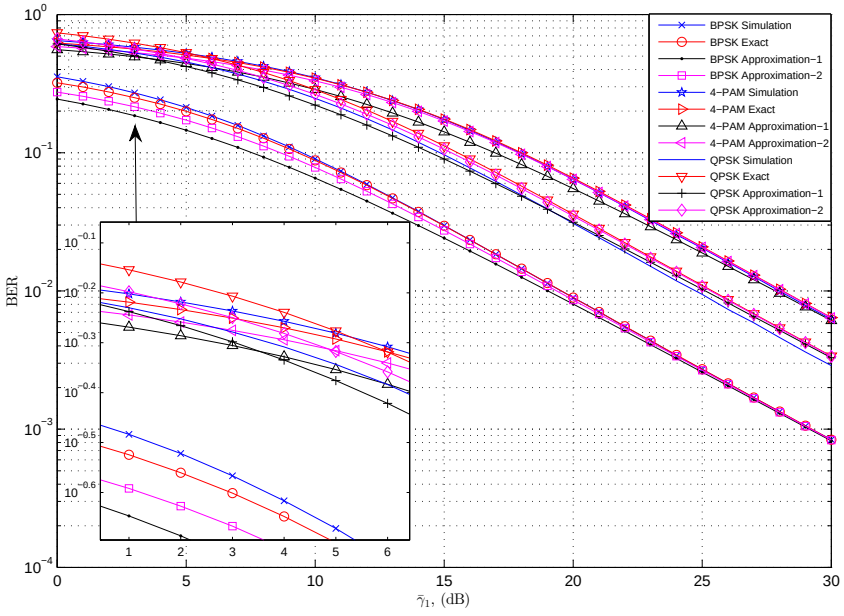

(b)

Figure 3.3: BER vs. $\bar{\gamma}_1$ for AF in DCE. (a) when h_1 is estimated but with the perfect knowledge of h_2. (b) when both h_1 and h_2 are estimated with $\gamma_{\varepsilon_2} = -10$ dB.

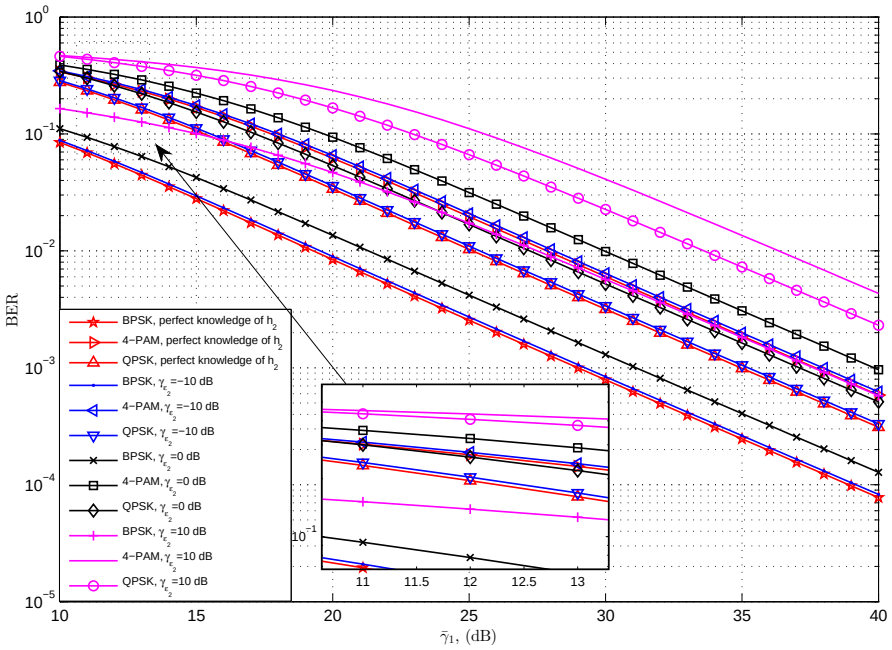

Figure 3.4: Comparison of BERs between the case when h_1 is estimated but with perfect knowledge of h_2 and the case when both h_1 and h_2 are estimated in DCE.

ulation, "Exact" in (3.54) and "Approximation-1" in (3.55) in CCE using $G_{d_{fix_2}}$ and $G_{w_{fix_2}}$. $\gamma_{\varepsilon_2} = -10$ dB is set. One sees from Fig. 3.5 (a) and Fig. 3.5 (b) that there are considerable differences between "Exact" in (3.48) or (3.54), "Approximation-1" in (3.49) or (3.55) and simulation for BPSK, QPSK and 4-PAM, respectively, when $\bar{\gamma}_1$ is small. In particular, the differences between "Exact", "Approximation-1" and simulation for QPSK are the largest. Generally, when $\bar{\gamma}_1$ increases, their difference increases. That is because n_w in (3.13) is assumed as Gaussian in order to get tractable results in CCE for BPSK, QPSK and 4-PAM. When $\bar{\gamma}_1$ increases, the approximation errors increase accordingly. Specifically, $G_{d_{fix_1}}$ and $G_{w_{fix_1}}$ are larger than $G_{d_{fix_2}}$ and $G_{w_{fix_2}}$, respectively, in the same conditions. Therefore the gap between "Exact" and simulation in Fig. 3.5 (a) increases quicker than the gap between "Exact" and simulation in Fig. 3.5 (b) when $\bar{\gamma}_1$ increases. $G^2_{d_{fix_1}} \approx \frac{E_s}{N_1}$ and $G^2_{w_{fix_1}} \approx \frac{E_{w_2}}{N_{w_1}}$ are used to approximate $G^2_{d_{fix_1}}$ and $G^2_{w_{fix_1}}$, respectively for "Approximation-1" in Fig. 3.5 (a). Interestingly, "Approximation-1" is nearly 1 dB lower than "Exact" when $\bar{\gamma}_1$ is above 15 dB such that the fitting performance of "Approximation-1" for simulation is better than "Exact" in Fig. 3.5 (a). But when $\bar{\gamma}_1$ is below 10 dB, "Exact" still has better performance than "Approximation-1" in Fig. 3.5 (a). $G^2_{d_{fix_2}} \approx \frac{E_s}{E_d \Omega_1}$ and $G^2_{w_{fix_2}} \approx \frac{E_{w_2}}{E_{w_1} \Omega_1}$ are used to approximate $G^2_{d_{fix_2}}$ and $G^2_{w_{fix_2}}$, respectively for "Approximation-1" in Fig. 3.5 (b). It is obvious that when the value of $\bar{\gamma}_1$ is large, there is no gap between "Approximation-1" and "Exact" in Fig. 3.5 (b). Similarly, when the value of $\bar{\gamma}_1$ is below 10 dB, "Exact" has better performance than "Approximation-1" in Fig. 3.5 (b). However, the use of the approximation for $G_{d_{fix_1}}$, $G_{w_{fix_1}}$, $G_{d_{fix_2}}$ and $G_{d_{fix_2}}$ can significantly simplify the BER expressions, with slightly deteriorated performance. More importantly, these approximations do not af-

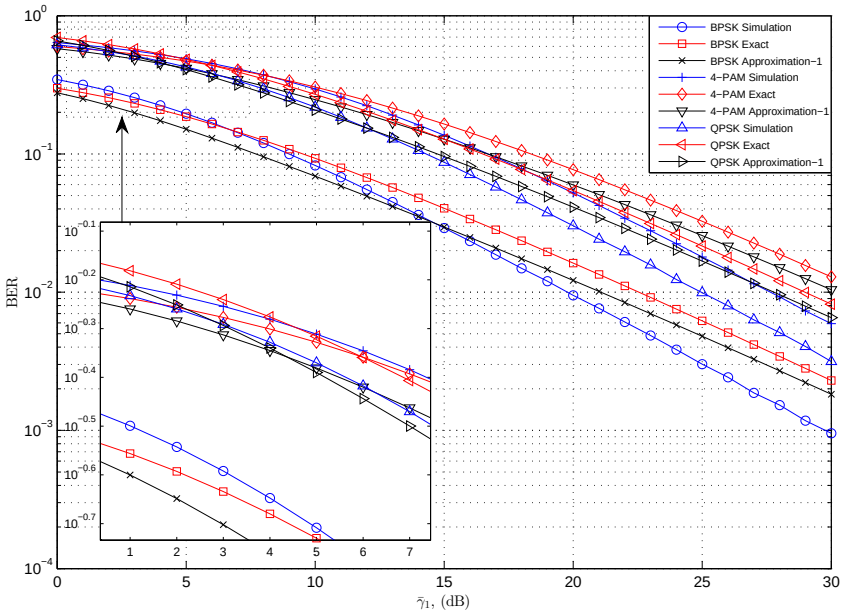

(a)

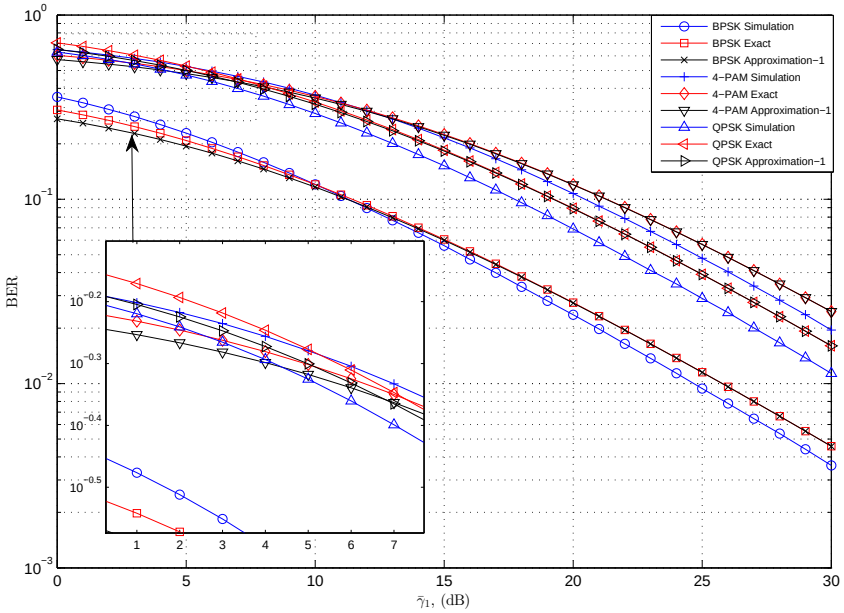

(b)

Figure 3.5: BER vs. $\bar{\gamma}_1$ for AF in CCE. (a) when $G_{d_{fix_1}}$ and $G_{w_{fix_1}}$ are used. (b) when $G_{d_{fix_2}}$ and $G_{w_{fix_2}}$ are used.

fect the choice of the optimal energy allocation obtained by using these BER expressions, as will be shown later. In other words, although these curves mismatch, their troughs with respect to the pilot energy are located very close to each other.

3.6.2 Optimal Energy Allocation Evaluation

This part uses the BER performance to check the optimal energy values obtained from our BER expressions. "Exact" of (3.21) is used in DCE when h_1 is estimated, (3.30) is used in DCE when both h_1 and h_2 are estimated, (3.48) is used in CCE with the amplification gain $G_{d_{fix_1}}$, $G_{w_{fix_1}}$ and (3.54) is used in CCE with the amplification gain $G_{d_{fix_2}}$, $G_{w_{fix_2}}$ in Fig. 3.6- Fig. 3.10. Fig. 3.6 - Fig. 3.8 examine the optimal allocation between P_d and P_{w_1} under fixed P_1 and the optimal allocation between P_s and P_{w_2} under fixed P_2, respectively.

Fig. 3.6 shows the BERs vs. E_{w_1} when h_1 is estimated but with the perfect knowledge of h_2 in DCE. Fig. 3.7 shows the BERs vs. E_{w_1} when $G_{d_{fix_1}}$ and $G_{w_{fix_1}}$ are used in CCE. Monte-Carlo simulation has been used in Fig. 3.6 and Fig. 3.7. In Fig. 3.6 and Fig. 3.7, $N_1 = 1$, $N_2 = 1$, $N_{w_1} = 1$ and $N_{w_2} = 1$ are assumed. $P_1 = 30$ dB and $P_1 = 40$ dB are examined in Fig. 3.6 while $P_1 = 30$ dB, $P_2 = 30$ dB and $P_1 = 40$ dB, $P_2 = 40$ dB are examined in Fig. 3.7. Also, $\bar{\gamma}_2 = 30$ dB is set in Fig. 3.6 while $E_{w_1} = E_{w_2}$ is set in Fig. 3.7. Consider both the case when the relay is close to the source and the destination ($d_1 = 0.5$, $d_2 = 0.5$) and the case when the relay is far from the source and the destination ($d_1 = 1$, $d_2 = 1$) in Fig. 3.6 and Fig. 3.7.

In these figures, the BER performances become worse when d_1 and d_2 increase (the distance between source and relay, and the distance between

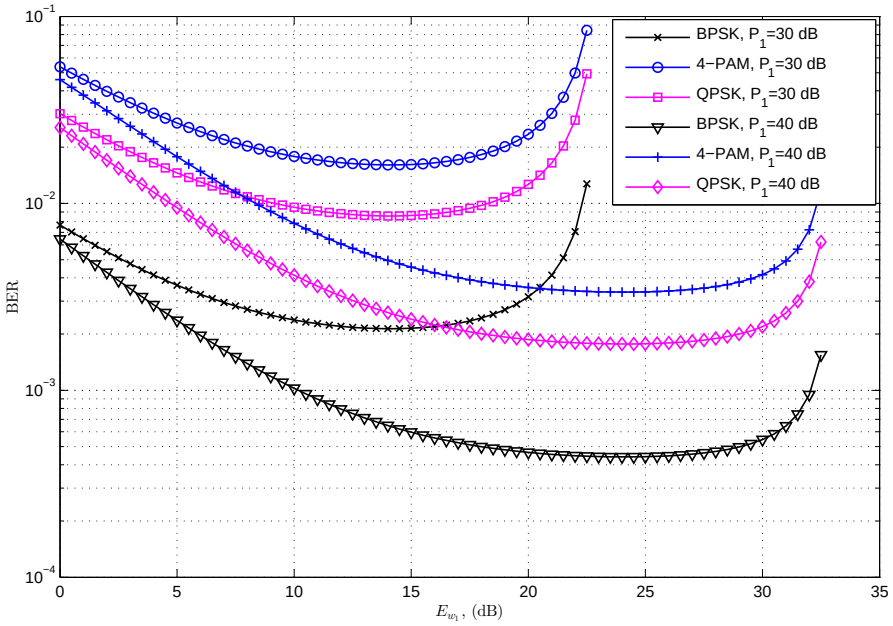

(a)

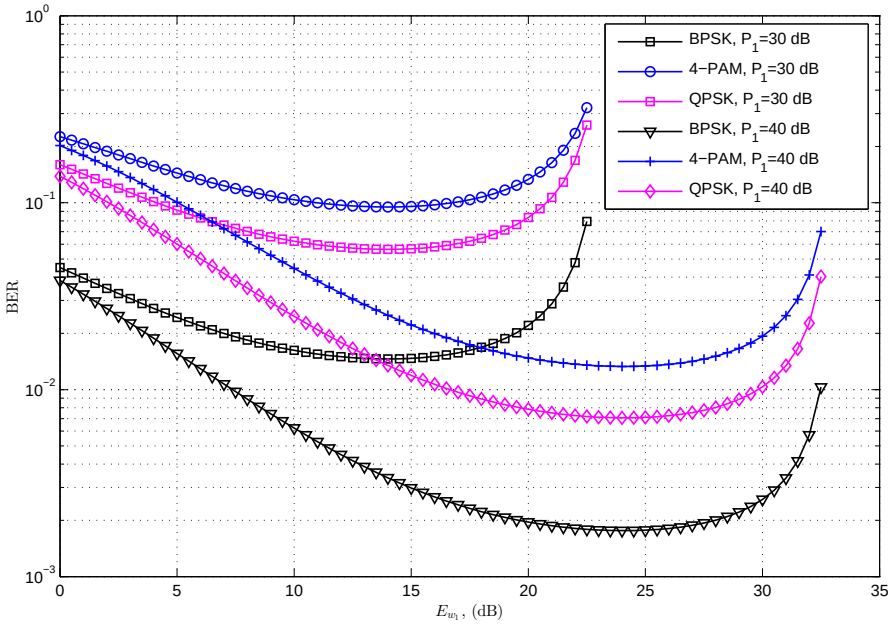

(b)

Figure 3.6: BERs vs. E_{w_1} for AF in DCE when h_1 is estimated but with the perfect knowledge of h_2 with $\bar{\gamma}_2 = 30$ dB. (a) $d_1 = 0.5$, $d_2 = 0.5$. (b) $d_1 = 1$, $d_2 = 1$.

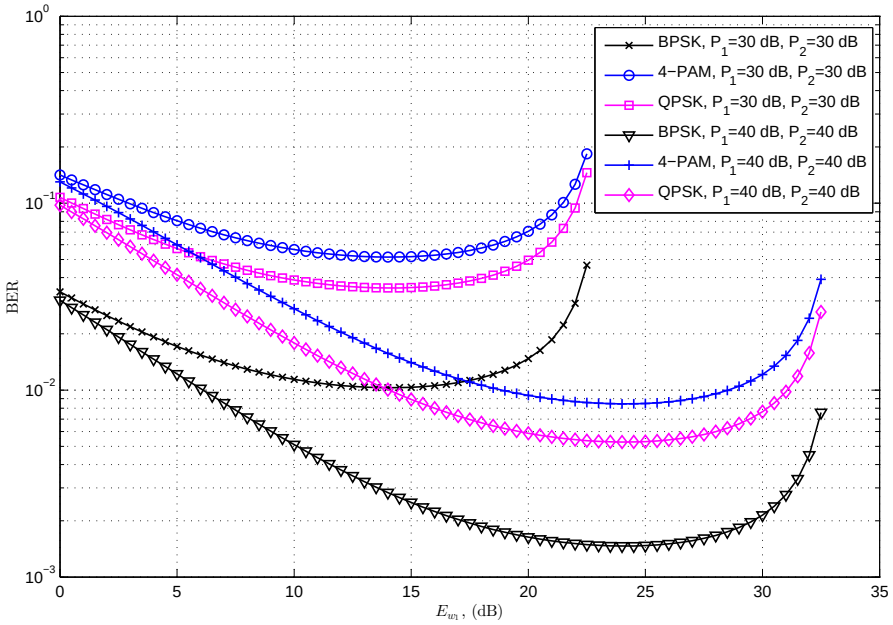

(a)

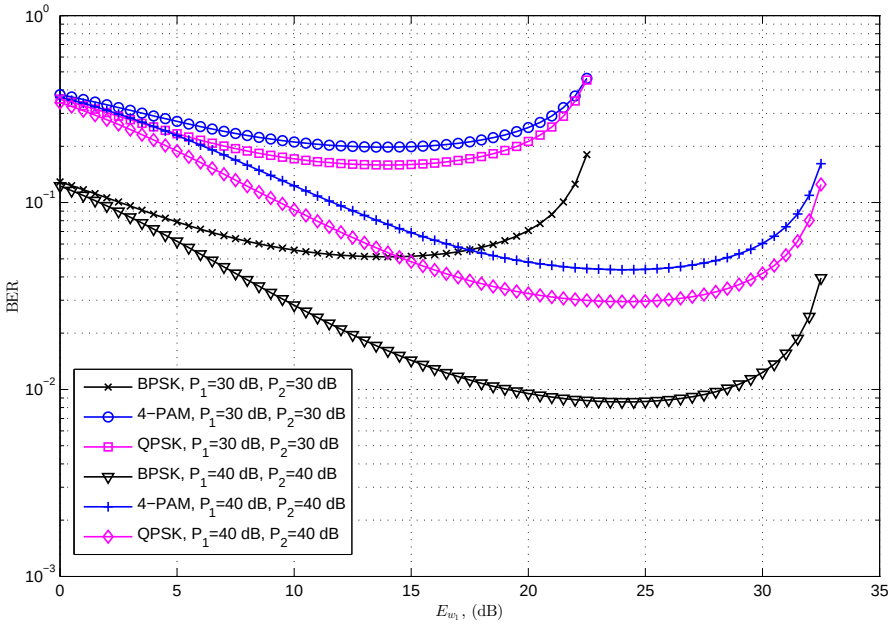

(b)

Figure 3.7: BER vs. E_{w_1} for AF in CCE when $G_{d_{fix_1}}$ and $G_{w_{fix_1}}$ are used. (a) $d_1 = 0.5$, $d_2 = 0.5$. (b) $d_1 = 1$, $d_2 = 1$.

relay and destination, respectively). This shows that the distance between nodes and therefore the average energy, have significant impact on system performance.

It is understandable that if E_{w_1} (the pilot power) decreases, the BER performance will decrease even with increasing data power. This is because the system cannot obtain good approximate channel information without enough pilot power. Similarly, if E_{w_1} (the pilot power) increases too much, the BER performance will also decrease even with perfect channel information. This is because the system cannot perform well without enough data transmission power. This explains Fig. 3.6 and Fig. 3.7, where one can see that all the BER curves are concave and thus first decrease and then increase, when E_{w_1} (the pilot power) increases.

Also, one can see from Fig. 3.6 and Fig. 3.7 that the minimum BERs are achieved at the same E_{w_1} for BPSK, 4-PAM and QPSK. It proves why our optimal energy allocation schemes do not include modulation-specific constants a and b such as (3.25), (3.52) and (3.53). The minimum BER is achieved at around $E_{w_1} = 14$ dB for $P_1 = 30$ dB and $E_{w_1} = 24$ dB for $P_1 = 40$ dB in all the BER curves for DCE in Fig. 3.6. From (3.25), one can calculate the optimal total pilot power at the source as $E_{w_1} = 14.1267$ dB for $P_1 = 30$ dB and $E_{w_1} = 24.1394$ dB for $P_1 = 40$ dB in Fig. 3.6 (a), while one can get optimal pilot power $E_{w_1} = 14.0257$ dB for $P_1 = 30$ dB and $E_{w_1} = 24.1295$ dB for $P_1 = 40$ dB in Fig. 3.6 (b). Thus, the optimal power allocation from our theoretical analysis is nearly the same as what is observed from Fig. 3.6. Similarly, the minimum BER is achieved at around $E_{w_1} = 14$ dB for $P_1 = 30$ dB, $P_2 = 30$ dB and $E_{w_2} = 24$ dB for $P_1 = 40$ dB, $P_2 = 40$ dB in all the BER curves for CCE in Fig. 3.7. From (3.52) and (3.53), one can calculate $E_{w_1} = 14.1267$

dB, $E_{w_2} = 13.573$ dB for $P_1 = 30$ dB, $P_2 = 30$ dB and $E_{w_1} = 24.1394$ dB, $E_{w_2} = 23.821$ dB for $P_1 = 40$ dB, $P_2 = 40$ dB in Fig. 3.7 (a). One can also calculate $E_{w_1} = 14.0257$ dB, $E_{w_2} = 13.5158$ dB for $P_1 = 30$ dB, $P_2 = 30$ dB and $E_{w_1} = 24.1295$ dB, $E_{w_2} = 23.5745$ dB for $P_1 = 40$ dB, $P_2 = 40$ dB in Fig. 3.7 (b). Again, our theoretical value of the optimal allocation is nearly the same as that from the simulation. From Fig. 3.6 and Fig. 3.7, one can also see that the BERs with the optimal allocation have the lowest values, which implies that the energy allocation proposed in this chapter has better performance than all other allocation methods.

Fig. 3.8 compares BERs with optimal allocation between the case when h_1 is estimated but with perfect knowledge of h_2 and the case when both h_1 and h_2 are estimated in DCE. $d_1 = 1$, $d_2 = 1$, $N_1 = 1$, $N_2 = 1$, $N_{w_1} = 1$, $P_1 = P_2$ are assumed and 4-PAM modulation is examined. P_2 can be used all by data at the relay when the channel has perfect knowledge of h_2 while $N_{w_2} = 1, 10, 20, 30$ are assumed when h_2 are estimated, where P_2 has to be shared by data and pilot by using our optimal energy allocation in this case. As can be seen in Fig. 3.8, as P_1/H_1 (the power per symbol at the source) increases, all the BERs decrease. This is because with the total power increasing, the BER performance improves. One can also see that BERs with perfect knowledge of h_2 give the best performance and that when N_{w_2} (the noise power in pilot) increases, the BERs increase. This is because the increase of noise powers deteriorate the BER performances.

Fig. 3.9 and Fig. 3.10 compare the BER using the optimal energy allocation between P_d, P_s, P_{w_1}, P_{w_2} under fixed P_T with the BER using equal energy allocation without optimization where $P_d = \frac{P_T D}{H}$, $P_s = \frac{P_T D}{H}$, $P_{w_1} = \frac{P_T W_1}{H}$ and $P_{w_2} = \frac{P_T W_2}{H}$. $d_2 = 1$ and $N_1 = 1$ are set in Fig. 3.9 and Fig. 3.10.

4-PAM modulation is used as examples and other modulation can be checked in a similar way.

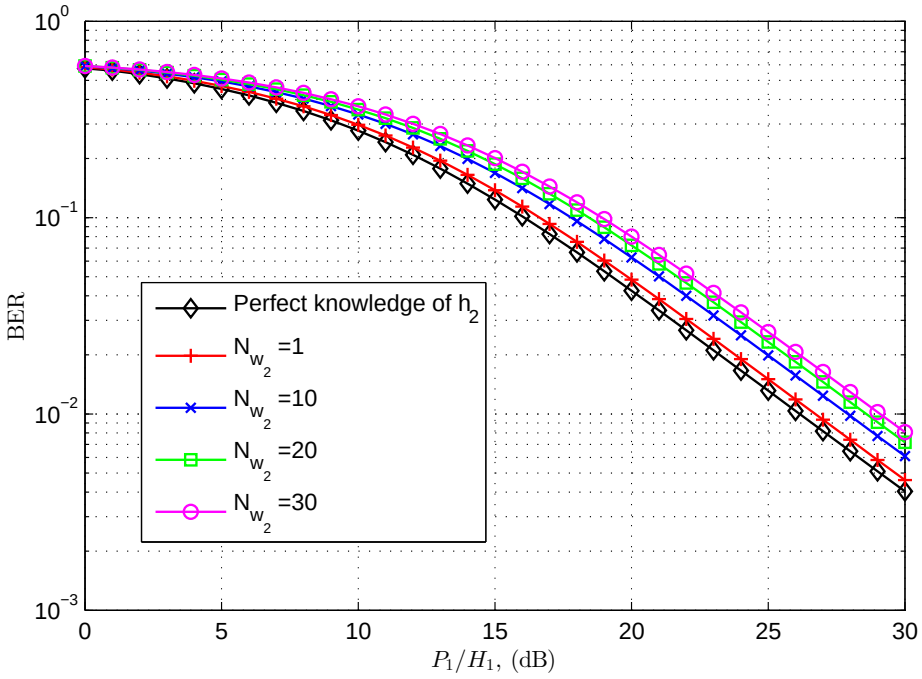

Figure 3.8: Comparison of BERs with optimal allocation between the case when h_1 is estimated but with perfect knowledge of h_2 and the case when both h_1 and h_2 are estimated in DCE.

Fig. 3.9 shows the BERs vs. P_T/H when both h_1 and h_2 are estimated in DCE. Fig. 3.10 shows the BERs vs. P_T/H when $G_{d_{fix_2}}$ and $G_{w_{fix_2}}$ are used in CCE. d_1 is decreased from 1/4 d_2 in Fig. 3.9 (a) and Fig. 3.10 (a) to 1/10 d_2 in Fig. 3.9 (b) and Fig. 3.10 (b), respectively. From Fig. 3.9 and Fig. 3.10, one can see that the BERs with optimal energy allocation outperform the BERs with equal allocation under the same conditions.

Comparing the system with $N_{w_2} = N_{w_1} = N_2 = N_1$ in Fig. 3.9 (a) and Fig. 3.9 (b), one can see that the BER improves when d_1 (the distance between source and relay) decreases. This is because when d_1 decreases, the

average power increases and thus, the BER performance improves.

Also, in this case, as d_1 is decreased from 1/4 d_2 in Fig. 3.9 (a) to 1/10 d_2 in Fig. 3.9 (b), the performance gain of optimal allocation over equal allocation is increased from 2 dB to 3 dB. This is because equal allocation cannot perform well when the status of source-to-relay channel is different from that of the relay-to-destination channel. Therefore, with the decrease of d_1, the difference between d_1 and d_2 becomes larger such that the performance gain will increase accordingly. As can be seen in Fig. 3.9 (a), with the increase of N_{w_2} and N_2 from N_1 to $3N_1$, the performance gain increases from 2 dB to 2.25 dB. Also, with the increase of N_{w_2} and N_{w_1} from N_1 to $3N_1$, the performance gain increases from 2 dB to 2.4 dB. This is also because that with the increase of difference of noise power between source-to-relay and relay-to-destination channel or between data transmission and pilot transmission, the performance gain increases. In Fig. 3.9 (b), as the increase of N_{w_2} and N_{w_1} from $10N_1$ to $20N_1$, the performance gain increases from 4.8 dB to 5.5 dB with the same reason above.

Similar analysis and conclusion can be made from Fig. 8 (a) and Fig. 8 (b) in CCE. Moreover, when setting $d_1 = 1$, $d_2 = 1/4\ d_1$ and $d_2 = 1/10\ d_1$ in Fig. 3.9 and Fig. 3.10, similar performance gain can be obtained. These figures are omitted here to save space.

3.7 Conclusions

The BER and the outage probability of AF relaying systems using variable gain in DCE and fixed gains in CCE have been derived when different channel gains are estimated using the pilot-aided ML estimation for slowly fading Rayleigh

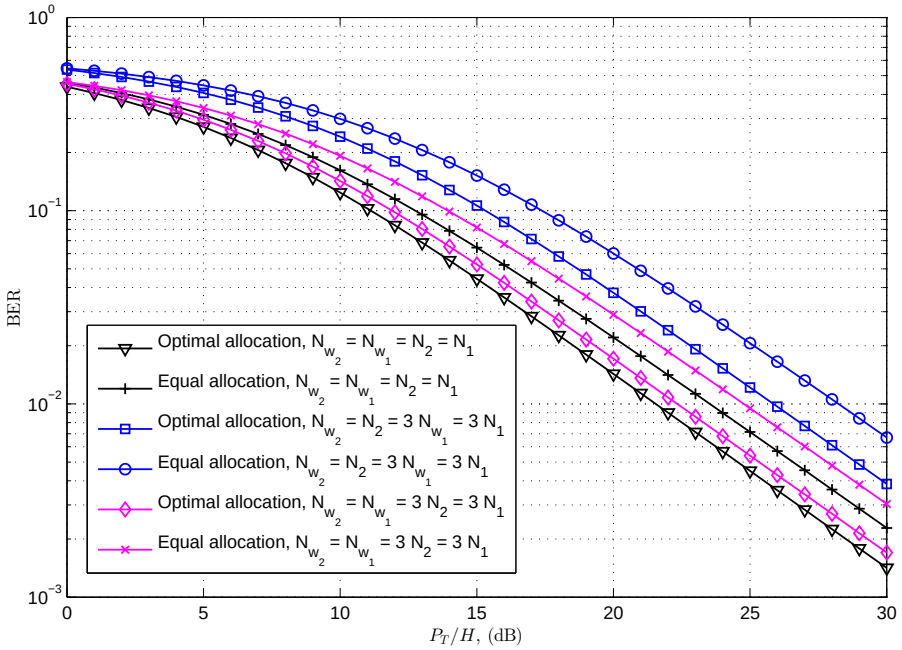

(a)

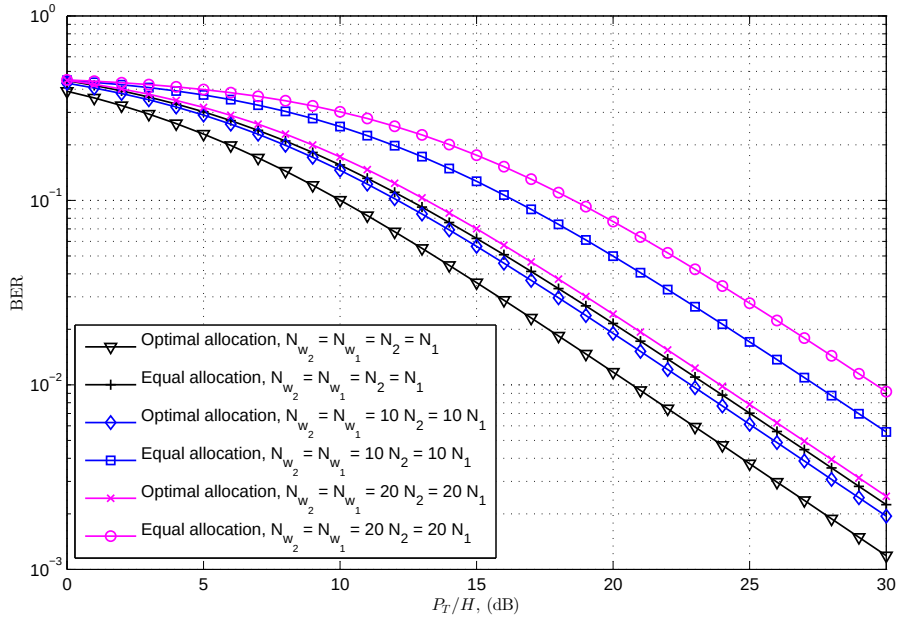

(b)

Figure 3.9: BER vs. P_T/H for AF in DCE when both h_1 and h_2 are estimated. (a) $d_1 = 1/4\ d_2$. (b) $d_1 = 1/10\ d_2$.

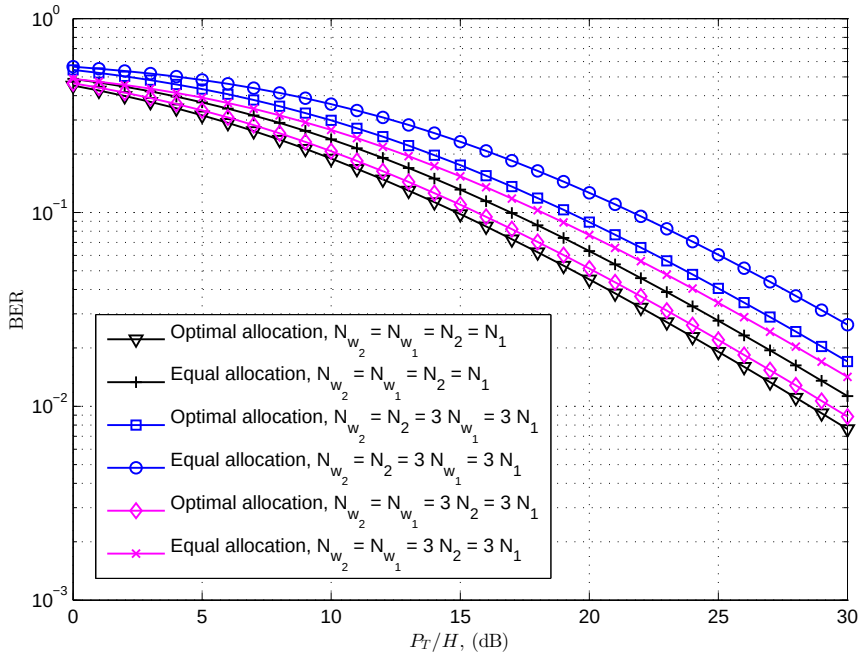

(a)

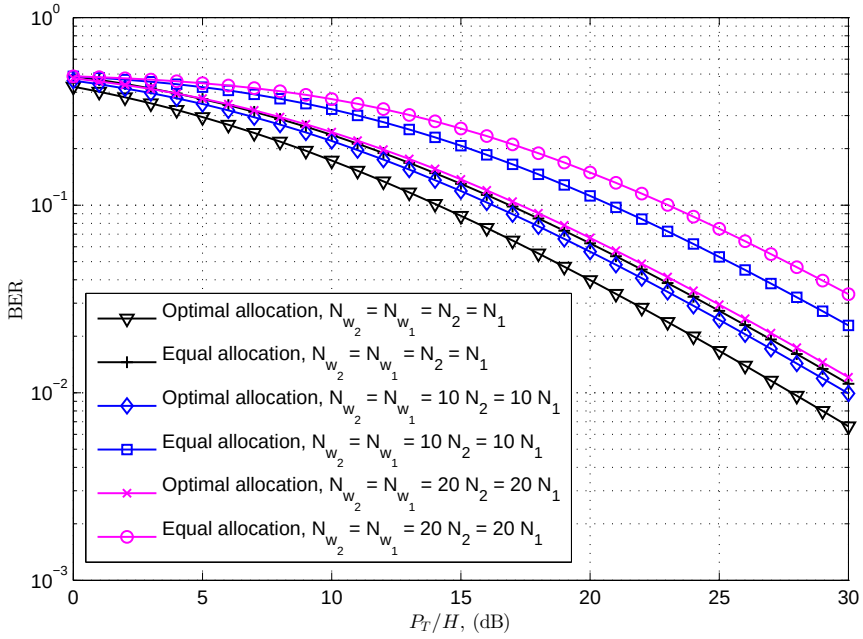

(b)

Figure 3.10: BER vs. P_T/H for AF in CCE when $G_{d_{fix_2}}$ and $G_{w_{fix_2}}$ are used. (a) $d_1 = 1/4\ d_2$. (b) $d_1 = 1/10\ d_2$.

channels. Based on these BERs, two kinds of optimal energy allocation have been studied. From the derivation, one can see that the BER expressions for CCE are more complex than those for DCE, as they include the Meijer's G - function.

Numerical results have confirmed the accuracy of the analysis. They have shown that the optimal energy allocation methods outperform the conventional system without optimal energy allocation, which could be as large as several dB's in some cases. Note that this chapter considers a single carrier system. The optimization only needs to be done once using channel statistics and can be offline. An interesting future work is to extend it to multi-carrier systems with higher spectral efficiency, provided that closed-form expressions for BER can be obtained.

Chapter 4

Performance Analysis for Amplify-and-Forward Relaying with Randomly Distributed and Fixed Interferers

4.1 Introduction

Wireless relaying can extend the network coverage by using idle nodes as relays in the network. It can also provide diversity gain by using idle nodes as virtual antennas [9]. In practical systems, it is often the case that more than one idle node is available at the same time such that multiple relays can be used by the source. If all the idle nodes are used in wireless relaying, orthogonal channels between relays have to be used in the second relaying phase such that the relayed signals will not interfere with each other. This will reduce the usage efficiency of the system resources considerably. To solve this problem, relay

selection can be used by choosing only one node out of all available idle nodes in the second phase [66]. It can be shown that relay selection can achieve the same diversity gain as the scheme that uses all available idle nodes, with proper designs [17]. Thus, this chapter focuses on relay selection using AF as an effective technology to achieve reliable communications.

Several researchers have studied the performance of relay selection using AF. In [117], the optimal relay selection criterion was proposed by selecting the relay with the largest instantaneous end-to-end or global SNR for forwarding. The performance of this criterion was analyzed in [118]. In [67], two suboptimal relay selection schemes based on two upper bounds to the instantaneous global SNR were proposed and analyzed. Reference [70] proposed partial relay selection scheme where relay selection is based on only the instantaneous SNR of the first hop. In [66], both the optimal selection scheme and the partial selection scheme were analyzed for Nakagami-m fading channels. However, none of these works has considered the interferences from other transmitting sources in the network.

In a multiple-access system or a frequency-reused cell, interferences from other transmitting sources, such as interferers, may cause performance degradation and therefore, cannot be ignored. Moreover, the positions of the nodes may not be optimized such that interferers may be randomly distributed. In this case, the spatially averaged (over the distributions of the positions) performance metrics may be of more practical use for system design and optimization by considering random locations of interferers.

Reference [119] provided the closed-form expression of the outage probability of dual-hop AF relaying in the presence of interference at the destination over Rayleigh fading channels. Reference [53] analyzed the outage probabil-

ity of a dual-hop AF relaying system where both relay and destination are interfered by a single source in Nakagami-m fading channel. However these two works either considered interferers only at the destination over Rayleigh fading channels or only a signal interferer of fixed location.

In this chapter, a comprehensive analytical framework is provided to derive the outage probability performance of an AF relay selection system where the relays suffer from path loss, independent but non-identically distributed Nakagami-m fading as well as Nakagami-m interferences. The optimal criterion that selects the relay with the largest instantaneous global SINR is studied. The contributions and findings of this chapter can be summarized as follows:

• First, it is assumed the interferers have random number and locations. This is the case for multiple-access systems with mobile nodes. With the help of GGA, the exact outage probability of this case in the form of one-dimensional integral is derived. Then, lower bound of this outage probability with simplified form is given. More importantly, asymptotic expression are provided to show several insights and intuitions. Special cases (i.e. dominant interferences in both relay and destination, Rayleigh distributed signals) are also proposed.

• Then, it is assumed the interferers have fixed number and locations. This is the case for fixed-access wireless systems where wireless interconnections are mainly provided to replace wires with considerably low or little mobility. The exact outage probability in terms of one-dimensional integral is derived. Then, closed-form lower bound of this outage probability is given. Moreover, asymptotic expression of outage probability with simplified form is presented for large SINR values. Special cases (i.e. i.i.d. interferences, domi-

nant interferences, Rayleigh distributed signals) are also proposed with several insights.

• Finally, numerical results are presented to show the accuracy of our analysis and therefore to examine the effects of the number and the locations of the interferences on relay selection using AF. They show that with the increase of SINR, the outage probability decreases accordingly for both random and fixed interferers. They also show that with the change of interference-to-noise ratio (INR) but with the SINR fixed, the outage probability for random interferers change correspondingly while the outage probability for fixed interferers remains almost the same.

The remainder of this chapter is organized as follows. Section 4.2 introduces the system model. Section 4.3 considers the case when the interferers have random number and locations, while Section 4.4 studies the case when the interferers have fixed number and locations. Numerical results are presented to examine our theoretical analysis in Section 4.5, followed by concluding remarks in Section 4.6.

4.2 System Model

Consider a wireless relaying system with one source S, one destination D and J relays R_j, $j = 1, 2, \cdots, J$, as shown in Fig. 4.1. Assume there is no direct link between the source and destination, which is the case when relays are used to extend network coverage and is the focus of this chapter. All nodes have a single antenna and are in half-duplex mode.

Assume that there are I^{sj} interferers denoted by I_i^{sj}, $i = 1, 2, \cdots, I^{sj}$, and I^{jd} interferers denoted by I_v^{jd}, $v = 1, 2, \cdots, I^{jd}$, that are transmitting at

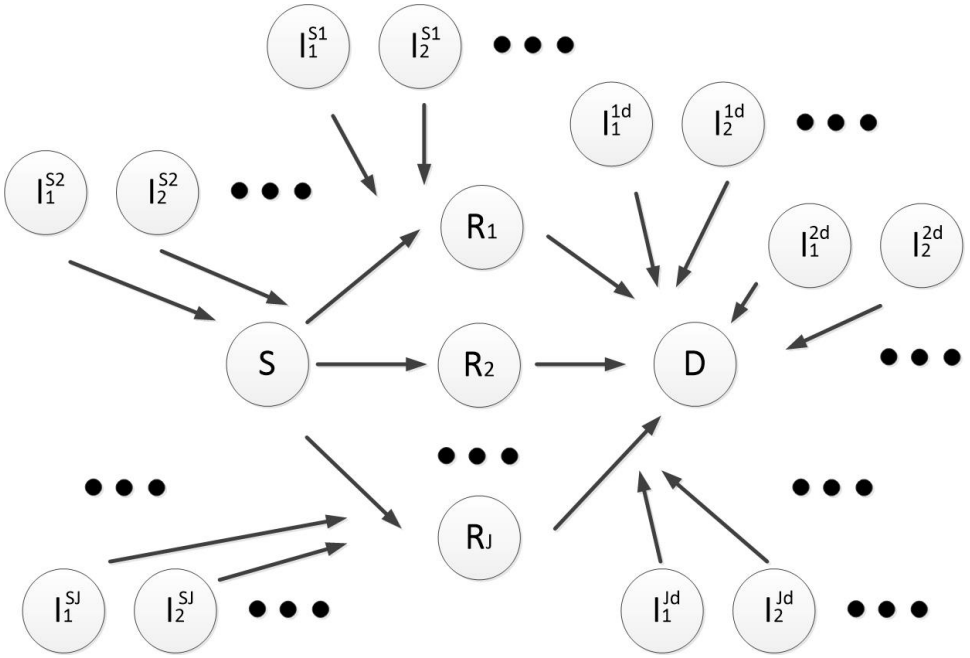

Figure 4.1: System model.

the same time as the source to the j-th relay and the j-th relay to the destination, causing interference to the j-th relay and the destination, respectively. Assume that the distance between the source S and the j-th relay R_j, the j-th relay R_j and the destination D, the i-th interferer I_i^{sj} and the j-th relay R_j and the v-th interferer I_v^{jd} and the destination D are l_{sj}, l_{jd}, l_{ij} and l_{vj}, respectively. Also, assume that the path loss between S and R_j, R_j and D, I_i^{sj} and R_j, I_v^{jd} and D are $\eta(l_{sj})$, $\eta(l_{jd})$, $\eta(l_{ij})$ and $\eta(l_{vj})$, respectively. As the singular path loss model always leads to impractical power condition in the network when $l < 1$, the non-singular model for the path loss is assumed as [120]

$$\eta(l) = \frac{1}{l^{\beta} + 1} \tag{4.1}$$

where β is the path loss exponent.

In the case when the interferers have random number and locations,

this chapter assumes the numbers I^{sj}, I^{jd} and the distances l_{ij}, l_{vj} are random. Also, assume a Poisson point process (PPP) with density λ_I for the spatial distribution of the interferers. Then, the PDF of the number of interferers is given as

$$Pr\{i = I\} = \frac{(\lambda_I A_I)^I}{I!} e^{-\lambda_I A_I},\ I = 0, 1, \cdots \tag{4.2}$$

where A_I is the distribution area of interferers. Also, this chapter assumes that the distance l follows a general distribution with a PDF of $f_l(x)$ which can be specified for different applications considered. In the case when the interferers have fixed locations, both the number of interferers and their locations are fixed such that I^{sj}, I^{jd}, l_{ij} and l_{vj} are deterministic values.

The received signal from the source S to the j-th relay R_j is given by

$$y_{sj} = \sqrt{\Omega_{sj}} h_{sj} x + \sum_{i=1}^{I^{sj}} \sqrt{\Omega_{ij}} h_{ij} x_{ij} + n_{sj} \tag{4.3}$$

and it can be further amplified and forwarded such that the received signal at the destination is given by

$$y_{jd} = \sqrt{\Omega_{jd}} h_{jd} \cdot G_j \cdot y_{sj} + \sum_{v=1}^{I^{jd}} \sqrt{\Omega_{vj}} h_{vj} x_{vj} + n_{jd} \tag{4.4}$$

where $\Omega_{sj} = K_{sj} P_{sj} \eta(l_{sj})$, $\Omega_{jd} = K_{jd} P_{jd} \eta(l_{jd})$, $\Omega_{ij} = K_{ij} P_{ij} \eta(l_{ij})$ and $\Omega_{vj} = K_{vj} P_{vj} \eta(l_{vj})$ are the average power of the Nakagami-m fading gain in the channel between the source S and the j-th relay R_j, the j-th relay R_j and the destination D, the i-th interferer I_i^{sj} and the j-th relay R_j, and the v-th interferer I_v^{jd} and the destination D, respectively, P_{sj}, P_{jd}, P_{ij} and P_{vj} are the transmitted power of S, R_j, I_i^{sj} and I_v^{jd}, respectively, K_{sj}, K_{jd}, K_{ij} and K_{vj} are constants that take other power factors, such as antenna gains and the

average signal power factors, into account, h_{sj}, h_{jd}, h_{ij} and h_{vj} are the fading gains with unit average power between S and R_j, R_j and D, I_i^{sj} and R_j, I_v^{jd} and D, respectively, x, x_{ij} and x_{vj} are the transmitted symbol of S, I_i^{sj} and I_v^{jd}, respectively, n_{sj}, n_{jd} are the additive white Gaussian noise (AWGN) in the channel between S and R_j, R_j and D, respectively, and G_j is the amplification factor.

In the above, assume enough distances between relays, and between source and relays, and between relays and destination such that $|h_{sj}|$, $j = 1, 2, \cdots, J$, are independent of each other, $|h_{jd}|$, $j = 1, 2, \cdots, J$ are independent of each other and $|h_{sj}|$ are independent of $|h_{jd}|$. Similarly, assume that n_{sj} are independent of each other for different j, n_{jd} are independent of each other for different j, and n_{sj} are independent of n_{jd}. Also, assume enough distances between interferers at the relay and between interferers at the destination such that I_i^{sj}, $|h_{ij}|$, $i = 1, 2, \cdots, I^{sj}$, at R_j are independent of each other, respectively, and I_v^{jd}, $|h_{vj}|$, $v = 1, 2, \cdots, I^{jd}$, at D are independent of each other, respectively. Also assume that interferers change from broadcasting phase to relaying phase such that interferences at the destination are independent of those at the relays.

Note that I_i^{sj}, $|h_{ij}|$ are independent of I_v^{jd}, $|h_{vj}|$, respectively, for different values of j, as it is not possible to have the same interferences in the signals from different relays to destination. Otherwise, the relays have to transmit their signals at the same time in the same frequency band and the destination will not be able to tell which signal is from which relay.

Based on the discussions above, this chapter assumes the independent Nakagami-m fading channels such that the fading powers $|h_{sj}|^2$, $|h_{jd}|^2$, $|h_{ij}|^2$, and $|h_{vj}|^2$ are independent Gamma RVs with shape parameters m_{sj}, m_{jd}, m_{ij},

m_{vj} and scale parameters $1/m_{sj}$, $1/m_{jd}$, $1/m_{ij}$, $1/m_{vj}$, respectively, where the Nakagami-m parameters are assumed to be integers. Also, assume $E(|x|^2) = 1$, $E(|x_{ij}|^2) = 1$ and $E(|x_{vj}|^2) = 1$ such that the actual average signal power is absorbed by Ω_{sj}, Ω_{ij} and Ω_{vj}, respectively.

Denote $\sigma_{sj}^2 = E(|n_{sj}|^2)$ as the noise power at R_j, and $\sigma_{jd}^2 = E(|n_{jd}|^2)$ as the noise power at D. Let $Y_{sj} = \sum_{i=1}^{I^{sj}} \Omega_{ij}|h_{ij}|^2$ and $Y_{jd} = \sum_{v=1}^{I^{jd}} \Omega_{vj}|h_{vj}|^2$. Define the SNR at R_j and D as $\gamma_{sj}^{SNR} = \frac{E(\Omega_{sj}|h_{sj}|^2)}{\sigma_{sj}^2}$ and $\gamma_{jd}^{SNR} = \frac{E(\Omega_{jd}|h_{jd}|^2)}{\sigma_{jd}^2}$, respectively, the INR at R_j and D as $\gamma_{sj}^{INR} = \frac{E(Y_{sj})}{\sigma_{sj}^2}$ and $\gamma_{jd}^{INR} = \frac{E(Y_{jd})}{\sigma_{jd}^2}$, respectively, and the SINR at R_j and D as $\gamma_{sj}^{SINR} = \frac{E(\Omega_{sj}|h_{sj}|^2)}{\sigma_{sj}^2+E(Y_{sj})}$ and $\gamma_{jd}^{SINR} = \frac{E(\Omega_{jd}|h_{jd}|^2)}{\sigma_{jd}^2+E(Y_{jd})}$, respectively.

Using these assumptions, for variable-gain relaying, the amplification factor considering interference is given by

$$G_j = \frac{1}{\sqrt{\Omega_{sj}|h_{sj}|^2 + \sigma_{sj}^2 + \sum_{i=1}^{I^{sj}} \Omega_{ij}|h_{ij}|^2}}. \tag{4.5}$$

Using (4.5) in (4.4), the instantaneous end-to-end SINR of the j-th relaying link can be derived as

$$\Gamma_j = \frac{\Gamma_{sj}\Gamma_{jd}}{\Gamma_{sj} + \Gamma_{jd} + 1} \tag{4.6}$$

where

$$\Gamma_{sj} = \frac{\Omega_{sj}|h_{sj}|^2}{\sigma_{sj}^2 + Y_{sj}} \tag{4.7}$$

and

$$\Gamma_{jd} = \frac{\Omega_{jd}|h_{jd}|^2}{\sigma_{jd}^2 + Y_{jd}}. \tag{4.8}$$

In relay selection, the relay with the largest end-to-end instantaneous SINR is selected. Thus, the outage probability for a threshold of γ_{th} is given

by

$$P_o(\gamma_{th}) = Pr\{\max\{\Gamma_j\} < \gamma_{th}\}, \quad j = 1, 2, \cdots, J. \tag{4.9}$$

In the next sections, this outage probability is derived for different cases.

4.3 Random Interferers

First, the case when the interferers have random number and locations is considered. In this case, the randomness comes from the Nakagami-m fading powers, the number of interferers I^{sj} and I^{jd} as well as the distances l_{ij} and l_{vj}. In the first subsection, the PDFs of Y_{sj} and Y_{jd} are derived using the GGA, as their closed-form expressions are difficult to obtain, if not impossible. Then, closed-form expressions of the PDF and CDF for Γ_{sj} and Γ_{jd} are derived. In the third subsection, outage probability is derived when the relay with the largest instantaneous end-to-end SINR is selected. Last in this section, special cases are given with the simplified expressions. Note that the analysis of outage probability in this section can also be considered as an exact result when each relay and the destination have only one fixed interferer following GG distribution.

4.3.1 PDF of Y_{sj} and Y_{jd}

Exact closed-form expressions for the PDFs of Y_{sj} and Y_{jd} are not available and are difficult to obtain. As a result, only MGFs of Y_{sj} and Y_{jd} for i.i.d. channels are available in the literature [121], which use either two- or three-dimensional integrals and thus are very complicated and not convenient to use. Therefore, it is nearly impossible to get the closed-form expressions for

the PDFs and CDFs of Y_{sj} and Y_{jd} from these MGFs because the inverse Laplace transform is further needed. Thus, in the following, GGA will be used by matching the first-order, second-order and third-order moments of Y_{sj} and Y_{jd} to the first-order, second-order and third-order moments of a GG RV. To the best of the authors' knowledge, none of the works in the literature have considered using GGA to approximate the distribution of random interferers. Numerical results in Section 4.5 will show that the GGA approximation has a very good match with the simulation results.

As Y_{sj} and Y_{jd} have the same distribution but with different parameters, the distribution of Y_{sj} is approximated first. One can get the approximate PDF of Y_{sj} using GGA (introduced in Section 2.6) as

$$f_{Y_{sj}}(x; a_{sj}, d_{sj}, p_{sj}) = \frac{p_{sj}\ a_{sj}^{-d_{sj}} x^{d_{sj}-1} e^{-\left(\frac{x}{a_{sj}}\right)^{p_{sj}}}}{\Gamma\left(\frac{d_{sj}}{p_{sj}}\right)}, x > 0 \tag{4.10}$$

where $d_{sj} > 0, p_{sj} > 0$ are shape parameters and $a_{sj} > 0$ is the scale parameter to be determined. It is shown in Appendix B.1 that one can calculate p_{sj} and d_{sj} in (4.10) by solving the two equations as

$$\begin{cases} B\left(\frac{d_{sj}+1}{p_{sj}}, \frac{d_{sj}+2}{p_{sj}}\right) = \frac{E(Y_{sj})E(Y_{sj}^2)}{E(Y_{sj}^3)} B\left(\frac{d_{sj}}{p_{sj}}, \frac{d_{sj}+3}{p_{sj}}\right) \\ B\left(\frac{d_{sj}+1}{p_{sj}}, \frac{d_{sj}+1}{p_{sj}}\right) = \frac{E(Y_{sj})^2}{E(Y_{sj}^2)} B\left(\frac{d_{sj}}{p_{sj}}, \frac{d_{sj}+2}{p_{sj}}\right) \end{cases} \tag{4.11}$$

where $E(Y_{sj})$, $E(Y_{sj}^2)$ and $E(Y_{sj}^3)$ can be found in equations (B.2), (B.3) and (B.4), respectively, and then one can calculate a_{sj} by inserting the solved values of p_{sj} and d_{sj} into one of the equations in (B.5). Also, when all the interferers are i.i.d., with the help of $e^{\lambda} = \sum_{I=0}^{\infty} \frac{\lambda^I}{I!}$, $e^{\lambda} = \frac{1}{\lambda} \sum_{I=1}^{\infty} I \frac{\lambda^I}{I!}$ or $e^{\lambda} = \frac{1}{\lambda^2} \sum_{I=1}^{\infty} I(I-1) \frac{\lambda^I}{I!}$, $e^{\lambda} = \frac{1}{\lambda^3} \sum_{I=1}^{\infty} I(I-1)(I-2) \frac{\lambda^I}{I!}$ [87], $E(Y_{sj})$, $E(Y_{sj}^2)$ and

$E(Y_{sj}^3)$ can be simplified as

$$\begin{cases} E(Y_{sj}) = I^{sj} K_{ij} P_{ij} \eta_{1,ij} \\ E(Y_{sj}^2) = I^{sj} K_{ij}^2 P_{ij}^2 \eta_{2,ij} \frac{m_{ij}+1}{m_{ij}} + (I^{sj})^2 K_{i_1 j} P_{i_1 j} K_{i_2 j} P_{i_2 j} \eta_{1,ij}^2 \\ E(Y_{sj}^3) = I^{sj} K_{ij}^3 P_{ij}^3 \frac{(m_{ij}+1)(m_{ij}+2)}{m_{ij}^2} \eta_{3,ij} + (I^{sj})^2 K_{i_1 j}^2 P_{i_1 j}^2 K_{i_2 j} P_{i_2 j} \frac{m_{ij}+1}{m_{ij}} \\ \times \eta_{2,ij} \eta_{1,ij} + (I^{sj})^3 K_{i_1 j} P_{i_1 j} K_{i_2 j} P_{i_2 j} K_{i_3 j} P_{i_3 j} \eta_{1,ij}^3. \end{cases} \tag{4.12}$$

The PDF expression $f_{Y_{jd}}(x; a_{jd}, d_{jd}, p_{jd})$ of Y_{jd} can be obtained using the same method as

$$f_{Y_{jd}}(x; a_{jd}, d_{jd}, p_{jd}) = \frac{p_{jd}\, a_{jd}^{-d_{jd}} x^{d_{jd}-1} e^{-\left(\frac{x}{a_{jd}}\right)^{p_{jd}}}}{\Gamma\left(\frac{d_{jd}}{p_{jd}}\right)}, x > 0, \tag{4.13}$$

where $d_{jd} > 0, p_{jd} > 0$ are shape parameters and $a_{jd} > 0$ is the scale parameter to be determined.

4.3.2 PDF and CDF of Γ_{sj} and Γ_{jd}

Denote $W_{sj} = \Omega_{sj} |h_{sj}|^2$. Since $|h_{sj}|^2$ is a Gamma RV with shape parameter m_{sj} and scale parameter $1/m_{sj}$, W_{sj} is also a Gamma RV with PDF

$$f_{W_{sj}}(x) = \left(\frac{m_{sj}}{\Omega_{sj}}\right)^{m_{sj}} \frac{x^{m_{sj}-1}}{\Gamma(m_{sj})} e^{-\frac{m_{sj}}{\Omega_{sj}} x}, x \geq 0. \tag{4.14}$$

Also, denote $Z_{sj} = Y_{sj} + \sigma_{sj}^2$, where the PDF of Z_{sj} is determined by $f_{Z_{sj}}(x) = f_{Y_{sj}}(x - \sigma_{sj}^2)$ for $x \geq \sigma_{sj}^2$. Thus, one has $\Gamma_{sj} = \frac{W_{sj}}{Z_{sj}}$ and the PDF of Γ_{sj} is given by

$$f_{\Gamma_{sj}}(u) = \int_{-\infty}^{\infty} |x|\, f_{W_{sj}}(xu)\, f_{Y_{sj}}\left(x - \sigma_{sj}^2\right) dx. \tag{4.15}$$

Using (4.10) and (4.14) in (4.15) and defining $p_{sj} = l_{sj}/k_{sj}$ and also assuming $gcd(l_{sj}, k_{sj}) = 1$ where $gcd(\cdot,\cdot)$ is the greatest common devisor operator [36], one has

$$f_{\Gamma_{sj}}(u) = \sum_{r_1=0}^{m_{sj}} \mu_{1,sj,r_1} e^{-\frac{m_{sj}\sigma_{sj}^2 u}{\Omega_{sj}}} u^{-d_{sj}+m_{sj}-r_1-1} \times G_{l_{sj},k_{sj}}^{k_{sj},l_{sj}}\left(\mu_{0,sj}u^{-l_{sj}}\middle| \begin{matrix} I(l_{sj}, 1-d_{sj}-r_1) \\ I(k_{sj},0) \end{matrix}\right), \tag{4.16}$$

where $\mu_{0,sj} = k_{sj}^{-k_{sj}} l_{sj}^{l_{sj}} a_{sj}^{-k_{sj}p_{sj}} \left(\frac{m_{sj}}{\Omega_{sj}}\right)^{-l_{sj}}$,

$\mu_{1,sj,r_1} = \frac{l_{sj}^{d_{sj}+r_1-\frac{1}{2}} \sigma_{sj}^{2(m_{sj}-r_1)} \left(\frac{m_{sj}}{\Omega_{sj}}\right)^{-d_{sj}+m_{sj}-r_1} \sqrt{k_{sj}} p_{sj} m_{sj}! a_{sj}^{-d_{sj}} (2\pi)^{-\frac{k_{sj}}{2}-\frac{l_{sj}}{2}+1}}{r_1!(m_{sj}-r_1)!\Gamma(m_{sj})\Gamma\left(\frac{d_{sj}}{p_{sj}}\right)}$,

$I(n,\xi) = (\xi/n, (\xi+1)/n, \cdots, (\xi+n-1)/n)$ and $G_{a,b}^{c,d}(\cdot)$ denotes the Meijer'G-function [36] which is available as a built-in function in many mathematical software packages, such as MATLAB, MATHEMATICA and MAPLE.

Proof: See Appendix B.2.

Also, one can get the CDF of Γ_{sj} as

$$F_{\Gamma_{sj}}(u) = 1 - \sum_{r_2=0}^{m_{sj}-1} \sum_{r_3=0}^{r_2} \mu_{2,sj,r_2,r_3} e^{-\frac{m_{sj}\sigma_{sj}^2 u}{\Omega_{sj}}} u^{-d_{sj}+r_2-r_3} \times G_{l_{sj},k_{sj}}^{k_{sj},l_{sj}}\left(\mu_{0,sj}u^{-l_{sj}}\middle| \begin{matrix} I(l_{sj}, 1-d_{sj}-r_3) \\ I(k_{sj},0) \end{matrix}\right) \tag{4.17}$$

where $\mu_{2,sj,r_2,r_3} = \frac{l_{sj}^{d_{sj}+r_3-\frac{1}{2}} \sigma_{sj}^{2(r_2-r_3)} \left(\frac{m_{sj}}{\Omega_{sj}}\right)^{-d_{sj}+r_2-r_3} \sqrt{k_{sj}} p_{sj} a_{sj}^{-d_{sj}} (2\pi)^{-\frac{k_{sj}}{2}-\frac{l_{sj}}{2}+1}}{r_3!(r_2-r_3)!\Gamma\left(\frac{d_{sj}}{p_{sj}}\right)}$.

Proof: See Appendix B.3.

The PDF and CDF of Γ_{sj} in (4.16) and (4.17) in terms of the Meijer'G-function are computationally complex. Therefore, the high SINR approximations that have simpler forms are provided next. Using the following Taylor's

series expansion

$$e^x = \sum_{n=0}^{N} \frac{x^n}{n!} + o(x^N), \qquad \text{as} \quad x \to 0, \tag{4.18}$$

where N is the positive integer and $o(x)$ denotes the higher-order term of an arbitrary function $a(x)$, one can get the PDF and CDF of Γ_{sj} as (4.19) and (4.20), respectively.

$$\begin{aligned} f_{\Gamma_{sj}}(u) = &\sum_{n_1=0}^{N_1} \sum_{n_3=0}^{N_3} \sum_{r_1=0}^{m_{sj}} \mu_{5,sj,r_1,n_1,n_3} u^{m_{sj}+n_1+n_3-1} + o\left[(u/\Omega_{sj})^{N_1}\right] \\ &+ o\left[(\sigma_{sj}^2 u/\Omega_{sj})^{N_3}\right], \end{aligned} \tag{4.19}$$

where $\mu_{5,sj,r_1,n_1,n_3} = \frac{(-1)^{n_1+n_3} a_{sj}^{n_1+r_1} m_{sj}^{m_{sj}+n_1+n_3+1} \Omega_{sj}^{-m_{sj}-n_1-n_3} \sigma_{sj}^{2(m_{sj}-r_1+n_3)} \Gamma\left(\frac{d_{sj}+n_1+r_1}{p_{sj}}\right)}{n_1! n_3! \Gamma(r_1+1)\Gamma(m_{sj}-r_1+1)\Gamma\left(\frac{d_{sj}}{p_{sj}}\right)}$, and N_1, N_3 are the positive integers.

$$\begin{aligned} F_{\Gamma_{sj}}(u) = 1 - &\sum_{n_2=0}^{N_2} \sum_{n_4=0}^{N_4} \sum_{r_2=0}^{m_{sj}-1} \sum_{r_3=0}^{r_2} \mu_{6,sj,r_2,r_3,n_2,n_4} u^{n_2+r_2+n_4} \\ &+ o\left[(u/\Omega_{sj})^{N_2}\right] + o\left[(\sigma_{sj}^2 u/\Omega_{sj})^{N_4}\right], \end{aligned} \tag{4.20}$$

where $\mu_{6,sj,r_2,r_3,n_2,n_4} = \frac{(-1)^{n_2+n_4} a_{sj}^{n_2+r_3} \sigma_{sj}^{2(r_2-r_3+n_4)} \left(\frac{m_{sj}}{\Omega_{sj}}\right)^{n_2+r_2+n_4} \Gamma\left(\frac{d_{sj}+n_2+r_3}{p_{sj}}\right)}{n_2! n_4! r_3! (r_2-r_3)! \Gamma\left(\frac{d_{sj}}{p_{sj}}\right)}$, and N_2, N_4 are the positive integers.

Proof: See Appendix B.4.

In high SINR conditions when $\Omega_{sj} \to \infty$ or $\sigma_{sj}^2 \to 0$ or in the low outage regime when $u \to 0$, one can set $N_1 = N_2 = N_3 = N_4 = 1$ and get rid of $o\left[(u/\Omega_{sj})^{N_1}\right]$, $o\left[(u/\Omega_{sj})^{N_2}\right]$, $o\left[(\sigma_{sj}^2 u/\Omega_{sj})^{N_3}\right]$ and $o\left[(\sigma_{sj}^2 u/\Omega_{sj})^{N_4}\right]$ in (4.19) and (4.20) to obtain corresponding approximations, respectively.

The PDF and CDF expressions $f_{\Gamma_{jd}}(u)$ and $F_{\Gamma_{jd}}(u)$ and their high SINR approximations can be obtained using the same method as above. They can be found in Appendix B.5.

4.3.3 Outage Probability

Using the derived PDF and CDFs of Γ_{sj} and Γ_{jd} in the previous subsection, the CDF of the instantaneous end-to-end SINR in (4.6) can be derived as [66]

$$\begin{aligned} F_{\Gamma_j}^{E}(x) &= \int_0^{\infty} Pr\left\{\frac{\Gamma_{sj}\Gamma_{jd}}{\Gamma_{sj}+\Gamma_{jd}+1} \leq x | t\right\} f_{\Gamma_{sj}}(t)dt \\ &= F_{\Gamma_{sj}}(x) + \int_0^{\infty} F_{\Gamma_{jd}}\left(\frac{x^2+x+xt}{t}\right) f_{\Gamma_{sj}}(t+x)dt. \end{aligned} \tag{4.21}$$

One can see that (4.21) only has a one-dimensional integral, which can be calculated numerically using mathematical software. Also, by using the lower bound as

$$F_{\Gamma_j}(x) \geqslant 1 - \left[1 - F_{\Gamma_{sj}}(x)\right]\left[1 - F_{\Gamma_{jd}}(x)\right] = F_{\Gamma_j}^{LB}(x), \tag{4.22}$$

one can get the lower bound to the CDF as

$$\begin{aligned} F_{\Gamma_j}^{LB}(x) = 1 - &\sum_{r_2=0}^{m_{sj}-1}\sum_{r_3=0}^{r_2}\sum_{r_2'=0}^{m_{jd}-1}\sum_{r_3'=0}^{r_2'} \mu_{2,sj,r_2,r_3}\mu_{2,jd,r_2',r_3'} e^{-\frac{m_{sj}\sigma_{sj}^2 x}{\Omega_{sj}} - \frac{m_{jd}\sigma_{jd}^2 x}{\Omega_{jd}}} \\ &\times x^{-d_{sj}+r_2-r_3-d_{jd}+r_2'-r_3'} G_{l_{sj},k_{sj}}^{k_{sj},l_{sj}}\left(\mu_{0,sj}x^{-l_{sj}}\middle|\begin{matrix} I(l_{sj}, 1-d_{sj}-r_3) \\ I(k_{sj},0) \end{matrix}\right) \\ &\times G_{l_{jd},k_{jd}}^{k_{jd},l_{jd}}\left(\mu_{0,jd}x^{-l_{jd}}\middle|\begin{matrix} I(l_{jd}, 1-d_{jd}-r_3') \\ I(k_{jd},0) \end{matrix}\right), \end{aligned} \tag{4.23}$$

where $\mu_{0,jd} = k_{jd}^{-k_{jd}} l_{jd}^{l_{jd}} a_{jd}^{-k_{jd}p_{jd}} \left(\frac{m_{jd}}{\Omega_{jd}}\right)^{-l_{jd}}$, and

$$\mu_{2,jd,r_2',r_3'} = \frac{l_{jd}^{d_{jd}+r_3'-\frac{1}{2}} \sigma_{jd}^{2(r_2'-r_3')} \left(\frac{m_{jd}}{\Omega_{jd}}\right)^{-d_{jd}+r_2'-r_3'} \sqrt{k_{jd}} p_{jd} a_{jd}^{-d_{jd}} (2\pi)^{-\frac{k_{jd}}{2}-\frac{l_{jd}}{2}+1}}{r_3'!(r_2'-r_3')!\Gamma\left(\frac{d_{jd}}{p_{jd}}\right)}.$$

Also, if one inserts the CDFs of high SINR approximations into (4.22) and with the help of (B.1), one can get the asymptotic expression of the CDF as

$$\begin{aligned} F_{\Gamma_j}^{\infty}(x) = 1 - \sum_{n_2=0}^{N_2} \sum_{n_4=0}^{N_4} \sum_{r_2=0}^{m_{sj}-1} \sum_{r_3=0}^{r_2} \sum_{n_2'=0}^{N_2'} \sum_{n_4'=0}^{N_4'} \sum_{r_2'=0}^{m_{jd}-1} \sum_{r_3'=0}^{r_2'} x^{n_2+r_2+n_4+n_2'+r_2'+n_4'} \\ \times \left(\frac{m_{sj}}{\Omega_{sj}}\right)^{n_2+r_2+n_4} \left(\frac{m_{jd}}{\Omega_{jd}}\right)^{n_2'+r_2'+n_4'} E\left(Y_{sj}^{n_2+r_3}\right) E\left(Y_{jd}^{n_2'+r_3'}\right) \\ \times \frac{(-1)^{n_2+n_4+n_2'+n_4'} \sigma_{sj}^{2(r_2-r_3+n_4)} \sigma_{jd}^{2(r_2'-r_3'+n_4')}}{n_2! n_4! r_3! (r_2-r_3)! n_2'! n_4'! r_3'! (r_2'-r_3')!} \end{aligned} \tag{4.24}$$

where $E\left(Y_{sj}^{n_2+r_3}\right) = \frac{a_{sj}^{n_2+r_3}\Gamma\left(\frac{d_{sj}+n_2+r_3}{p_{sj}}\right)}{\Gamma\left(\frac{d_{sj}}{p_{sj}}\right)}$, $E\left(Y_{jd}^{n_2'+r_3'}\right) = \frac{a_{jd}^{n_2'+r_3'}\Gamma\left(\frac{d_{jd}+n_2'+r_3'}{p_{jd}}\right)}{\Gamma\left(\frac{d_{jd}}{p_{jd}}\right)}$.

Then, the outage probability for AF relay selection is given by

$$P_o^{\Psi}(\gamma_{th}) = \prod_{j=1}^{J} F_{\Gamma_j}^{\Psi}(\gamma_{th}) \tag{4.25}$$

where Ψ in (4.25) can be E using $F_{\Gamma_j}^{E}(x)$ to get the exact outage probability, LB using $F_{\Gamma_j}^{LB}(x)$ to get lower bound, and ∞ using $F_{\Gamma_j}^{\infty}(\gamma_{th})$ to get the asymptotic expression for the outage probability.

Using the simple form in (4.24), several insights can be obtained. For example, in the low outage regime when $\gamma_{th} \to 0$, the above result becomes exact. Also, one can see from (4.24) that when the Nakagami-m parameters of the interference m_{ij} or m_{vj} ($\gg 1$) are large and increase, the outage probability remains almost unchanged. This is because m_{ij} or m_{vj} only have an influence

on the order of interference power, as can be seen from (B.2), (B.3) and (B.4) in Appendix B.1, where the c-th order moment of interference power $E\left(Y_{sj}\right)$ or $E\left(Y_{jd}\right)$ remains almost unchanged when m_{ij} or m_{vj} are large. For small values of m_{ij} or m_{vj} (≈ 1), they still have some influence on the outage probability, as $\frac{m_{ij}+1}{m_{ij}}$ in (B.3) and $\frac{(m_{ij}+1)(m_{ij}+2)}{m_{ij}^2}$ in (B.4) cannot be ignored if $m_{ij} \approx 1$ (They approach 1 when $m_{ij} \to 0$). This phenomenon will be shown in Fig. 4.2 by simulation in Section 4.5.

Also, one can see from (4.24) that, when the SINR increases (i.e. Ω_{sj} or Ω_{jd} increase, or σ_{sj}^2 or σ_{jd}^2 decrease, or $E\left(Y_{sj}\right)$ or $E\left(Y_{jd}\right)$ decrease), the outage probability decreases accordingly, which will be shown in Fig. 4.4 and Fig. 4.5 in Section 4.5. Further, for fixed SINR, if one decreases INR (i.e. decreases the interference power $E\left(Y_{sj}\right)$ or $E\left(Y_{jd}\right)$), the outage probability still decreases. This is because the order of the interference power $E\left(Y_{sj}^{n_2+r_3}\right)$ or $E\left(Y_{jd}^{n_2'+r_3'}\right)$ in (4.24) also affects the outage probability. The rate of decrease becomes small when the diversity order (determined by m_{sj} or m_{jd}) is small. Therefore, when the signal experiences Rayleigh fading (i.e. $m_{sj} = 1$ or $m_{jd} = 1$), the outage probability remains almost unchanged if one changes INR but keeps SINR fixed. These explanations will be verified in Fig. 4.3 and Fig. 4.4 in Section 4.5.

Furthermore, since the possible boundary of the interferers and the pass loss between the interferer and the signal have influence on the order of interference power (referring to (B.2), (B.3) and (B.4) in Appendix B.1), changing the possible boundary and the pass loss also changes the outage probability, even if one keeps the SINR and INR fixed. Similar to before, for the Rayleigh case, the outage probability changes little if one keeps SINR and INR fixed. These discussions will be verified in Fig. 4.6 and Fig. 4.7 in Section

4.5.

Another insight that can be obtained from (4.24) is that, when m_{sj} or m_{jd} increase, the outage probability decreases, as m_{sj} or m_{jd} are in the upper limits of the summations in (4.24), which will also be examined in Fig. 4.3 - Fig. 4.7 in Section 4.5.

4.3.4 Special Cases

For the sake of simplicity, this subsection now focus on the case when the interferences are dominant at both relay and destination. By setting $\sigma_{sj}^2 \approx 0$ and $\sigma_{jd}^2 \approx 0$ in (4.24), one can get the asymptotic CDF in this case as

$$F_{\Gamma_j}^{\infty}(x) = 1 - \sum_{n_2=0}^{N_2} \sum_{r_2=0}^{m_{sj}-1} \sum_{n_2'=0}^{N_2'} \sum_{r_2'=0}^{m_{jd}-1} x^{n_2+r_2+n_2'+r_2'} \frac{(-1)^{n_2+n_2'} \left(\frac{m_{sj}}{\Omega_{sj}}\right)^{n_2+r_2} \left(\frac{m_{jd}}{\Omega_{jd}}\right)^{n_2'+r_2'} E\left(Y_{sj}^{n_2+r_2}\right) E\left(Y_{jd}^{n_2'+r_2'}\right)}{n_2! r_2! n_2'! r_2'!}, \tag{4.26}$$

where $E\left(Y_{sj}^{n_2+r_2}\right) = \frac{a_{sj}^{n_2+r_2} \Gamma\left(\frac{d_{sj}+n_2+r_2}{p_{sj}}\right)}{\Gamma\left(\frac{d_{sj}}{p_{sj}}\right)}$, $E\left(Y_{jd}^{n_2'+r_2'}\right) = \frac{a_{jd}^{n_2'+r_2'} \Gamma\left(\frac{d_{jd}+n_2'+r_2'}{p_{jd}}\right)}{\Gamma\left(\frac{d_{jd}}{p_{jd}}\right)}$.

In another special case when the signal experiences Rayleigh fading channel, by setting $m_{sj} = 1$ and $m_{jd} = 1$, (4.24) is specialized to

$$F_{\Gamma_j}^{\infty}(x) = 1 - \sum_{n_2=0}^{N_2} \sum_{n_4=0}^{N_4} \sum_{n_2'=0}^{N_2'} \sum_{n_4'=0}^{N_4'} x^{n_2+n_4+n_2'+n_4'} \frac{(-1)^{n_2+n_4+n_2'+n_4'} \Omega_{sj}^{-n_2-n_4} \Omega_{jd}^{-n_2'-n_4'} \sigma_{sj}^{2n_4} \sigma_{jd}^{2n_4'} E\left(Y_{sj}^{n_2}\right) E\left(Y_{jd}^{n_2'}\right)}{n_2! n_4! n_2'! n_4'!}, \tag{4.27}$$

where $E\left(Y_{sj}^{n_2}\right) = \frac{a_{sj}^{n_2} \Gamma\left(\frac{d_{sj}+n_2}{p_{sj}}\right)}{\Gamma\left(\frac{d_{sj}}{p_{sj}}\right)}$, $E\left(Y_{jd}^{n_2'}\right) = \frac{a_{jd}^{n_2'} \Gamma\left(\frac{d_{jd}+n_2'}{p_{jd}}\right)}{\Gamma\left(\frac{d_{jd}}{p_{jd}}\right)}$.

Then, using (4.25), the outage probability for the two special cases above can be obtained.

4.4 Fixed Interferers

In this section, the case when the interferers have fixed number and locations are considered. In this case, the numbers of interferers I^{sj} and I^{jd} as well as the distances l_{ij} and l_{vj} are deterministic such that they can be all treated as constants. The only randomness comes from the Nakagami-m fading. Thus, Γ_{sj} is a function of only the random channel gains.

Note that similar derivations have also been conducted for dual-hop AF relaying without relay selection in the literature [53–55, 122–128]. However, they either consider interference at only one of the relay and the destination [54, 122–124, 126], only a single interferer [53], for fixed-gain relaying [125], for performance upper bounds [127], for interference-limited case with identical Nakagami-m channels [55], or for Rayleigh channels [128]. In the following, the exact performance for the case when both the relay and the destination suffer from multiple non-identically distributed Nakagami-m interferers will be derived and relay selection will also be considered in our derivation.

4.4.1 PDF and CDF of Γ_{sj} and Γ_{jd}

Similarly, the PDF and CDF of Γ_{sj} are derived first. Since $Y_{sj} = \sum_{i=1}^{I^{sj}} \Omega_{ij}|h_{ij}|^2$ and $|h_{ij}|^2$ are independent Gamma RVs, by proper scaling, Y_{sj} is actually a sum of independent Gamma RVs. A closed-form expression for the PDF of this sum was derived in [129]. However, this expression uses an infinite series in order to consider the general case of arbitrary shape parameters and scale

parameters. To avoid this infinite series in our result, this section uses the PDF in [130] for the case when the Nakagami-m parameters could be different but are integers. In this case, the PDF of Y_{sj} is given by [130, (4)]

$$f_{Y_{sj}}(x) = \left[\prod_{i^*=1}^{I^{sj}} \left(-\frac{\Omega_{i^*j}}{m_{i^*j}}\right)^{-m_{i^*j}}\right] \sum_{i=1}^{I^{sj}} \sum_{r=1}^{m_{ij}} \frac{(-1)^r b_{ir}}{(r-1)!} x^{r-1} e^{-\frac{m_{ij}}{\Omega_{ij}}x}, x > 0 \quad (4.28)$$

where b_{ir} is a constant given by [130, (5)], Ω_{i^*j}, m_{i^*j} are the same as Ω_{ij}, m_{ij}, respectively for the same i and j and all other symbols are defined as before. It is derived in Appendix B.6 that the PDF of Γ_{sj} can be written as

$$f_{\Gamma_{sj}}(u) = \sum_{i=1}^{I^{sj}} \sum_{r=1}^{m_{ij}} \sum_{f=0}^{m_{sj}} \varphi_{1,sj,ij,i,r,f} \frac{u^{m_{sj}-1} e^{-\frac{m_{sj}}{\Omega_{sj}}\sigma_{sj}^2 u}}{(\frac{m_{sj}}{\Omega_{sj}}u + \frac{m_{ij}}{\Omega_{ij}})^{f+r}}, \quad (4.29)$$

where $\varphi_{1,sj,ij,i,r,f} = \left[\prod_{i^*=1}^{I^{sj}} \left(-\frac{\Omega_{i^*j}}{m_{i^*j}}\right)^{-m_{i^*j}}\right] \frac{(-1)^r b_{ir} \left(\frac{m_{sj}}{\Omega_{sj}}\right)^{m_{sj}} \binom{m_{sj}}{f} (\sigma_{sj}^2)^{m_{sj}-f} \Gamma(f+r)}{\Gamma(m_{sj})(r-1)!}$,
and the CDF of Γ_{sj} can be derived as

$$F_{\Gamma_{sj}}(u) = 1 - \sum_{i=1}^{I^{sj}} \sum_{r=1}^{m_{ij}} \sum_{f=0}^{m_{sj}-1} \sum_{h=0}^{f} \varphi_{2,sj,ij,i,r,f,h} \frac{u^f e^{-\frac{m_{sj}}{\Omega_{sj}}\sigma_{sj}^2 u}}{(\frac{m_{sj}}{\Omega_{sj}}u + \frac{m_{ij}}{\Omega_{ij}})^{h+r}}, \quad (4.30)$$

where $\varphi_{2,sj,ij,i,r,f,h} = \left[\prod_{i^*=1}^{I^{sj}} \left(-\frac{\Omega_{i^*j}}{m_{i^*j}}\right)^{-m_{i^*j}}\right] \frac{(-1)^r b_{ir} \left(\frac{m_{sj}}{\Omega_{sj}}\right)^{f} \binom{f}{h} (\sigma_{sj}^2)^{f-h} \Gamma(h+r)}{(r-1)!f!}$.
Using (4.18) and the following Taylor's series expansion

$$(1+x)^{-n} = \sum_{i=0}^{N} \binom{-n}{i} x^i + o(x^N), \quad \text{as} \quad x \to 0, \quad (4.31)$$

where n and N are positive integers, one can get the high SINR approximations ($\sigma_{sj}^2/\Omega_{sj} \to 0$ and $\Omega_{ij}/\Omega_{sj} \to 0$) for PDF and CDF of Γ_{sj} as (4.32) and (4.33),

respectively.

$$f_{\Gamma_{sj}}(u) = \sum_{i=1}^{I^{sj}} \sum_{n_5=0}^{N_5} \sum_{n_6=0}^{N_6} \sum_{r=1}^{m_{ij}} \sum_{f=0}^{m_{sj}} \varphi_{3,sj,ij,i,r,f,n_5,n_6} u^{m_{sj}+n_5+n_6-1} + o\left[(\sigma_{sj}^2 u/\Omega_{sj})^{N_5}\right] + o\left[(u\Omega_{ij}/\Omega_{sj})^{N_6}\right] \tag{4.32}$$

where $\varphi_{3,sj,ij,i,r,f,n_5,n_6} = \left[\prod_{i^*=1}^{I^{sj}} \left(-\frac{\Omega_{i^*j}}{m_{i^*j}}\right)^{-m_{i^*j}}\right] \times \frac{(-1)^{r+n_5} b_{ir} \left(\frac{m_{sj}}{\Omega_{sj}}\right)^{m_{sj}+n_5+n_6} \left(\frac{m_{ij}}{\Omega_{ij}}\right)^{-f-r-n_6} \binom{m_{sj}}{f} \binom{-f-r}{n_6} (\sigma_{sj}^2)^{m_{sj}-f+n_5} \Gamma(f+r)}{\Gamma(m_{sj})(r-1)!n_5!}$,

$$F_{\Gamma_{sj}}(u) = 1 - \sum_{i=1}^{I^{sj}} \sum_{n_7=0}^{N_7} \sum_{n_8=0}^{N_8} \sum_{r=1}^{m_{ij}} \sum_{f=0}^{m_{sj}-1} \sum_{h=0}^{f} \varphi_{4,sj,ij,i,r,f,h,n_7,n_8} u^{f+n_7+n_8} + o\left[(\sigma_{sj}^2 u/\Omega_{sj})^{N_7}\right] + o\left[(u\Omega_{ij}/\Omega_{sj})^{N_8}\right], \tag{4.33}$$

where $\varphi_{4,sj,ij,i,r,f,h,n_7,n_8} = \left[\prod_{i^*=1}^{I^{sj}} \left(-\frac{\Omega_{i^*j}}{m_{i^*j}}\right)^{-m_{i^*j}}\right] \times \frac{(-1)^{r+n_7} b_{ir} \left(\frac{m_{sj}}{\Omega_{sj}}\right)^{f+n_7+n_8} \left(\frac{m_{ij}}{\Omega_{ij}}\right)^{-h-r-n_8} \binom{f}{h} \binom{-h-r}{n_8} (\sigma_{sj}^2)^{f-h+n_7} \Gamma(h+r)}{(r-1)!f!n_7!}$, and N_5, N_6, N_7, N_8 are the positive integers.

In high SINR conditions, $o\left[(\sigma_{sj}^2 u/\Omega_{sj})^{N_5}\right]$, $o\left[(u\Omega_{ij}/\Omega_{sj})^{N_6}\right]$, $o\left[(\sigma_{sj}^2 u/\Omega_{sj})^{N_7}\right]$ and $o\left[(u\Omega_{ij}/\Omega_{sj})^{N_8}\right]$ in the above equations can be removed to obtain corresponding approximations.

The PDF and CDF expressions $f_{\Gamma_{jd}}(u)$ and $F_{\Gamma_{jd}}(u)$ and their high SINR approximations can be also obtained using the same methods. They can be found in Appendix B.7.

4.4.2 Outage Probability

Using the derived exact PDF and CDFs of Γ_{sj} and Γ_{jd} into (4.21), one can get the CDF of the instantaneous end-to-end SINR in one-dimensional integral, which can be calculated numerically using mathematical software.

Then, following the same process as in Section 4.3, one can get the lower bound of the CDF as (4.34), when the exact CDFs of Γ_{sj} and Γ_{jd} are used,

$$F_{\Gamma_j}(x) \geqslant 1 - \sum_{i=1}^{I^{sj}} \sum_{r=1}^{m_{ij}} \sum_{f=0}^{m_{sj}-1} \sum_{h=0}^{f} \sum_{v=1}^{I^{jd}} \sum_{r'=1}^{m_{vj}} \sum_{f'=0}^{m_{jd}-1} \sum_{h'=0}^{f'} \frac{u^f e^{-\frac{m_{sj}}{\Omega_{sj}}\sigma_{sj}^2 u}}{(\frac{m_{sj}}{\Omega_{sj}}u + \frac{m_{ij}}{\Omega_{ij}})^{h+r}} \times \frac{u^{f'} e^{-\frac{m_{jd}}{\Omega_{jd}}\sigma_{jd}^2 u}}{(\frac{m_{jd}}{\Omega_{jd}}u + \frac{m_{vj}}{\Omega_{vj}})^{h'+r'}} \varphi_{2,sj,ij,i,r,f,h} \varphi_{2,jd,vj,v,r',f',h'} = F_{\Gamma_j}^{LB}(x), \tag{4.34}$$

where $\varphi_{2,jd,vj,v,r',f',h'} = \left[\prod_{v^*=1}^{I^{jd}} \left(-\frac{\Omega_{v^*j}}{m_{v^*j}}\right)^{-m_{v^*j}}\right] \frac{(-1)^{r'} b_{vr'} \left(\frac{m_{jd}}{\Omega_{jd}}\right)^{f'} \binom{f'}{h'} (\sigma_{jd}^2)^{f'-h'} \Gamma(h'+r')}{(r'-1)! f'!}$.

Also, using high SINR approximations of $F_{\Gamma_{sj}}$ and $F_{\Gamma_{jd}}$, one can get the asymptotic expression of the CDF as

$$F_{\Gamma_j}^{\infty}(x) = 1 - \sum_{i=1}^{I^{sj}} \sum_{n_7=0}^{N_7} \sum_{n_8=0}^{N_8} \sum_{r=1}^{m_{ij}} \sum_{f=0}^{m_{sj}-1} \sum_{h=0}^{f} \sum_{v=1}^{I^{jd}} \sum_{n_7'=0}^{N_7'} \sum_{n_8'=0}^{N_8'} \sum_{r'=1}^{m_{vj}} \sum_{f'=0}^{m_{jd}-1} \sum_{h'=0}^{f'} u^{f+n_7+n_8+f'+n_7'+n_8'} \varphi_{4,sj,ij,i,r,f,h,n_7,n_8} \varphi_{4,jd,vj,v,r',f',h',n_7',n_8'}, \tag{4.35}$$

where $\varphi_{4,jd,vj,v,r',f',h',n_7',n_8'} = \left[\prod_{v^*=1}^{I^{jd}} \left(-\frac{\Omega_{v^*j}}{m_{v^*j}}\right)^{-m_{v^*j}}\right] \frac{(-1)^{r'+n_7'} b_{vr'} \left(\frac{m_{jd}}{\Omega_{jd}}\right)^{f'+n_7'+n_8'} \left(\frac{m_{vj}}{\Omega_{vj}}\right)^{-h'-r'-n_8'} \binom{f'}{h'} \binom{-h'-r'}{n_8'} (\sigma_{jd}^2)^{f'-h'+n_7'} \Gamma(h'+r')}{(r'-1)! f'! n_7'!}$.

Then, using (4.25), the outage probability can be obtained.

4.4.3 Dominant Interferences

In the case when the interferences are dominant at both relay and destination such that $\sigma_{sj}^2 \approx 0$ and $\sigma_{jd}^2 \approx 0$, exact CDF expression (4.21) can be solved in closed-form as

$$F_{\Gamma_j}(x) = F_{\Gamma_{sj}}(x) + \sum_{i=1}^{I^{sj}} \sum_{r_1=1}^{m_{ij}} \varphi_7 \varphi_9(x) - \sum_{i=1}^{I^{sj}} \sum_{v=1}^{I^{jd}} \sum_{r_1=1}^{m_{ij}} \sum_{r_2=1}^{m_{vj}} \sum_{f=0}^{m_{jd}-1} \sum_{j_1=0}^{m_{sj}-1} \sum_{j_2=0}^{f} \varphi_8 \varphi_{10}(x) \quad (4.36)$$

where $\varphi_7 = \left(\frac{m_{sj}}{\Omega_{sj}}\right)^{-r_1} \left[\prod_{i^*=1}^{I^{sj}} \left(-\frac{\Omega_{i^*j}}{m_{i^*j}}\right)^{-m_{i^*j}}\right] \frac{(-1)^{r_1} b_{ir_1} \Gamma(m_{sj}+r_1) B(1,r_1)}{\Gamma(m_{sj})(r_1-1)!}$,

$\varphi_8 = \left(\frac{m_{sj}}{\Omega_{sj}}\right)^{m_{sj}} \left[\prod_{i^*=1}^{I^{sj}} \left(-\frac{\Omega_{i^*j}}{m_{i^*j}}\right)^{-m_{i^*j}}\right] \left[\prod_{v^*=1}^{I^{jd}} \left(-\frac{\Omega_{v^*j}}{m_{v^*j}}\right)^{-m_{v^*j}}\right] \binom{f}{j_2} \binom{m_{sj}-1}{j_1}$

$\times \frac{(-1)^{r_1+r_2} b_{ir_1} b_{vr_2} \Gamma(m_{sj}+r_1)\Gamma(f+r_2) \Omega_{jd}^{r_2} (\Omega_{ij}\Omega_{sj})^{m_{sj}+r_1} m_{jd}^{j_1+j_2+1} \Omega_{vj}^{j_1+j_2+r_2+1}}{(r_2-1)! f! \Gamma(m_{sj})(r_1-1)!}$

$\times B(j_1+j_2+r_2+1, m_{sj}+r_1-j_1-j_2+f-1)$,

$\varphi_9(x) = {}_2F_1\left(1, 1-m_{sj}; r_1+1; -\frac{m_{ij}\Omega_{sj}}{m_{sj}\Omega_{ij}x}\right) \left(\frac{m_{ij}\Omega_{sj}}{m_{sj}\Omega_{ij}} + x\right)^{-m_{sj}-r_1+1} x^{m_{sj}-1}$,

$\varphi_{10}(x) = (x+1)^{j_1+1} x^{j_2+m_{sj}} (m_{ij}\Omega_{sj} + m_{sj}\Omega_{ij}x)^{-m_{sj}-r_1} \times$

$(m_{jd}\Omega_{vj}x + m_{vj}\Omega_{jd})^{-j_1-j_2-r_2-1}\, {}_2F_1(m_{sj}+r_1, j_1+j_2+r_2+1; m_{sj}+r_1+f+r_2; 1 - \frac{m_{jd}\Omega_{vj} m_{sj}\Omega_{ij}\left(x^2+x\right)}{(m_{ij}\Omega_{sj}+m_{sj}\Omega_{ij}x)(m_{vj}\Omega_{jd}+m_{jd}\Omega_{vj}x)})$ and ${}_2F_1(\cdot,\cdot;\cdot;\cdot)$ is the hypergeometric function.

Proof: See Appendix B.8.

Note that (4.36) is a very good closed-form approximation to the exact CDF when INR is large in the case of fixed interferences.

4.4.4 I.i.d. Interferences

This subsection focuses on the case when all the interferences are i.i.d. One can see that the PDF $f_{Y_{sj}}(x)$ in (4.28) is only suitable when the Nakagami-m

parameters of interferences are different. When all the interferences are i.i.d., (4.28) simply becomes

$$f_{Y_{sj}}(x) = \left(\frac{m_{ij}}{\Omega_{ij}}\right)^{I^{sj}m_{ij}} \frac{x^{I^{sj}m_{ij}-1}}{\Gamma(I^{sj}m_{ij})} e^{-\frac{m_{ij}}{\Omega_{ij}}x}, x > 0 \tag{4.37}$$

where b_{ir} does not exist any more and all other symbols are defined as before. Using (4.14), (4.15), (4.22) and (4.37), the lower bound can be derived as

$$F_{\Gamma_j}(x) \geqslant 1 - \varphi_{12} \sum_{v_1=0}^{m_{sj}-1} \sum_{v_2=0}^{m_{jd}-1} \sum_{s_1=0}^{v_1} \sum_{s_2=0}^{v_2} \varphi_{13}\varphi_{14}(x) = F_{\Gamma_j}^{LB}(x) \tag{4.38}$$

where $\varphi_{12} = \frac{\left(\frac{\Omega_{vj}}{m_{vj}}\right)^{-I^{jd}m_{vj}} \left(\frac{\Omega_{ij}}{m_{ij}}\right)^{-I^{sj}m_{ij}} e^{-\frac{m_{jd}\sigma_{jd}^2 x}{\Omega_{jd}} - \frac{m_{sj}\sigma_{sj}^2 x}{\Omega_{sj}}}}{\Gamma(I^{jd}m_{vj})\Gamma(I^{sj}m_{ij})}$,

$\varphi_{13} = \frac{\left(\frac{\Omega_{jd}}{m_{jd}}\right)^{-v_2} \left(\frac{\Omega_{sj}}{m_{sj}}\right)^{-v_1} (\sigma_{jd}^2)^{v_2-s_2} (\sigma_{sj}^2)^{v_1-s_1} \Gamma(I^{jd}m_{vj}+s_2)\Gamma(I^{sj}m_{ij}+s_1)}{s_1!s_2!(v_1-s_1)!(v_2-s_2)!}$,

$\varphi_{14}(x) = x^{v_1+v_2} \left(\frac{m_{jd}x}{\Omega_{jd}} + \frac{m_{vj}}{\Omega_{vj}}\right)^{-I^{jd}m_{vj}-s_2} \left(\frac{m_{ij}}{\Omega_{ij}} + \frac{m_{sj}x}{\Omega_{sj}}\right)^{-I^{sj}m_{ij}-s_1}$.

Similarly, the asymptotic expression can be derived as

$$F_{\Gamma_j}^{\infty}(x) = 1 - \sum_{v_1=0}^{m_{sj}-1} \sum_{v_2=0}^{m_{jd}-1} \sum_{s_1=0}^{v_1} \sum_{s_2=0}^{v_2} \sum_{n_9=0}^{N_9} \sum_{n_{10}=0}^{N_{10}} \sum_{n_{11}=0}^{N_{11}} \sum_{n_{12}=0}^{N_{12}} \varphi_{15}\varphi_{16} \; x^{n_{10}+n_{11}+n_{12}+n_9+v_1+v_2}, \tag{4.39}$$

where $\varphi_{15} = \frac{(-1)^{n_{10}+n_9}\Gamma(I^{jd}m_{vj}+s_2)\Gamma(I^{sj}m_{ij}+s_1)\binom{-I^{jd}m_{vj}-s_2}{n_{12}}\binom{-I^{sj}m_{ij}-s_1}{n_{11}}}{n_{10}!n_9!s_1!s_2!(v_1-s_1)!(v_2-s_2)!\Gamma(I^{jd}m_{vj})\Gamma(I^{sj}m_{ij})}$,

$\varphi_{16} = \left(\frac{\Omega_{ij}}{m_{ij}}\right)^{n_{11}+s_1} \left(\frac{\Omega_{vj}}{m_{vj}}\right)^{n_{12}+s_2} (\sigma_{jd}^2)^{n_{10}-s_2+v_2} (\sigma_{sj}^2)^{n_9-s_1+v_1} \left(\frac{\Omega_{jd}}{m_{jd}}\right)^{-n_{10}-n_{12}-v_2} \left(\frac{\Omega_{sj}}{m_{sj}}\right)^{-n_{11}-n_9-v_1}$.

Then, the lower bound and asymptotic expression for the outage probability can be derived by using (4.38) and (4.39) in (4.25). Several insights can be obtained from the simulation for i.i.d. fixed interferers. For example,

one can see that with the increase of the Nakagami-m parameters of the interference m_{ij} or m_{vj}, the outage probability remains almost the same, which can be seen from Fig. 4.8. Similar to the analysis for random interferers, with the increase of SINR, the outage probability for fixed interferer decreases accordingly, which will be examined in Fig. 4.10 and Fig. 4.11 in Section 4.5. However, different from random interferers, changing INR will not have a great influence on the outage probability for fixed interferers if the SINR is fixed. This is because SINR dominates the outage probability for fixed interferes and changing INR just change the ratio between the noise power and the interference power but has negligible influence on the overall outage probability, which will be shown in Fig. 4.9 and Fig. 4.10 in Section 4.5.

Another insight that can be obtained from (4.39) is that, with the increase of m_{sj} or m_{jd}, the outage probability decreases, as m_{sj} or m_{jd} are in the upper limits of the summations in (4.39), which will be examined in Fig. 4.9 - Fig. 4.11 via simulation in Section 4.5.

In the i.i.d. case when the interferences are dominant at both the relay and the destination, one can further get the closed-form expression of the CDF as

$$F_{\Gamma_j}(x) = 1 - \sum_{f_1=0}^{m_{sj}-1} \varphi_{17} x^{f_1} \left(\frac{m_{ij}}{\Omega_{ij}} + \frac{m_{sj}x}{\Omega_{sj}} \right)^{-f_1 - I^{sj} m_{ij}} + \varphi_{18}\varphi_{20}(x) - \sum_{f_2=0}^{m_{jd}-1} \sum_{s_1=0}^{f_2} \sum_{s_2=0}^{m_{sj}-1} \varphi_{19}\varphi_{21}(x) \tag{4.40}$$

where $\varphi_{17} = \frac{\Gamma(f_1 + I^{sj} m_{ij})}{f_1! \left(\frac{\Omega_{sj}}{m_{sj}}\right)^{f_1} \left(\frac{\Omega_{ij}}{m_{ij}}\right)^{I^{sj} m_{ij}} \Gamma(I^{sj} m_{ij})}$,

$\varphi_{18} = \frac{m_{sj}^{-I^{sj} m_{ij}} \left(\frac{\Omega_{ij}}{m_{ij}}\right)^{-I^{sj} m_{ij}} \Omega_{sj}^{I^{sj} m_{ij}} B(1, I^{sj} m_{ij})}{B(I^{sj} m_{ij}, m_{sj})}$,

$$\varphi_{19} =$$
$$\frac{\Gamma(f_2+I^{jd}m_{vj})m_{jd}^{-I^{jd}m_{vj}}\Omega_{jd}^{I^{jd}m_{vj}}\left(\frac{\Omega_{vj}}{m_{vj}}\right)^{-I^{jd}m_{vj}}m_{sj}^{-I^{sj}m_{ij}}\left(\frac{\Omega_{ij}}{m_{ij}}\right)^{-I^{sj}m_{ij}}\Omega_{sj}^{I^{sj}m_{ij}}\Gamma(I^{sj}m_{ij}+m_{sj})}{\Gamma(I^{jd}m_{vj})\Gamma(I^{sj}m_{ij})s_1!s_2!(f_2-s_1)!\Gamma(m_{sj}-s_2)}$$
$$\times B(I^{jd}m_{vj}+s_1+s_2+1, f_2+I^{sj}m_{ij}+m_{sj}-s_1-s_2-1),$$
$$\varphi_{20}(x) =$$
$$x^{m_{sj}-1}\left(\frac{\Omega_{sj}m_{ij}}{m_{sj}\Omega_{ij}}+x\right)^{-I^{sj}m_{ij}-m_{sj}+1}{}_2F_1\left(1, 1-m_{sj}; I^{sj}m_{ij}+1; -\frac{m_{ij}\Omega_{sj}}{m_{sj}\Omega_{ij}x}\right),$$
$$\varphi_{21}(x) = (x+1)^{s_2+1}x^{m_{sj}+s_1}\left(\frac{m_{sj}\Omega_{ij}}{m_{sj}\Omega_{ij}x+m_{ij}\Omega_{sj}}\right)^{I^{sj}m_{ij}+m_{sj}}$$
$$\left(\frac{m_{jd}\Omega_{vj}}{m_{jd}\Omega_{vj}x+m_{vj}\Omega_{jd}}\right)^{I^{jd}m_{vj}+s_1+s_2+1}{}_2F_1(I^{sj}m_{ij}+m_{sj}, I^{jd}m_{vj}+s_1+s_2+1; f_2+$$
$$I^{sj}m_{ij}+m_{sj}+I^{jd}m_{vj}; 1-\frac{m_{jd}m_{sj}\Omega_{vj}\Omega_{ij}x(x+1)}{\left(\Omega_{jd}m_{vj}m_{ij}+m_{jd}\Omega_{vj}m_{ij}x\right)(\Omega_{sj}m_{vj}m_{ij}+\Omega_{ij}m_{sj}xm_{vj})}).$$

Again, (4.40) is a very good closed-form approximation for the exact CDF when INR is large in the case of i.i.d fixed interferences.

Using (4.25), the outage probability is obtained. Simulations in Fig. 4.12 in Section 4.5 will show that this approximation has a very good match with the exact outage probability when INR is large or interferences are dominant.

4.4.5 Rayleigh Fading Signal

In another special case when the signal experiences Rayleigh fading channel, (4.40) is further specialized to

$$F_{\Gamma_j}(x) = 1 - I^{sj}m_{ij}\Omega_{jd}^{I^{jd}m_{vj}}\Omega_{sj}^{I^{sj}m_{ij}}B(I^{jd}m_{vj}+1, I^{sj}m_{ij})\left(\frac{\Omega_{vj}x}{m_{vj}}+\Omega_{jd}\right)^{-I^{jd}m_{vj}}$$
$$\times {}_2F_1\left(I^{jd}m_{vj}+1, I^{sj}m_{ij}+1; I^{sj}m_{ij}+I^{jd}m_{vj}+1; 1-\varphi_{22}(x)\right)\varphi_{22}(x)$$
$$\times\left(\frac{\Omega_{ij}x}{m_{ij}}+\Omega_{sj}\right)^{-I^{sj}m_{ij}} \tag{4.41}$$

where $\varphi_{22}(x) = \frac{\Omega_{ij}\Omega_{vj}x(x+1)}{(m_{ij}\Omega_{sj}+\Omega_{ij}x)(m_{vj}\Omega_{jd}+\Omega_{vj}x)}$.

In the high SINR condition such that $\Omega_{sj} \to \infty$ and $\Omega_{jd} \to \infty$, using [36, (9.1)] as

$$\lim_{\varphi \to 0} \varphi \cdot {}_2F_1(a+1, b+1; a+b+1; 1-\varphi) = \frac{\Gamma(a+b+1)}{\Gamma(a+1)\Gamma(b+1)} \tag{4.42}$$

in (4.41), one can get the high SINR approximation of (4.41) as

$$F_{\Gamma_j}(x) = 1 - \left(\frac{\Omega_{ij} x}{\Omega_{sj} m_{ij}} + 1\right)^{-I^{sj} m_{ij}} \left(\frac{\Omega_{vj} x}{\Omega_{jd} m_{vj}} + 1\right)^{-I^{jd} m_{vj}}. \tag{4.43}$$

Using (4.25), the outage probability is obtained. From (4.43) and (4.25), one has several insights as follows: (1) with the increase of the number of interferers at the relay I^{sj} or at the destination I^{jd}, the outage probability increases; (2) with the increase of the average power of signal at the relay Ω_{sj} or at the destination Ω_{jd}, the outage probability decreases; (3) with the increase of the average power of interferers at the relay Ω_{ij} or at the destination Ω_{vj}, the outage probability increases.

4.5 Numerical Results and Discussion

In this section, numerical examples are presented to show the effects of the number and locations of interferers by using the outage probability expressions derived in the previous sections.

Assume $\bar{\gamma}^{SINR} = b_{sj}\bar{\gamma}_{sj}^{SINR} = b_{jd}\bar{\gamma}_{jd}^{SINR}$, $\bar{\gamma}^{INR} = c_{sj}\bar{\gamma}_{sj}^{INR} = c_{jd}\bar{\gamma}_{jd}^{INR}$, $\beta = \beta_{ij} = \beta_{vj}$ and $K_{ij}P_{ij} = K_{vj}P_{vj} = 1$. In the examples where the interferers have random number and locations, let $\lambda = \lambda_I A_I$ and assume that the distances l_{ij} and l_{vj} follow the uniform distribution as $f_l(l) = \frac{2l}{L^2}$, $0 < l < L$, where L is the maximum radius of the disc. Assume $\lambda = \lambda_{sj} = \lambda_{jd}$ and $L = L_{sj} =$

L_{jd} in this case. In the examples where the interferers have fixed number and locations, the distances l_{ij}, l_{vj} and the number of interferers I^{sj}, I^{jd} are constant. Therefore, assume $l = l_{ij} = l_{vj} = 2$, $I = I^{sj} = I^{jd} = 10$ and $\beta = 3$. In this case, there still exists path loss if the distances between nodes are large. The path loss is determined by l and β. This influence can be checked by examining Ω_{ij} and Ω_{vj}, as l and β can be absorbed by Ω_{ij} and Ω_{vj} as part of the average powers of the interference.

In the calculations for both cases above, assume the number of relays $J = 2$, $b_{sj} = c_{sj} = c_{jd} = 1$ and $b_{jd} = 10$. Also, let the values of m_{sj} be the same for any j; m_{jd} be the same for any j; m_{ij} be the same for any i, j; m_{vj} be the same for any v, j. Note that our results are general enough to include other cases but these settings are used here as examples.

Figs. 4.2 - 4.7 show the outage probability vs. γ_{th} in the case when the interferers have random number and locations. The GGA curve is obtained by using (4.16), (4.17) and (4.21) in (4.25) with numerical integration, the lower bound curve is obtained by using (4.23) in (4.25) while the asymptotic curve is obtained by using (4.24) in (4.25).

In general, one can see that the outage probability decreases when the value of γ_{th} decreases or when the channel condition changes from Rayleigh fading to general Nakagami-m fading (or with the increase of m in Nakagami-m fading).

The influence of m_{ij} and m_{vj} is examined in Fig. 4.2 for $\bar{\gamma}^{SINR} = 15$ dB, $\bar{\gamma}^{INR} = 0$ dB, $\lambda = 50$, $\beta = 3$, $L = 10$, $m_{sj} = 4$ and $m_{jd} = 5$. One can see that the curves for $m_{ij} = 1$ and $m_{vj} = 1$ have a slightly worse outage probability than the curves for $m_{ij} = 2$, $m_{vj} = 3$ and $m_{ij} = 6$, $m_{vj} = 7$ while the curves for $m_{ij} = 2$, $m_{vj} = 3$ and $m_{ij} = 6$, $m_{vj} = 7$ are nearly the same for the reasons

explained in Section 4.3.3.

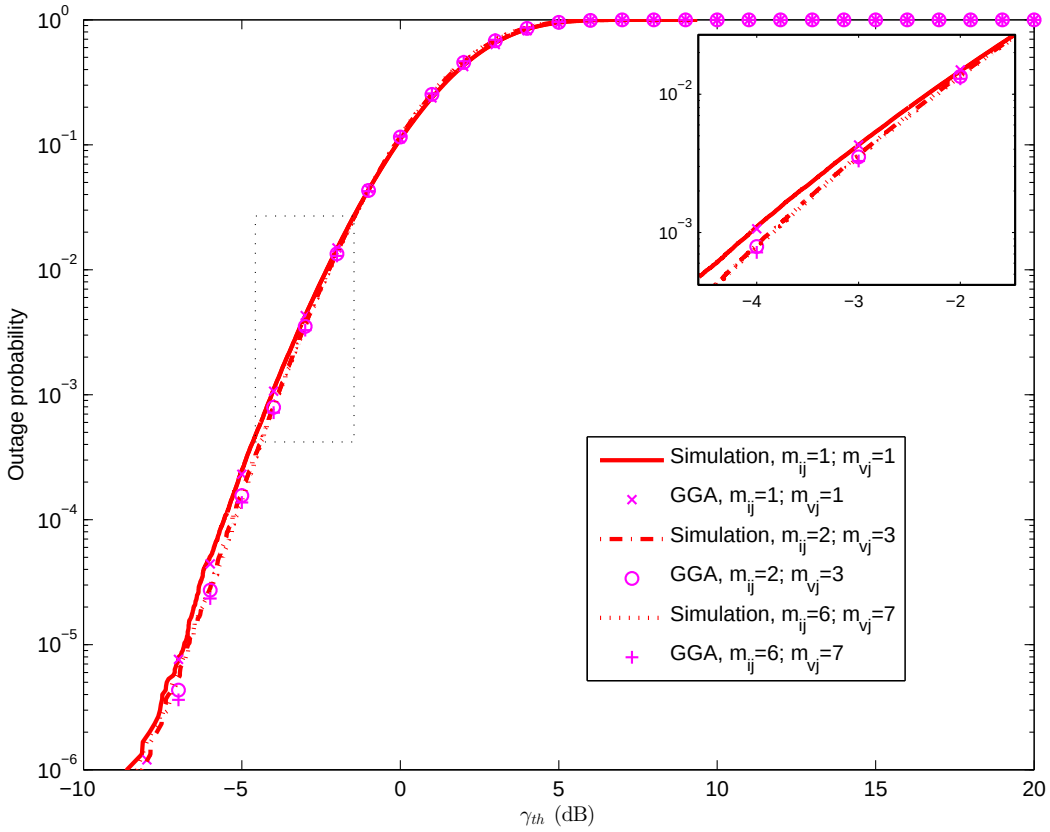

Figure 4.2: Outage probability vs. γ_{th} for random interferers when $\bar{\gamma}^{SINR} = 15$ dB, $\bar{\gamma}^{INR} = 0$ dB, $\lambda = 50$, $L = 10$, $\beta = 3$, $m_{sj} = 4$ and $m_{jd} = 5$.

Fig. 4.3 shows the result for $\bar{\gamma}^{SINR} = 15$ dB, $\bar{\gamma}^{INR} = 0$ dB, $\lambda = 50$, $\beta = 3$, and $L = 10$ while Fig. 4.4 shows the result for the same conditions except that $\bar{\gamma}^{INR}$ is increased from 0 dB in Fig. 4.3 to 20 dB in Fig. 4.4. One can see the outage probability for $m_{sj} = 2$, $m_{jd} = 3$, $m_{sj} = 2$, $m_{jd} = 3$ and $m_{sj} = 4$, $m_{jd} = 5$, $m_{sj} = 6$, $m_{jd} = 7$ deteriorate when $\bar{\gamma}^{INR}$ increases and the deteriorate rate for $m_{sj} = 2$, $m_{jd} = 3$, $m_{sj} = 2$, $m_{jd} = 3$ is slightly smaller than that for $m_{sj} = 4$, $m_{jd} = 5$, $m_{sj} = 6$, $m_{jd} = 7$. However, the outage probability remains nearly unchanged for the Rayleigh case in these two figures for the reasons explained in Section 4.3.3.

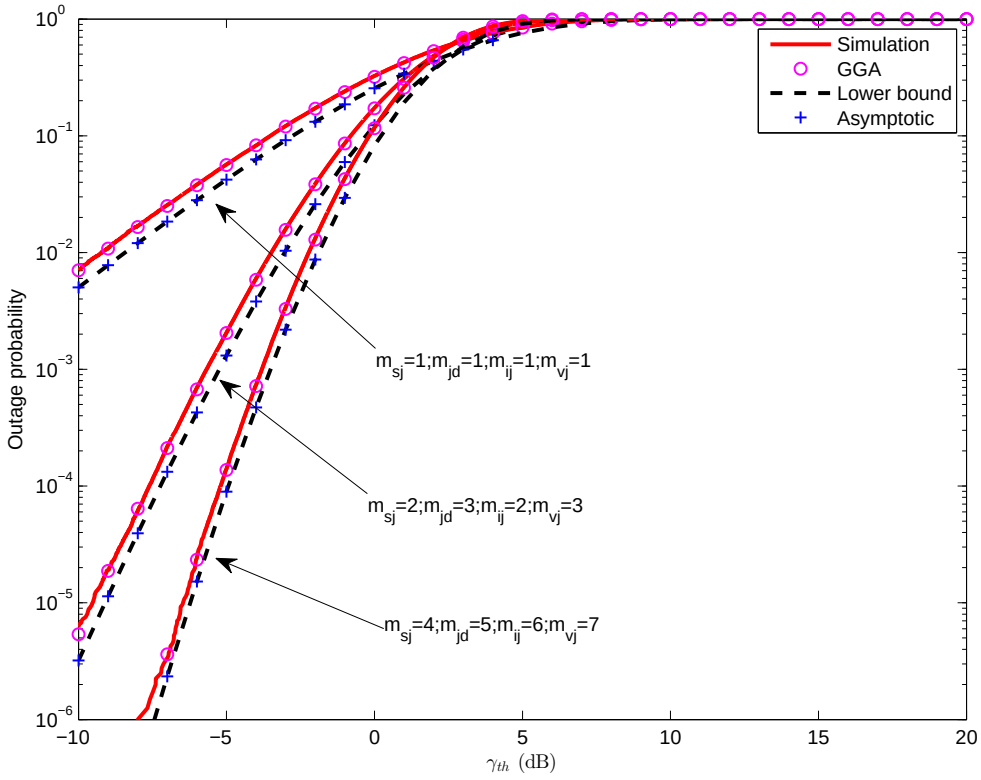

Figure 4.3: Outage probability vs. γ_{th} for random interferers when $\bar{\gamma}^{SINR} = 15$ dB, $\bar{\gamma}^{INR} = 0$ dB, $\lambda = 50$, $L = 10$ and $\beta = 3$.

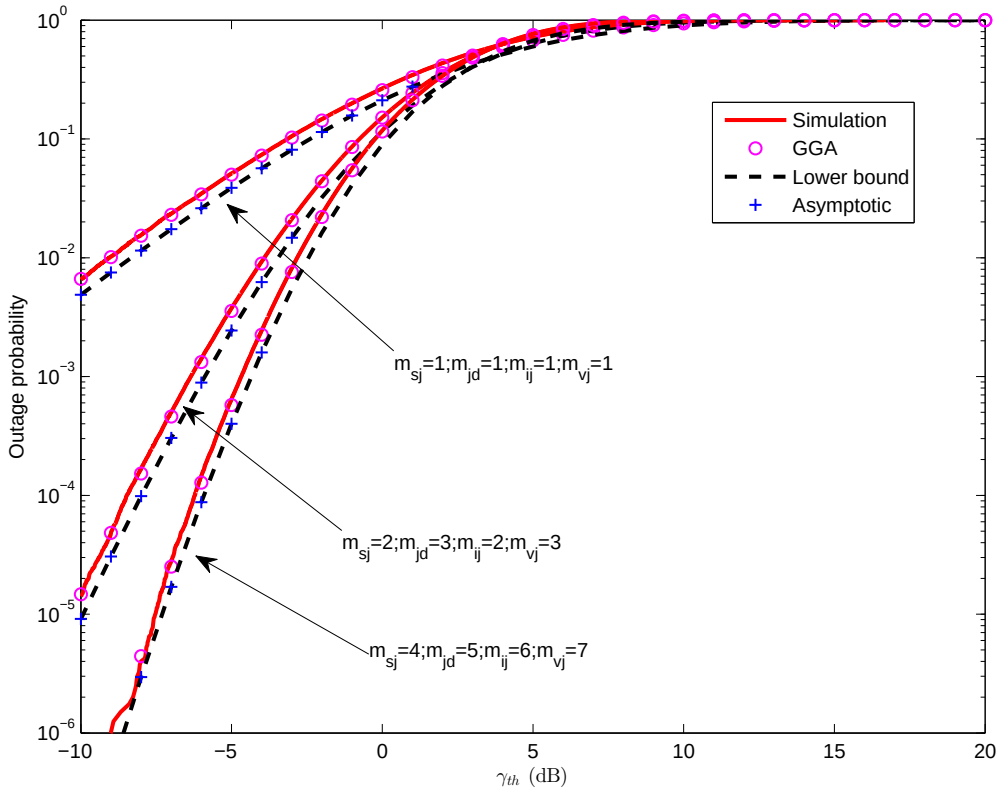

Figure 4.4: Outage probability vs. γ_{th} for random interferers when $\bar{\gamma}^{SINR} = 15$ dB, $\bar{\gamma}^{INR} = 20$ dB, $\lambda = 50$, $L = 10$ and $\beta = 3$.

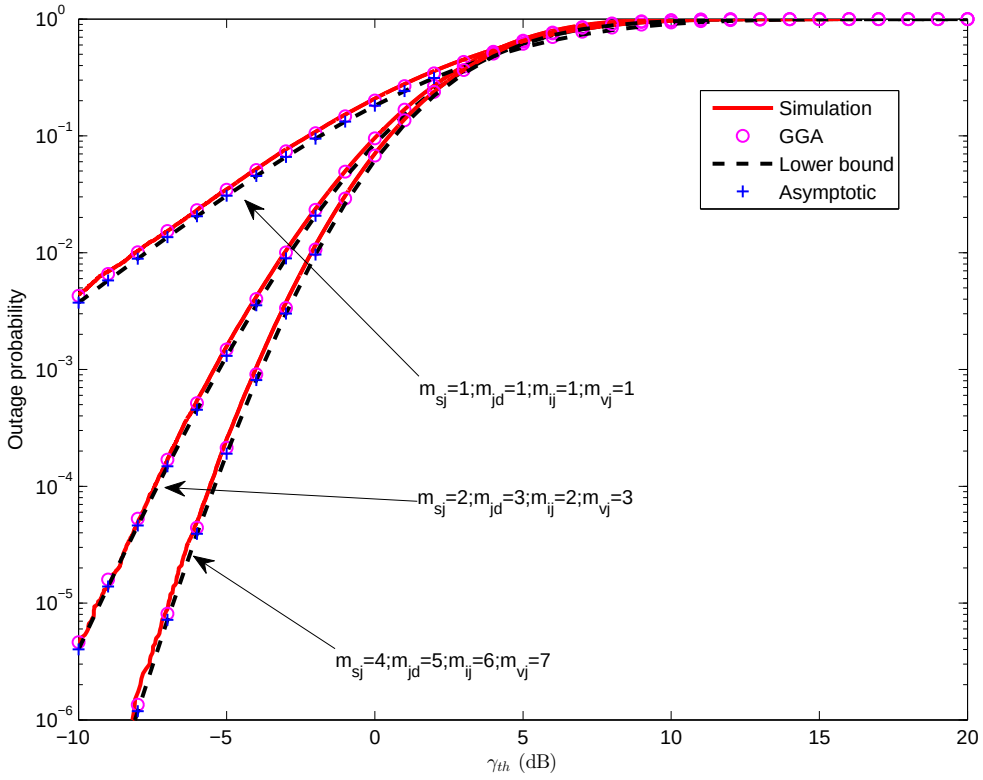

Figure 4.5: Outage probability vs. γ_{th} for random interferers when $\bar{\gamma}^{SINR} = 20$ dB, $\bar{\gamma}^{INR} = 20$ dB, $\lambda = 50$, $L = 10$ and $\beta = 3$.

Fig. 4.5 shows the same conditions as Fig. 4.4 except $\bar{\gamma}^{SINR}$ is increased from 15 dB in Fig. 4.4 to 20 dB in Fig. 4.5. One can see that the outage probability decreases with the increase of $\bar{\gamma}^{SINR}$, as expected.

Also, comparing Fig. 4.3 with Fig. 4.6, one can see that the outage probability for $m_{sj} = 2$, $m_{jd} = 3$, $m_{sj} = 2$, $m_{jd} = 3$ and $m_{sj} = 4$, $m_{jd} = 5$, $m_{sj} = 6$, $m_{jd} = 7$ increases when the value of β changes from 3 in Fig. 4.3 to 5 in Fig. 4.6.

Comparing Fig. 4.3 with Fig. 4.7, one can see that the outage probability for $m_{sj} = 2$, $m_{jd} = 3$, $m_{sj} = 2$, $m_{jd} = 3$ and $m_{sj} = 4$, $m_{jd} = 5$, $m_{sj} = 6$, $m_{jd} = 7$ increases when the value of L increases from 10 in Fig. 4.3 to 20 in Fig. 4.7. However, the outage performances for the Rayleigh case in these two cases above keep almost unchanged for the reasons explained in Section 4.3.3.

In all these cases above, the results based on GGA match very well with the simulation results, showing the accuracy of the approximation and the usefulness of our results. Also, from Figs. 4.3 - 4.7, one can see that the lower bounds have considerable match with the simulation while the asymptotic curves match well with the simulation for small γ_{th}. On the other hand, one can see that the gap between lower bound and simulation decreases when $\bar{\gamma}^{SINR}$ increases, as expected, when comparing Fig. 4.5 with other figures above.

Figs. 4.8 - 4.12 show the outage probability vs. γ_{th} in the case when the interferers have fixed number and locations. The exact curve is obtained by using (4.21) (4.29) and (4.30) in (4.25) with numerical integration, the lower bound curve is obtained by using (4.38) in (4.25) while the asymptotic curve is obtained by using (4.38) and (4.18) in (4.25).

In general, one sees that the outage probability decreases when the value of γ_{th} decreases or when the Nakagami-m parameter increases. Also,

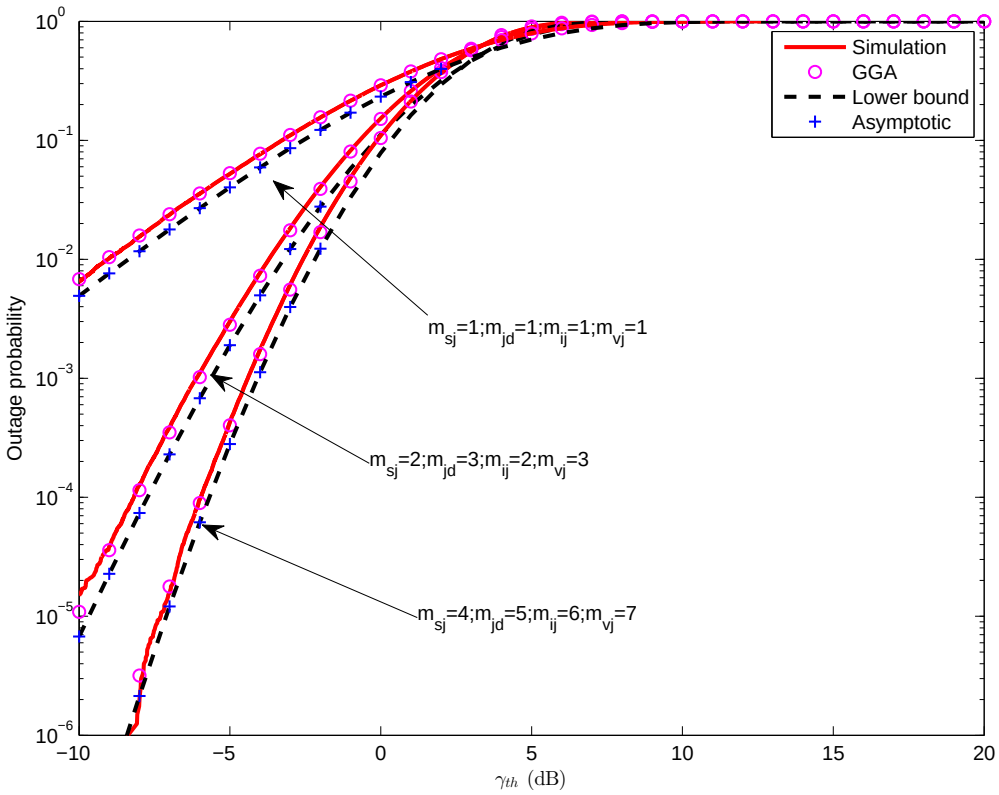

Figure 4.6: Outage probability vs. γ_{th} for random interferers when $\bar{\gamma}^{SINR} = 15$ dB, $\bar{\gamma}^{INR} = 0$ dB, $\lambda = 50$, $L = 10$ and $\beta = 5$.

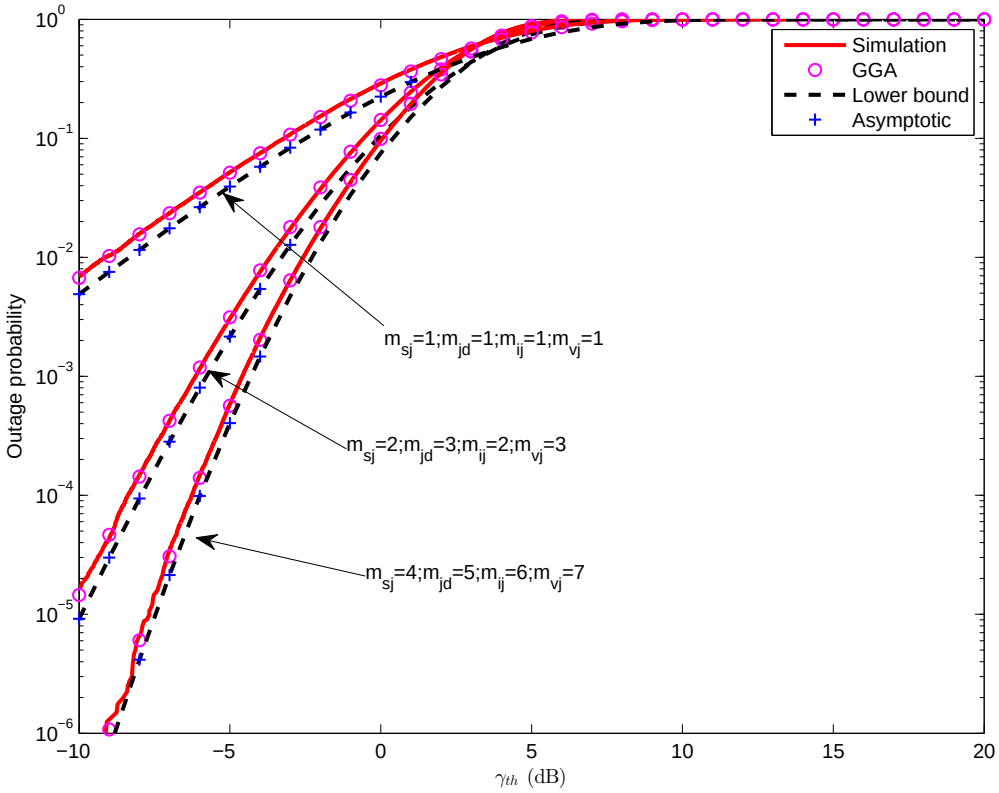

Figure 4.7: Outage probability vs. γ_{th} for random interferers when $\bar{\gamma}^{SINR} = 15$ dB, $\bar{\gamma}^{INR} = 0$ dB, $\lambda = 50$, $L = 20$ and $\beta = 3$.

our derived exact results match very well with the simulation results and our derived lower bounds and asymptotic curves have considerable matches with the simulation, especially for small γ_{th} in these figures, which verify the accuracy of our analysis.

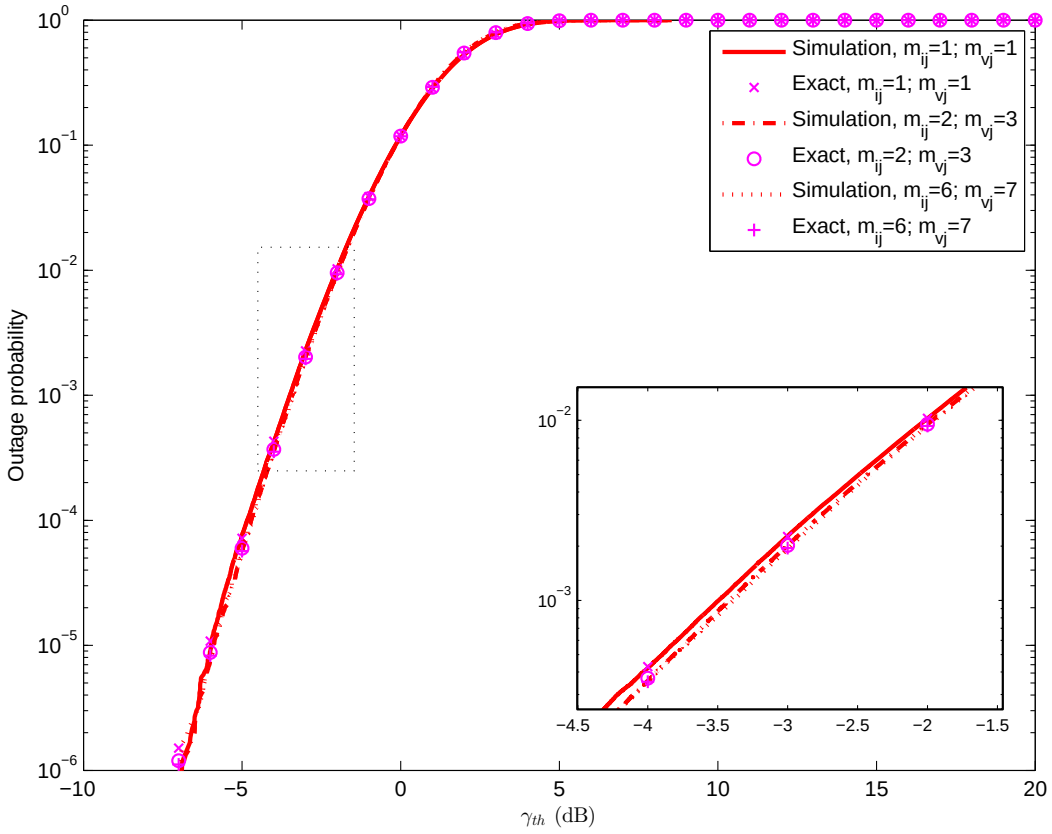

Figure 4.8: Outage probability vs. γ_{th} for fixed interferers when $\bar{\gamma}^{SINR} = 15$ dB, $\bar{\gamma}^{INR} = 0$ dB, $m_{sj} = 4$ and $m_{jd} = 5$.

The influence of m_{ij} and m_{vj} is examined in Fig. 4.8 for $\bar{\gamma}^{SINR} = 15$ dB, $\bar{\gamma}^{INR} = 0$ dB, $m_{sj} = 4$ and $m_{jd} = 5$. One can see that the curves with $m_{ij} = 1$ and $m_{vj} = 1$ has a slightly worse outage probability than the curves with $m_{ij} = 2$, $m_{vj} = 3$ and $m_{ij} = 6$, $m_{vj} = 7$ while the curves with $m_{ij} = 2$, $m_{vj} = 3$ are almost the same as the curves with $m_{ij} = 6$, $m_{vj} = 7$.

Fig. 4.9 shows the result for $\bar{\gamma}^{SINR} = 15$ dB, $\bar{\gamma}^{INR} = 0$ dB while Fig. 4.10

shows the result for the same conditions except that $\bar{\gamma}^{INR}$ is increased from 0 dB in Fig. 4.9 to 20 dB in Fig. 4.10. One can see that the outage probability from simulation remains almost unchanged, as the SINR dominates the outage probability in the case of fixed interferers and the influence of changing INR can be ignored in this case.

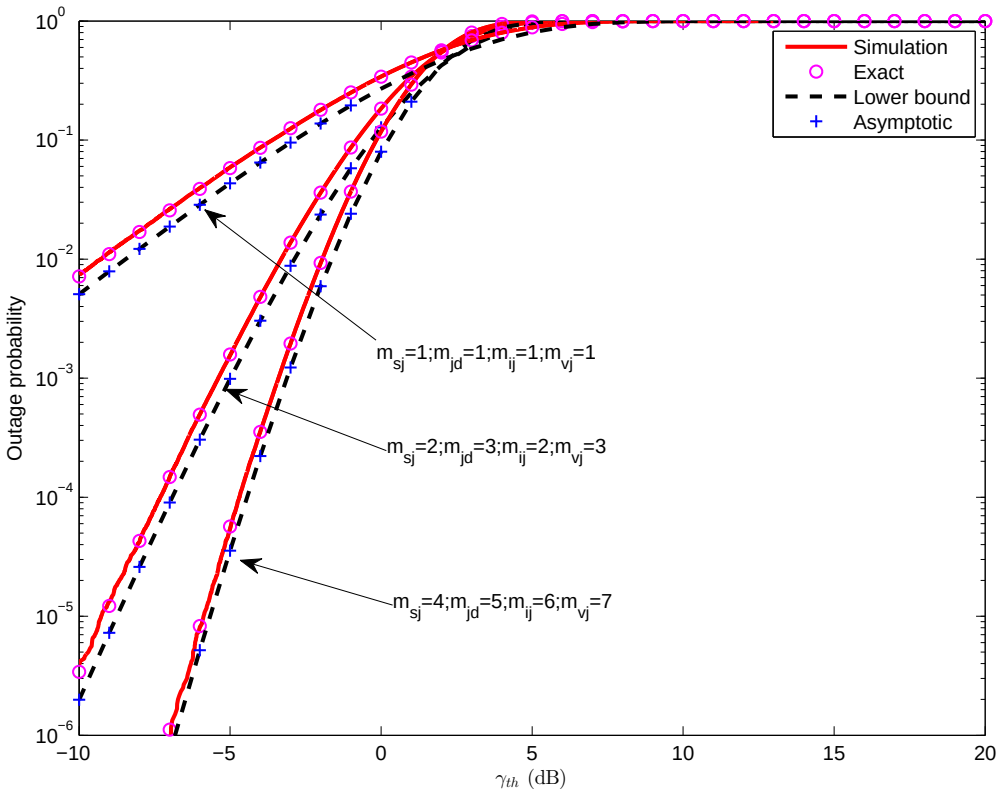

Figure 4.9: Outage probability vs. γ_{th} for fixed interferers when $\bar{\gamma}^{SINR} = 15$ dB and $\bar{\gamma}^{INR} = 0$ dB.

Fig. 4.11 shows the same conditions as Fig. 4.10 except that $\bar{\gamma}^{SINR}$ is increased from 15 dB in Fig. 4.10 to 20 dB in Fig. 4.11. One can see that the outage probability decreases with the increase of $\bar{\gamma}^{SINR}$, as expected.

Next, our derived closed-form approximations to the exact outage probability in the case of fixed interferences is examined in Fig. 4.12 where (4.40)

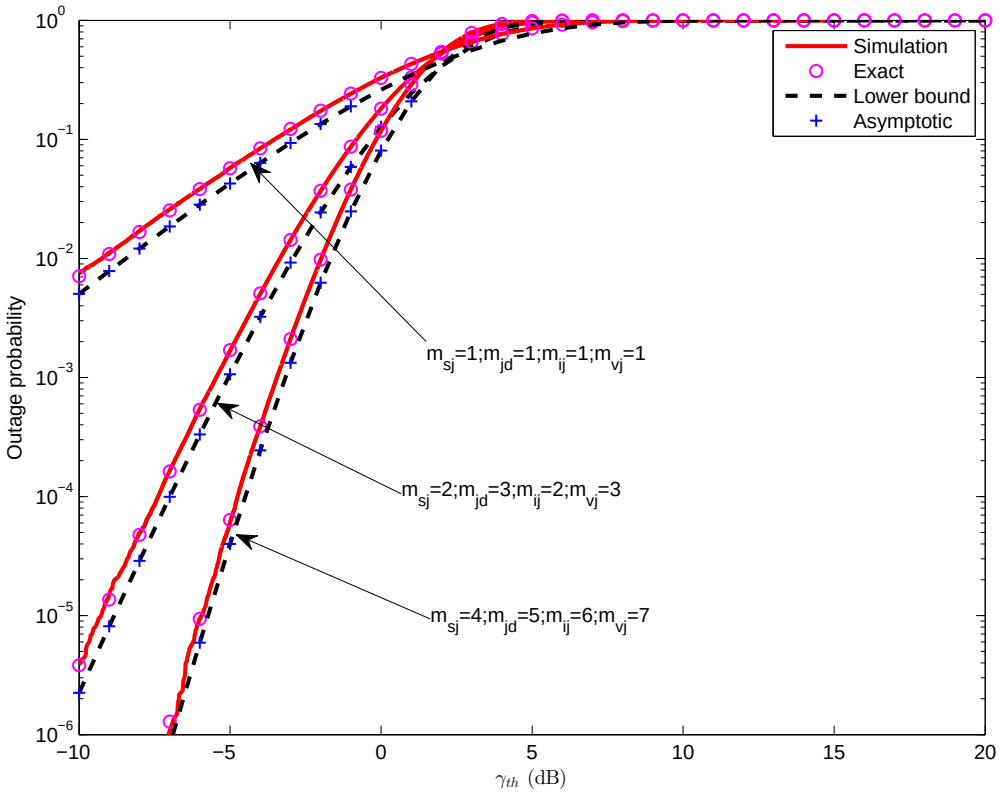

Figure 4.10: Outage probability vs. γ_{th} for fixed interferers when $\bar{\gamma}^{SINR} = 15$ dB and $\bar{\gamma}^{INR} = 20$ dB.

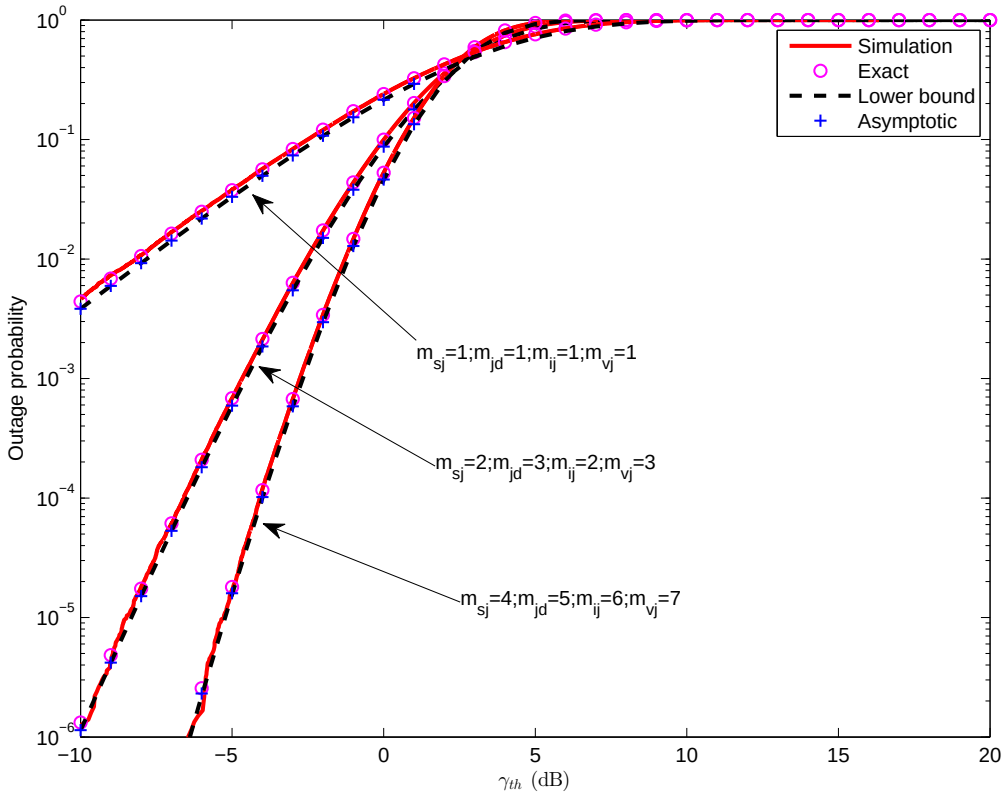

Figure 4.11: Outage probability vs. γ_{th} for fixed interferers when $\bar{\gamma}^{SINR} = 20$ dB and $\bar{\gamma}^{INR} = 20$ dB.

is used as the approximation curve and $\bar{\gamma}^{SINR} = 10$ dB, $m_{sj} = 2$, $m_{jd} = 3$, $m_{sj} = 2$, $m_{jd} = 3$. One can see that the simulation curves for INR $\bar{\gamma}^{INR} = 10$, 15 and 20 dB remain almost unchanged, as $\bar{\gamma}^{SINR}$ is fixed in these curves. One can see that the approximation curve with $\bar{\gamma}^{INR} = 10$ dB is closer to the exact curve in Fig. 4.12 but still have a slight approximation error. With the increase of $\bar{\gamma}^{INR}$, these approximation errors decrease. In the case of $\bar{\gamma}^{INR} = 20$ dB, this approximation error can be ignored.

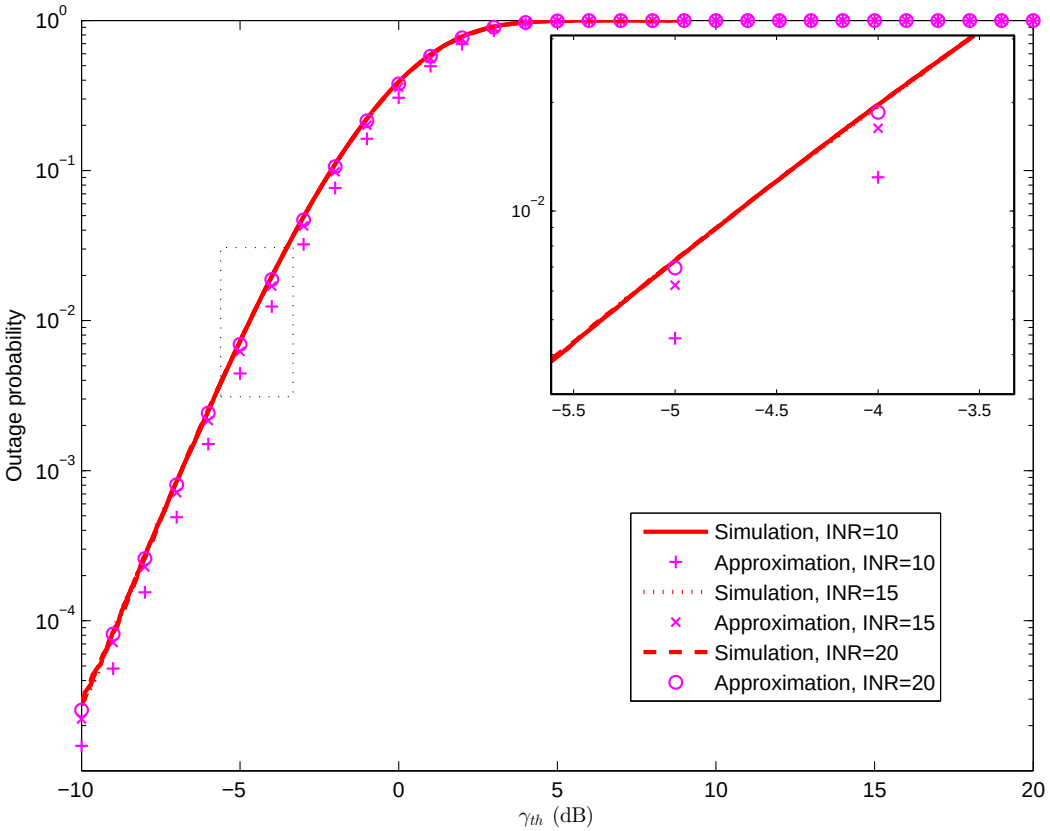

Figure 4.12: Outage probability vs. γ_{th} for fixed interferers when $\bar{\gamma}^{SINR} = 10$ dB, $m_{sj} = 2$, $m_{jd} = 3$, $m_{ij} = 2$ and $m_{vj} = 3$.

4.6 Conclusions

The outage probability performance of a dual-hop AF selective relaying system with relay selection based on the global instantaneous SINR has been analyzed for different cases of interferer's number and locations. Exact analytical expressions in terms of one-dimensional integral for the general cases have been derived. Closed-form expressions for its lower bounds and asymptotic bounds have been obtained. Special cases for dominant interferences, i.i.d Nakagami-m fading interferers and Rayleigh fading channel have also been studied.

Numerical examples have been presented to show the accuracy of the analysis by examining the effects of interferences and their locations, which are otherwise not possible using previous results. These examples have confirmed that the outage performance improves when the SINR increases and provided useful insights on the effects of different system parameters on the outage performance.

Chapter 5

Performance Analysis for Multihop Relaying and Multiple Scattering over α - μ Fading Channels

5.1 Introduction

Multihop communication has been extensively used in our daily lives, such as vehicular ad hoc networks (VANETs) to provide support for road management, traffic information, safety or other applications by enabling vehicle-to-vehicle communications [131]. As introduced before, AF can be further divided into disintegrated channel and cascaded channel [30]. CSI is often required in disintegrated channel, resulting in a variable-gain (or variable amplification factor). However, CSI is not necessarily needed in cascaded channel, leading to a fixed-gain (or fixed amplification factor).

Several researchers have studied the performance of wireless multihop relaying with AF in cascaded channel using fixed amplification gain due to its lower complexity and higher usage efficiency. Reference [56] has studied the lower bounds for the performance of multihop transmissions in cascaded channel over Nakagami-m fading channels, while [132] has derived the closed-form expression of the outage probability over N*Nakagami fading in terms of the Meijer's G-function. In [133], the closed-form expression of the CDF of cascaded channel with multihop relaying over GG fading channels has been obtained and closed-form expressions for bounds of EGC over GG have also been derived. But these works either use infinite series or special functions that are computationally complicated.

Reference [95] has presented the approximations to the statistics of products of independent RVs but without considering relay combining. Reference [60] has proposed the approximations to EGC and MRC of GG variables without considering multihop transmission. Also, none of these works has considered the multihop interference from other transmitting sources in the network. In a multiple-access system or a frequency-reused cell, interference from other transmitting sources may cause a performance degradation and therefore cannot be ignored. Similar research has been done in the multiple scattering (keyhole) channel [134], in which the electromagnetic wave propagates through several keyholes. Then, the overall channel gain can be modeled as the linear combination of product of RVs, but this reference did not consider interference.

To fill in this gap, this chapter derives the exact PDF and CDF in terms of one-dimensional integral for the SRP and the SP of independent α - μ RVs. To reduce the computational complexity, the approximate PDF and CDF of

SRP in closed-form expressions using the GGRA and GRA are proposed. Also, GGA and GA are presented to approximate the SP.

Then, SRP can be used to calculate the outage probability of EGC or MRC receivers for wireless relaying systems. In this case, statistically independent multiple hops are used with AF protocol and fixed amplification gain. SP can be used to calculate the outage probability of EGC or MRC receivers of the same channel but without interferences. Also, SRP can be applied to model the channel gain in multiple scattering system with interferences, while SP can be applied to model the channel gain in multiple scattering system without interferences.

Moreover, GRA is used to approximate RSP of α-μ RVs that models the SIR and the corresponding outage probability in the scattering channels. The contributions of this chapter can be summarized as follows:

• Based on the existing works on the products and ratios of α-μ RVs, the exact MGF of the products and ratios of α-μ RVs are derived. Two special cases are considered, i.e. SRP and SP of independent α - μ RVs.

• Based on the derived exact MGFs, the PDFs and CDFs of the above results are obtained in terms of one-dimensional integral. Also, the closed-form expressions of the PDFs and CDFs using a finite series are given. They can be applied to calculate the outage probability of wireless multihop relaying systems or multiple scattering channels with interferences or without interferences.

• More importantly, new approximation methods, i.e. GGRA and GRA are proposed to calculate SRP and RSP while approximation methods, i.e. GGA and GA are presented to calculate SP in closed-form and simplified structure.

• Numerical results are provided to show the accuracy of the derived exact expressions and the derived approximate expressions. They have shown that the exact result derived agree very well with the simulations and that the GGRA and GGA approximations have a good match with the simulations while the GRA and GA have acceptable performances only in certain cases but with a simpler structure.

The remainder of this chapter is organized as follows. Section 5.2 introduces the system model including SRP, SP and RSP of independent α-μ RVs. Section 5.3 derives the exact CDF of the SRP and SP using MGF in the form of one-dimensional integral while Section 5.4 presents the approximate methods using GGRA, GRA, GGA and GA, followed by applications in Section 5.5. Numerical results are given in Section 5.6. Finally, concluding remarks are made in Section 5.7.

5.2 System Model

This chapter considers independent α - μ RVs $\{X_{jl}\}_{j=1,l=1}^{k,L}$, each having PDF as [40]

$$f_{X_{jl}}(x) = \frac{\alpha_{jl}\mu_{jl}^{\mu_{jl}}}{\Gamma(\mu_{jl})\hat{\gamma_{jl}}^{\alpha_{jl}\mu_{jl}}} x^{\alpha_{jl}\mu_{jl}-1} e^{-\frac{\mu_{jl}x^{\alpha_{jl}}}{\hat{\gamma_{jl}}^{\alpha_{jl}}}}, x \geq 0 \tag{5.1}$$

As introduced before, the significant character of the α - μ fading channel is that it includes the Nakagami-m fading ($\alpha_{jl} = 1$), Weibull fading ($\mu_{jl} = 1$), and Rayleigh fading ($\alpha_{jl} = \mu_{jl} = 1$), as special cases. As can be seen from (5.1), α - μ general fading distribution is written in terms of two physical parameters, i.e. α and μ. μ is referred to the number of multipath clusters while α is associated to the non-linearity of the environment [60].

5.2.1 Sum of Ratios of Products of α - μ RVs

Define a RV R as the SRP of independent α-μ RVs $\{X_{jl}\}_{j=1,l=1}^{k,L}$, giving

$$R = \sum_{l=1}^{L} R_l \tag{5.2}$$

and

$$R_l = \omega_l \frac{\prod_{j=1}^{m} X_{jl}}{\prod_{j=m+1}^{k} X_{jl}} \tag{5.3}$$

where ω_l is constant. This SRP can be used to calculate the outage probability of EGC or MRC receivers for wireless multihop relaying system [56] considering interferences. Also, in multiple scattering channels [134], if each scattering is affected by interferences, the overall channel gain can be described as a linear combination of the ratios of signal to interference and following that, outage probability in multiple scattering channels can also be obtained.

5.2.2 Sum of Products of α - μ RVs

Define a RV P as the SP of independent α-μ RVs $\{X_{jl}\}_{j=1,l=1}^{m,L}$, giving

$$P = \sum_{l=1}^{L} P_l \tag{5.4}$$

and

$$P_l = \omega_l \prod_{j=1}^{m} X_{jl} \tag{5.5}$$

where ω_l is constant. This SP can be used to calculate the outage probability of the EGC or MRC receivers for wireless multihop relaying system without interferences [56]. Also, it can be used to model the overall channel gain in multiple scattering system [134] and based on that, outage probability in

multiple scattering channels can be obtained.

5.2.3 Ratio of Sums of Products of α - μ RVs

Define a RV Z as the RSP of independent α-μ RVs $\{X_{jl}\}_{j=1,l=1}^{k,L}$, giving

$$Z = \frac{P^{(1)}}{P^{(2)}} \tag{5.6}$$

where $P^{(1)} = \sum_{l=1}^{L^{(1)}} \omega_l \prod_{j=1}^{m} X_{jl}$ and $P^{(2)} = \sum_{l=1}^{L^{(2)}} \omega_l \prod_{j=m+1}^{k} X_{jl}$. If we consider $P^{(1)}$ as a linear combination of signal components and $P^{(2)}$ as a linear combination of interferer components, the square of this RSP can be considered as the SIR in a multiple scattering system [134] with interferences. Thus, the outage probability for the SIR in multiple scattering channels can be further obtained.

These simple expressions give the relationships between outage probability and important system parameters, such as the number of hops, the number of links, the weighting factors and signal powers. They could be optimized for different applications.

5.3 Exact Results

This section will derive the PDF and CDF of the SRP R in (5.2) and SP P in (5.4). The first subsection will derive the closed-form expressions for the MGF of R_l in (5.3) and P_l in (5.5). The second subsection will provide the expressions for the PDF and CDF of R and P in both integral form and finite series form.

5.3.1 MGF

If the α-μ RVs are independent, the MGF of R_l can be derived as

$$M_{R_l}(s) = \frac{C_l \alpha_l^{\frac{1}{2}}}{2\pi^{\frac{\alpha_l - 1}{2}}} \times G_{n'+\alpha_l, m'}^{m', n'+\alpha_l} \left(\left(\frac{\alpha_l}{\omega_l} \right)^{\alpha_l} \frac{t_l}{s^{\alpha_l}} \right. \\ \left. \Big| \begin{matrix} \Delta(\alpha_l, 1), 1 - \frac{\mu_{jl}}{m_{jl}} - \frac{r_l}{m_{jl}}, r_l = 0, 1, \cdots, m_{jl} - 1, j = m+1, \cdots, k \\ \frac{\mu_{jl}}{m_{jl}} + \frac{r_l}{m_{jl}}, r_l = 0, 1, \cdots, m_{jl} - 1, j = 1, \cdots, m \end{matrix} \right) \tag{5.7}$$

where $G_{a,b}^{c,d}(\cdot)$ is the Meijer's G-function [36], α_l and m_{jl} are positive integers with $\alpha_{jl} = \frac{\alpha_l}{m_{jl}}$, $j = 1, 2, \cdots, k$, $C_l = 1/\left(\prod_{j=1}^{k} \prod_{r_l=0}^{m_{jl}-1} \Gamma(\frac{\mu_{jl}}{m_{jl}} + \frac{r_l}{m_{jl}}) \right)$, $t_l = \prod_{j=1}^{m} \left(\frac{\mu_{jl}}{\hat{\gamma}_{jl}^{\alpha_{jl}}} \right)^{m_{jl}} / \prod_{j=m+1}^{k} \left(\frac{\mu_{jl}}{\hat{\gamma}_{jl}^{\alpha_{jl}}} \right)^{m_{jl}}$, $m' = \sum_{j=1}^{m} m_{jl}$, $n' = \sum_{j=m+1}^{k} m_{jl}$ and $\Delta(a, b) \triangleq b/a, \cdots, (b+a-1)/a$.

See Appendix C.1 for proof.

If the α-μ RVs are i.i.d, α_{jl}, μ_{jl} and $\hat{\gamma_{jl}}$ become α, μ and $\hat{\gamma}$, respectively. Therefore, the MGF of R_l in (5.7) is specialized to

$$M_{R_l}(s) = \frac{\alpha e^{(m+n)(\mu - \frac{1}{2}) + 1}}{\Gamma^k(\mu) f^{\frac{1}{2}} 2\pi^{(e-1)(\frac{n+m}{2}) + \frac{f-1}{2}}} \times \\ G_{en+f, em}^{em, en+f} \left(\frac{f^f}{\omega_l^{\alpha e} s^l} \left(\frac{\mu}{\hat{\gamma}^{\alpha} e} \right)^{(m-n)e} \Big| \begin{matrix} \Delta(f, 1), \Delta(e, 1-\mu), \cdots, \Delta(e, 1-\mu) \\ \Delta(e, \mu), \cdots, \Delta(e, \mu) \end{matrix} \right) \tag{5.8}$$

where $n = k - m$, f and e are relatively prime integers satisfying $\alpha = f/e$.

Also, when the α-μ RVs are independent, the MGF of P_l can be derived

as

$$M_{P_l}(s) = \frac{C_l \alpha_l^{\frac{1}{2}}}{2\pi^{\frac{\alpha_l - 1}{2}}} \times$$
$$G_{\alpha_l, m'}^{m', \alpha_l} \left(\left(\frac{\alpha_l}{\omega_l} \right)^{\alpha_l} \frac{t_l}{s^{\alpha_l}} | \begin{matrix} \Delta(\alpha_l, 1) \\ \frac{\mu_{jl}}{m_{jl}} + \frac{r_l}{m_{jl}}, r_l = 0, 1, \cdots, m_{jl} - 1, j = 1, \cdots, m \end{matrix} \right) \tag{5.9}$$

by setting $k = m$ in (5.7), where $C_l = 1/\left(\prod_{j=1}^{m} \prod_{r_l=0}^{m_{jl}-1} \Gamma(\frac{\mu_{jl}}{m_{jl}} + \frac{r_l}{m_{jl}}) \right)$, and $t_l = \prod_{j=1}^{m} \left(\frac{\mu_{jl}}{\hat{\gamma}_{jl}^{\alpha_{jl}}} \right)^{m_{jl}}$.

If the α-μ RVs in P_l are i.i.d, the MGF of P_l is specialized to

$$M_{P_l}(s) = \frac{\alpha e^{m(\mu - \frac{1}{2}) + 1}}{\Gamma^m(\mu) f^{\frac{1}{2}} 2\pi^{(e-1)\frac{m}{2} + \frac{f-1}{2}}} \times$$
$$G_{f,em}^{em,f} \left(\frac{f^f}{\omega_l^{\alpha e} s^l} \left(\frac{\mu}{\hat{\gamma}^{\alpha} e} \right)^{me} | \begin{matrix} \Delta(f, 1) \\ \Delta(e, \mu), \cdots, \Delta(e, \mu) \end{matrix} \right) \tag{5.10}$$

Thus, the MGF of R and P is given by

$$M_R(s) = \prod_{l=1}^{L} M_{R_l}(s) \tag{5.11}$$

and

$$M_P(s) = \prod_{l=1}^{L} M_{P_l}(s) \tag{5.12}$$

respectively.

5.3.2 PDF and CDF

The PDF and CDF of R can be expressed as [36]

$$f_R(x) = \frac{1}{2\pi i} \oint_C M_R(s) e^{-sx} ds \tag{5.13}$$

and

$$F_R(y) = \frac{1}{2\pi i} \oint_C \frac{M_R(s) e^{-sy}}{s} ds \tag{5.14}$$

respectively. The contour integral in (5.13) and (5.14) may not be solved in closed-form easily but can be calculated numerically by using mathematical software packages, such as MATLAB, MATHEMATICA and MAPLE.

Following the same process of [135], (5.13) can be approximated using a finite series in closed-form as [135, (9)]

$$\begin{aligned} f_R(x) \approx & \sum_{q=0}^{Q} 2^{-Q} \binom{Q}{q} \left[\frac{e^{A/2}}{x} \sum_{n=0}^{N+q} \frac{(-1)^n}{\beta_n} \Re \left\{ M_R \left(\frac{A + 2\pi j n}{2x} \right) \right\} \right] \\ & + E(A) + E(N, Q), \\ \beta_n = & \begin{cases} 2, & n = 0 \\ 1, & n = 1, 2, \cdots, N \end{cases} \end{aligned} \tag{5.15}$$

where the discretization error can be bounded as $|E(A)| \leq e^{-A}$ and the truncation error can be estimated as $E(N, Q) \simeq \frac{e^{A/2}}{x} \sum_{q=0}^{Q} 2^{-Q} (-1)^{N+q+1} \binom{Q}{q}$ $\Re \left\{ M_R \left(\frac{A + 2\pi j (N+q+1)}{2x} \right) \right\}$.

Similarly, (5.14) can be approximated as [135, (11)]

$$F_R(y) \approx \frac{2^{-Q}e^{A/2}}{y} \sum_{q=0}^{Q} \binom{Q}{q} \sum_{n=0}^{N+q} \frac{(-1)^n}{\beta_n} \Re \left\{ \frac{M_R\left(-\frac{A+2\pi jn}{2y}\right)}{\frac{A+2\pi jn}{2y}} \right\} + E(A,Q,N) \tag{5.16}$$

where the overall error term is approximately bounded by $|E(A,Q,N)| \simeq \frac{e^{-A}}{1-e^{-A}} + \left| \frac{2^{-Q}e^{A/2}}{y} \sum_{q=0}^{Q} (-1)^{N+1+q} \binom{Q}{q} \Re \left\{ \frac{M_R\left(-\frac{A+2\pi j(N+q+1)}{2y}\right)}{\frac{A+2\pi j(N+q+1)}{2y}} \right\} \right|$.

The PDF $f_P(x)$ and CDF $F_P(y)$ of P can be obtained by simply replacing $M_{R_l}(s)$ with $M_{P_l}(s)$ in $f_R(x)$ and $F_R(y)$, respectively. No exact results for Z are available due to the difficulty in obtaining them.

Note also that [136] provides the PDF of products, quotients and powers of Fox H-function variates. Although Fox H-function variates include α - μ variates, the result in this reference is only a special case of this chapter when summation is not considered.

5.4 Approximate Results

The exact PDF and CDF expressions in integral or series in the previous subsection are complicated and not convenient to use. Thus, in the following, new approximation methods GGRA and GRA to approximate R and GRA to approximate Z will be presented. Also, this section proposes to use the conventional approximation methods GGA and GA to approximate P.

In the first subsection, two new approximate methods GGRA and GGA are proposed and two conventional approximate methods GGA and GA are reviewed. In the second subsection, the w-th order moment of GGRA, GRA, GGA and GA are shown. In the third subsection, moment-matching method for determining the unknown parameters of GGRA, GRA, GGA and GA are

presented.

5.4.1 Approximate PDF and CDF

The PDF and CDF of GGRA are given by

$$f_{X_{GGRA}}(x) = \frac{pk^{-\frac{d_1}{p}} x^{d_1-1}(1+k^{-1}\ x^p)^{-\frac{d_1+d_2}{p}}}{B(\frac{d_1}{p},\frac{d_2}{p})}, x>0 \tag{5.17}$$

and

$$F_{X_{GGRA}}(y) = \frac{k^{-\frac{d_1}{p}} y^{d_1}\ {}_2F_1\left(\frac{d_1}{p},\frac{d_1}{p}+\frac{d_2}{p};1+\frac{d_1}{p};-k^{-1}y^p\right)}{\frac{d_1}{p}B(\frac{d_1}{p},\frac{d_2}{p})} \tag{5.18}$$

respectively, where d_1, d_2, p, $k>0$ are the parameters to be determined.

Proof: See Appendix C.2.

GGRA can be used to approximate the SRP of α-μ RVs R in (5.2) and it has a very good match although four unknown parameters need to be determined. To simplify the parameters calculation, GRA is proposed by setting $p=1$ in GGRA. Therefore, the PDF and CDF of GRA are given by

$$f_{X_{GRA}}(x) = \frac{k^{-d_1}x^{d_1-1}(1+xk^{-1})^{-d_1-d_2}}{B(d_1,d_2)}, x>0 \tag{5.19}$$

and

$$F_{X_{GRA}}(y) = \frac{y^{d_1}k^{-d_1}\ {}_2F_1\left(d_1,d_1+d_2;1+d_1;-yk^{-1}\right)}{d_1B(d_1,d_2)} \tag{5.20}$$

respectively.

Proof: See Appendix C.2.

GRA can be used to approximate R in (5.2) as well with a simplified form as only three parameters need to be determined. Also, GRA can be used to approximate Z in (5.6). Numerical results in Section 5.6 will show that

GRA has a slightly worse performance than GGRA when approximating the SRP but has a very good match with the RSP Z in (5.6).

On the other hand, one can use GGA (as introduced in Section 2.6), which has the PDF and CDF as

$$f_{X_{GGA}}(x) = \frac{p\, a^{-d} x^{d-1} e^{-\left(\frac{x}{a}\right)^p}}{\Gamma\left(\frac{d}{p}\right)}, x \geq 0 \tag{5.21}$$

and

$$F_{X_{GGA}}(y) = \frac{\gamma(d/p, (y/a)^p)}{\Gamma(d/p)} \tag{5.22}$$

respectively, where $d > 0, p > 0$, $a > 0$ are the parameters to be determined. The GGA can be used to approximate P in (5.4).

Moreover, one can get the PDF and CDF of GA as

$$f_{X_{GA}}(x) = \frac{x^{d-1} e^{-\frac{x}{a}}}{a^d \Gamma(d)} \tag{5.23}$$

and

$$F_{X_{GA}}(y) = \frac{\gamma(d, y/a)}{\Gamma(d)} \tag{5.24}$$

by setting $p = 1$ in (5.21) and (5.22), respectively. The GA can be also used to approximate P in (5.4) but with a simplified form compared with GGA.

5.4.2 The w-th Order Moment

This subsection gives the w-th order moment of GGRA, GRA, GGA and GA, and the 1-th, 2-th, 3-th and 4-th order moment of R and P.

The w-th order moment of GGRA and GRA

The w-th order moment of GGRA is given by [137]

$$E\left(X_{GGRA}^{w}\right)=k^{w/p}\frac{\Gamma(\frac{d_1}{p}+\frac{w}{p})}{\Gamma(\frac{d_1}{p})}\frac{\Gamma(\frac{d_2}{p}-\frac{w}{p})}{\Gamma(\frac{d_2}{p})}. \tag{5.25}$$

By setting $p=1$ in (5.25), one can get the w-th order moment of GRA as

$$E\left(X_{GRA}^{w}\right)=\frac{k^{w}\Gamma(d_2-w)\Gamma(d_1+w)}{\Gamma(d_1)\Gamma(d_2)}. \tag{5.26}$$

The w-th order moment of GGA and GA

The w-th order moment of GGA is given by [40, (5)]

$$E(X_{GGA}^{w})=\frac{a^{w}\Gamma\left(\frac{d+w}{p}\right)}{\Gamma\left(\frac{d}{p}\right)}. \tag{5.27}$$

By setting $p=1$ in (5.27), one can get the w-th order moment of GA as [138, (7)]

$$E(X_{GA}^{w})=\frac{a^{w}\Gamma\left(d+w\right)}{\Gamma\left(d\right)}. \tag{5.28}$$

The 1-st to 4-th order moments of R and P

The w-th order moment for X_{jl} in (5.1) is given by [40]

$$E(X_{jl}^{w})=\frac{\hat{\gamma_{jl}}^{w}\Gamma(\mu_{jl}+w/\alpha_{jl})}{\mu_{jl}^{w/\gamma_{jl}}\Gamma(\mu_{jl})} \tag{5.29}$$

and the w-th order moment for $\frac{1}{X_{jl}}$ in (5.1) is given by

$$E(\frac{1}{X_{jl}^w}) = \frac{\hat{\gamma_{jl}}^{-w}\Gamma(\mu_{jl} - w/\alpha_{jl})}{\mu_{jl}^{-w/\gamma_{jl}}\Gamma(\mu_{jl})}. \tag{5.30}$$

Thus, the first order moment of R in (5.2) is given by

$$E(R) = \sum_{l=1}^{L} \omega_l \prod_{j=1}^{m} E(X_{jl}) \prod_{j=m+1}^{k} E(\frac{1}{X_{jl}}), \tag{5.31}$$

the second order moment of R in (5.2) is given by

$$\begin{aligned} E(R^2) &= \sum_{l=1}^{L} \omega_l^2 \prod_{j=1}^{m} E(X_{jl}^2) \prod_{j=m+1}^{k} E(\frac{1}{X_{jl}^2}) \\ &+ \sum_{l_1=1}^{L} \sum_{l_2 \neq l_1=1}^{L} \omega_{l_1}\omega_{l_2} \prod_{j=1}^{m} E(X_{jl_1})E(X_{jl_2}) \prod_{j=m+1}^{k} E(\frac{1}{X_{jl_1}})E(\frac{1}{X_{jl_2}}), \end{aligned} \tag{5.32}$$

the third order moment of R in (5.2) is given by

$$\begin{aligned} E(R^3) &= \sum_{l=1}^{L} \omega_l^3 \prod_{j=1}^{m} E(X_{jl}^3) \prod_{j=m+1}^{k} E(\frac{1}{X_{jl}^3}) + \sum_{l_1=1}^{L} \sum_{l_2 \neq l_1=1}^{L} \omega_{l_1}^2\omega_{l_2} \prod_{j=1}^{m} E(X_{jl_1}^2) \\ &\times E(X_{jl_2}) \prod_{j=m+1}^{k} E(\frac{1}{X_{jl_1}^2})E(\frac{1}{X_{jl_2}}) + \sum_{l_1=1}^{L} \sum_{l_2 \neq l_1=1}^{L} \sum_{l_3 \neq l_2 \neq l_1=1}^{L} \omega_{l_1}\omega_{l_2}\omega_{l_3} \\ &\times \prod_{j=1}^{m} E(X_{jl_1})E(X_{jl_2})E(X_{jl_3}) \prod_{j=m+1}^{k} E(\frac{1}{X_{jl_1}})E(\frac{1}{X_{jl_2}})E(\frac{1}{X_{jl_3}}) \end{aligned} \tag{5.33}$$

and the fourth order moment of R in (5.2) is given by

$$
\begin{aligned}
E(R^4) = & \sum_{l=1}^{L} \omega_l^4 \prod_{j=1}^{m} E(X_{jl}^4) \prod_{j=m+1}^{k} E(\frac{1}{X_{jl}^4}) + \sum_{l_1=1}^{L} \sum_{l_2 \neq l_1=1}^{L} \omega_{l_1}^3 \omega_{l_2} \prod_{j=1}^{m} E(X_{jl_1}^3) \\
& \times E(X_{jl_2}) \prod_{j=m+1}^{k} E(\frac{1}{X_{jl_1}^3}) E(\frac{1}{X_{jl_2}}) + \sum_{l_1=1}^{L} \sum_{l_2 \neq l_1=1}^{L} \sum_{l_3 \neq l_2 \neq l_1=1}^{L} \omega_{l_1}^2 \omega_{l_2} \omega_{l_3} \\
& \times \prod_{j=1}^{m} E(X_{jl_1}^2) E(X_{jl_2}) E(X_{jl_3}) \prod_{j=m+1}^{k} E(\frac{1}{X_{jl_1}^2}) E(\frac{1}{X_{jl_2}}) E(\frac{1}{X_{jl_3}}) \\
& + \sum_{l_1=1}^{L} \sum_{l_2 \neq l_1=1}^{L} \sum_{l_3 \neq l_2 \neq l_1=1}^{L} \sum_{l_4 \neq l_3 \neq l_2 \neq l_1=1}^{L} \omega_{l_1} \omega_{l_2} \omega_{l_3} \omega_{l_4} \prod_{j=1}^{m} E(X_{jl_1}) E(X_{jl_2}) E(X_{jl_3}) \\
& E(X_{jl_4}) \prod_{j=m+1}^{k} E(\frac{1}{X_{jl_1}}) E(\frac{1}{X_{jl_2}}) E(\frac{1}{X_{jl_3}}) E(\frac{1}{X_{jl_4}}).
\end{aligned}
\tag{5.34}
$$

Using similar method, one can easily get $E(P)$, $E(P^2)$, $E(P^3)$ and $E(P^4)$ from (5.31), (5.32), (5.33) and (5.34), respectively, by setting $k = m$ and ignoring $E(\frac{1}{X_{jl}})$.

5.4.3 Moment-Matching Approximations

This subsection uses the moment-matching method to determine the unknown parameters in GGRA, GRA to approximate R, those in GGA and GA to approximate P and those in GRA to approximate Z.

Approximation of R

For GGRA, d_1, d_2, p and k are determined by matching the first, second, third and fourth order moment of R with the first, second, third and fourth order

moment of GGRA. Thus, one can get the values of d_1, d_2, p and k by solving

$$\begin{cases} E(R) = k^{1/p}\frac{\Gamma(\frac{d_1}{p}+\frac{1}{p})}{\Gamma(\frac{d_1}{p})}\frac{\Gamma(\frac{d_2}{p}-\frac{1}{p})}{\Gamma(\frac{d_2}{p})} \\ E(R^2) = k^{2/p}\frac{\Gamma(\frac{d_1}{p}+\frac{2}{p})}{\Gamma(\frac{d_1}{p})}\frac{\Gamma(\frac{d_2}{p}-\frac{2}{p})}{\Gamma(\frac{d_2}{p})} \\ E(R^3) = k^{3/p}\frac{\Gamma(\frac{d_1}{p}+\frac{3}{p})}{\Gamma(\frac{d_1}{p})}\frac{\Gamma(\frac{d_2}{p}-\frac{3}{p})}{\Gamma(\frac{d_2}{p})} \\ E(R^4) = k^{4/p}\frac{\Gamma(\frac{d_1}{p}+\frac{4}{p})}{\Gamma(\frac{d_1}{p})}\frac{\Gamma(\frac{d_2}{p}-\frac{4}{p})}{\Gamma(\frac{d_2}{p})} \end{cases}. \tag{5.35}$$

Further, one can simplify (5.35) by getting rid of k as

$$\begin{cases} \frac{E(R^2)}{E^2\{R\}} = \frac{\Gamma(\frac{d_1}{p})\Gamma(\frac{d_2}{p})\Gamma\left(\frac{d_1}{p}+\frac{2}{p}\right)\Gamma\left(\frac{d_2}{p}-\frac{2}{p}\right)}{\Gamma\left(\frac{d_1}{p}+\frac{1}{p}\right)^2\Gamma\left(\frac{d_2}{p}-\frac{1}{p}\right)^2} \\ \frac{E(R^3)}{E^3\{R\}} = \frac{\Gamma(\frac{d_1}{p})^2\Gamma(\frac{d_2}{p})^2\Gamma\left(\frac{d_1}{p}+\frac{3}{p}\right)\Gamma\left(\frac{d_2}{p}-\frac{3}{p}\right)}{\Gamma\left(\frac{d_1}{p}+\frac{1}{p}\right)^3\Gamma\left(\frac{d_2}{p}-\frac{1}{p}\right)^3} \\ \frac{E(R^4)}{E^4\{R\}} = \frac{\Gamma(\frac{d_1}{p})^3\Gamma(\frac{d_2}{p})^3\Gamma\left(\frac{d_1}{p}+\frac{4}{p}\right)\Gamma\left(\frac{d_2}{p}-\frac{4}{p}\right)}{\Gamma\left(\frac{d_1}{p}+\frac{1}{p}\right)^4\Gamma\left(\frac{d_2}{p}-\frac{1}{p}\right)^4} \end{cases}. \tag{5.36}$$

Equations (5.36) can be solved for d_1, d_2, p numerically by using mathematical software packages. Then, k can be obtained by using the values of d_1, d_2, p from (5.36) in (5.35).

For GRA, d_1, d_2, and k are determined by matching the first, second and third order moment of R with the first, second and third moment of GRA. Therefore, one can calculate the values of d_1, d_2 and k by solving

$$\begin{cases} E(R) = \frac{k\Gamma(d_2-1)\Gamma(d_1+1)}{\Gamma(d_1)\Gamma(d_2)} \\ E(R^2) = \frac{k^2\Gamma(d_2-2)\Gamma(d_1+2)}{\Gamma(d_1)\Gamma(d_2)} \\ E(R^3) = \frac{k^3\Gamma(d_2-3)\Gamma(d_1+3)}{\Gamma(d_1)\Gamma(d_2)} \end{cases}. \tag{5.37}$$

Further, one can simplify (5.37) by getting rid of k as

$$\begin{cases} \frac{E(R^2)}{E^2\{R\}} = \frac{(d_1+1)(d_2-1)}{d_1(d_2-2)} \\ \frac{E(R^3)}{E(R^2)E(R)} = \frac{(d_1+2)(d_2-1)}{d_1(d_2-3)} \end{cases}. \tag{5.38}$$

Then, one can get the values of d_1, d_2 and k by

$$d_1 = \frac{2E(R)\left(E^2\{R^2\} - E(R)E(R^3)\right)}{2E^2\{R\}E(R^3) - E(R)E^2\{R^2\} - E(R^2)E(R^3)}, \tag{5.39}$$

$$d_2 = \frac{E^2\{R\}E(R^2) + 3E(R)E(R^3) - 4E^2\{R^2\}}{E^2\{R\}E(R^2) + E(R)E(R^3) - 2E^2\{R^2\}} \tag{5.40}$$

and

$$k = \frac{-2E(R)^2E(R^3) + E(R)E(R^2)^2 + E(R^2)E(R^3)}{E(R)^2E(R^2) + E(R)E(R^3) - 2E(R^2)^2} \tag{5.41}$$

respectively. Unlike (5.36), the parameters are calculated without numerical solutions to the equations.

Approximation of P

For GGA, a, d and p are determined by matching the first, second and third order moment of P with the first, second and third order moment of GGA as

$$\begin{cases} E(P) = \frac{a\Gamma\left(\frac{d+1}{p}\right)}{\Gamma\left(\frac{d}{p}\right)} \\ E(P^2) = \frac{a^2\Gamma\left(\frac{d+2}{p}\right)}{\Gamma\left(\frac{d}{p}\right)} \\ E(P^3) = \frac{a^3\Gamma\left(\frac{d+3}{p}\right)}{\Gamma\left(\frac{d}{p}\right)} \end{cases}. \tag{5.42}$$

Furthermore, with the help of Beta function $B(\cdot,\cdot)$ function [36, (8.384)], one has

$$\begin{cases} B\left(\frac{d+1}{p},\frac{d+2}{p}\right)=\frac{E(P)E(P^2)}{E(P^3)}B\left(\frac{d}{p},\frac{d+3}{p}\right) \\ B\left(\frac{d+1}{p},\frac{d+1}{p}\right)=\frac{E(P)^2}{E(P^2)}B\left(\frac{d}{p},\frac{d+2}{p}\right) \end{cases}. \tag{5.43}$$

Then one can solve d and p numerically by using mathematical software packages. Then, a can be obtained by using the values of d and p from (5.43) in (5.42).

For GA, a and d are decided by matching the first and second order moment of P with the first and second order moment of GA. Therefore, one can calculate the values of a and d by solving

$$\begin{cases} E(P)=\frac{a\Gamma(d+1)}{\Gamma(d)} \\ E(P^2)=\frac{a^2\Gamma(d+2)}{\Gamma(d)} \end{cases}. \tag{5.44}$$

Then, one can get the values of a and d by

$$a=\frac{E(P)-E^2(P)}{E(P)} \tag{5.45}$$

and

$$d=\frac{E^2(P)}{E(P)-E^2(P)} \tag{5.46}$$

respectively.

Approximation of Z

It is not easy to get the closed form of w-th order moment for Z. However, it is shown in Appendix C.2 that GRA can be considered as the ratio of two

GAs. Therefore the values of d_1 and d_2 can be decided by

$$d_1 = \frac{E^2(P^{(1)})}{E(P^{(1)}) - E^2(P^{(1)})} \tag{5.47}$$

and

$$d_2 = \frac{E^2(P^{(2)})}{E(P^{(2)}) - E^2(P^{(2)})} \tag{5.48}$$

respectively, and k can be solved by $k = \frac{a_1}{a_2}$, where

$$a_1 = \frac{E(P^{(1)}) - E^2(P^{(1)})}{E(P^{(1)})} \tag{5.49}$$

and

$$a_2 = \frac{E(P^{(2)}) - E^2(P^{(2)})}{E(P^{(2)})}. \tag{5.50}$$

5.5 Applications

In this section, the exact and approximate CDFs derived in the previous section are adopted to calculate the outage probability for wireless multihop relaying and multiple scattering systems.

For L-branch EGC receivers of wireless relaying system through statistically independent multihop using AF protocol with fixed amplification gain over α - μ fading channel considering interferences, the instantaneous end-to-end SIR is given by

$$\gamma_R = \frac{1}{L}\left(\sum_{l=1}^{L}\sqrt{\gamma_l}\right)^2 \tag{5.51}$$

where $\gamma_l = \frac{E_s}{K_0}R_l^2$, $R_l = \omega_l \frac{\prod_{j=1}^{m} X_{jl}}{\prod_{j=m+1}^{k} X_{jl}}$, $\omega_l = 1$, E_s is the transmitted power, K_0 is the constant that takes other necessary power factors into account, $\prod_{j=1}^{m} X_{jl}$

represents the product of fading coefficient of signal through m hop in the lth path [56], and $\prod_{j=m+1}^{k} X_{jl}$ represents the product of fading coefficient of the interferer through $k-m$ hop in the lth path. Note that the system model in this chapter does not consider noise or considers there is little noise which can be ignored. Using (5.2), one can rewrite (5.51) as

$$\gamma_R' = \frac{1}{L}\frac{E_s}{K_0}R^2 \tag{5.52}$$

which can be seen as the instantaneous SIR in multiple scattering radio channel. In this case, R can be seen as the overall channel gain considering interferences in each scattering, R^2 can be seen as the fading power, ω_l in (5.3) can be seen as the weight which is a nonnegative real-valued constant that determines the mixture weight of the multiple scattering component, and the channel gain can be described as a linear combination of signal components with constant, Rayleigh, double-Rayleigh, etc., distributed amplitude [134].

Define the corresponding average SIR in wireless multihop relaying system or multiple scattering channel as

$$\bar{\gamma_R} = \frac{1}{L}\frac{E_s}{K_0}E\left(\left(\sum_{l=1}^{L} R_l\right)^2\right). \tag{5.53}$$

By normalizing (5.51) or (5.52) with respect to the average end-to-end SIR in (5.53) and using (5.2), one has

$$\hat{\gamma_R} = \frac{R^2}{E\left(R^2\right)}. \tag{5.54}$$

The outage probability is defined as the probability that the SNR of γ_R is

below a certain threshold as $P_o = Pr\{\gamma_R < \gamma_0\}$. By normalizing both sides of the inequality with the positive value of $\bar{\gamma_R}$ and letting $\gamma_{th} = (\gamma_0/\bar{\gamma_R})$, one has

$$P_o = Pr\{\hat{\gamma_R} < \gamma_{th}\}. \tag{5.55}$$

Then, using the CDF of R in (5.14) and in (5.16), one has

$$P_o = F_R\left(\sqrt{\gamma_{th}} E^{\frac{1}{2}}\left(R^2\right)\right). \tag{5.56}$$

Also, using the CDF of GGRA in (5.18) and the CDF of GRA in (5.20), one can get approximate outage probability of $\hat{\gamma_R}$ in (5.54) as

$$P_o = F_{GGRA}\left(\sqrt{\gamma_{th}} E^{\frac{1}{2}}\left(R^2\right)\right) \tag{5.57}$$

and

$$P_o = F_{GRA}\left(\sqrt{\gamma_{th}} E^{\frac{1}{2}}\left(R^2\right)\right). \tag{5.58}$$

Similarly, for L-branch EGC receivers of wireless multihop relaying system without interferences or for transmitting signal in multiple scattering radio channel without interference, the exact results of outage probability are given by substituting $M_R(s)$ with $M_P(s)$ in (5.14) and (5.16) as

$$P_o = F_P\left(\sqrt{\gamma_{th}} \cdot E^{\frac{1}{2}}\{P^2\}\right). \tag{5.59}$$

Also, using the CDF of GGA in (5.22) and the CDF of GA in (5.24), one can get the approximate outage probability as

$$P_o = F_{GGA}\left(\sqrt{\gamma_{th}} \cdot E^{\frac{1}{2}}\{P^2\}\right) \tag{5.60}$$

and

$$P_o = F_{GA}\left(\sqrt{\gamma_{th}} \cdot E^{\frac{1}{2}}\{P^2\}\right), \tag{5.61}$$

respectively.

Note that the exact and approximate results of outage probability derived above can also be applied to L-branch MRC receivers of wireless multihop relaying system with proper modifications. For the exact results, a variable substitution of x by x^2 is needed in (5.1) and in the following MGF expressions. For the approximate results, moment-matching should be done by considering $E(R^2)$, $E(R^4)$, $E(R^6)$, $E(R^8)$, $E(P^2)$, $E(P^4)$, $E(P^6)$, $E(P^8)$ with the corresponding moments of GGRA, GRA, GGA, GA.

However, EGC is simpler to implement and its performance is very close to that of MRC although MRC is the optimal combining scheme [139]. Thus, EGC is considered from here on.

Next, the outage probability for SIR in multiple scattering radio channel is considered. In this case, the SIR I_Z is given by

$$I_Z = Z^2 = \frac{Z_1}{Z_2} \tag{5.62}$$

where $Z_1 = (P^{(1)})^2 = (\sum_{l=1}^{L^{(1)}} \omega_l \prod_{j=1}^{m} X_{jl})^2$ represents the signal power in multiple scattering channel and $Z_2 = (P^{(2)})^2 = (\sum_{l=1}^{L^{(2)}} \omega_l \prod_{j=m+1}^{k} X_{jl})^2$ represents the interference power in the same channel. Due to the complexity of the exact expression of outage probability of I_Z and the high accuracy of the approximate result of GRA to I_Z, which will be seen from the numerical results in the next section, this chapter only provides the approximate expression GGA

for I_Z. Thus, the outage probability of SIR in (5.62) can be

$$P_o = F_{GGA}\left(\sqrt{\gamma_{th}} \cdot E^{\frac{1}{2}}\{Z^2\}\right). \tag{5.63}$$

In the next section, numerical results and discussion are given to show the accuracy of the proposed exact and approximate expressions.

5.6 Numerical Results and Discussion

In this section, numerical results are presented to show the performance of the derived exact and approximate expressions. In these examples, the exact results in Section 5.3 are evaluated using the series forms in (5.15) [135, (9)] and (5.16) [135, (11)] with $A = 23.026$, $N = 15$ and $Q = 10$, whereas the approximate results are calculated using our proposed closed-form approximations in Section 5.4. Let $\alpha_{jl} = 2$, $\mu_{jl} = 4$ and $\hat{\gamma_{jl}} = 5$ for all j and l. Note that our results are general enough to include other cases but these settings are used here as examples.

Tables 5.1 and 5.2 compare the exact and approximate PDFs and CDFs of $R = 2\frac{X_{11}}{X_{21}X_{31}} + 3\frac{X_{12}X_{22}X_{32}}{X_{42}X_{52}}$, respectively. One can see that the PDF and CDF of the GGRA approximation match very well with the exact result. The GRA approximation also matches well with the exact result in most values examined but with a simplified form.

Fig. 5.1 and Fig. 5.2 show the outage probability vs. γ_{th} using EGC receivers in wireless multihop relaying system over α - μ channels. Fig. 5.1 describes the signal model as $R = \frac{X_{11}}{X_{21}} + \frac{X_{12}X_{22}}{X_{32}X_{42}}$ which assumes $L = 2$ with interference while Fig. 5.2 describes the signal model as $R = X_{11} + X_{12}X_{22} +$

Table 5.1: Comparison of exact and approximate PDFs of $R = 2\frac{X_{11}}{X_{21}X_{31}} + 3\frac{X_{12}X_{22}X_{32}}{X_{42}X_{52}}$.

R	Exact	GGRA	GRA
3	0.005123366578	0.00553831	0.00657853
6	0.03437761985	0.0340766	0.0339683
9	0.05414392525	0.0538482	0.0528716
12	0.055066531	0.0550564	0.0544886
15	0.04670142108	0.0468074	0.0467473
18	0.03634886	0.0364498	0.0366334
21	0.027117528	0.0271797	0.0274094
24	0.019823972	0.0198519	0.0200418
27	0.014372777	0.014379	0.0145091
30	0.01040560788	0.0104009	0.0104784
33	0.007553075	0.00754393	0.0075832
36	0.00550956	0.00549977	0.00551409
39	0.0040442581	0.00403557	0.00403502
42	0.002989825	0.00298263	0.00297411
45	0.00222678	0.00222117	0.00220904
48	0.001670996	0.00166687	0.00165373
51	0.00126327	0.00126047	0.00124778
54	0.0009624243	0.00096032	0.000948797
57	0.0007384826	0.00073699	0.000726922
60	0.00057033	0.000569594	0.000561023

Table 5.2: Comparison of exact and approximate CDFs of $R = 2\frac{X_{11}}{X_{21}X_{31}} + 3\frac{X_{12}X_{22}X_{32}}{X_{42}X_{52}}$.

R	Exact	GGRA	GRA
3	0.002918777902	0.00343157	0.00456575
6	0.05963044177	0.0603741	0.0635416
9	0.1977381439	0.197387	0.198466
12	0.3651634794	0.36438	0.363
15	0.5189965633	0.518401	0.516134
18	0.6435316511	0.643263	0.641246
21	0.7382844348	0.738262	0.736898
24	0.8082033983	0.808312	0.807589
27	0.8590801037	0.859235	0.858993
30	0.8959262807	0.89608	0.896146
33	0.9226282412	0.922759	0.922997
36	0.9420521725	0.942154	0.942469
39	0.9562621779	0.956336	0.956669
42	0.9667270005	0.966777	0.967096
45	0.9744897491	0.974522	0.974809
48	0.9802920019	0.980311	0.980559
51	0.9846609351	0.984671	0.98488
54	0.9879744607	0.987979	0.988152
57	0.9905062535	0.990509	0.990649
60	0.9924555580	0.992457	0.992569

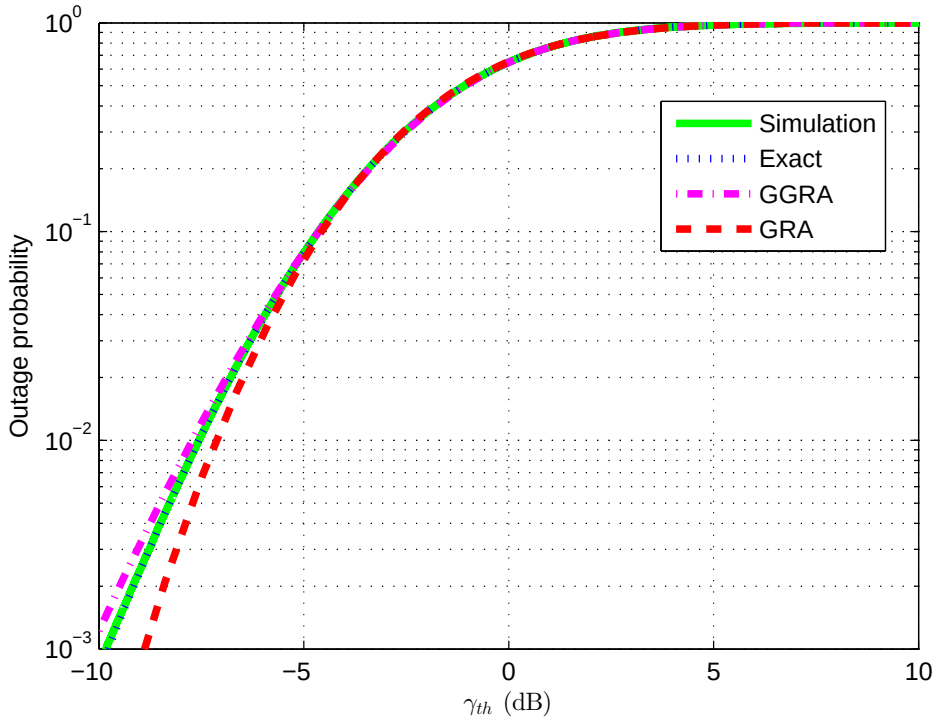

Figure 5.1: Outage probability vs. γ_{th} using EGC receivers in wireless multi-hop relaying system with interferences.

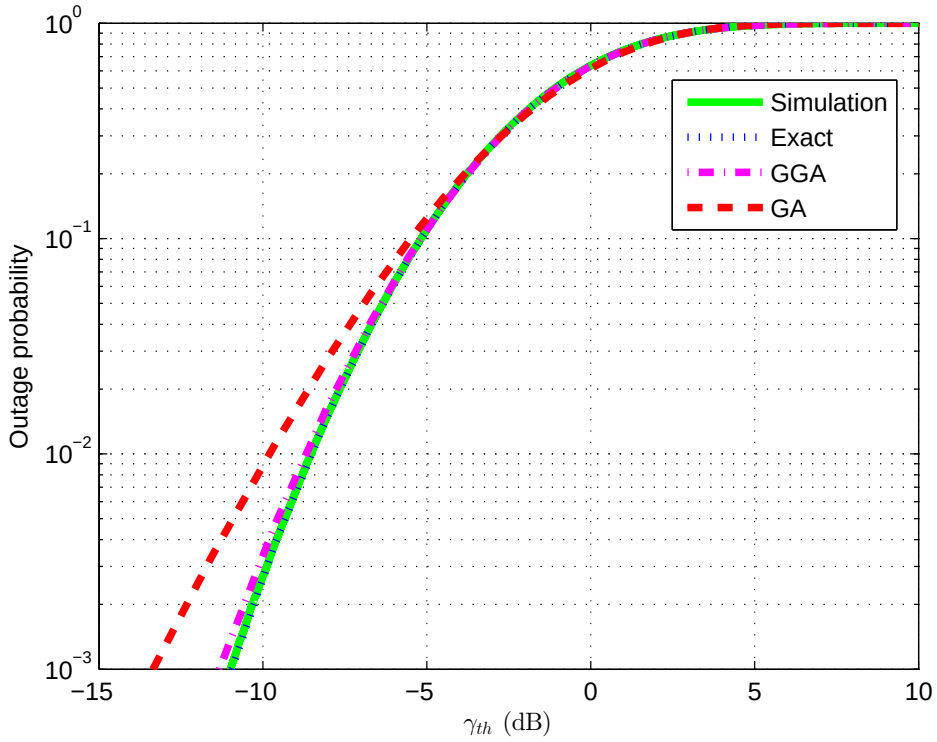

Figure 5.2: Outage probability vs. γ_{th} using EGC receivers in wireless multi-hop relaying system without interferences.

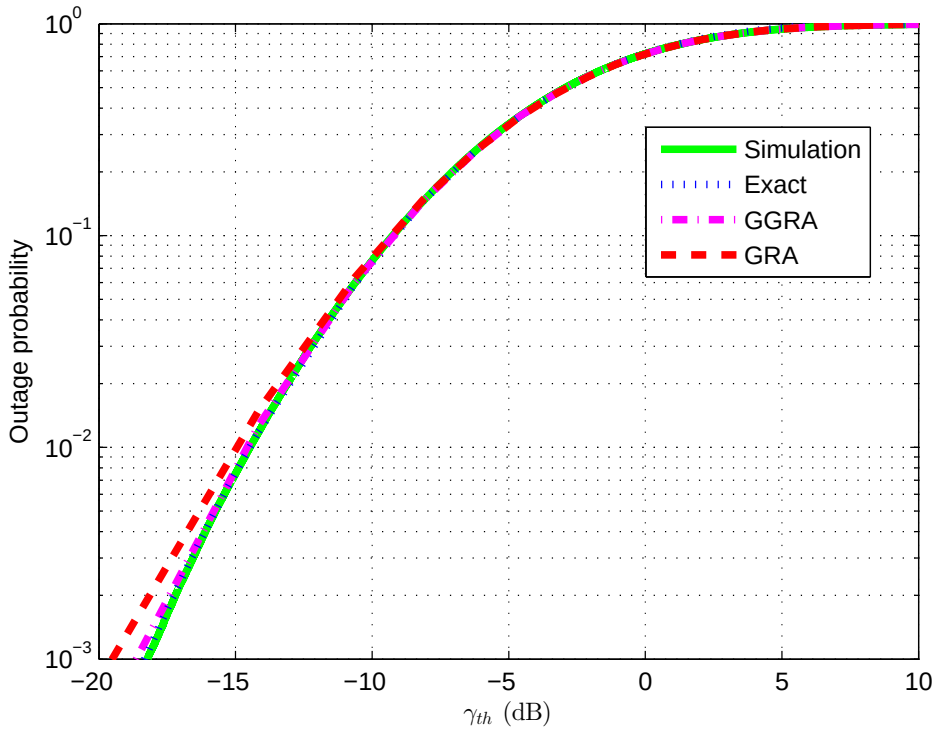

Figure 5.3: Outage probability vs. γ_{th} in multiple scattering channel with interferences.

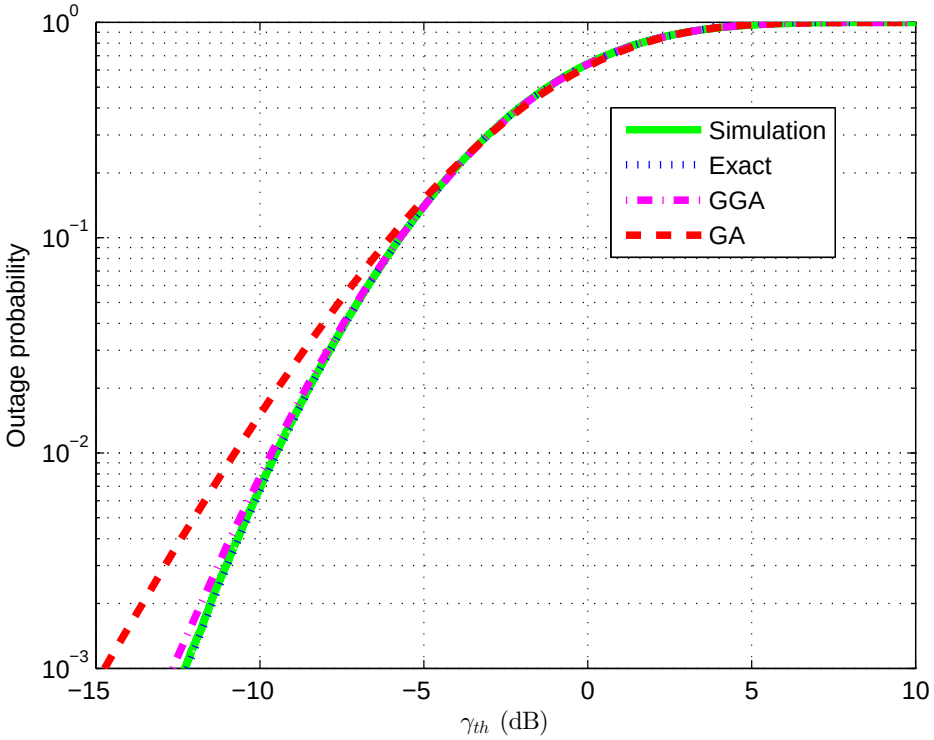

Figure 5.4: Outage probability vs. γ_{th} in multiple scattering channel without interferences.

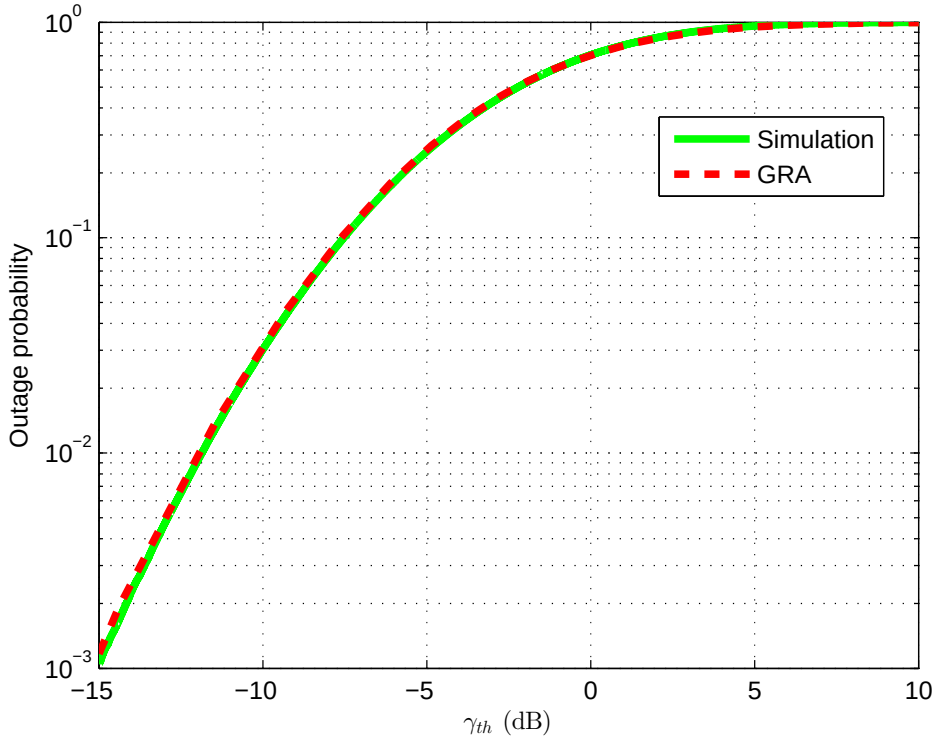

Figure 5.5: Outage probability vs. γ_{th} in terms of SIR in multiple scattering channel with interferences.

$X_{13}X_{23}X_{33}$ which assumes $L = 3$ and does not consider interferences.

Fig. 5.3 and Fig. 5.4 show the outage probability vs. γ_{th} in multiple scattering channels, in which Fig. 5.3 describes the signal model with interferences as $R = 2\frac{X_{11}}{X_{21}X_{31}} + 3\frac{X_{12}X_{22}X_{32}}{X_{42}X_{52}}$ while Fig. 5.4 describes the signal model without interferences as $R = X_{11} + 2X_{12}X_{22} + 3X_{13}X_{23}X_{33}$.

Moreover, Fig. 5.5 shows the outage probability vs. γ_{th} in terms of SIR in multiple scattering channel. In this case, the SIR can be described as $I_z = Z^2$, where $Z = \frac{X_{11}+X_{21}X_{31}}{X_{42}+X_{52}X_{62}+X_{72}X_{82}X_{92}}$.

From Figs. 5.1 - 5.5, one can see that the outage probability increases when the SIR threshold increases, as expected. In the extreme case when the SIR threshold goes to infinity, the outage probability will approach one. Furthermore, the exact results of outage probability agree very well with the simulations in Figs. 5.1 - 5.4. The approximate results based on GGRA match very well with simulations in Fig. 5.1 and Fig. 5.3 while GGA matches very well with simulations in Fig. 5.2 and Fig. 5.4, showing the usefulness of our approximate expressions. The approximate result based on GRA matches well with the simulations in Fig. 5.1 and Fig. 5.3 and GA matches well with the simulations in Fig. 5.2 and Fig. 5.4, both between 10^{-1} to 1 but with simple structures. Moreover, GRA has a very good match with the simulation in Fig. 5.5.

5.7 Conclusions

The exact results of CDF of the SRP and the SP of independent α - μ RVs in the form of one-dimensional integral have been derived. Also, the closed-form approximations for the CDF using GGRA, GRA, GGA and GA have

been obtained. Applications for the outage probability of EGC receivers in wireless multihop relaying considering interferences or no interferences have been discussed. Moreover, applications for the outage probability of signal transmitting in multiple scattering channels considering interferences or no interferences have also been provided.

Numerical examples have shown that the exact result derived agree very well with the simulations and that the GGRA and GGA approximations have a good match with the simulations while the GRA and GA approximations have acceptable performances only in certain cases but with a simpler structure.

Chapter 6

Performance Analysis for Hard-Decision Fusion with Arbitrary Numbers of Bits for Different Samples

6.1 Introduction

Data fusion is a technique which can combine data from different mobile nodes, multiple sensors, secondary users and diversity branches to achieve improved accuracies and performance. For example, vehicle navigation and detection systems were proposed using fusion methods, in which each node takes a local observation and then transmits it to a fusion centre for joint processing to track and detect vehicles [140], [141].

In these applications, communication consumes a significant portion of the total power as compared with other parts [142]. Therefore, developing

power-efficient transmission strategies has motivated a wide range of studies [143]. In [144, 145], distributed decision system with multiple nodes have been studied, where [144] proposed the MRC statistic approach to approximate the likelihood-based fusion rule for low SNR and [145] developed the channel-aware decision fusion rules for multi-hop transmission.

Popular decision rules such as ML and maximum a posteriori probability have been introduced in [1]. Optimal decision rule in multiple node systems has been studied in [77]. In [77], individual decisions are weighted according to the reliability of the detector information and then a threshold comparison is conducted to get the global decision. Optimal partial decision combining rule in diversity systems is proposed in [146]. In [146], the suboptimal diversity receivers that combine hard decisions have been studied. Their performances in terms of noncoherent frequency-shift-keying (NCFSK) have also been analyzed and compared to the voting and selection diversity in Rayleigh fading channel.

Moreover, in [32, 78, 146, 147], hard decision fusion based on one, two or several bits has been examined. However, all these works have assumed the same numbers of bits sampled from data collected at all nodes. In reality, data at some nodes may be more reliable than others. For example, some nodes may be closer to the place where the event happens than others. As a result, data collected at those nodes will be more informative. It will be more efficient if these data can be sampled with more bits to increase their weights in hard decision fusion. It is therefore necessary for the fusion centre to conduct hard decision fusion where different nodes send different numbers of bits sampled from the collected data.

In this chapter, the optimal hard decision fusion rule that combines

different numbers of bits sent from different nodes is derived. The BER performance and the best thresholds for special cases are also provided, followed by the simulation and discussion. The contributions of this chapter can be summarized as follows:

• First of all, the optimum rule that minimizes the probability of error for fusing the decisions from different nodes with different numbers of bits following a likelihood ratio test are derived.

• As special cases of this result above, the optimal hard decision fusion rules in the previous literature that combines one bit or two bits sent from each node are also generalized to the derived case when each node sends the arbitrary number of bits.

• Then, the BER performance for hard decision fusion with one bit from each node is derived for BPSK and then extended to NCFSK while the BER for hard decision fusion with more than one bit are simulated using our derived expressions.

• Next, the optimum thresholds for hard decision fusion rules with more than one bit are obtained through simulation. The performance of this new fusion rule is simulated for different fading channels by taking both the energy penalty and the BER penalty into account.

• Numerical results show that this new scheme can achieve better performance with higher energy efficiency. Compared with existing hard decision fusion rules that combine the same number of bits from different nodes, the proposed new rule has great flexibility that allows different nodes to transmit the minimum number of bits for their samples in order to save energy. Importantly, this chapter shows that when the fusion is accurate enough, it is not necessary to transmit too many bits for the data samples as the energy

penalty is larger in doing this.

The remainder of this chapter is organized as follows. Section 6.2 introduces the system model. Section 6.3 proposes the optimal hard decision fusion rule with arbitrary numbers of bits while Section 6.4 presents the BER expression of decision fusion with one bit using characteristic function. Numerical results are presented in Section 6.5, followed by concluding remarks and discussions in Section 6.6.

6.2 System Model and Technical Background

6.2.1 System Model

This chapter considers a system where several nodes are deployed to collect binary source information with two hypotheses as H_0 and H_1. Each node collects a noisy and fading observation from the source. Assume that BPSK is used. The observation or the data is sampled using different numbers of bits based on their reliability. After that, different numbers of bits representing data will be sent to the fusion centre where an overall decision is made, as shown in Fig. 6.1.

The observation at the i-th node can be expressed as

$$v_i = b \cdot s_i + a_i \tag{6.1}$$

where $i = 1, 2, ..., L$ index different node, $b = -1$ if H_0 is true and $b = 1$ if H_1 is true, s_i is the fading amplitude, a_i is the Gaussian noise with mean zero and variance σ_i^2. Then, the quantized data will be sent to the fusion centre through a control channel corrupted by fading and Gaussian noise with

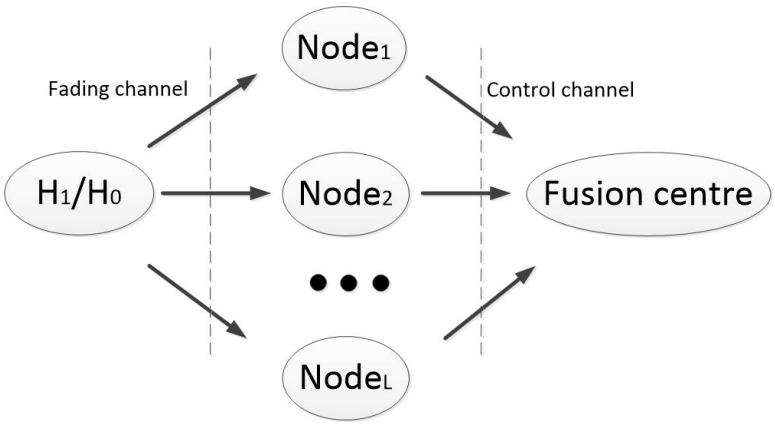

Figure 6.1: System model.

mean zero and variance β_i^2. $b = -1$ and $b = 1$ are assumed to have equal probabilities. Also assume that all the received signals are independent and that fading is independent of noise.

6.2.2 Technical Background

In [82, 83], partial data fusion combining has been studied for an additive white Gaussian noise channel. In [148], partial decision combining has been considered for direct-sequence code-division-multiplex-access systems. In [32], one-bit and two-bit combining schemes for partial decisions were derived for Rayleigh fading channels. [146] has proposed the optimal hard decision fusion rule using one bit according to the maximum likelihood principle as

$$\hat{b} = sign\left(\sum_{i=1}^{L} d_i \cdot ln\frac{P_{c|s_i}}{P_{e|s_i}}\right) \tag{6.2}$$

where $P_{c|s_i}$ and $P_{e|s_i}$ are the correct rate and the error rate of each hard limiter, respectively, with $P_{c|s_i} = 1 - P_{e|s_i} = 1 - Q(\frac{s_i}{\sigma_i})$ and $d_i = sign\,(v_i)$ where $sign(\cdot)$ is the signum function with $sign(\cdot) = 1$ if $x > 0$, $sign(\cdot) = -1$ if $x < 0$ and

$sign(\cdot) = 0$ if $x = 0$.

Using the device, $x = |x|sign(x)$, MRC in [34] can be easily rewritten as

$$\hat{b} = sign\left(\sum_{i=1}^{L} d_i \cdot ln\frac{s_i\,|v_i|}{\sigma_i^2}\right) \tag{6.3}$$

which requires knowledge of $|v_i|$ in addition to s_i. This can be considered as an optimal hard decision fusion rule using an infinite number of bits for the data collected at each sensor.

In [32], the optimal hard decision fusion rule using two bits representing data collected at each node was derived as

$$\hat{b} = sign\left(\sum_{i=1}^{L} d_{i1}\left[ln\frac{P_{1i}P_{3i}}{P_{2i}P_{4i}} + d_{i2}ln\frac{P_{1i}P_{4i}}{P_{2i}P_{3i}}\right]\right) \tag{6.4}$$

where $[d_{i1}, d_{i2}] = \begin{cases} [-1 \quad +1] & v_i < -T \\ [-1 \quad -1] & -T \le v_i < 0 \\ [+1 \quad -1] & 0 \le v_i < T \\ [+1 \quad +1] & T \le v_i \end{cases}$,

and T is the threshold for quantization, $P_{1i} = Pr(v_i > T)$, $P_{2i} = Pr(v_i < -T)$, $P_{3i} = Pr(0 < v_i < T)$ and $P_{4i} = Pr(-T < v_i < 0)$.

In the following, (6.2) and (6.4) will be generalized to the case when an arbitrary number of bits for different samples are used to represent the data collected at each node.

6.3 Optimal Hard-Decision Fusion Rule

The optimum rule that minimizes the probability of error for fusing the decisions from different nodes with different numbers of bits follows a likelihood

ratio test [77, 146]. The data decision selects $\hat{b} = 1$ if

$$P(\{d_i\}_{i=1}^{L}, \{s_i\}_{i=1}^{L}|b = 1) > P(\{d_i\}_{i=1}^{L}, \{s_i\}_{i=1}^{L}|b = -1). \tag{6.5}$$

Assume that fading is independent of noise. It can be obtained from (6.5) that

$$\begin{aligned} &P(\{d_i\}_{i=1}^{L}|\{s_i\}_{i=1}^{L}, b = 1)P(\{s_i\}_{i=1}^{L}|b = 1) > \\ &P(\{d_i\}_{i=1}^{L}|\{s_i\}_{i=1}^{L}, b = -1)P(\{s_i\}_{i=1}^{L}|b = -1). \end{aligned} \tag{6.6}$$

Further, assume that fading is independent of the transmitted signal. Thus (6.6) can be rewritten as

$$\prod_{i=1}^{L} \frac{P(d_i|s_i, b = 1)}{P(d_i|s_i, b = -1)} > 1. \tag{6.7}$$

If $b = 1$ is sent and the received signal v_i at the i-th node is divided into intervals, one has

$$P_{ij|1} = P(T_{i,j-1} < v_i \leq T_{i,j}|s_i, b = 1) \tag{6.8}$$

where $i = 1, 2, \cdots, L$ is the node index, $j = 1, 2, \cdots, 2^{n_i}$ is the interval index, n_i is the number of bits that the observed sample has been quantized with, $T_{i,j}$ is the j-th threshold of the i-th node and $T_{i,j} = -T_{i,2^{n_i}-j}$ assuming symmetry. One has $T_{i,0} = -\infty$ and $T_{i,2^{n_i}} = +\infty$. Similarly, if $b = -1$ is sent, one has

$$P_{ij|-1} = P(T_{i,j-1} < v_i \leq T_{i,j}|s_i, b = -1). \tag{6.9}$$

One can see that $P_{ij|-1}$ is the symmetric interval of $P_{2^{n_i}-j+1|-1}$. Assume that k_{ijm} can represent the interval corresponding to the m-th bit of the j-th interval

of the i-th node and k_{ijm} should also satisfy the symmetric criterion. For instance, when $b = 1$ is sent and 3 bits is assumed, if [1 -1 -1] is used to represent $P_{ij|1}$, then [-1 1 1] should be used to represent $P_{2^{n_i}-j+1|1}$ in order to meet the symmetric criterion. In the quantization of the observation, denote the m-th bit of the i-th node as d_{im}, $m = 1, 2, \cdots, n_i$. d_{im} should be the same as k_{ijm} if the received signal v_i falls into the same j-th interval.

Using these expressions, (6.7) can be rewritten as

$$\prod_{i=1}^{L}\prod_{j=1}^{2^{n_i}}(\frac{P_{ij|1}}{P_{ij|-1}})^{\Pi_{m=1}^{n_i}\frac{1+k_{ijm}d_{im}}{2}} > 1. \tag{6.10}$$

Taking logarithms on both sides of (6.10), one has

$$\sum_{i=1}^{L}\sum_{j=1}^{2^{n_i}}(\prod_{m=1}^{n_i}\frac{1+k_{ijm}d_{im}}{2})\cdot ln\frac{P_{ij|1}}{P_{ij|-1}} > 0. \tag{6.11}$$

Using the symmetric criterion, one has $P_{ij|-1} = P(T_{i,j-1} < -1\cdot s_i + n_i \leq T_{i,j}) = P(T_{i,j-1} < -s_i - n_i \leq T_{i,j}) = P(T_{i,2^{n_i}-j} < s_i + n_i \leq T_{i,2^{n_i}-j+1}) = P_{2^{n_i}-j+1|1}$. Therefore the fusion rule can be simplified as

$$\begin{aligned}\hat{b} = sign\Bigg[&\sum_{i=1}^{L}\sum_{j=1}^{2^{n_i-1}}\left(\prod_{m=1}^{n_i}\left(\frac{1+k_{ijm}d_{im}}{2}\right)-\prod_{m=1}^{n_i}\left(\frac{1-k_{ijm}d_{im}}{2}\right)\right)\\ &\times ln\frac{P_{ij|1}}{P_{2^{n_i}-j+1|1}}\Bigg]\end{aligned} \tag{6.12}$$

Note that (6.12) is the sum of the multi-bit decisions from L nodes, each with a different number of bits weighted by a reliability term. Each weight is determined by first estimating the fading gain of the channel s_i and then using the analytical expression as (6.12). By replacing n_i with n and removing $\frac{1}{2^{n_i}}$

in (6.12), one can have

$$\hat{b} = sign\left[\sum_{i=1}^{L}\sum_{j=1}^{2^{n-1}}\left(\prod_{m=1}^{n}(1+k_{ijm}d_{im}) - \prod_{m=1}^{n}(1-k_{ijm}d_{im})\right) \times ln\frac{P_{ij|1}}{P_{2^n-j+1|1}}\right], \tag{6.13}$$

a special case when all the L nodes have the same n bits to represent the observation. It can be easily verified that (6.2) and (6.4) are special cases of (6.13) when $n = 1$ and $n = 2$, respectively.

This scheme can also be used in cognitive radio systems [149,150] where measurements from different secondary users must be combined at a base station to decide the presence of the primary user. Also, this scheme can be used in autonomous vehicle navigation using fusion with multi-bit quantized data representing multi-node information [141].

6.4 BER of Decision Fusion with 1 Bit

In a Nakagami-m fading channel (as introduced in Section 2.1.3), the received SNR per symbol γ is distributed according to a Gamma distribution as

$$f_\Gamma(\gamma) = \frac{m^m \gamma^{m-1}}{\gamma_0^m \Gamma(m)} e^{-\frac{m\gamma}{\gamma_0}},\ \gamma \geq 0 \tag{6.14}$$

where the instantaneous SNR γ is defined as $E_s s^2/N_0$, s is the fading amplitude, E_s is the received power per node, N_0 is the noise power, m is the fading parameter ranging from 1/2 to ∞, m=1 gives the Rayleigh model and $\Gamma(z) = \int_0^\infty t^{z-1}e^{-t}dt$ [36]. Simulators for Rayleigh and Nakagami fading channels were reported in [37, 38].

The approximate characteristic function $\Phi_X(w)$ of hard decision fusion for BPSK using one bit and $L = 1$ in a Rayleigh fading channel is derived in Appendix D.1. Using this characteristic function in (D.8) in Appendix D.1, the BER of the decision fusion with one bit in (6.2) for BPSK can be expressed as [151]

$$P_e \approx \frac{1}{2} - \frac{1}{\pi} \int_0^\infty \frac{\Im\left\{(\Phi_X(w))^L\right\}}{w} dw \tag{6.15}$$

where $\Im\{x\}$ denotes the imaginary part of x. It is very difficult to obtain closed-form expressions for the BERs of other rules or when $m \neq 1$. They will be evaluated by simulation in the next section.

6.5 Numerical Results and Discussion

The first part of this section assumes a perfect control channel (without considering energy penalty). The best values of thresholds for the fusion rules using more than one bit in a Rayleigh fading channel are calculated by minimizing the BERs using simulation.

In the second part of this section, the performances of decision fusion rule based on arbitrary numbers of bits are evaluated when energy penalty is considered, where σ_i and β_i are fixed at 1.

Also, denote that the SNR between the source and the relay nodes as γ_1 or SNR_1, while the SNR between the relay nodes and the fusion centre as γ_2 or SNR_2 for the control channel. When energy penalty is considered, denote the unit energy as E and assume that the node consumes E, $2E$, $3E$, $4E$ when 1 bit, 2 bits, 3 bits and 4 bits are sent to the fusion centre that represent the observations, respectively. For MRC in (6.3), this chapter assumes that it

consumes $16E$ (2 bytes) when sending the whole sample to the fusion centre from the nodes. Also, assume the total energy is fixed at $16E$ in the relay nodes.

In all the figures below, denote (a, b, c) as the first, second and third relay node each using a number of a, b, c bits, respectively, to represent the observations made at different nodes.

6.5.1 Best Thresholds and BERs Assuming a Perfect Control Channel

This subsection uses simulation to calculate the best thresholds for 2 bits, 3 bits and 4 bits that represent the quantized observations made at different nodes in a Rayleigh fading channel. Fig. 6.2 gives the BER curves for fusion rules using 2 bits, 3 bits and 4 bits as functions of T_1, T_3, T_7 respectively, at $\gamma_1 = 5$ dB and $L = 3$.

In the simulation, $T_2 = 0$ for the fusion rule using 2 bits and $T_4 = 0$, $T_2 = 2T_3$, $T_1 = 3T_3$ for the fusion rule using 3 bits and $T_8 = 0$, $T_6 = 2T_7$, $T_5 = 3T_7$, $T_4 = 4T_7$, $T_3 = 5T_7$, $T_2 = 6T_7$, $T_1 = 7T_7$ for the fusion rule using 4 bits. One can see that BER curve reaches the lowest point at 0.01379 when $T_1 = 0.5s_i$ for the fusion rule using 2 bits, at 0.01173 when $T_3 = 0.4s_i$ for the fusion rule using 3 bits and at 0.01107 when $T_7 = 0.3s_i$ for the fusion rule using 4 bits.

Our examinations also find that the best thresholds for other values of SNR, other numbers of bits and other values of m in a Nakagami-m fading channel are almost the same, although the thresholds do slightly decrease when the SNR increases due to the fact that when the SNR increases, the

signal is dominant and the channel condition gets better so that only one bit of the sample is enough with all thresholds approaching zero to achieve this. Because when SNR is large, the probability of having a large value of the received signal is also large so that the values of the thresholds become small. Also, these best thresholds can apply to the case when the control channel is not perfect. To simplify our discussion and design, these thresholds (see Table 6.1) are used for all the following figures.

Table 6.1: The values of best thresholds using 1 bit, 2 bits, 3 bits and 4 bits used in Figs. 6.4-6.8.

Number of bits	Threshold
1	$T_1 = 0$
2	$T_2 = 0,\ T_1 = 0.5s_i$
3	$T_4 = 0,\ T_3 = 0.4s_i,\ T_2 = 0.8s_i,\ T_1 = 1.2s_i$
4	$T_8 = 0,\ T_7 = 0.3s_i,\ T_6 = 0.6s_i,\ T_5 = 0.9s_i$ $T_4 = 1.2s_i,\ T_3 = 1.5s_i,\ T_2 = 1.8s_i,\ T_1 = 2.1s_i$

Fig. 6.3 gives the BER curve comparing the simulation result using (6.2) and the approximation result using numerical integration of (6.15) at $L = 1, 2, 3, 4$. One can see that the fusion performance improves as the number of nodes increases. The small mismatching errors between simulation result and approximation result may be caused by using the approximation of Gaussian-Q function and the numerical integration.

Fig. 6.4 gives the BER curves for fusion rules using MRC, using 1 bit (1, 1, 1), using 2 bits (2, 2, 2), using 3 bits (3, 3, 3) and using 4 bits (4, 4, 4) in Rayleigh fading channels. The curves for MRC, (1, 1, 1), (2, 2, 2) are the existing fusion rules in (6.3), (6.2) and (6.4) respectively, while (3, 3, 3) and (4, 4, 4) are the new fusion rules obtained from (6.12) when $n_i = 3$ and $n_i = 4$

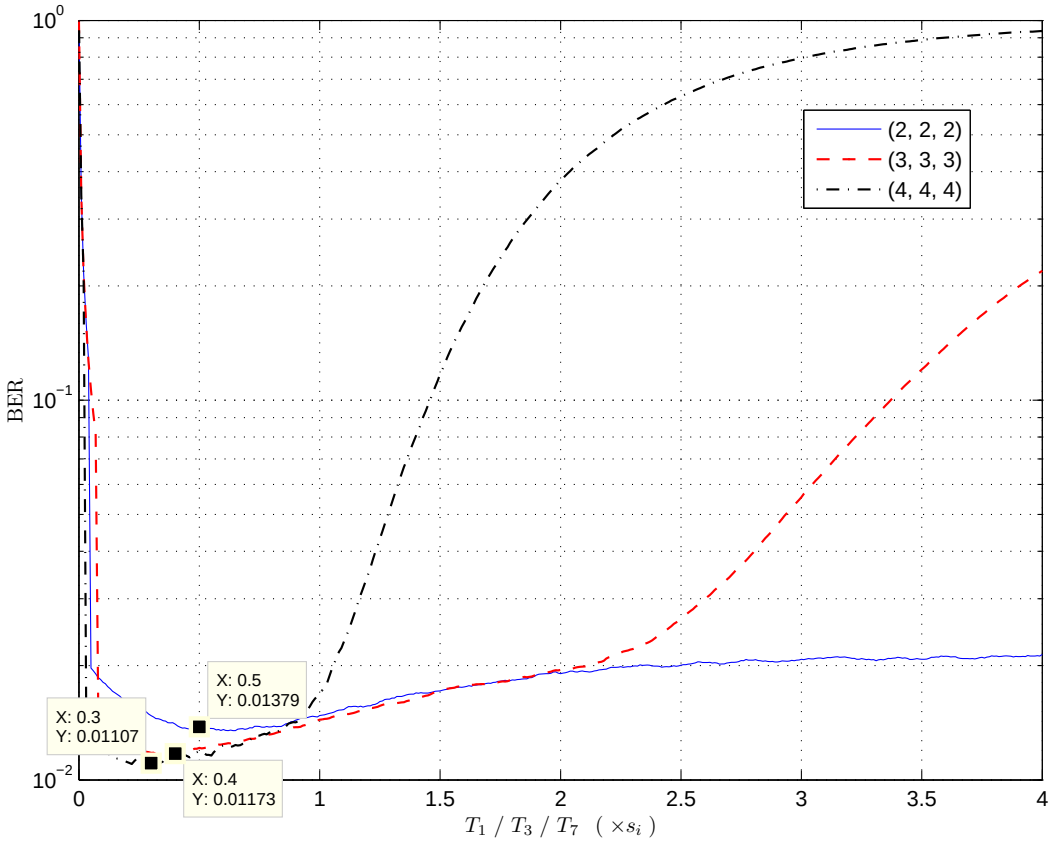

Figure 6.2: Choices of the best thresholds for the fusion rules using 2 bits, 3 bits and 4 bits at γ_1=5 dB and L=3 in Rayleigh fading channels.

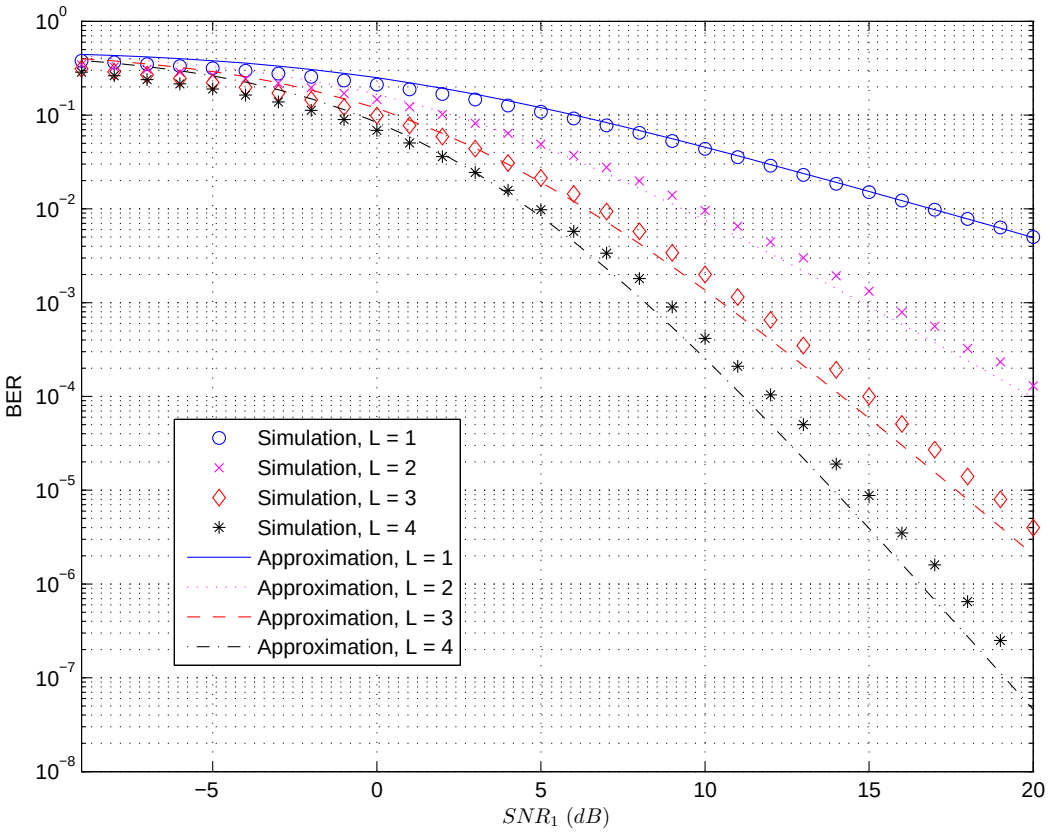

Figure 6.3: BER curves comparing the simulation and the approximation results using 1 bit to represent the observations made at $L = 1, 2, 3, 4$.

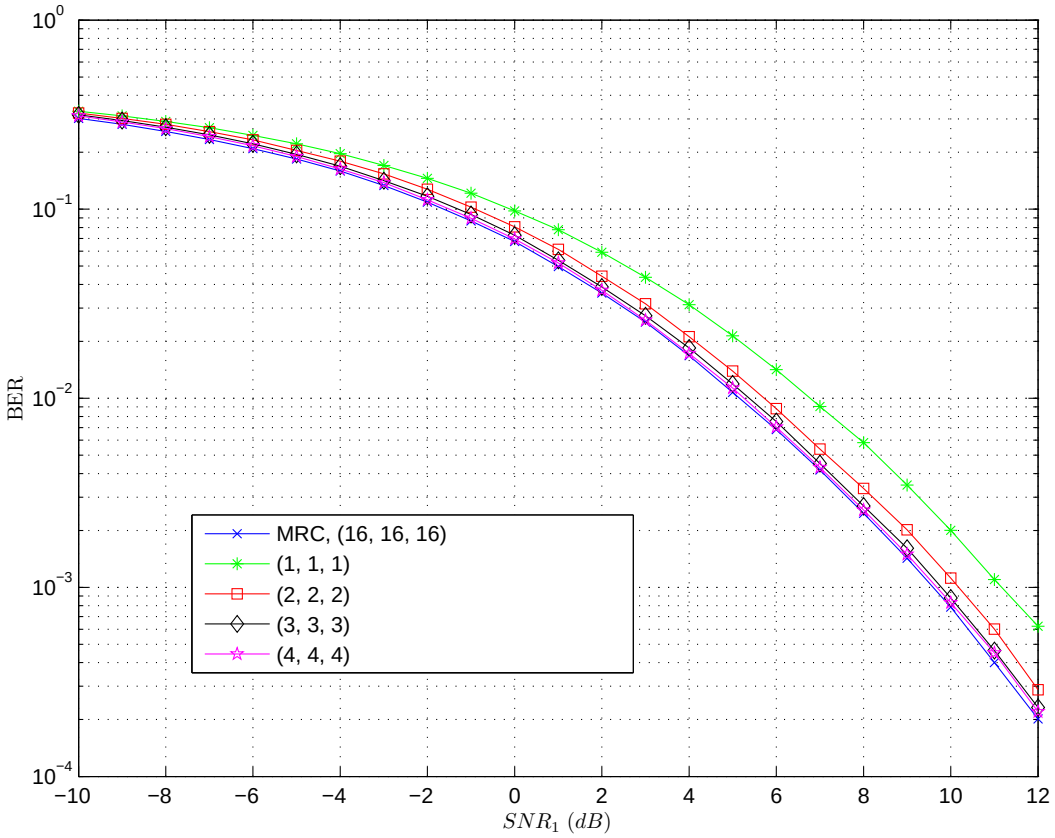

Figure 6.4: Comparison of BER curves for the decision rules using MRC, using 1 bit, using 2 bits, using 3 bits and using 4 bits in Rayleigh fading channels.

respectively. One can see that if one does not consider energy penalty, MRC performs the best, followed by the fusion rule using 4 bits, the fusion rule using 3 bits, the fusion rule using 2 bits, while the fusion rule using 1 bit performs the worst, as expected. However, more bits require more energy. Therefore the energy penalty is needed to take into account in the next subsection.

6.5.2 Simulation of Arbitrary Bits Decision Fusion Rule

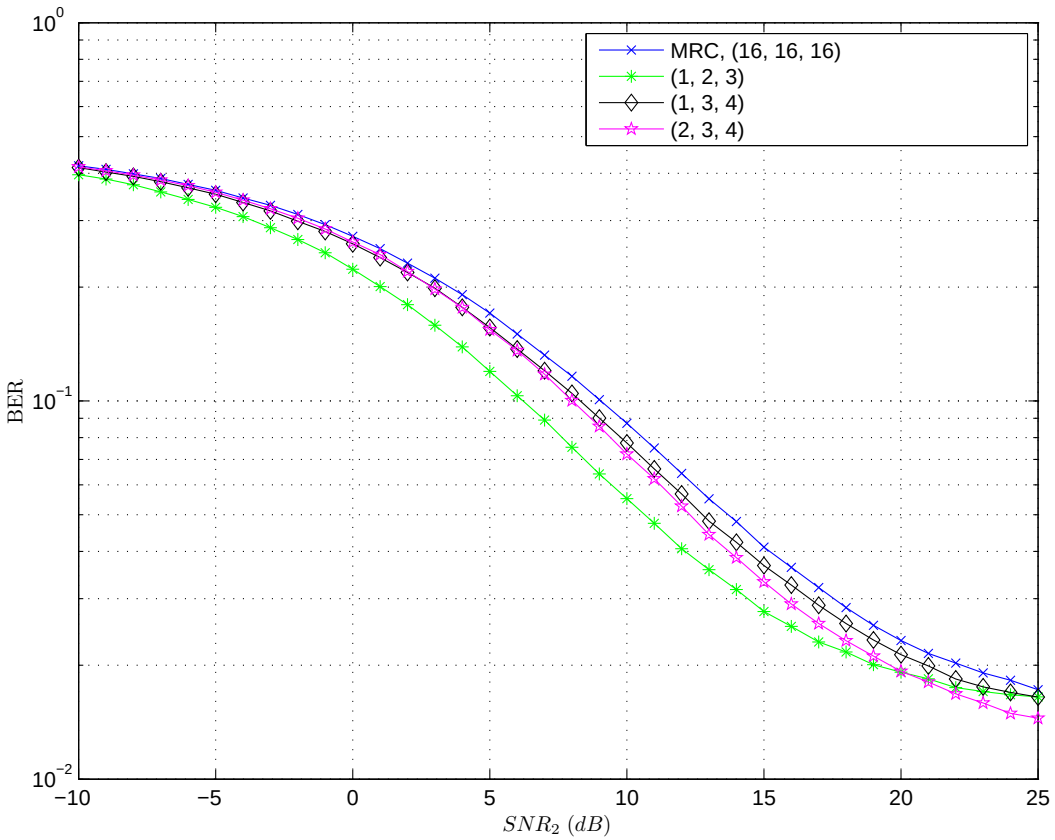

Figure 6.5: BER curves of MRC, (1, 2, 3), (1, 3, 4) and (2, 3, 4) fusion rules at $\gamma_1 = 5$ dB in Rayleigh fading channels.

In this subsection, the performances of the arbitrary bits decision fusion rule derived in the Section 6.3 are evaluated via simulation, where the value

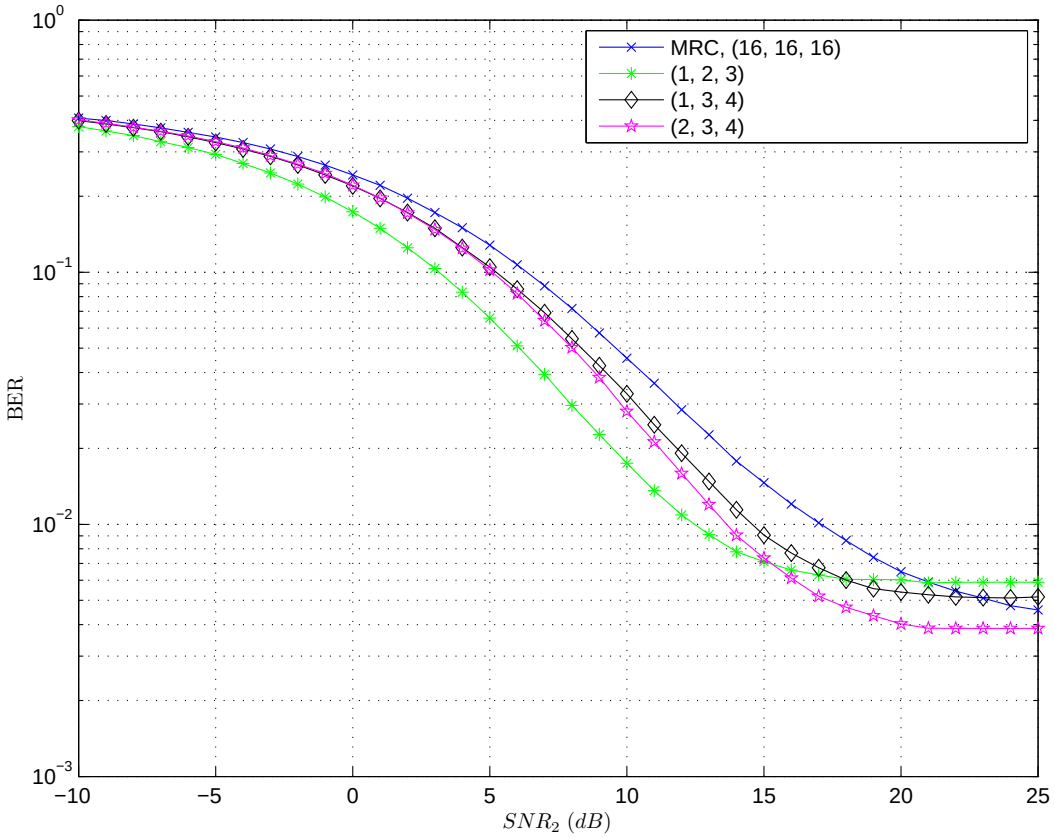

Figure 6.6: BER curves of MRC, (1, 2, 3), (1, 3, 4), (2, 3, 4) fusion rules at $\gamma_1 = 5$ dB in Nakagami-m fading channels with $m = 3$.

of threshold for the fusion rule using 1 bit, 2 bits, 3 bits and 4 bits are chosen from Table 6.1 and energy penalty is considered.

Fig. 6.5 shows the BER curves for MRC, (1, 2, 3), (1, 3, 4) and (2, 3, 4) fusion rules at $\gamma_1 = 5$ dB in Rayleigh fading channels. One can see that the (1, 2, 3) fusion rule performs the best between γ_2 = -10 dB and $\gamma_2 = 20$ dB while the (2, 3, 4) fusion rule performs the best when γ_2 is higher than 20 dB. On the other hand, MRC performs the worst in the whole range of γ_2 due to the energy penalty incurred in sending 2 bytes.

Fig. 6.6 shows the BER curves for MRC, (1, 2, 3), (1, 3, 4) and (2, 3, 4) fusion rules at $\gamma_1 = 5$ dB in Nakagami-m fading channels with $m = 3$. One can see that the performances of MRC, (1, 2, 3), (1, 3, 4) and (2, 3, 4) fusion rules improve as the value of m increases, as expected. Also, one can see that the (1, 2, 3) fusion rule is still the best fusion rule but only between γ_2 = -10 dB and $\gamma_2 = 15$ dB. The (2, 3, 4) fusion rule performs the best when $\gamma_2 > 15$ dB. One also sees that the performances of (1, 2, 3), (1, 3, 4) and (2, 3, 4) fusion rules reach an error floor when γ_2 is higher than 17 dB. In this case, we cannot obtain better BER performances unless we increase γ_1.

Fig. 6.7 shows the BER curves for MRC, (1, 2, 3), (1, 3, 4) and (2, 3, 4) fusion rules at $\gamma_2 = 10$ dB in Rayleigh fading channels. One can see that the performances of the (1, 2, 3), (1, 3, 4) and (2, 3, 4) fusion rules are nearly the same when -10 dB $< \gamma_1 <$ -2 dB. However, the BER difference between the (1, 2, 3) fusion rule and the other two rules increases as the value of γ_1 increases. In this case, MRC performs the worst when γ_1 is lower than 6 dB but becomes the best when γ_1 is higher than 8 dB. This is due to the fact that MRC has the worst performance due to its largest energy penalty, but when γ_1 increases, the performance gain of MRC increases quickly to compensate

the energy penalty.

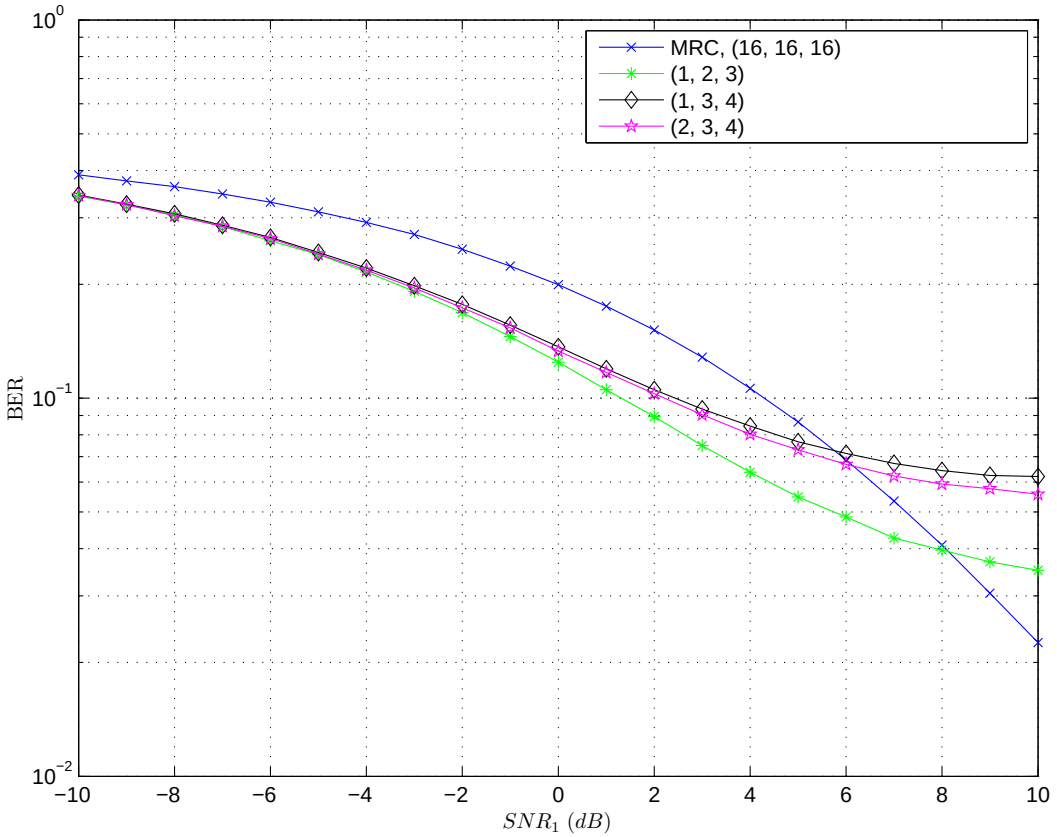

Figure 6.7: BER curves of MRC, (1, 2, 3), (1, 3, 4) and (2, 3, 4) fusion rules at $\gamma_2 = 10$ dB in Rayleigh fading channels.

Fig. 6.8 shows that BER curves of MRC, (1, 2, 3), (1, 3, 4) and (2, 3, 4) fusion rules at $\gamma_2 = 10$ dB in Nakagami-m fading channels with $m = 3$. One can see that the performances of MRC, (1, 2, 3), (1, 3, 4) and (2, 3, 4) fusion rules improve as the value of m increases, as expected. The BER difference between (1, 2, 3), (1, 3, 4) and (2, 3, 4) fusion rules is larger compared with Fig. 6.7.

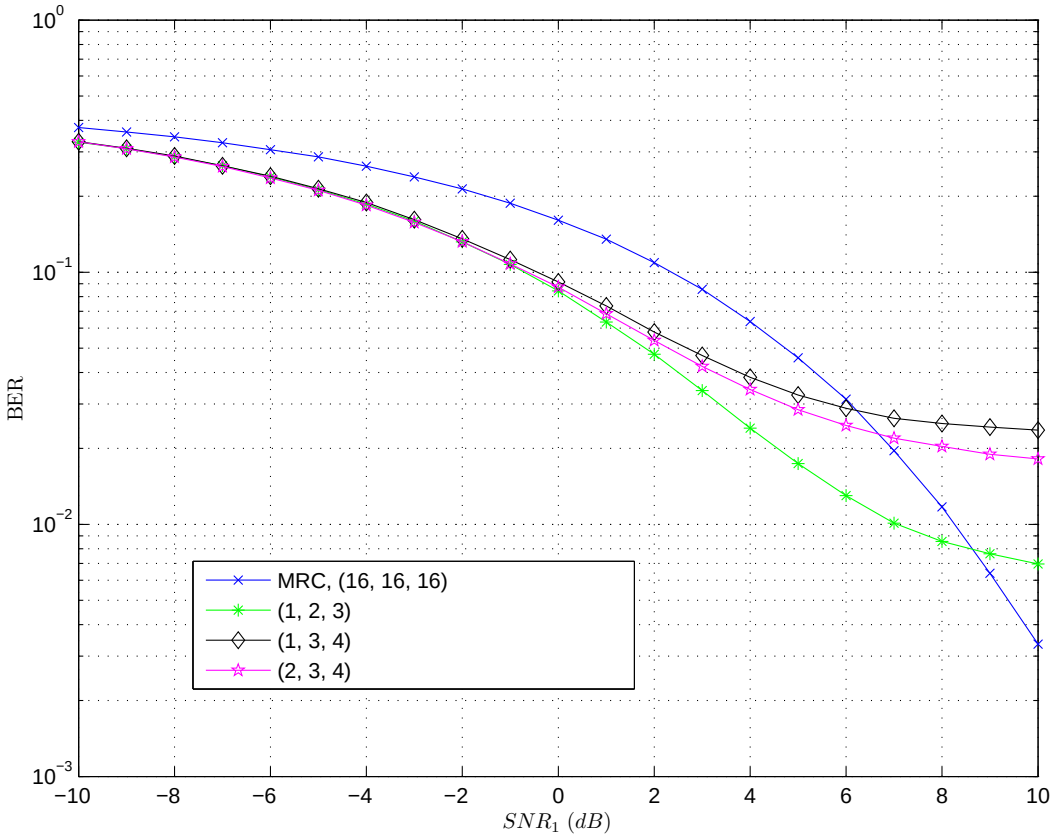

Figure 6.8: BER curves of MRC, (1, 2, 3), (1, 3, 4) and (2, 3, 4) fusion rules at $\gamma_2 = 10$ dB in Nakagami-m fading channels with $m = 3$.

6.6 Conclusions

A new hard decision fusion rule where each node can transmit an arbitrary number of bits has been derived. Compared with the existing hard decision fusion rules that combine the same number of bits from different nodes, the new rule has great flexibility that allows different nodes to transmit the minimum number of bits for their samples in order to save energy.

Numerical results have shown that this new scheme can achieve better performance with higher energy efficiency. The proposed fusion rule is very useful in mobile networks, such as in a vehicular system, in which the nodes are battery-powered and energy saving is an important issue for efficient decision-making.

Future work will be aimed at lifetime maximization and energy-related optimization because energy cost often equals to the number of bits multiplied by the energy per bit.

Chapter 7

Conclusions and Future Work

In this thesis, we have focused on the performance analysis for cooperative wireless communications by considering several realistic situations, such as the system with unknown channel state information, with limited transmission power, with random and fixed interferers. We have tried to use approximate methods with simplified form to model complex system channels. Also, decision methods have been studied and evaluated in this thesis.

In this chapter, the main contributions and findings of this thesis are summarized in Section 7.1 and future works are suggested in Section 7.2.

7.1 Conclusions

The purpose of this thesis is to present an analytical performance evaluation of the cooperative wireless system and provide guidance to the practical system design.

First of all, an overview of cooperative wireless communications is given in Chapter 1, including the advantage of wireless communications, evolution

of mobile communication and introduction to cooperative relaying systems.

Then, a detailed background is shown in Chapter 2, which includes important fading channels, essential modulation schemes, popular data fusion methods, widely used system performance measures and related methods applied in this thesis. More importantly, a comprehensive overview of the cooperative wireless relaying is given and its applications in the LTE-Advanced standard is introduced.

Third, performance analysis and optimal energy allocation for amplify-and-forward relaying systems using pilot-aided maximum likelihood estimation in slowly fading Rayleigh channel are studied. They can be used in applications with high data rate transmission or the channel with coherence time much larger than the bit interval. Generalized BER expression including high order modulations for both disintegrated channel and cascaded channel are presented. Their closed-form approximations are also given. Based on the these BER results, optimal energy allocation for disintegrated channel and cascaded channel are derived in two cases. In the first case, the optimal values of pilot energy under the total transmitting energy constraints at the source and the optimal values of pilot energy under the total transmitting energy constraints at the relay are obtained, separately. This can be applied to the case when the source, relay or destination are battery-limited moving nodes. In the second case, the optimal energy allocation between the pilot energy at the source, the pilot energy at the relay, the data energy at the source and the data energy at the relay are obtained when their total transmitting energy is fixed. This can be used to the case when the source, relay and destination are fixed nodes which can be charged.

Fourth, performance analysis for amplify-and-forward relaying systems

with global relay selection is studied. This part considers that the relays and the destination suffer from path loss, independent but non-identically distributed Nakagami-m fading as well as multiple Nakagami-m interferences. However, this part assumes perfect channel state information in order to simplify the system model and analysis. Two cases (i.e. randomly distributed and fixed interferers) are considered in this part. For randomly distributed interferers, the number and the location of the interferers are random. This is the case for multiple-access systems with mobile nodes. For fixed interferers, the number and the location of the interferers are fixed. This is the case for fixed-access wireless systems where wireless interconnections are mainly provided to replace wires with considerably low or little mobility. The outage probability of the instantaneous end-to-end SINR are obtained in the form of one-dimensional integral for both cases. Closed-form lower bound of this outage probability and asymptotic expressions are also given to provide readers with several useful insights. The special cases when the interferences are i.i.d and when the signal experiences Rayleigh fading are also examined.

Fifth, performance analysis for multihop relaying and multiple scattering system over α - μ fading channels are studied. In this part, the systems with interferers and without interferers are considered. Three system model (i.e. SRP, SP and RSP of independent α - μ RVs) are proposed in this part. SRP can be used to calculate the outage probability for wireless multihop relaying systems or multiple scattering channels with interferences. SP can be used to calculate the outage probability for above systems without interferences. Moreover, RSP is proposed to calculate the outage probability of the SIR in multiple scattering system with interference. Exact results of MGF for the SRP and the SP in closed-from are derived, based on which, the exact

PDFs and CDFs of the SRP and the SP in the form of one-dimensional integral is derived while the closed-form finite series form of these PDFs and CDFs are also given. More importantly, new closed-form approximation methods, GGRA is proposed to approximate SRP while GRA is proposed to approximate SRP and the RSP. Also, two conventional approximation methods GGA and GA are applied to approximate SP. Moment-matching approximations are used to determine the unknown parameters of the above approximation methods.

Finally, a new hard-decision fusion rule that combines arbitrary numbers of bits for different samples taken at different nodes is proposed. The best thresholds of the hard decision fusion rules with more than one bit are obtained through simulation. The performance of this new fusion rule is simulated for Nakagami-m fading channel by taking both the energy penalty and the BER penalty into account. The exact BER expression for hard decision fusion with one bit for each node is derived for BPSK and extended to NCFSK while the BER for hard decision fusion with more than one bit is simulated. Importantly, this part shows that when the fusion is accurate enough, it is not necessary to transmit too many bits for the data samples as the energy penalty is larger in doing this.

7.2 Future Work

The work presented in this thesis also provide good guidelines and suggestions for the potential future research. Some of them are listed below.

• This thesis considers a single carrier system during the amplify-and-forward transmission. An interesting future work is to extend it to multi-

carrier systems with higher spectral efficiency.

• This thesis considers a full pilot-aided estimation system. This work can be extended to the case which applies the scattered pilots through the data transmission. It will make the system have better performance and lower complexity.

• This thesis considers a single relay system with channel state information aided. However, it assumes perfect channel state information when considering multiple relays or multihop transmission in order to get tractable results. Future work can be done in more practical situation, i.e. channel state information should be estimated in all relays and in all hops. In this case, new effective approximations should be developed to analyze the system performance.

• Randomly distributed and fixed interferers, along with the channel state information estimation and relay selection should be considered at the same time in the future, to provide a comprehensive evaluation to the system performance.

• This thesis only addresses the concern about the optimal energy allocation in a single relay system. Optimal energy allocation between pilots and data can be also investigated in multihop transmission, provided that closed-form expressions for BERs or outage probability can be obtained. Interference can also be considered in this case.

• Moreover, optimal energy allocation between each hop can be further studied in multihop transmission if randomly distributed or fixed interferers is considered.

• Other performance measures, other than BER and outage probability, can be studied in the future to provide more insights to the analysis and design

of practical system, such as examining diversity order, diversity gain, capacity of the system.

• The optimal fusion rule proposed in this thesis can be extended to other area, such as detection of the secondary user in cognitive radio.

• Similar performance analyses and measure in this thesis can be extended to other wireless cooperative relaying system, such as decode-and-forward, compress-and-forward systems.

• In future, relevant experiments can be designed and implemented to verify our proposed methods and systems in this thesis.

Appendix A

Derivation for DCE and CCE

A.1 Derivation of Outage Probability for the First Case in DCE

The CDF of the end-to-end SNR in (3.19) can be derived as

$$\begin{aligned} F_{\gamma_{end_1}}(\gamma_{th}) &= \int_0^\infty P\left(\frac{\gamma_2\hat{\gamma}_1}{\gamma_2+\hat{\gamma}_1+1+\gamma_{\varepsilon_1}\ \gamma_2} \leq \gamma_{th}|\gamma_2\right) f(\gamma_2)d\gamma_2 \\ &= 1-\int_{\gamma_{th}}^\infty e^{-\frac{\gamma_{th}\gamma_2+\gamma_{th}+\gamma_{\varepsilon_1}\ \gamma_{th}\gamma_2}{\bar{\gamma}_1(\gamma_2-\gamma_{th})}} f(\gamma_2)d\gamma_2. \end{aligned} \tag{A.1}$$

By using $z=\gamma_2-\gamma_{th}$, one has.

$$F_{\gamma_{end_1}}(\gamma_{th}) = 1-\frac{1}{\bar{\gamma}_2}\int_0^\infty e^{-\frac{(z+\gamma_{th})\gamma_{th}+\gamma_{th}+(z+\gamma_{th})\gamma_{th}\ \gamma_{\varepsilon_1}}{\bar{\gamma}_1 z}-\frac{z+\gamma_{th}}{\bar{\gamma}_2}} dz. \tag{A.2}$$

Using [36, (3.471)], the CDF can be derived as (3.20).

A.2 Derivation of the First BER Approximation for the First Case in DCE

In the asymptotic case, we have $\bar{\bar{\gamma}}_1, \bar{\gamma}_2 \to \infty$. Using the approximation of [36]

$$K_\nu(x) \approx \frac{2^{\nu-1}\Gamma(\nu)}{x} \tag{A.3}$$

in (3.20), one has

$$F_{\gamma_{end_1}}(\gamma_{th}) \approx 1 - e^{-\gamma_{th}\beta_2}. \tag{A.4}$$

Then using (3.21) and (A.4), one can obtain the approximate BER as (3.22).

A.3 Derivation of the Second BER Approximation for the First Case in DCE

When $\gamma_{\varepsilon_1}\ \gamma_{th} + \gamma_{th} \gg 1$, we have $\gamma_{\varepsilon_1}\ \gamma_{th} + \gamma_{th} + 1 \approx \gamma_{\varepsilon_1}\ \gamma_{th} + \gamma_{th}$. Then (3.20) can be approximated as

$$F_{\gamma_{end_1}}(\gamma_{th}) \approx 1 - \beta_1\gamma_{th}e^{-\gamma_{th}\beta_2}K_1(\gamma_{th}\beta_1). \tag{A.5}$$

One can use (A.5) in (3.21) with [36, (6.621)] to solve the integral as (3.23).

A.4 Derivation of Outage Probability for the Second Case in DCE

The CDF of the end-to-end SNR in (3.28) can be written as

$$\begin{aligned} & F_{\gamma_{end_2}}(\gamma_{th}) \\ & = \int_0^\infty P\left(\frac{\hat{\gamma}_2\hat{\gamma}_1}{\hat{\gamma}_2\gamma_{\varepsilon_1} + \hat{\gamma}_1\gamma_{\varepsilon_2} + \gamma_{\varepsilon_1}\,\gamma_{\varepsilon_2} + \hat{\gamma}_2 + \hat{\gamma}_1 + 1 + \gamma_{\varepsilon_2}} \leq \gamma_{th}|\hat{\gamma}_2\right) f(\hat{\gamma}_2)d\hat{\gamma}_2 \\ & = 1 - \int_{\gamma_{th}}^\infty e^{-\frac{\hat{\gamma}_2(\gamma_{th}\gamma_{\varepsilon_1}+\gamma_{th})+\gamma_{\varepsilon_1}\gamma_{\varepsilon_2}\gamma_{th}+\gamma_{\varepsilon_2}\gamma_{th}+\gamma_{th}}{\hat{\gamma}_1(\hat{\gamma}_2-\gamma_{\varepsilon_2}\gamma_{th}-\gamma_{th})}} f(\hat{\gamma}_2)d\hat{\gamma}_2. \end{aligned} \tag{A.6}$$

Let $z = \hat{\gamma}_2 - \gamma_{\varepsilon_2}\gamma_{th} - \gamma_{th}$ and using [36, (3.471)], the CDF can be derived as (3.29).

A.5 Derivation of Outage Probability for CCE

By substituting $\hat{H}$ with $\hat{H}^2$ in (3.15), one can get the PDF of $\hat{H}^2$ as

$$f_{\hat{H}^2}(x) = \frac{2K_0\left(2\sqrt{\frac{x}{\Omega}}\right)}{\Omega},\ x > 0. \tag{A.7}$$

Then, one can get the CDF of $\hat{H}^2$ as

$$F_{\hat{H}^2}(y) = 1 - 2\sqrt{\frac{y}{\Omega}}K_1\left(2\sqrt{\frac{y}{\Omega}}\right). \tag{A.8}$$

Using (3.45), $\hat{H}^2$ can be written as

$$\hat{H}^2 = \frac{\gamma_{fix}(E_d\Omega_\varepsilon G_{d_{fix_1}}^2 + N)}{E_d G_{d_{fix_1}}^2}. \tag{A.9}$$

Then, using (A.8) and (A.9), the outage probability can be derived as (3.46).

Appendix B

Derivation for Random Interferers and Fixed Interferers

B.1 Derivation of PDF of Y_{sj} for Random Interferers

One has the c-th order moment of (4.10) as [94]

$$E(Y_{sj}^c) = \frac{a_{sj}^c \Gamma\left(\frac{d_{sj}+c}{p_{sj}}\right)}{\Gamma\left(\frac{d_{sj}}{p_{sj}}\right)} \tag{B.1}$$

where c represents the c-th order moment. Denote $\eta_{1,ij} = \int_0^\infty f_l(l_{ij})\eta(l_{ij})dl_{ij}$, $\eta_{2,ij} = \int_0^\infty f_l(l_{ij})\eta^2(l_{ij})dl_{ij}$ and $\eta_{3,ij} = \int_0^\infty f_l(l_{ij})\eta^3(l_{ij})dl_{ij}$. One can derive the

first-order moment of Y_{sj} as

$$\begin{aligned} E(Y_{sj}) &= \sum_{I=0}^{\infty} \frac{e^{-\lambda_I A_I}(\lambda_I A_I)^I}{I!} \sum_{i=1}^{I} E(\Omega_{ij}) E(|h_{ij}|^2) \\ &= \sum_{I=0}^{\infty} \frac{e^{-\lambda_I A_I}(\lambda_I A_I)^I}{I!} \sum_{i=1}^{I} K_{ij} P_{ij} \eta_{1,ij}, \end{aligned} \tag{B.2}$$

the second-order moment of Y_{sj} as

$$\begin{aligned} E(Y_{sj}^2) &= \sum_{I=0}^{\infty} \frac{e^{-\lambda_I A_I}(\lambda_I A_I)^I}{I!} E\left\{ \left(\sum_{i_1=1}^{I} \Omega_{i_1 j} \ |h_{i_1 j}|^2 \right) \left(\sum_{i_2=1}^{I} \Omega_{i_2 j} \ |h_{i_2 j}|^2 \right) \right\} \\ &= \sum_{I=0}^{\infty} \frac{e^{-\lambda_I A_I}(\lambda_I A_I)^I}{I!} \left(\sum_{i=1}^{I} K_{ij}^2 P_{ij}^2 \eta_{2,ij} \frac{m_{ij}+1}{m_{ij}} + \sum_{i_1=1}^{I} \sum_{i_2 \neq i_1 = 1}^{I} \right. \\ &\left. K_{i_1 j} P_{i_1 j} K_{i_2 j} P_{i_2 j} \eta_{1,ij}^2 \right) \end{aligned} \tag{B.3}$$

and the third-order moment of Y_{sj} as

$$\begin{aligned} E(Y_{sj}^3) &= \sum_{I=0}^{\infty} \frac{e^{-\lambda_I A_I}(\lambda_I A_I)^I}{I!} \\ &\times E\left\{ \left(\sum_{i_1=1}^{I} \Omega_{i_1 j} \ |h_{i_1 j}|^2 \right) \left(\sum_{i_2=1}^{I} \Omega_{i_2 j} \ |h_{i_2 j}|^2 \right) \left(\sum_{i_1=1}^{I} \Omega_{i_3 j} \ |h_{i_3 j}|^2 \right) \right\} \\ &= \sum_{I=0}^{\infty} \frac{e^{-\lambda_I A_I}(\lambda_I A_I)^I}{I!} \left(\sum_{i=1}^{I} K_{ij}^3 P_{ij}^3 \eta_{3,ij} \frac{(m_{ij}+1)(m_{ij}+2)}{m_{ij}^2} \right. \\ &+ \sum_{i_1=1}^{I} \sum_{i_2 \neq i_1 = 1}^{I} K_{i_1 j}^2 P_{i_1 j}^2 K_{i_2 j} P_{i_2 j} \eta_{2,ij} \eta_{1,ij} \frac{m_{ij}+1}{m_{ij}} \\ &\left. + \sum_{i_1=1}^{I} \sum_{i_2 \neq i_1 = 1}^{I} \sum_{i_3 \neq i_2 \neq i_1 = 1}^{I} K_{i_1 j} P_{i_1 j} K_{i_2 j} P_{i_2 j} K_{i_3 j} P_{i_3 j} \eta_{1,ij}^3 \right). \end{aligned} \tag{B.4}$$

Note that (B.2), (B.3) and (B.4) require an infinite series. However, in reality, one does not need to include many terms in the calculation as $\frac{e^{-\lambda_I A_I}(\lambda_I A_I)^I}{I!}$

decreases quickly with I. Therefore approximations of (B.2), (B.3) and (B.4) can be made by choosing finite series. Then, one can calculate the values of a_{sj}, p_{sj} and d_{sj} in (4.10) by solving

$$\begin{cases} E(Y_{sj}) = \dfrac{a_{sj}\Gamma\left(\frac{d_{sj}+1}{p_{sj}}\right)}{\Gamma\left(\frac{d_{sj}}{p_{sj}}\right)} \\ E(Y_{sj}^2) = \dfrac{a_{sj}^2\Gamma\left(\frac{d_{sj}+2}{p_{sj}}\right)}{\Gamma\left(\frac{d_{sj}}{p_{sj}}\right)} \\ E(Y_{sj}^3) = \dfrac{a_{sj}^3\Gamma\left(\frac{d_{sj}+3}{p_{sj}}\right)}{\Gamma\left(\frac{d_{sj}}{p_{sj}}\right)}. \end{cases} \tag{B.5}$$

Furthermore, with the help of Beta function $B(\cdot,\cdot)$ [36, (8.384)], one can simplify (B.5) as (4.11), which can be solved numerically by using popular mathematical software packages, such as MATLAB, MATHEMATICA and MAPLE.

B.2 Derivation of PDF of Γ_{sj} for Random Interferers

Assume independent RVs $u, x > 0$ in the equations below. Using (4.10) and (4.14) in (4.15) and after some manipulations, one has

$$\begin{aligned} f_{\Gamma_{sj}}(u) &= \frac{p_{sj}\left(\frac{m_{sj}}{\Omega_{sj}}\right)^{m_{sj}} u^{m_{sj}-1}}{a_{sj}^{d_{sj}}\Gamma(m_{sj})\Gamma\left(\frac{d_{sj}}{p_{sj}}\right)} \\ &\times \int_{\sigma_{sj}^2}^{\infty} (x-\sigma_{sj}^2)^{d_{sj}-1} x^{m_{sj}} \exp\left(-\left(\frac{x-\sigma_{sj}^2}{a_{sj}}\right)^{p_{sj}} - \frac{m_{sj}xu}{\Omega_{sj}}\right) dx. \end{aligned} \tag{B.6}$$

Using binomial expansion and variable substitution, (B.6) becomes

$$f_{\Gamma_{sj}}(u) = \sum_{r_1=0}^{m_{sj}} \frac{p_{sj} m_{sj}! a_{sj}^{-d_{sj}} \left(\frac{m_{sj}}{\Omega_{sj}}\right)^{m_{sj}} \sigma_{sj}^{2(m_{sj}-r_1)} u^{m_{sj}-1} e^{-\frac{m_{sj}\sigma_{sj}^2 u}{\Omega_{sj}}}}{\Gamma(m_{sj})\Gamma\left(\frac{d_{sj}}{p_{sj}}\right) r_1!(m_{sj}-r_1)!} \times \int_0^\infty x^{d_{sj}+r_1-1} e^{-\left(\frac{x}{a_{sj}}\right)^{p_{sj}}} e^{-\frac{m_{sj} u x}{\Omega_{sj}}} dx. \tag{B.7}$$

The integral in (B.7) can be transformed by replacing the exponential functions with the Meijer's G-function as [113, pp. 346]

$$f_{\Gamma_{sj}}(u) = \sum_{r_1=0}^{m_{sj}} \frac{p_{sj} m_{sj}! a_{sj}^{-d_{sj}} \left(\frac{m_{sj}}{\Omega_{sj}}\right)^{m_{sj}} \sigma_{sj}^{2(m_{sj}-r_1)} u^{m_{sj}-1} e^{-\frac{m_{sj}\sigma_{sj}^2 u}{\Omega_{sj}}}}{\Gamma(m_{sj})\Gamma\left(\frac{d_{sj}}{p_{sj}}\right) r_1!(m_{sj}-r_1)!} \times \int_0^\infty x^{d_{sj}+r_1-1} G_{0,1}^{1,0}\left(\left(\frac{x}{a_{sj}}\right)^{p_{sj}} \Big| \begin{matrix} - \\ 0 \end{matrix}\right) G_{0,1}^{1,0}\left(\frac{m_{sj} u x}{\Omega_{sj}} \Big| \begin{matrix} - \\ 0 \end{matrix}\right) dx. \tag{B.8}$$

This integral can be solved by using [152] as (4.16).

B.3 Derivation of CDF of Γ_{sj} for Random Interferers

Using the definition of CDF and (B.6), one has

$$F_{\Gamma_{sj}}(u) = \int_0^u f_{\Gamma_{sj}}(t)dt = \frac{p_{sj}\left(\frac{m_{sj}}{\Omega_{sj}}\right)^{m_{sj}}}{a_{sj}^{d_{sj}}\Gamma(m_{sj})\Gamma\left(\frac{d_{sj}}{p_{sj}}\right)} \times \int_0^u \int_{\sigma_{sj}^2}^\infty t^{m_{sj}-1}(x-\sigma_{sj}^2)^{d_{sj}-1} x^{m_{sj}} \exp\left(-\left(\frac{x-\sigma_{sj}^2}{a_{sj}}\right)^{p_{sj}} - \frac{m_{sj} x t}{\Omega_{sj}}\right) dxdt. \tag{B.9}$$

By interchanging the order of integration and solving the integration over t first using [36, (3.351)], one can get

$$\begin{aligned} F_{\Gamma_{sj}}(u) &= \frac{p_{sj} x^{d_{sj}-1}}{a_{sj}^{d_{sj}} \Gamma(m_{sj}) \Gamma\left(\frac{d_{sj}}{p_{sj}}\right)} \\ &\times \int_0^\infty \exp\left(-\left(\frac{x}{a_{sj}}\right)^{p_{sj}}\right) \gamma\left(m_{sj}, \frac{m_{sj}(\sigma_{sj}^2 + x)u}{\Omega_{sj}}\right) dx \end{aligned} \tag{B.10}$$

where $\gamma(\cdot,\cdot)$ is the lower incomplete Gamma function [36]. Then, using [36, (8.352)] to expand the lower incomplete Gamma function as a finite series, one can get

$$\begin{aligned} F_{\Gamma_{sj}}(u) = \frac{p_{sj}(m_{sj}-1)! a_{sj}^{-d_{sj}}}{\Gamma(m_{sj}) \Gamma\left(\frac{d_{sj}}{p_{sj}}\right)} \Bigg(& \int_0^\infty x^{d_{sj}-1} e^{-\left(\frac{x}{a_{sj}}\right)^{p_{sj}}} dx \\ - \sum_{r_2=0}^{m_{sj}-1} \sum_{r_3=0}^{r_2} & \frac{\sigma_{sj}^{2(r_2-r_3)} e^{-\frac{m_{sj}\sigma_{sj}^2 u}{\Omega_{sj}}} \left(\frac{m_{sj}u}{\Omega_{sj}}\right)^{r_2}}{r_3!(r_2-r_3)!} \int_0^\infty x^{d_{sj}+r_3-1} e^{-\left(\frac{x}{a_{sj}}\right)^{p_{sj}}} e^{-\frac{m_{sj}ux}{\Omega_{sj}}} dx \Bigg). \end{aligned} \tag{B.11}$$

By using [36, (3.381)] and using the same method as that for (B.8) twice, one can get the CDF of Γ_{sj} as (4.17).

B.4 Derivation of the High SINR Approximations for PDF and CDF of Γ_{sj} for Random Interferers

Using Taylor's series expansion of (4.18) and [36, (3.381)] into (B.7) and (B.11), one can calculate the PDF and CDF of Γ_{sj} as (B.12) and (B.13), respectively,

$$f_{\Gamma_{sj}}(u) = \sum_{n_1=0}^{N_1} \sum_{r_1=0}^{m_{sj}} \mu_{3,sj,r_1,n_1} e^{-\frac{m_{sj}\sigma_{sj}^2 u}{\Omega_{sj}}} u^{m_{sj}+n_1-1} + o\left[(u/\Omega_{sj})^{N_1}\right], \tag{B.12}$$

where $\mu_{3,sj,r_1,n_1} = \dfrac{(-1)^{n_1} m_{sj}^{m_{sj}+n_1+1} \Omega_{sj}^{-m_{sj}-n_1} \sigma_{sj}^{2(m_{sj}-r_1)} a_{sj}^{d_{sj}+n_1+r_1} \Gamma\left(\frac{d_{sj}+n_1+r_1}{p_{sj}}\right) a_{sj}^{-d_{sj}}}{n_1!\Gamma(r_1+1)\Gamma(m_{sj}-r_1+1)\Gamma\left(\frac{d_{sj}}{p_{sj}}\right)}$,

$$F_{\Gamma_{sj}}(u) = 1 - \sum_{n_2=0}^{N_2} \sum_{r_2=0}^{m_{sj}-1} \sum_{r_3=0}^{r_2} \mu_{4,sj,r_2,r_3,n_2} u^{n_2+r_2} e^{-\frac{m_{sj}\sigma_{sj}^2 u}{\Omega_{sj}}} + o\left[(u/\Omega_{sj})^{N_2}\right], \tag{B.13}$$

where $\mu_{4,sj,r_2,r_3,n_2} = \dfrac{(-1)^{n_2} a_{sj}^{n_2+r_3} \sigma_{sj}^{2(r_2-r_3)} \left(\frac{m_{sj}}{\Omega_{sj}}\right)^{n_2+r_2} \Gamma\left(\frac{d_{sj}+n_2+r_3}{p_{sj}}\right)}{n_2! r_3! (r_2-r_3)! \Gamma\left(\frac{d_{sj}}{p_{sj}}\right)}$.

Furthermore, using (4.18) in (B.12) and (B.13) again, one can get (4.19) and (4.20).

B.5 Derivation of PDF and CDF of Γ_{jd} for Random Interferers

The PDF $f_{\Gamma_{jd}}(u)$ is as follows

$$f_{\Gamma_{jd}}(u) = \sum_{r_1=0}^{m_{jd}} \mu_{1,jd,r_1} e^{-\frac{m_{jd}\sigma_{jd}^2 u}{\Omega_{jd}}} u^{-d_{jd}+m_{jd}-r_1-1} \times G_{l_{jd},k_{jd}}^{k_{jd},l_{jd}} \left(\mu_{0,jd} u^{-l_{jd}} \middle| \begin{matrix} I(l_{jd}, 1-d_{jd}-r_1) \\ I(k_{jd}, 0) \end{matrix} \right), \tag{B.14}$$

where $\mu_{0,jd} = k_{jd}^{-k_{jd}} l_{jd}^{l_{jd}} a_{jd}^{-k_{jd}p_{jd}} \left(\frac{m_{jd}}{\Omega_{jd}}\right)^{-l_{jd}}$, and

$\mu_{1,jd,r_1} = \frac{l_{jd}^{d_{jd}+r_1-\frac{1}{2}} \sigma_{jd}^{2(m_{jd}-r_1)} \left(\frac{m_{jd}}{\Omega_{jd}}\right)^{-d_{jd}+m_{jd}-r_1} \sqrt{k_{jd}} p_{jd} m_{jd}! a_{jd}^{-d_{jd}} (2\pi)^{-\frac{k_{jd}}{2}-\frac{l_{jd}}{2}+1}}{r_1!(m_{jd}-r_1)!\Gamma(m_{jd})\Gamma\left(\frac{d_{jd}}{p_{jd}}\right)}$.

The CDF $F_{\Gamma_{jd}}(u)$ is as follows

$$F_{\Gamma_{jd}}(u) = 1 - \sum_{r_2=0}^{m_{jd}-1} \sum_{r_3=0}^{r_2} \mu_{2,jd,r_2,r_3} e^{-\frac{m_{jd}\sigma_{jd}^2 u}{\Omega_{jd}}} u^{-d_{jd}+r_2-r_3} \times G_{l_{jd},k_{jd}}^{k_{jd},l_{jd}} \left(\mu_{0,jd} u^{-l_{jd}} \middle| \begin{matrix} I(l_{jd}, 1-d_{jd}-r_3) \\ I(k_{jd}, 0) \end{matrix} \right) \tag{B.15}$$

where $\mu_{2,jd,r_2,r_3} = \frac{l_{jd}^{d_{jd}+r_3-\frac{1}{2}} \sigma_{jd}^{2(r_2-r_3)} \left(\frac{m_{jd}}{\Omega_{jd}}\right)^{-d_{jd}+r_2-r_3} \sqrt{k_{jd}} p_{jd} a_{jd}^{-d_{jd}} (2\pi)^{-\frac{k_{jd}}{2}-\frac{l_{jd}}{2}+1}}{r_3!(r_2-r_3)!\Gamma\left(\frac{d_{jd}}{p_{jd}}\right)}$.

The high SINR approximation of PDF is as follows

$$f_{\Gamma_{jd}}(u) = \sum_{n_1=0}^{N_1} \sum_{n_3=0}^{N_3} \sum_{r_1=0}^{m_{jd}} \mu_{5,jd,r_1,n_1,n_3} u^{m_{jd}+n_1+n_3-1} + o\left[(u/\Omega_{jd})^{N_1}\right] + o\left[(\sigma_{jd}^2 u/\Omega_{jd})^{N_3}\right], \tag{B.16}$$

where $\mu_{5,jd,r_1,n_1,n_3} =$

$$\frac{(-1)^{n_1+n_3}a_{jd}^{n_1+r_1}m_{jd}^{m_{jd}+n_1+n_3+1}\Omega_{jd}^{-m_{jd}-n_1-n_3}\sigma_{jd}^{2(m_{jd}-r_1+n_3)}\Gamma\left(\frac{d_{jd}+n_1+r_1}{p_{jd}}\right)}{n_1!n_3!\Gamma(r_1+1)\Gamma(m_{jd}-r_1+1)\Gamma\left(\frac{d_{jd}}{p_{jd}}\right)}.$$

The high SINR approximation of CDF is as follows

$$\begin{aligned} F_{\Gamma_{jd}}(u) &= 1-\sum_{n_2=0}^{N_2}\sum_{n_4=0}^{N_4}\sum_{r_2=0}^{m_{jd}-1}\sum_{r_3=0}^{r_2}\mu_{6,jd,r_2,r_3,n_2,n_4}u^{n_2+r_2+n_4} \\ &+ o\left[(u/\Omega_{jd})^{N_2}\right]+o\left[(\sigma_{jd}^2u/\Omega_{jd})^{N_4}\right], \end{aligned} \tag{B.17}$$

where $\mu_{6,jd,r_2,r_3,n_2,n_4}=\frac{(-1)^{n_2+n_4}a_{jd}^{n_2+r_3}\sigma_{jd}^{2(r_2-r_3+n_4)}\left(\frac{m_{jd}}{\Omega_{jd}}\right)^{n_2+r_2+n_4}\Gamma\left(\frac{d_{jd}+n_2+r_3}{p_{jd}}\right)}{n_2!n_4!r_3!(r_2-r_3)!\Gamma\left(\frac{d_{jd}}{p_{jd}}\right)}$.

B.6 Derivation of PDF and CDF of Γ_{sj} for Fixed Interferers

The PDF of Γ_{sj} can be calculated using (4.14) and (4.28) as

$$\begin{aligned} f_{\Gamma_{sj}}(u) &= \int_{-\infty}^{\infty}|x|\,f_{W_j}(xu)\,f_{Y_{sj}}\left(x-\sigma_{sj}^2\right)dz_j \\ &= \left(\frac{m_{sj}}{\Omega_{sj}}\right)^{m_{sj}}\left[\prod_{i^*=1}^{I^{sj}}\left(-\frac{\Omega_{i^*j}}{m_{i^*j}}\right)^{-m_{i^*j}}\right]\sum_{i=1}^{I^{sj}}\sum_{r=1}^{m_{ij}}\frac{(-1)^r b_{ir}u^{m_{sj}-1}}{\Gamma(m_{sj})(r-1)!} \\ &\times \int_{\sigma_{sj}^2}^{\infty}z^{m_{sj}}(z-\sigma_{sj}^2)^{r-1}e^{-\frac{m_{sj}}{\Omega_{sj}}uz-\frac{m_{ij}}{\Omega_{ij}}(z-\sigma_{sj}^2)}dz. \end{aligned} \tag{B.18}$$

This integral can be solved by using [36, (3.351)] as (4.29).

Using the definition of CDF and (B.18), one has

$$\begin{aligned} F_{\Gamma_{sj}}(u) &= \int_0^u f_{\Gamma_{sj}}(t)dt \\ &= \left(\frac{m_{sj}}{\Omega_{sj}}\right)^{m_{sj}} \left[\prod_{i^*=1}^{I^{sj}} \left(-\frac{\Omega_{i^*j}}{m_{i^*j}}\right)^{-m_{i^*j}}\right] \sum_{i=1}^{I^{sj}} \sum_{r=1}^{m_{ij}} \frac{(-1)^r b_{ir}}{\Gamma(m_{sj})(r-1)!} \\ &\times \int_0^u \int_{\sigma_{sj}^2}^{\infty} t^{m_{sj}-1} z^{m_{sj}} (z-\sigma_{sj}^2)^{r-1} e^{-\frac{m_{sj}}{\Omega_{sj}}tz - \frac{m_{ij}}{\Omega_{ij}}(z-\sigma_{sj}^2)} dz dt. \end{aligned} \tag{B.19}$$

By interchanging the order of integration and solving the integration over t first using [36, (3.351)], one further has

$$\begin{aligned} F_{\Gamma_{sj}}(u) &= \left[\prod_{i^*=1}^{I^{sj}} \left(-\frac{\Omega_{i^*j}}{m_{i^*j}}\right)^{-m_{i^*j}}\right] \sum_{i=1}^{I^{sj}} \sum_{r=1}^{m_{ij}} \frac{(-1)^r b_{ir}}{\Gamma(m_{sj})(r-1)!} \\ &\times \int_0^{\infty} z'^{r-1} e^{-\frac{m_{ij}}{\Omega_{ij}}z'} \gamma(m_{sj}, \frac{m_{sj}}{\Omega_{sj}}(z'+\sigma_{sj}^2)u) dz'. \end{aligned} \tag{B.20}$$

Then, one can derive the CDF of Γ_{sj} by using [36, (8.352)] and [36, (3.381)] in closed-form as (4.30).

B.7 Derivation of PDF and CDF of Γ_{jd} for Fixed Interferers

The PDF of Γ_{jd} can be written as

$$f_{\Gamma_{jd}}(u) = \sum_{v=1}^{I^{jd}} \sum_{r=1}^{m_{vj}} \sum_{f=0}^{m_{jd}} \varphi_{1,jd,vj,v,r,f} \frac{u^{m_{jd}-1} e^{-\frac{m_{jd}}{\Omega_{jd}}\sigma_{jd}^2 u}}{(\frac{m_{jd}}{\Omega_{jd}}u + \frac{m_{vj}}{\Omega_{vj}})^{f+r}}, \tag{B.21}$$

where $\varphi_{1,jd,vj,v,r,f} = \left[\prod_{v^*=1}^{I^{jd}} \left(-\frac{\Omega_{v^*j}}{m_{v^*j}}\right)^{-m_{v^*j}}\right] \frac{(-1)^r b_{vr} \left(\frac{m_{jd}}{\Omega_{jd}}\right)^{m_{jd}} \binom{m_{jd}}{f} (\sigma_{jd}^2)^{m_{jd}-f} \Gamma(f+r)}{\Gamma(m_{jd})(r-1)!}$.

The CDF of Γ_{jd} can be written as

$$F_{\Gamma_{jd}}(u) = 1 - \sum_{v=1}^{I^{jd}} \sum_{r=1}^{m_{vj}} \sum_{f=0}^{m_{jd}-1} \sum_{h=0}^{f} \varphi_{2,jd,vj,v,r,f,h} \frac{u^f e^{-\frac{m_{jd}}{\Omega_{jd}}\sigma_{jd}^2 u}}{(\frac{m_{jd}}{\Omega_{jd}}u + \frac{m_{vj}}{\Omega_{vj}})^{h+r}}, \quad \text{(B.22)}$$

where $\varphi_{2,jd,vj,v,r,f,h} = \left[\prod_{v^*=1}^{I^{jd}} \left(-\frac{\Omega_{v^*j}}{m_{v^*j}}\right)^{-m_{v^*j}}\right] \frac{(-1)^r b_{vr} \left(\frac{m_{jd}}{\Omega_{jd}}\right)^f \binom{f}{h} (\sigma_{jd}^2)^{f-h} \Gamma(h+r)}{(r-1)!f!}$.

The high SINR approximation for PDF is

$$\begin{aligned} f_{\Gamma_{jd}}(u) &= \sum_{v=1}^{I^{jd}} \sum_{n_5=0}^{N_5} \sum_{n_6=0}^{N_6} \sum_{r=1}^{m_{vj}} \sum_{f=0}^{m_{jd}} \varphi_{3,jd,vj,v,r,f,n_5,n_6} u^{m_{jd}+n_5+n_6-1} \\ &+ o\left[(\sigma_{jd}^2 u/\Omega_{jd})^{N_5}\right] + o\left[(u\Omega_{vj}/\Omega_{jd})^{N_6}\right] \end{aligned} \quad \text{(B.23)}$$

where $\varphi_{3,jd,vj,v,r,f,n_5,n_6} = \left[\prod_{v^*=1}^{I^{jd}} \left(-\frac{\Omega_{v^*j}}{m_{v^*j}}\right)^{-m_{v^*j}}\right]$
$\times \frac{(-1)^{r+n_5} b_{vr} \left(\frac{m_{jd}}{\Omega_{jd}}\right)^{m_{jd}+n_5+n_6} \left(\frac{m_{vj}}{\Omega_{vj}}\right)^{-f-r-n_6} \binom{m_{jd}}{f} \binom{-f-r}{n_6} (\sigma_{jd}^2)^{m_{jd}-f+n_5} \Gamma(f+r)}{\Gamma(m_{jd})(r-1)!n_5!}$.

The high SINR approximation for CDF is

$$\begin{aligned} F_{\Gamma_{jd}}(u) &= 1 - \sum_{v=1}^{I^{jd}} \sum_{n_7=0}^{N_7} \sum_{n_8=0}^{N_8} \sum_{r=1}^{m_{vj}} \sum_{f=0}^{m_{jd}-1} \sum_{h=0}^{f} \varphi_{4,jd,vj,v,r,f,h,n_7,n_8} u^{f+n_7+n_8} \\ &+ o\left[(\sigma_{jd}^2 u/\Omega_{jd})^{N_7}\right] + o\left[(u\Omega_{vj}/\Omega_{jd})^{N_8}\right], \end{aligned} \quad \text{(B.24)}$$

where $\varphi_{4,jd,vj,v,r,f,h,n_7,n_8} = \left[\prod_{v^*=1}^{I^{jd}} \left(-\frac{\Omega_{v^*j}}{m_{v^*j}}\right)^{-m_{v^*j}}\right]$
$\times \frac{(-1)^{r+n_7} b_{vr} \left(\frac{m_{jd}}{\Omega_{jd}}\right)^{f+n_7+n_8} \left(\frac{m_{vj}}{\Omega_{vj}}\right)^{-h-r-n_8} \binom{f}{h} \binom{-h-r}{n_8} (\sigma_{jd}^2)^{f-h+n_7} \Gamma(h+r)}{(r-1)!f!n_7!}$.

B.8 Derivation of CDF of Γ_j for the Dominant Fixed Interferences

When the interference is dominant such that the noise can be ignored, one further has $\sigma_{sj}^2 \approx 0$ in (4.29) to give the PDF as

$$f_{\Gamma_{sj}}(u) = \sum_{i=1}^{I^{sj}} \sum_{r=1}^{m_{ij}} \varphi_{5,sj,ij,i,r} \frac{u^{m_{sj}-1}}{(\frac{m_{sj}}{\Omega_{sj}}u + \frac{m_{ij}}{\Omega_{ij}})^{m_{sj}+r}}, \tag{B.25}$$

where $\varphi_{5,sj,ij,i,r} = \left[\prod_{i^*=1}^{I^{sj}} \left(-\frac{\Omega_{i^*j}}{m_{i^*j}}\right)^{-m_{i^*j}}\right] \left(\frac{m_{sj}}{\Omega_{sj}}\right)^{m_{sj}} \frac{(-1)^r b_{ir} \Gamma(m_{sj}+r)}{\Gamma(m_{sj})(r-1)!}$.
Also, the CDF of Γ_{sj} in (4.30) becomes

$$F_{\Gamma_{sj}}(u) = 1 - \sum_{i=1}^{I^{sj}} \sum_{r=1}^{m_{ij}} \sum_{f=0}^{m_{sj}-1} \varphi_{6,sj,ij,i,r,f} \frac{u^f}{(\frac{m_{sj}}{\Omega_{sj}}u + \frac{m_{ij}}{\Omega_{ij}})^{f+r}}, \tag{B.26}$$

where $\varphi_{6,sj,ij,i,r,f} = \left[\prod_{i^*=1}^{I^{sj}} \left(-\frac{\Omega_{i^*j}}{m_{i^*j}}\right)^{-m_{i^*j}}\right] \left(\frac{m_{sj}}{\Omega_{sj}}\right)^{f} \frac{(-1)^r b_{ir} \Gamma(f+r)}{(r-1)!f!}$.

Therefore, (4.21) can be solved as (4.36) with the help of [36, (3.197)].

Appendix C

Derivation for α-μ RVs

C.1 Derivation of MGF for Sum of Ratios of Products of α-μ RVs

If α-μ RVs $\{X_{jl}\}_{j=1,l=1}^{k,L}$ in (5.3) are independent, from [153] and using variable transformation, one can get the PDF of R_l in (5.3) as

$$f_{R_l}(x) = C_l x^{-1} \alpha_l \times$$
$$G_{n',m'}^{m',n'}\left(t_l \left(\frac{x}{\omega_l}\right)^{\alpha_l} \Bigg| \begin{matrix} 1 - \frac{\mu_{jl}}{m_{jl}} - \frac{r_l}{m_{jl}}, r_l = 0, 1, \cdots, m_{jl} - 1, j = m+1, \cdots, k \\ \frac{\mu_{jl}}{m_{jl}} + \frac{r_l}{m_{jl}}, r_l = 0, 1, \cdots, m_{jl} - 1, j = 1, \cdots, m \end{matrix} \right). \tag{C.1}$$

The moment generating function (MGF) of R_l is defined as

$$M_{R_l}(s) = \int_0^\infty e^{xs} f_{R_l}(x) dx. \tag{C.2}$$

With the help of the Meijer's G-function identity [152], [112, 07.34.22.0003.01], [112, 07.34.02.0004.01] and [112, 07.34.02.0005.01], one can get MGF of R_l as

(5.7).

If α-μ RVs $\{X_{jl}\}_{j=1,l=1}^{k,L}$ in (5.3) are i.i.d, α_{jl}, μ_{jl} and $\hat{\gamma_{jl}}$ become α, μ and $\hat{\gamma}$. Therefore, the PDF of R_l in (C.1) becomes

$$f_{R_l}(x) = \frac{\alpha}{\Gamma^k(\mu)x} G_{n,m}^{m,n}\left(\left(\frac{\mu}{\hat{\gamma}^\alpha}\right)^{m-n} \left(\frac{x}{\omega_l}\right)^{\alpha} \Big| \begin{matrix} 1-\mu,\cdots,1-\mu \\ \mu,\cdots,\mu \end{matrix} \right). \tag{C.3}$$

Using (C.3) in (C.2), the MGF of R_l is derived as (5.8).

If α-μ RVs $\{X_{jl}\}_{j=1,l=1}^{m,L}$ in (5.5) are independent, the PDF of P_l in (5.5) can be obtained as (C.4) when $k = m$ in (C.1).

$$\begin{aligned} &f_{P_l}(x) = C_l x^{-1}\alpha_l \times \\ &G_{0,m'}^{m',0}\left(t_l \left(\frac{x}{\omega_l}\right)^{\alpha_l} \Big| \begin{matrix} - \\ \frac{\mu_{jl}}{m_{jl}} + \frac{r_l}{m_{jl}}, r_l = 0,1,\cdots,m_{jl}-1, j = 1,\cdots,m \end{matrix} \right). \end{aligned} \tag{C.4}$$

Using (C.4) in (C.2), the PDF of P_l can be derived as (5.9).

If α-μ RVs $\{X_{jl}\}_{j=1,l=1}^{m,L}$ in (5.5) are i.i.d, then the PDF of P_l in (5.5) can be obtained as

$$f_{P_l}(x) = \frac{\alpha}{\Gamma^m(\mu)x} G_{0,m}^{m,0}\left(\left(\frac{\mu}{\hat{\gamma}^\alpha}\right)^{m} \left(\frac{x}{\omega_l}\right)^{\alpha} \Big| \begin{matrix} - \\ \mu,\cdots,\mu \end{matrix} \right). \tag{C.5}$$

Using (C.5) in (C.2), the MGF of P_l is derived as (5.10).

C.2 Derivation of GGRA and GRA Approximation

From R in (5.2), one can see that it is a sum of ratios of products. Therefore, we propose to use the ratio of GG distribution to approximate R. Let $x = \frac{r_1}{r_2}$, where r_1 and r_2 follow GG distribution with the PDFs of

$$f_1(r_1; a_1, d_1, p) = \frac{p\, a_1^{-d_1} r_1^{d_1-1} e^{-\left(\frac{r_1}{a_1}\right)^p}}{\Gamma\left(\frac{d_1}{p}\right)}, r_1 > 0, \tag{C.6}$$

and

$$f_2(r_2; a_2, d_2, p) = \frac{p\, a_2^{-d_2} r_2^{d_2-1} e^{-\left(\frac{r_2}{a_2}\right)^p}}{\Gamma\left(\frac{d_2}{p}\right)}, r_2 > 0 \tag{C.7}$$

respectively. Then, one has the PDF of x as

$$f_{GGRA}(x) = \int_0^\infty |r|\, f_1(rx)\, f_2(r)\, dr. \tag{C.8}$$

After simplification and using [137], one can get

$$f_{GGRA}(x) = \frac{p a_1^{-d_1} a_2^{d_1} x^{d_1-1} (1 + (\frac{a_2}{a_1})^p\, x^p)^{-\frac{d_1+d_2}{p}}}{B(\frac{d_1}{p}, \frac{d_2}{p})}. \tag{C.9}$$

Using $k = (\frac{a_1}{a_2})^p$ in (C.9), one can get the PDF of GGRA as (5.17). The CDF of GGRA is given by

$$F_{GGRA}(y) = \int_0^y f_{GGRA}(x) dx. \tag{C.10}$$

Using (5.17) in (C.10) and with the help of [36, (3.259)], one can get the CDF of GGRA as (5.18). One can see that there are four unknown parameters in

GGRA. Therefore, we propose another approximate method with the name of GRA which has only three unknown parameters. GRA can be seen as the ratio of Gamma distribution. Thus when $p = 1$ in (C.6) and (C.7), they become

$$f_1(r_1) = \frac{r_1^{d_1-1} e^{-r_1/a_1}}{a_1^{d_1}\Gamma(d_1)}, r_1 > 0 \tag{C.11}$$

and

$$f_2(r_2) = \frac{r_2^{d_2-1} e^{-r_2/a_2}}{a_2^{d_2}\Gamma(d_2)}, r_2 > 0 \tag{C.12}$$

respectively. Using (C.11), (C.12) and $k = \frac{a_1}{a_2}$, one can get the PDF and CDF of GRA as (5.19) and (5.20), respectively.

Appendix D

Derivation for Hard-Decision Fusion Rule

D.1 Derivation of the Characteristic Function of Hard-Decision Fusion with 1 Bit for BPSK

For BPSK, using the approximation of the Gaussian-Q function (as introduced in Section 2.1.1),

$$Q(x) \approx \frac{1}{2} e^{-\frac{x^2}{2}}, \tag{D.1}$$

the ideal BPSK receiver with instantaneous SNR γ has a BER of

$$\begin{aligned} p_e(\gamma) &= Q(\sqrt{2\gamma}) \\ &\approx \frac{1}{2} e^{-\gamma}. \end{aligned} \tag{D.2}$$

The decision variable X for the fusion rule using one bit in (6.2) when $L = 1$ can be defined as

$$X \triangleq d_1 \cdot ln\frac{p_c}{p_e} \tag{D.3}$$

where $p_c = P_{c|s_1}$, $p_e = P_{e|s_1}$ and $d_1 = sign(v_1)$ when $L = 1$ in (6.2). Using (6.14) when setting $m = 1$ and (D.2), one can derive the PDF of X as

$$f_X(x) = \begin{cases} \frac{1}{\gamma_0} 2^{\frac{1}{\gamma_0}} e^{-x} \left(1 + e^{-x}\right)^{-2-\frac{1}{\gamma_0}} & x < 0 \\ \frac{1}{\gamma_0} 2^{\frac{1}{\gamma_0}} e^{2x} \left(1 + e^{x}\right)^{-2-\frac{1}{\gamma_0}} & x > 0. \end{cases} \tag{D.4}$$

The characteristic function of X is defined as

$$\Phi_X(w) = E(e^{iwx}) = \int_{-\infty}^{\infty} f_X(x) e^{iwx} dx \tag{D.5}$$

where $E(\cdot)$ denotes the expectation operation and $i = \sqrt{-1}$. Thus, for $x < 0$, we can get

$$\int_{-\infty}^{0} f_X(x) e^{iwx} dx = \left(\left(-\frac{1}{2} \right)^{-1/\gamma_0} e^{\pi w} \Gamma\left(-\frac{1}{\gamma_0} \right) \right.$$
$$\left. \times \Gamma\left(1 + \frac{1}{\gamma_0} + iw \right) \right) \Big/ \left(\left(1 + \gamma_0\right) \Gamma\left(iw\right) \right) + 1/\left(2 + 2\gamma_0\right) \; {}_2F_1\left(1, iw, -\frac{1}{\gamma_0}, 2 \right) \tag{D.6}$$

Similarly, we can get the characteristic function of $f_X(x)$ for $x > 0$ as

$$\begin{aligned}
&\int_0^\infty f_X(x)e^{jwx}dx = 1\,/\left(2\left(-1+\gamma_0^2\right)\Gamma((1-iw)\right)(-1)^{-1/\gamma_0}e^{-\pi w} \\
&\times\left(-2^{1+\frac{1}{r}}\gamma_0^2 w(-i+w)\Gamma\left(2-\frac{1}{\gamma_0}\right)\Gamma\left(\frac{1}{\gamma_0}-iw\right)+\Gamma(1-iw)\right. \\
&\times\left((-1)^{\frac{1}{\gamma_0}}e^{\pi w}\ {}_2F_1\left(1,-iw,-\frac{1}{\gamma_0},2\right)+2(1+\gamma_0)\left((-1)^{\frac{1}{\gamma_0}}e^{\pi w}\right.\right. \\
&\left.{}_2F_1\left(1,1-iw,\frac{-1+\gamma_0}{\gamma_0},2\right)+\gamma_0\ {}_2F_1\left(-\frac{1}{\gamma_0},-\frac{1}{\gamma_0}+iw,\frac{-1+\gamma_0}{\gamma_0},2\right)\right. \\
&\left.\left.-2\ {}_2F_1\left(\frac{-1+\gamma_0}{\gamma_0},1-\frac{1}{\gamma_0}+iw,2-\frac{1}{\gamma_0},2\right)\right)+\gamma_0\right. \\
&\left.\times\ {}_2F_1\left(-\frac{1+\gamma_0}{\gamma_0},-\frac{1}{\gamma_0}+iw,-\frac{1}{\gamma_0},2\right)\right)\right).
\end{aligned} \tag{D.7}$$

Therefore, the characteristic function of hard decision fusion with one bit for BPSK is given by

$$\begin{aligned}
&\Phi_X(w) = \int_{-\infty}^0 f_X(x)e^{iwx}dx + \int_0^\infty f_X(x)e^{iwx}dx \\
&= \frac{1}{2}\left(\frac{i}{i+\gamma_0 w}+\frac{1}{1+\gamma_0}\times\ {}_2F_1\left(1,iw,-\frac{1}{\gamma_0},2\right)+\Gamma\left(-\frac{1+\gamma_0}{\gamma_0}\right)\right. \\
&\left(\frac{1}{i+\gamma_0 w}(-i+w)\ {}_2F_1R\left(1,-iw,-\frac{1}{\gamma_0},2\right)+\frac{1}{\pi\gamma_0}2^{1+\frac{1}{\gamma_0}}e^{-\pi\left(\frac{i}{\gamma_0}+w\right)}\right. \\
&\left.\left.\left(i\Gamma\left(\frac{1}{\gamma_0}-iw\right)\Gamma(2+iw)-e^{2\pi w}w\Gamma\left(1+\frac{1}{\gamma_0}+iw\right)\Gamma(-iw)\right)\sinh(\pi w)\right)\right)
\end{aligned} \tag{D.8}$$

where ${}_2F_1R(a,b,c,z) = {}_2F_1(a,b,c,z)/\Gamma(c)$.

This result can be extended to NCFSK with the BER of [1]

$$p_e(\gamma) = \frac{1}{2}e^{-\gamma/2}. \tag{D.9}$$

Using similar procedures, one can have the characteristic function of hard

decision fusion with one bit for NCFSK as

$$\Phi_X(w) = \Bigg((-1)^{-2/\gamma_0} e^{-\pi w} \Bigg(4ie^{\pi\left(\frac{2i}{\gamma_0}+w\right)} \pi \left(-4+\gamma_0^2\right) \times \ (i+\gamma_0 w) + \\ \gamma_0^2 \Gamma\left(2-\frac{2}{\gamma_0}\right) \left(-4^{\frac{1}{\gamma_0}} e^{-\pi w} \times \left(e^{2\pi w}-1\right) \gamma_0 w \right. \\ \times \left(\gamma_0 \Gamma\left(1+\frac{2}{\gamma_0}-iw\right) \Gamma(2+iw) + e^{2\pi w} w(2i+\gamma_0 w) \Gamma\left(1+\frac{2}{\gamma_0}+iw\right) \right. \\ \left. \Gamma(-iw)) + 1 \Big/ \Gamma\left(-\frac{2}{\gamma_0}\right) e^{\pi\left(\frac{2i}{\gamma_0}+w\right)} \pi \left(\gamma_0^2 w(-i+w) \ {}_2F_1\left(1,-iw,-\frac{2}{\gamma_0},2\right) \right. \right. \\ \left. \left. - (2i+\gamma_0 w) \left(-i(2+\gamma_0)+\gamma_0 w \ {}_2F_1\left(1,iw,-\frac{2}{\gamma_0},2\right)\right)\right)\right)\right)\Bigg) \\ \Big/ \left(2\pi\gamma_0 \left(-4+\gamma_0^2\right) w(2i+\gamma_0 w)\right). \tag{D.10}$$

References

[1] J. G. Proakis and M. Salehi, *Digital Communications*. New York: McGraw-Hill, 2008.

[2] J. Kahn and J. Barry, "Wireless infrared communications," *Proceedings of the IEEE*, vol. 85, no. 2, pp. 265–298, Feb 1997.

[3] T. Rappaport, S. Sun, R. Mayzus, H. Zhao, Y. Azar, K. Wang, G. Wong, J. Schulz, M. Samimi, and F. Gutierrez, "Millimeter wave mobile communications for 5g cellular: It will work!" *IEEE Access*, vol. 1, pp. 335–349, 2013.

[4] J. Andrews, S. Buzzi, W. Choi, S. Hanly, A. Lozano, A. Soong, and J. Zhang, "What will 5g be?" *IEEE Journal on Selected Areas in Communications*, vol. 32, no. 6, pp. 1065–1082, June 2014.

[5] WiMAX, "Wimax forum," *The WiMAX Forum Site*, http://www.wimaxforum.org.

[6] Q. Li, R. Hu, Y. Qian, and G. Wu, "Cooperative communications for wireless networks: techniques and applications in LTE-Advanced systems," *IEEE Wireless Communications*, vol. 19, no. 2, April 2012.

[7] A. Nosratinia, T. Hunter, and A. Hedayat, "Cooperative communication in wireless networks," *IEEE Communications Magazine*, vol. 42, no. 10, pp. 74–80, Oct. 2004.

[8] S. Alamouti, "A simple transmit diversity technique for wireless communications," *IEEE Journal on Selected Areas in Communications*, vol. 16, no. 8, pp. 1451–1458, Oct 1998.

[9] J. Laneman and G. Wornell, "Energy-efficient antenna sharing and relaying for wireless networks," in *2000 IEEE Wireless Communications and Networking Confernce*, vol. 1, 2000, pp. 7–12.

[10] J. Laneman, D. Tse, and G. W. Wornell, "Cooperative diversity in wireless networks: Efficient protocols and outage behavior," *IEEE Transactions on Information Theory*, vol. 50, no. 12, pp. 3062–3080, Dec 2004.

[11] J. Boyer, D. Falconer, and H. Yanikomeroglu, "Multihop diversity in wireless relaying channels," *IEEE Transactions on Communications*, vol. 52, no. 10, pp. 1820–1830, Oct. 2004.

[12] R. Bhatia and M. Kodialam, "On power efficient communication over multi-hop wireless networks: joint routing, scheduling and power control," in *INFOCOM 2004*, vol. 2, March 2004, pp. 1457–1466.

[13] M. Dohler and Y. H. Li, *Cooperative communications: hardware, channel and PHY*. John Wiley Sons Ltd, 2010.

[14] A. Narula, M. Trott, and G. W. Wornell, "Performance limits of coded diversity methods for transmitter antenna arrays," *IEEE Transactions on Information Theory*, vol. 45, no. 7, pp. 2418–2433, Nov 1999.

[15] J. Laneman and G. W. Wornell, "Distributed space-time-coded protocols for exploiting cooperative diversity in wireless networks," *IEEE Transactions on Information Theory*, vol. 49, no. 10, pp. 2415–2425, Oct 2003.

[16] K. Azarian, H. El Gamal, and P. Schniter, "On the achievable diversity-multiplexing tradeoff in half-duplex cooperative channels," *IEEE Transactions on Information Theory*, vol. 51, no. 12, pp. 4152–4172, Dec 2005.

[17] Y. Jing and H. Jafarkhani, "Single and multiple relay selection schemes and their achievable diversity orders," *IEEE Transactions on Wireless Communications*, vol. 8, no. 3, pp. 1414–1423, March 2009.

[18] J. Luo, R. Blum, L. Cimini, L. Greenstein, and A. Haimovich, "Power allocation in a transmit diversity system with mean channel gain information," *IEEE Communications Letters*, vol. 9, no. 7, pp. 616–618, July 2005.

[19] S. Talwar, Y. Jing, and S. ShahbazPanahi, "Joint relay selection and power allocation for two-way relay networks," *IEEE Signal Processing Letters*, vol. 18, no. 2, pp. 91–94, Feb 2011.

[20] Z. Mo, W. Su, S. Batalama, and J. Matyjas, "Cooperative communication protocol designs based on optimum power and time allocation," *IEEE Transactions on Wireless Communications*, vol. 13, no. 8, pp. 4283–4296, Aug 2014.

[21] L. Cao, J. Zhang, and N. Kanno, "Multi-user cooperative communications with relay-coding for uplink imt-advanced 4g systems," in *IEEE Global Telecommunications Conference (GLOBECOM 2009)*, Nov 2009, pp. 1–6.

[22] E. Yilmaz, R. Knopp, F. Kaltenberger, and D. Gesbert, "Low-complexity multiple-relay strategies for improving uplink coverage in 4g wireless networks," in *Conference Record of the Forty Fourth Asilomar Conference on Signals, Systems and Computers (2010 ASILOMAR)*, Nov 2010, pp. 1305–1310.

[23] W. Yang and Y. Cai, "On the performance of the block-based selective ofdm decode-and-forward relaying scheme for 4g mobile communication systems," *Journal of Communications and Networks*, vol. 13, no. 1, pp. 56–62, Feb 2011.

[24] R. Pabst, D. Schultz, and B. H. Walke, "Performance evaluation of a relay-based 4g network deployment with combined sdma/ofdma and resource partitioning," in *IEEE Vehicular Technology Conference (VTC Spring 2008)*, May 2008, pp. 2001–2005.

[25] E. Yilmaz, D. Gesbert, and R. Knopp, "Interference relay channel in 4g wireless networks," in *IEEE Wireless Communications and Networking Conference (2012 WCNC)*, April 2012, pp. 364–368.

[26] K. Ratajczak, K. Bakowski, and K. Wesolowski, "Two-way relaying for 5g systems: Comparison of network coding and MIMO techniques," in *IEEE Wireless Communications and Networking Conference (2014 WCNC)*, April 2014, pp. 376–381.

[27] Y. Yang, H. Hu, J. Xu, and G. Mao, "Relay technologies for WiMax and LTE-Advanced mobile systems," *IEEE Communications Magazine*, vol. 47, no. 10, pp. 100–105, October 2009.

[28] R. Pabst, B. H. Walke, D. Schultz, P. Herhold, H. Yanikomeroglu, S. Mukherjee, H. Viswanathan, M. Lott, W. Zirwas, M. Dohler, H. Aghvami, D. Falconer, and G. Fettweis, "Relay-based deployment concepts for wireless and mobile broadband radio," *IEEE Communications Magazine*, vol. 42, no. 9, pp. 80–89, Sept 2004.

[29] Y. Jing and X. Yu, "ML-based channel estimations for non-regenerative relay networks with multiple transmit and receive antennas," *IEEE Journal on Selected Areas in Communications*, vol. 30, no. 8, pp. 1428–1439, September 2012.

[30] O. Amin, B. Gedik, and M. Uysal, "Channel estimation for amplify-and-forward relaying: Cascaded against disintegrated estimators," *IET Communications*, vol. 4, no. 10, pp. 1207 –1216, Jul. 2010.

[31] I. Krikidis, J. Thompson, S. McLaughlin, and N. Goertz, "Max-min relay selection for legacy amplify-and-forward systems with interference," *IEEE Transactions on Wireless Communications*, vol. 8, no. 6, pp. 3016–3027, June 2009.

[32] Y. Chen and N. C. Beaulieu, "Novel partial decision combining schemes for Rayleigh fading," *Transactions on Emerging Telecommunications Technologies*, vol. 23, no. 1, pp. 67–75, Sep. 2011.

[33] Y. Chen, K. Wang, and J. Chen, "Hard-decision fusion with arbitrary numbers of bits for different samples," *IEEE Transactions on Vehicular Technology*, vol. 62, no. 2, pp. 879–884, Feb 2013.

[34] M. K. Simon and M.-S. Alouini, *Digital Communication over Fading Channels*. New York, 2005.

[35] Wikimedia, "Rayleigh fading," *wikipedia*, http://en.wikipedia.org/wiki/Rayleigh_fading.

[36] I. S. Gradshteyn and I. M. Ryzhik, *Table of Integrals, Series, and Products, 7th ed.* San Diego, CA: Academic, 2007.

[37] N. C. Beaulieu and C. Cheng, "Efficient Nakagami-m fading channel simulation," *IEEE Transactions on Vehicular Technology*, vol. 54, no. 2, pp. 413 – 424, Mar. 2005.

[38] M. Z. Win, N. C. Beaulieu, L. A. Shepp, J. Logan, B F., and J. H. Winters, "On the SNR penalty of mpsk with hybrid selection/maximal ratio combining over i.i.d. Rayleigh fading channels," *IEEE Transactions on Communications*, vol. 51, no. 6, pp. 1012 – 1023, Jun. 2003.

[39] H. Suzuki, "A statistical model for urban radio propogation," *IEEE Transactions on Communications*, vol. 25, no. 7, pp. 673–680, Jul 1977.

[40] M. Yacoub, "The α - μ distribution: A physical fading model for the stacy distribution," *IEEE Transactions on Vehicular Technology*, vol. 56, no. 1, pp. 27–34, 2007.

[41] W. Braun and U. Dersch, "A physical mobile radio channel model," *IEEE Transactions on Vehicular Technology*, vol. 40, no. 2, pp. 472–482, May 1991.

[42] S. Stein, "Fading channel issues in system engineering," *IEEE Journal on Selected Areas in Communications*, vol. 5, no. 2, pp. 68–89, Feb 1987.

[43] U. Dias and M. Yacoub, "On the α - μ autocorrelation and power spectrum functions: Field trials and validation," in *IEEE Global Telecommunications Conference (GLOBECOM 2009)*, Nov 2009, pp. 1–6.

[44] T. A. Tsiftsis, G. K. Karagiannidis, P. T. Mathiopoulos, and S. A. Kotsopoulos, "Nonregenerative dual-hop cooperative links with selection diversity," *EURASIP Journal on Wireless Communications and Networking*, pp. 1–8, April 2006.

[45] J. N. Laneman, G. W. Wornell, and D. Tse, "An efficient protocol for realizing cooperative diversity in wireless networks," in *IEEE International Symposium on Information Theory (ISIT'2001)*, 2001, p. 294.

[46] M. O. Hasna and M.-S. Alouini, "A performance study of dual-hop transmissions with fixed gain relays," *IEEE Transactions on Wireless Communications*, vol. 3, no. 6, pp. 1963 – 1968, Nov. 2004.

[47] ——, "End-to-end performance of transmission systems with relays over Rayleigh-fading channels," *IEEE Transactions on Wireless Communications*, vol. 2, no. 6, pp. 1126 – 1131, Nov. 2003.

[48] G. Kramer, M. Gastpar, and P. Gupta, "Cooperative strategies and capacity theorems for relay networks," *IEEE Transactions on Information Theory*, vol. 51, no. 9, pp. 3037–3063, Sept 2005.

[49] M. Janani, A. Hedayat, T. Hunter, and A. Nosratinia, "Coded cooperation in wireless communications: space-time transmission and iterative decoding," *IEEE Transactions on Signal Processing*, vol. 52, no. 2, pp. 362–371, Feb 2004.

[50] M. Iwamura, H. Takahashi, and S. Nagata, "Relay technology in LTE-Advanced," *NTT DOCOMO Technical Journal*, vol. 12, pp. 29–36, 2010.

[51] M. Xia, Y.-C. Wu, and S. Aissa, "Exact outage probability of dual-hop CSI-assisted AF relaying over Nakagami- m fading channels," *IEEE Transactions on Signal Processing*, vol. 60, no. 10, pp. 5578–5583, Oct 2012.

[52] M. Di Renzo, F. Graziosi, and F. Santucci, "A unified framework for performance analysis of CSI-assisted cooperative communications over fading channels," *IEEE Transactions on Communications*, vol. 57, no. 9, pp. 2551–2557, September 2009.

[53] H. Suraweera, D. Michalopoulos, and C. Yuen, "Performance analysis of fixed gain relay systems with a single interferer in Nakagami-m fading channels," *IEEE Transactions on Vehicular Technology*, vol. 61, no. 3, pp. 1457–1463, March 2012.

[54] F. Al-Qahtani, T. Duong, C. Zhong, K. Qaraqe, and H. Alnuweiri, "Performance analysis of dual-hop AF systems with interference in Nakagami- m fading channels," *IEEE Signal Processing Letters*, vol. 18, no. 8, pp. 454–457, Aug 2011.

[55] D. da Costa and M. Yacoub, "Outage performance of two hop AF relaying systems with co-channel interferers over Nakagami-m fading," *IEEE Communications Letters*, vol. 15, no. 9, pp. 980–982, September 2011.

[56] G. Karagiannidis, T. Tsiftsis, and R. Mallik, "Bounds for multihop relayed communications in Nakagami-m fading," *IEEE Transactions on Communications*, vol. 54, no. 1, pp. 18–22, Jan. 2006.

[57] M. Hasna and M.-S. Alouini, "Outage probability of multihop transmission over Nakagami fading channels," *IEEE Communications Letters*, vol. 7, no. 5, pp. 216–218, May. 2003.

[58] O. Oyman, N. Laneman, and S. Sandhu, "Multihop relaying for broadband wireless mesh networks: From theory to practice," *IEEE Communications Magazine*, vol. 45, no. 11, pp. 116–122, November 2007.

[59] V. Asghari, D. Benevides da Costa, and S. Aissa, "Performance analysis for multihop relaying channels with Nakagami-m fading: Ergodic capacity upper-bounds and outage probability," *IEEE Transactions on Communications*, vol. 60, no. 10, pp. 2761–2767, October 2012.

[60] D. Da Costa, M. Yacoub, and J. C. S. S. Filho, "Highly accurate closed-form approximations to the sum of α - μ variates and applications," *IEEE Transactions on Wireless Communications*, vol. 7, no. 9, pp. 3301–3306, 2008.

[61] B. Hamdaoui, T. Alshammari, and M. Guizani, "Exploiting 4g mobile user cooperation for energy conservation: challenges and opportunities," *IEEE Wireless Communications*, vol. 20, no. 5, pp. 62–67, October 2013.

[62] P. Anghel and M. Kaveh, "Exact symbol error probability of a cooperative network in a Rayleigh-fading environment," *IEEE Transactions on Wireless Communications*, vol. 3, no. 5, pp. 1416–1421, Sept. 2004.

[63] H. Shin and J. Song, "Mrc analysis of cooperative diversity with fixed-gain relays in Nakagami-m fading channels," *IEEE Transactions on Wireless Communications*, vol. 7, no. 6, pp. 2069–2074, June 2008.

[64] S. Ikki and M. Ahmed, "Performance of cooperative diversity using equal gain combining (EGC) over Nakagami-m fading channels," *IEEE Transactions on Wireless Communications*, vol. 8, no. 2, pp. 557–562, Feb 2009.

[65] M. Di Renzo, M. Iezzi, and F. Graziosi, "Error performance and diversity analysis of multi-source multi-relay wireless networks with binary network coding and cooperative mrc," *IEEE Transactions on Wireless Communications*, vol. 12, no. 6, pp. 2883–2903, June 2013.

[66] Y. Chen, C.-X. Wang, H. Xiao, and D. Yuan, "Novel partial selection schemes for AF relaying in Nakagami-m fading channels," *IEEE Transactions on Vehicular Technology*, vol. 60, no. 7, pp. 3497–3503, 2011.

[67] A. Bletsas, A. Khisti, D. Reed, and A. Lippman, "A simple cooperative diversity method based on network path selection," *IEEE Journal on Selected Areas in Communications*, vol. 24, no. 3, pp. 659–672, March 2006.

[68] A. Bletsas, H. Shin, and M. Win, "Outage optimality of opportunistic amplify-and-forward relaying," *IEEE Communications Letters*, vol. 11, no. 3, pp. 261–263, March 2007.

[69] G. Amarasuriya, M. Ardakani, and C. Tellambura, "Output-threshold multiple-relay-selection scheme for cooperative wireless networks," *IEEE Transactions on Vehicular Technology*, vol. 59, no. 6, pp. 3091–3097, July 2010.

[70] I. Krikidis, J. Thompson, S. McLaughlin, and N. Goertz, "Amplify-and-forward with partial relay selection," *IEEE Communications Letters*, vol. 12, no. 4, pp. 235–237, April 2008.

[71] W. Li and N. Beaulieu, "Effects of channel-estimation errors on receiver selection-combining schemes for alamouti MIMO systems with BPSK," *IEEE Transactions on Communications*, vol. 54, no. 1, pp. 169–178, Jan 2006.

[72] M. Selvaraj and R. Mallik, "Performance of full csi selection combining for cooperative diversity systems," *IEEE Transactions on Communications*, vol. 60, no. 9, pp. 2482–2488, September 2012.

[73] B. S. Tan, K. H. Li, and K. C. Teh, "Performance analysis of orthogonal space-time block code with minimum-selection generalized selection combining receiver over rayleigh fading," *IEEE Transactions on Vehicular Technology*, vol. 61, no. 3, pp. 1463–1467, March 2012.

[74] L. Yang, M.-S. Alouini, K. Qaraqe, and W. Liu, "On the performance of dual-hop systems with multiple antennas: Effects of spatial correlation, keyhole, and co-channel interference," *IEEE Transactions on Communications*, vol. 60, no. 12, pp. 3541–3547, December 2012.

[75] N. Suraweera and N. Beaulieu, "Outage probability of decode-and-forward relaying with optimum combining in the presence of co-channel interference and Nakagami fading," *IEEE Wireless Communications Letters*, vol. 2, no. 5, pp. 495–498, October 2013.

[76] Y. Chen and N. Beaulieu, "New partial decision combining schemes for spatial diversity," in *2010 IEEE International Conference on Communications (ICC)*, May 2010, pp. 1–5.

[77] Z. Chair and P. K. Varshney, "Optimal data fusion in multiple sensor detection systems," *IEEE Transactions on Aerospace and Electronic Systems*, vol. AES-22, no. 1, pp. 98 –101, Jan. 1986.

[78] A. Aziz, "A soft-decision fusion approach for multiple-sensor distributed binary detection systems," *IEEE Transactions on Aerospace and Electronic Systems*, vol. 47, no. 3, pp. 2208 –2216, Jul. 2011.

[79] R. R. Tenney and N. R. Sandell, "Detection with distributed sensors," *IEEE Transactions on Aerospace and Electronic Systems*, vol. AES-17, no. 4, pp. 501 –510, Jul. 1981.

[80] N. C. Beaulieu and C. Leung, "Optimal detection of hard-limited data signals in different noise environments," *IEEE Transactions on Communications*, vol. 34, no. 6, pp. 619 – 622, Jun. 1986.

[81] V. Milutinovic, "A comparison of suboptimal detection algorithms applied to the additive mix of orthogonal sinusoidal signals," *IEEE Transactions on Communications*, vol. 36, no. 5, pp. 538–543, May 1988.

[82] N. Beaulieu, "Penalties of sample-and-sum and weighted partial decision detectors in gaussian noise," *IEEE Transactions on Communications*, vol. 35, no. 8, pp. 777–785, Aug 1987.

[83] ——, "On the generalized multinomial distribution, optimal multinomial detectors, and generalized weighted partial decision detectors," *IEEE Transactions on Communications*, vol. 39, no. 2, pp. 193–194, Feb 1991.

[84] Y. Chau and J.-T. Sun, "Diversity with distributed decisions combining for direct-sequence cdma in a shadowed rician-fading land-mobile satellite channel," *IEEE Transactions on Vehicular Technology*, vol. 45, no. 2, pp. 237–247, May 1996.

[85] Y. Chen and N. Beaulieu, "Maximum likelihood estimation of SNR using digitally modulated signals," *IEEE Transactions on Wireless Communications*, vol. 6, no. 1, pp. 210–219, 2007.

[86] Y. Chen and C. Tellambura, "Distribution functions of selection combiner output in equally correlated Rayleigh, Rician, and Nakagami-m fading channels," *IEEE Transactions on Communications*, vol. 52, no. 11, pp. 1948–1956, 2004.

[87] A. Papoulis and S. U. Pillai, *Probability, Random Variables and Stochastic Processes, 4th ed.* McGraw-Hill, 2002.

[88] S. Ikki and M. Ahmed, "Performance analysis of cooperative diversity wireless networks over Nakagami-m fading channel," *IEEE Communications Letters*, vol. 11, no. 4, pp. 334–336, April 2007.

[89] G. Yang, M. Khalighi, S. Bourennane, and Z. Ghassemlooy, "Approximation to the sum of two correlated Gamma-Gamma variates and its applications in free-space optical communications," *IEEE Wireless Communications Letters*, vol. 1, no. 6, pp. 621–624, December 2012.

[90] J. C. S. S. Filho and M. D. Yacoub, "Nakagami-m approximation to the sum of M non-identical independent Nakagami-m variates," *Electronics Letters*, vol. 40, no. 15, pp. 951–952, July 2004.

[91] J. Filho and M. Yacoub, "Simple precise approximations to Weibull sums," *IEEE Communications Letters*, vol. 10, no. 8, pp. 614–616, Aug 2006.

[92] W. Hubbard, "The approximation of a poisson distribution by a gaussian distribution," *Proceedings of the IEEE*, vol. 58, no. 9, pp. 1374–1375, Sept 1970.

[93] H. Inaltekin, "Gaussian approximation for the wireless multi-access interference distribution," *IEEE Transactions on Signal Processing*, vol. 60, no. 11, pp. 6114–6120, Nov 2012.

[94] S. K. N. L. Johnson and N. Balakrishnan, *Continuous Univariate Distributions, 2nd Ed.* Wiley, 1994.

[95] Y. Chen, G. Karagiannidis, H. Lu, and N. Cao, "Novel approximations to the statistics of products of independent random variables and their applications in wireless communications," *IEEE Transactions on Vehicular Technology*, vol. 61, no. 2, pp. 443–454, 2012.

[96] K. Wang, T. Wang, Y. Chen, and M.-S. Alouini, "Statistics of α - μ random variables and their applications in wireless multihop relaying and multiple scattering channels," *IEEE Transactions on Vehicular Technology*, to appear.

[97] F. A. Khan, Y. Chen, and M.-S. Alouini, "Novel receivers for AF relaying with distributed stbc using cascaded and disintegrated channel estimation," *IEEE Transactions on Wireless Communications*, vol. 11, no. 4, pp. 1370 –1379, Apr. 2012.

[98] C. S. Patel and G. L. Stuber, "Channel estimation for amplify and forward relay based cooperation diversity systems," *IEEE Transactions on Wireless Communications*, vol. 6, no. 6, pp. 2348 –2356, Jun. 2007.

[99] F. Gao, T. Cui, and A. Nallanathan, "On channel estimation and optimal training design for amplify and forward relay networks," *IEEE Transactions on Wireless Communications*, vol. 7, no. 5, pp. 1907 –1916, May. 2008.

[100] H. Mheidat and M. Uysal, "Non-coherent and mismatched-coherent receivers for distributed stbcs with amplify-and-forward relaying," *IEEE Transactions on Wireless Communications*, vol. 6, no. 11, pp. 4060 – 4070, Nov. 2007.

[101] L. Tong, B. M. Sadler, and M. Dong, "Pilot-assisted wireless transmissions: general model, design criteria, and signal processing," *IEEE Signal Processing Magazine*, vol. 21, no. 6, pp. 12 – 25, Nov. 2004.

[102] Y. Wu and M. Patzold, "Parameter optimization for amplify-and-forward relaying with imperfect channel estimation," in *IEEE 69th Vehicular Technology Conference*, 2009, pp. 1–5.

[103] M. Mohammadi, P. Sadeghi, and M. Ardebilipour, "Node and symbol power allocation in time-varying amplify-and-forward dual-hop relay

channels," *IEEE Transactions on Vehicular Technology*, vol. 62, no. 1, pp. 432–439, 2013.

[104] A. Lalos, A. Rontogiannis, and K. Berberidis, "Frequency domain channel estimation for cooperative communication networks," *IEEE Transactions on Signal Processing*, vol. 58, no. 6, pp. 3400–3405, June 2010.

[105] Y. Gao, D. Lin, B. Li, and S. Li, "Optimal training power allocation for amplify and forward relay networks," in *2010 International Conference on Communications, Circuits and Systems (ICCCAS)*, 2010, pp. 73–77.

[106] B. Gedik, O. Amin, and M. Uysal, "Power allocation for cooperative systems with training-aided channel estimation," *IEEE Transactions on Wireless Communications*, vol. 8, no. 9, pp. 4773–4783, 2009.

[107] H. Rasouli and A. Anpalagan, "SNR-based vs. BER-based power allocation for an amplify-and-forward single-relay wireless system with mrc at destination," in *2010 25th Biennial Symposium on Communications (QBSC)*, 2010, pp. 429–432.

[108] F. Tabataba, P. Sadeghi, and M.-R. Pakravan, "Outage probability and power allocation of amplify and forward relaying with channel estimation errors," *IEEE Transactions on Wireless Communications*, vol. 10, no. 1, pp. 124–134, 2011.

[109] J. Cavers, "An analysis of pilot symbol assisted modulation for Rayleigh fading channels [mobile radio]," *IEEE Transactions on Vehicular Technology*, vol. 40, no. 4, pp. 686–693, Nov. 1991.

[110] G. Colavolpe and R. Raheli, "Noncoherent sequence detection in frequency nonselective slowly fading channels," *IEEE Journal on Selected Areas in Communications*, vol. 18, no. 11, pp. 2302–2311, Nov. 2000.

[111] V. Tarokh, N. Seshadri, and A. Calderbank, "Space-time codes for high data rate wireless communication: performance criterion and code construction," *IEEE Transactions on Information Theory*, vol. 44, no. 2, pp. 744–765, Mar. 1998.

[112] Wolfram, "Wolfram functions," *The Wolfram Functions Site*, http://functions.wolfram.com/NB/MeijerG.nb.

[113] Y. A. B. A. P. Prudnikov and O. I. Marichev, *Integrals and Series, Vol.3: More Special Functions.* Oxford University Press US, 1986.

[114] B. Hassibi and B. Hochwald, "How much training is needed in multiple-antenna wireless links?" *IEEE Transactions on Information Theory*, vol. 49, no. 4, pp. 951–963, 2003.

[115] R. U. Nabar, H. Bolcskei, and F. W. Kneubuhler, "Fading relay channels: performance limits and space-time signal design," *IEEE Journal on Selected Areas in Communications*, vol. 22, no. 6, pp. 1099 – 1109, Aug. 2004.

[116] M. K. Simon, *Probability Distributions Involving Gaussian Random Variables: A Handbook for Engineers and Scientists.* Boston, MA: Kluwer, 2002.

[117] Y. Zhao, R. Adve, and T. J. Lim, "Improving amplify-and-forward relay networks: optimal power allocation versus selection," *IEEE Transactions on Wireless Communications*, vol. 6, no. 8, pp. 3114–3123, August 2007.

[118] ——, "Symbol error rate of selection amplify-and-forward relay systems," *IEEE Communications Letters*, vol. 10, no. 11, pp. 757–759, November 2006.

[119] A. Guidotti, V. Buccigrossi, M. Di Renzo, G. Corazza, and F. Santucci, "Outage and symbol error probabilities of dual-hop AF relaying in a poisson field of interferers," in *2013 IEEE Wireless Communications and Networking Conference*, April 2013, pp. 3704–3709.

[120] J. Lee and C. Tepedelenlioglu, "Stochastic ordering of interference in large-scale wireless networks," *IEEE Transactions on Signal Processing*, vol. 62, no. 3, pp. 729–740, Feb 2014.

[121] M. Di Renzo, A. Guidotti, and G. Corazza, "Average rate of downlink heterogeneous cellular networks over generalized fading channels: A stochastic geometry approach," *IEEE Transactions on Communications*, vol. 61, no. 7, pp. 3050–3071, July 2013.

[122] C. Zhong, S. Jin, and K.-K. Wong, "Dual-hop systems with noisy relay and interference-limited destination," *IEEE Transactions on Communications*, vol. 58, no. 3, pp. 764–768, March 2010.

[123] H. Suraweera, H. Garg, and A. Nallanathan, "Performance analysis of two hop amplify-and-forward systems with interference at the relay," *IEEE Communications Letters*, vol. 14, no. 8, pp. 692–694, August 2010.

[124] D. Benevides da Costa, H. Ding, and J. Ge, "Interference-limited relaying transmissions in dual-hop cooperative networks over Nakagami-m fading," *IEEE Communications Letters*, vol. 15, no. 5, pp. 503–505, May 2011.

[125] F. Al-Qahtani, J. Yang, R. Radaydeh, C. Zhong, and H. Alnuweiri, "Exact outage analysis of dual-hop fixed-gain AF relaying with CCI under dissimilar Nakagami-m fading," *IEEE Communications Letters*, vol. 16, no. 11, pp. 1756–1759, November 2012.

[126] Z. Lin, X. Peng, F. Chin, and W. Feng, "Outage performance of relaying with directional antennas in the presence of co-channel interferences at relays," *IEEE Wireless Communications Letters*, vol. 1, no. 4, pp. 288–291, August 2012.

[127] S. Ikki and S. Aissa, "Performance evaluation and optimization of dual-hop communication over Nakagami-m fading channels in the presence of co-channel interferences," *IEEE Communications Letters*, vol. 16, no. 8, pp. 1149–1152, August 2012.

[128] D. Lee and J. H. Lee, "Outage probability for dual-hop relaying systems with multiple interferers over Rayleigh fading channels," *IEEE Transactions on Vehicular Technology*, vol. 60, no. 1, pp. 333–338, Jan 2011.

[129] P. G. Moschopoulos, "The distribution of the sum of independent Gamma random variables," *Ann. Inst. Statistical Math. (A)*, vol. 37, pp. 541–544, 1985.

[130] A. M. Mathai, "Storage capacity of a dam with Gamma type inputs," *Ann. Inst. Statist. Math. (A)*, vol. 34, pp. 591–597, 1982.

[131] J. Zhao and G. Cao, "VADD: Vehicle-assisted data delivery in vehicular ad hoc networks," *IEEE Transactions on Vehicular Technology*, vol. 57, no. 3, pp. 1910–1922, May 2008.

[132] G. Karagiannidis, N. Sagias, and P. Mathiopoulos, "N∗Nakagami: A novel stochastic model for cascaded fading channels," *IEEE Transactions on Communications*, vol. 55, no. 8, pp. 1453–1458, 2007.

[133] N. Sagias, G. Karagiannidis, P. Mathiopoulos, and T. Tsiftsis, "On the performance analysis of equal-gain diversity receivers over generalized Gamma fading channels," *IEEE Transactions on Wireless Communications*, vol. 5, no. 10, pp. 2967–2975, 2006.

[134] J. Salo, H. El-Sallabi, and P. Vainikainen, "Statistical analysis of the multiple scattering radio channel," *IEEE Transactions on Antennas and Propagation*, vol. 54, no. 11, pp. 3114–3124, 2006.

[135] Y.-C. Ko, M.-S. Alouini, and M. K. Simon, "Outage probability of diversity systems over generalized fading channels," *IEEE Transactions on Communications*, vol. 48, no. 11, pp. 1783–1787, 2000.

[136] C. B. D and M. D. Springer, "The distribution of products, quotients and powers of independent H-function variates," *SIAM J. Appl. Math.*, vol. 33, no. 4, pp. 542–558, 1977.

[137] C. A. Coelho and J. T. Mexia, "On the distribution of the product and ratio of independent generalized Gamma-ratio random variables," *The Indian Journal of Statistics*, vol. 62, no. 11, pp. 221–255, 2007.

[138] S. Al-Ahmadi and H. Yanikomeroglu, "On the approximation of the generalized-K distribution by a Gamma distribution for modeling composite fading channels," *IEEE Transactions on Wireless Communications*, vol. 9, no. 2, pp. 706–713, Feb. 2010.

[139] S. Navidpour, M. Uysal, and M. Kavehrad, "BER performance of free-space optical transmission with spatial diversity," *IEEE Transactions on Wireless Communications*, vol. 6, no. 8, pp. 2813–2819, 2007.

[140] D. Obradovic, H. Lenz, and M. Schupfner, "Fusion of sensor data in siemens car navigation system," *IEEE Transactions on Vehicular Technology*, vol. 56, no. 1, pp. 43 –50, Jan. 2007.

[141] G. Foresti and C. Regazzoni, "Multisensor data fusion for autonomous vehicle navigation in risky environments," *IEEE Transactions on Vehicular Technology*, vol. 51, no. 5, pp. 1165 – 1185, Sep. 2002.

[142] J. Fang and H. Li, "Power constrained distributed estimation with cluster-based sensor collaboration," *IEEE Transactions on Wireless Communications*, vol. 8, no. 7, pp. 3822 –3832, Jul. 2009.

[143] R. Yu, Z. Sun, and S. Mei, "Scalable topology and energy management in wireless sensor networks," in *2007 IEEE Wireless Communications and Networking Conference*, Hong Kong, Mar. 2007, pp. 3448 –3453.

[144] B. Chen, R. Jiang, T. Kasetkasem, and P. K. Varshney, "Channel aware decision fusion in wireless sensor networks," *IEEE Transactions on Signal Processing*, vol. 52, no. 12, pp. 3454 – 3458, Dec. 2004.

[145] Y. Lin, B. Chen, and P. K. Varshney, "Decision fusion rules in multi-hop wireless sensor networks," *IEEE Transactions on Aerospace and Electronic Systems*, vol. 41, no. 2, pp. 475 – 488, Apr. 2005.

[146] A. D. Kot and C. Leung, "Optimal partial decision combining in diversity systems," *IEEE Transactions on Communications*, vol. 38, no. 7, pp. 981 –991, Jul. 1990.

[147] R. S. Blum, "Distributed detection for diversity reception of fading signals in noise," *IEEE Transactions on Information Theory*, vol. 45, no. 1, pp. 158 –164, Jan. 1999.

[148] O. Ugweje, "Selection diversity for wireless communications in Nakagami-fading with arbitrary parameters," *IEEE Transactions on Vehicular Technology*, vol. 50, no. 6, pp. 1437–1448, Nov 2001.

[149] K. Letaief and W. Zhang, "Cooperative communications for cognitive radio networks," *Proceedings of the IEEE*, vol. 97, no. 5, pp. 878–893, May 2009.

[150] T. Yucek and H. Arslan, "A survey of spectrum sensing algorithms for cognitive radio applications," *IEEE Communications Surveys Tutorials*, vol. 11, no. 1, pp. 116–130, 2009.

[151] Q. Zhang, "Probability of error for equal-gain combiners over Rayleigh channels: some closed-form solutions," *IEEE Transactions on Communications*, vol. 45, no. 3, pp. 270 –273, Mar. 1997.

[152] A. P. Prudnikov and O. I. Marichev, "The algorithm for calculating integrals of hypergeometric type functions and its realization in reduce

system," in *Proceedings of the international symposium on Symbolic and algebraic computation*, 1990, pp. 212–224.

[153] A. M. Mathai, "Products and ratios of generalized Gamma variates," *Scandinavian Actuarial Journal*, vol. 1972, no. 2, pp. 193–198, 1972.